SPRFMO
South Pacific Regional Fisheries Management Organisation

11th MEETING OF THE SCIENTIFIC COMMITTEE

11 to 16 September 2023, Panama City, Panama

SC11 – DW07
Modelling vulnerable marine ecosystem (VME) indicator taxa

New Zealand

South Pacific Regional Fisheries Management Organisation

11th Meeting of the Scientific Committee

Panama City, Panama, 11-16 September 2023

Modelling vulnerable marine ecosystem (VME) indicator taxa

Jordi Tablada[1], Matthew Bennion[2], Anthony Charsley[2,3], Shane Geange[1], Owen Anderson[2], David Bowden[2], Ashley Rowden[2,3]

1. Department of Conservation, Wellington, New Zealand
2. National Institute of Water & Atmospheric Research, Wellington, New Zealand
3. Victoria University of Wellington, Wellington, New Zealand

12 August 2023

Contents

1. Purpose

The purpose of this paper is to update the Scientific Committee (SC) on the development of abundance models for Vulnerable Marine Ecosystem (VME) indicator taxa and outline their potential application, including for the identification of VMEs. This work will help reduce uncertainties in risk assessments for benthic habitats and VMEs and inform SC advice on the ongoing appropriateness of the management measures to ensure CMM-03-2023 continues to achieve its objective and the objectives of the Convention.

2. Background

Spatial management areas were established under CMM03-2019 to protect large proportions of suitable habitat for VME indicator taxa from the impacts of bottom fishing, while allowing bottom fishing within define bottom trawl management areas (BTMAs). The design of the BTMAs were informed by habitat suitability models for VME indicator taxa (Table 1), which predict the suitability of a location for a species, or group of species, based on their observed relationship with environmental conditions (Guisan and Zimmermann 2000; Elith and Leathwick, 2009). Habitat suitability models for VME indicator taxa have been progressively developed over the years for the SPRFMO Convention Area, or parts thereof (Anderson et al. 2016a, b, Rowden et al. 2017, Georgian et al. 2019. Stephenson et al. 2021, SC10-DW05). While habitat suitability models have been used within the SPRFMO context to predict the distribution of VME indicator taxa, they remain data-limited and do not generally include any information regarding the expected abundance of VME indicator taxa.

Recognising the limitations of habitat suitability models, and in particular their limited ability to infer taxon abundance, the 9th meeting of the SPRFMO SC noted that the "*estimation of the fraction of VME SC10-DW05 5 indicator taxa abundance protected [by the spatial management measures] depends strongly on the ability of the available habitat suitability models to infer abundance, noting that abundance models using survey presence-absence or abundance data and relevant environmental/benthic data could improve this accuracy*" (para 71 of the SC9-Report). Consequently, the item "Develop abundance models for VME [indicator] taxa" was added to the SC multi-annual workplan at the 10th SPRFMO Commission meeting, with a 2022+ timeline (Annex 4a of COMM10-Doc06_rev2).

Following the 10th SPRFMO Commission meeting, New Zealand trialled two methods for developing abundance models for VME indicator taxa: 1) a *data-driven* modelling approach underpinned by (limited) abundance data, and 2) a *principles-based* approach, i.e., where distribution of abundance of taxa are based on known or estimated relationships informed by experts.

The *data-driven* approach was trialled for two VME indicator taxa: *Goniocorella dumosa* (representing the order Scleractinia, stony corals) and Demospongiae (representing the phylum Porifera, sponges). Both abundance models produced credible predictions of spatial distributions of abundance with high correlations between modelled predictions and observed abundances (noting that these same data were also used to train the models).

A preliminary trial of abundance modelling using a *principles-based* approach (having only received input from a subset of experts, 5 out of 22 experts) provided spatial estimates which visually appeared

plausible, but which performed no better at predicting abundance than previously developed habitat suitability models. It was decided that further work was needed to fully assess the appropriateness of this approach, including the integration of responses from a greater number of experts (representing a variety of expertise and knowledge of the taxa) and possibly combining expert opinion using alternative elicitation methods than those tested. It was also decided that where sufficient abundance data exist to develop robust statistical models, a *data-driven* approach should be prioritised for estimating the distribution of VME indicator taxa abundances.

That results of that work was presented to the 10th meeting of the SPRFMO SC in SC10-DW05. Following discussion of SC10-DW05, in its report SC10 (para 122 SC10-Report) :

- **Recommended** the application of the *data-driven* approach described in this paper [in reference to SC10-DW05] to estimate spatial predictions of abundance for VME indicator taxa for which sufficient abundance data exists.
- **Recommended** further exploring the application of the *principles-based* approach where abundance data is insufficient to apply a *data-driven* approach until sufficient abundance data becomes available.

In response to recommendations of SC10, this paper presents abundance models for 15 VME indicator taxa within the evaluated area of the SPRFMO Convention Area using a *data-driven* approach and 4 taxa using a *principles-based* approach (Table 1). Additionally, to assess the utility of existing habitat suitability models and abundance models developed by this work for informing management decisions we also explore: 1. the relationship between models and historic benthic bycatch; and 2. the use of abundance models to develop VME indices.

As part of the on-going efforts to model abundance of VME indicator taxa within the SPRFMO Evaluated Area, a study to develop a spatial model using the vector autoregressive spatio-temporal (VAST) modelling platform (Thorson, 2019) was performed with Demospongiae selected as study taxon. Initial results from this case study are presented here. This work was funded separately by the EU, but under the same "Develop abundance models for VME [indicator] taxa" task in the SC multi-annual workplan.

Historic benthic bycatch data provide information on where VME indicator taxa are known to occur (or known to have previously occurred). Historic bycatch data therefore represent an opportunity to evaluate correlations between abundance models and habitat suitability models (when used as estimates or proxies for abundance) for VME indicator taxa distributions and historical records of benthic bycatch biomass to potentially validate the abundance models. This work addresses the SC multi-annual workplan tasks to "Investigate the relationship of benthic bycatch to abundance models of VME taxa" and to "Investigate the relationship between benthic bycatch from fishing vessels (including encounter events) and the habitat suitability models" (COMM11-Report Annex-4a).

The development of abundance models also potentially allows new applications that were not possible using habitat suitability models. Efforts by other Regional Fisheries Management Organisations to present SAIs on VMEs have combined the outputs of VME vulnerability assessments with spatially explicit distributions of VMEs and VME indicator taxa (and estimated levels of confidence), which has facilitated the mapping of a "VME index" (Morato et al 2018, Gros et al 2023. Here we provide an exploratory development of VME indices for 15 of the 17 newly developed VME

indicator taxa, based on the methods developed by Gros et al., 2023 and adapted by Stephenson et al., (in prep) using modelled distribution data.

Table 1 | Existing Habitat Suitability Models (providing the source) and newly developed Abundance Models (presented in this paper, shaded in light green), including approach taken, for each VME indicator taxon in the SPRFMO Evaluated Area.

FAO code	VME indicator taxon		Habitat Suitability Model	Abundance Model	
				Data-driven	***Principles-based***
PFR	Porifera	Demospongiae	Stephenson et al. 2021	Y	-
		Hexactinallida	Stephenson et al. 2021	Y	-
CSS	Scleractinia	*Enallopsammia rostrata*	Stephenson et al. 2021	-	Y
		Goniocorella Dumosa	Stephenson et al. 2021	Y	Y
		Madrepora oculata	Stephenson et al. 2021	-	Y
		Solenosmilia variabilis	Stephenson et al. 2021	Y	Y
AQZ	Antipatharia		Stephenson et al. 2021	Y	-
AJZ	Alcyonacea		Unpublished	Y	-
GGW	Gorgonian Alcyonacea		Stephenson et al. 2021	Y	-
NTW	Pennatulacea		Stephenson et al. 2021	Y	-
ATX	Actinaria		SC10-DW05	Y	-
ZOT	Zoantharia		SC10-DW05	Y	-
HQZ	Hydrozoa		SC10-DW05	Y	-
AXT	Stylasteridae		Stephenson et al. 2021	Y	-
BZN	Bryozoa		SC10-DW05	Y	-
BHZ	Brisingida		SC10-DW05	Y	-
CWD	Crinoidea		SC10-DW05	Y	-

3. Methods

3.1 Area of study

All the modelling work presented in this paper, hereby referred as the study area, covers the extent of the SPRFMO Evaluated Area (Figure 1), including the multiple (New Zealand, Australia, Norfolk Island, New Caledonia, Fiji, Tonga, Cook Islands and French Polynesia) Exclusive Economic Zone (EEZ) areas that are partly included within it. Any areas with depths outside of the 200-3,000m range are not part of the study area (Stephenson et al., 2021).

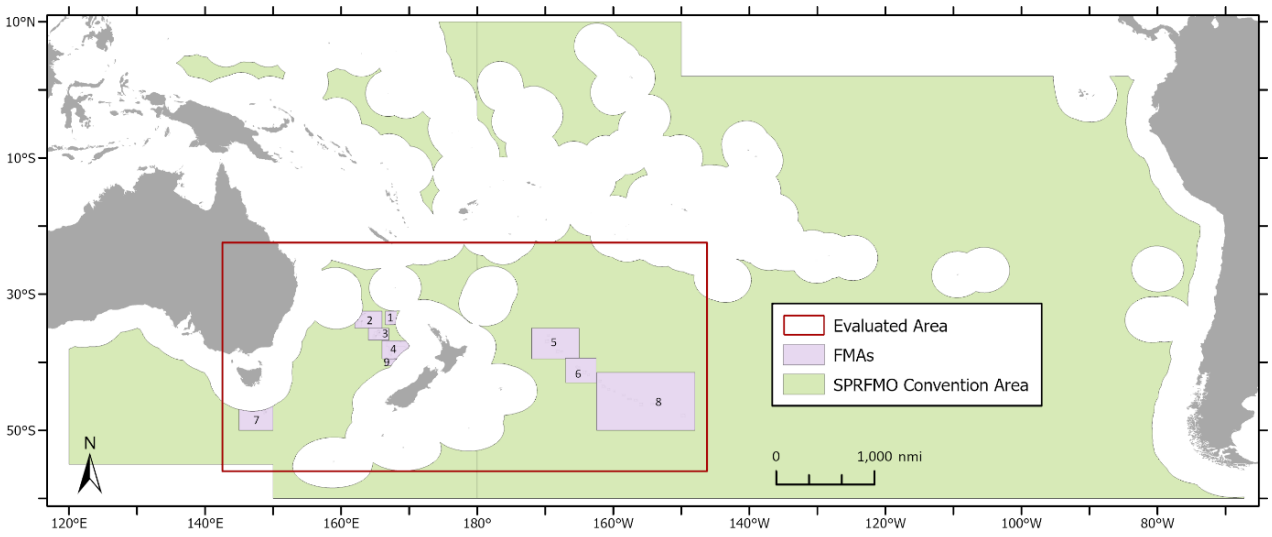

Figure 1 | SPRFMO Convention Area (light green area) including the extent of the Evaluated Area under SC9-DW10 (red boundaries) with all numbered Fisheries Management Areas (FMAs) defined under SPRFMO CMM03-2023 (pink polygons). FMAs numbered as 1) West Norfolk, 2) North Lord Howe Rise, 3) South Lord Howe Rise, 4) Northwest Challenger, 5) North Louisville Ridge, 6) Central Louisville Ridge, 7) South Tasman Rise, 8) South Louisville Ridge, and 9) Westpac Bank.

3.2 Modelling spatial estimates of density

The approach presented in SC10-DW05 for modelling the distribution of abundance is a two-part density (or hurdle) model. Briefly, density models firstly fit a binomial model for probability of occurrence, followed by a separate model with a Gaussian distribution to estimate density for locations where presence was recorded. Both models are then multiplied together (often referred to as 'hurdled', see Stephenson et al., 2021b) to obtain spatial estimates of density (number of individuals per square kilometre) conditional on presence (hereafter referred to as 'density'). The habitat suitability models of VME indicator taxa from both Stephenson et al. (2021a) and SC10-DW05 are binomial models and the first component of the models created here were developed in a similar way. The distinction here is that the image-based data used to train the *data-driven* models herein is presence-absence, so no pseudo-absence or target-group background absence generation methods were necessary. Additionally, as the predictions from the first component of these models are combined with the second, MaxEnt (maximum entropy) models were not used (as they are logistic regression based).

For the second component of the hurdle model, a *data-driven* approach and a *principles-based* approach (as described in SC10-DW05) were used (Table 1). As part of the *data-driven* approach, VME indicator taxa abundance data and spatially explicit environmental variables were analysed in a statistical model. The spatial outputs of the second component of the density model (conditioned to recorded presence for the *data-driven* approach) were then hurdled (multiplied) with the predictions of the habitat suitability models to produce spatial estimates of density (number of individuals per km^2). All VME indicator taxa were modelled using the *data-driven* approach except two species of stony corals (order Scleractinia), *Enallopsammia rostrata* and *Madrepora oculata* (Table 1) for which the existing abundance data was deemed insufficient. Instead, *Enallopsammia rostrata* and *Madrepora oculata* and two other taxa from the order Scleractinia, *Goniocorella dumosa* and

Solenosmilia variabilis were modelled using a *principles-based* approach. The *principles-based* approach, instead of using taxon occurrence records, used a set of environmental variables used to constraint taxon-specific suitable habitat by expert knowledge, producing what are known as relative environmental suitability (RES) models (Kaschner et al., 2006).

As an exploratory exercise, a spatial model was developed using the VAST modelling platform to predict the density of the class Demospongiae. Both Demospongiae abundance and presence-only data were combined with a set of environmental variables to produce a spatial representation of the predicted relative density of Demospongiae. The model included both spatial and environmental effects.

3.3 Data-driven approach

Biological data

Estimates of density data (number of individuals per km^2) for 17 VME indicator taxa (Table 1) was obtained from a database (Anderson et al., in press.) consisting of records of benthic invertebrates imagery data collected using NIWA's Deep Towed Imaging System (DTIS) at 949 seafloor sites compiled across 20 voyages: 358 sites from five surveys of Chatham Rise (Bowden et al. 2019), 172 sites from Campbell Plateau (Roberts et al. 2018, Anderson et al. 2020), 42 sites from the Challenger Plateau (Nodder 2007) 118 sites from the Louisville Seamount Chain (Clark et al. 2015), 18 sites from the Macquarie Ridge (RV Tangaroa voyage TAN0803) and 21 sites from the Kermadec Ridge (RV Tangaroa voyage TAN1612) and 61 sites from the Bay of Plenty Southern Kermadec Ridge (RV Tangaroa voyage TAN1206) (Anderson et al. in press). The training dataset was then limited to sites within the depth range of the study area (200-3000 m, Stephenson et al., 2021) leaving a total of 832 records with abundance data available for training the models, with 138 (17%) of those points being located within the boundaries of the evaluated area of the SPRFMO Convention Area (Figure 2). All 138 DTIS points in the SPRFMO Convention Area are located within FMAs, with 17 being located within the Northwest Challenger FMA (2%), 3 within the Westpac Bank FMA (0.4%), 73 within the North Louisville Ridge

FMA (9%), and 45 within the Central Louisville Ridge FMA (5.4%). The data included presence-absence data and estimates of density for all VME indicator taxa, which are included in Annex 1.

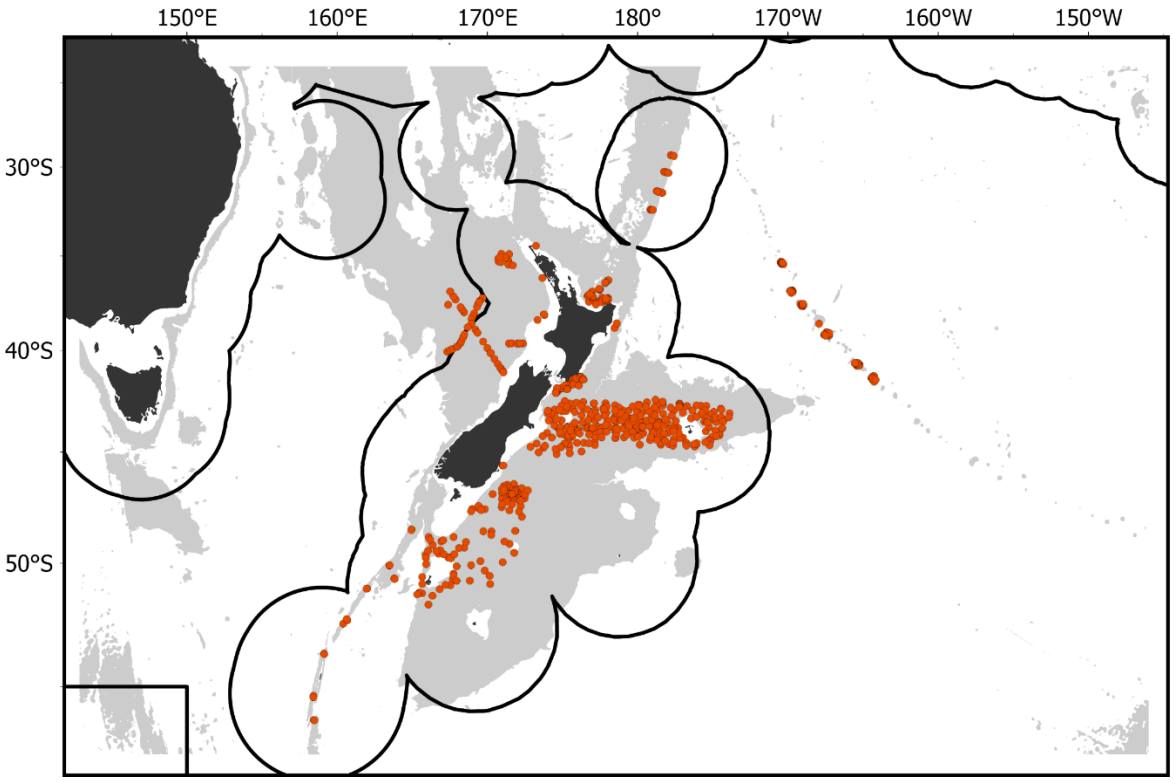

Figure 2 | DTIS sites (red dots) that provided estimates of VME indicator taxa abundance data. Black lines indicate the boundaries between the SPRFMO Evaluated Area and the multiple Exclusive Economic Zones.

Environmental data

The same environmental variables were used as predictors in the density distribution models as those used for the previously developed habitat suitability models (see open-access publications from Georgian et al., 2019 and Stephenson et al., 2021a for further details), except for an updated seamounts variable (Clark et al., 2022; Yesson et al., 2011). For each modelled VME indicator taxon, a subset of the environmental variables that appeared to drive the distribution of each taxon was used (Table *2*). Specific environmental variables were included or omitted based on the biology of modelled taxa. For example, calcium carbonate polymorph saturation state variables were included for certain taxa, where appropriate. For corals in the order Scleractinia aragonite saturation was included, whereas for Alcyonacea, for instance, calcite saturation was included (Stephenson et al., 2021; SC10-DW05). For density modelling (the second part of the hurdle/density model), a secondary environmental selection step using an automated variable selection procedure was employed. A random forest model was fitted with respective suites of taxon-specific environmental variables used by Stephenson et al. (2021a) and Stephenson et al. (2021b). This method takes account of any co-linearity between environmental variables through the implementation of a conditional approach to calculation of variable importance (Ellis et al., 2021; Stephenson et al., 2021b). Explanatory variables

with a relative influence greater than 100 divided by the number of environmental variables provided were retained for modelling.

Table 2 | Environmental variables used in the modelling of each VME indicator taxon using the *data-driven* approach. Taxon codes as: Actinaria (ATX), Alcyonacea (AJZ), Antipatharia (AQZ), Brisingida (BHZ), Bryozoa (BZN), Crionidea (CWD), Demospongiae (DEM), *Enallopsammia rostrata* (ERO)., *Goniocorella dumosa* (GDU), Gorgonian Alcyonacea (GGW), Hexactinellida (HEX), Hydrozoa (HQZ), *Madrepora oculata* (MOC), Pennatulacea (NTW), Solenosmilia variabilis (SVA), Stylasteridae (AXT), Zoantharia (ZOT).

	VME indicator taxon																
Environmental variable	ATX	AJZ	AQZ	BHZ	BZN	CWD	DEM	ERO	GDU	GGW	HEX	HQZ	MOC	NTW	SVA	AXT	ZOT
Aragonite saturation state at depth									X					X			
Calcite saturation state at depth		X		X	X					X							
Silicate							X				X						
Dissolved oxygen at depth			X	X			X		X	X		X		X			X
BPI-broad	X	X	X	X	X	X	X		X	X	X	X		X	X	X	X
Standard deviation of Slope	X	X	X	X	X	X	X			X					X		X
Ruggedness		X	X	X		X	X		X	X						X	
Percent gravel																	
Percent mud		X		X			X					X		X			X
Particulate organic carbon export	X	X		X	X	X	X		X	X	X	X		X		X	X
Seamounts (presence/absence)															X		
Temperature at depth	X		X	X	X		X		X		X	X		X			X

Density modelling

A bootstrap approach using Boosted Regression Trees (BRT) and Random Forests (RF) models was used to estimate density using a Gaussian error distribution, noting that the models are conditional on presence. Bootstrap models were fitted and geographical predictions (1 km x 1 km grid for depths between 200 and 3000 m) ensembled using the same approach as described in Stephenson et al. (2021b) (like Stephenson et al., 2021a but without the MaxEnt model contribution). Briefly, final ensemble models were produced by taking weighted averages of the spatial predictions from each model (BRT and RF). This procedure generates a two-part weighting for each component of the ensemble model, taking equal contributions from the overall model performance (R^2 value derived from the 'evaluation' dataset) and the uncertainty measure (CV) in each cell (see Stephenson et al., 2021b for further details). Within each bootstrap, spatial predictions from abundance models were hurdled with (multiplied by) the habitat suitability models (presence-absence) to produce spatial estimates of density. The accuracy of the spatial density estimates was assessed by comparing the predicted values with all the available abundance sample data for VME indicator taxa using Pearson's correlation measure, where 0.4 is considered good (based on a subjectively defined threshold). The performance of the models was evaluated at multiple spatial scales:

- At the SPRFMO Evaluated Area level
- At bioregions level, using the bioregions defined in Costello et al. (2017)
- At Fisheries Management Areas (FMAs) level

For comparison, scatter plots and Pearson's correlation were assessed using the DTIS abundance data (described above) for the final ensemble models from the density-driven approach and habitat suitability model outputs previously used as estimates (or proxies for) abundance (HSI-linear and HSI ROC-linear) (SC8-DW07-rev1).

Environmental coverage

Where predictions in "environmental space" (defined as the multidimensional space when considering each of the environmental variables as a dimension) occur where sampling is high, we may have more confidence in the predictions because they are well informed by empirical data. Conversely, where predictions occur in environmental space with low sampling coverage, we may have less confidence and predictions need to be carefully interpreted. To account for the lack of biological data used to predict density in some of the environmental space, a measure of "coverage of environmental space" (Pinkerton et al., 2010; Smith et al., 2013; Stephenson et al., 2020) was calculated following the same methodology as outlined by Stephenson et al. (2021a).

Briefly, VME indicator taxa presence-absence data (i.e., from DTIS observations) (Annex 1) was used to inform variation in sampling density within the environmental space by combining all presence-data locations with the same number of randomly selected sample cells from the environmental space (where there were no biological samples). A BRT model was used to model the relationship between these "present" (true) samples and "absent" (unsampled) samples for the 12 environmental variables (Table 2) used in the *data-driven* approach.

The predicted distribution of the coverage of the environmental space is bound between 0-1. Estimates of 0 indicate very low sampling of the environmental space, whereas estimates of 1 indicate a very high level of sampling (Stephenson et al., 2020; Stephenson et al., 2021a).

Spatially explicit estimates of environmental coverage were created based on all environmental data used for the *data-driven* approach (hereafter 'combined environmental coverage'). Then, separate taxon-specific environmental coverage was estimated, based on the environmental variables used for the density models (Table 2). This resulted in one combined environmental coverage layer and 15 taxon-specific environmental coverage layers.

3.4 Principles-based approach

Relative environmental suitability (RES) modelling is an approach to habitat suitability modelling that relies on expert knowledge rather than species observation data (Kaschner et al. 2006; Watson et al., 2013). Expert input is used to constrain suitable habitat based on known relationships between species presence and a suite of environmental variables. Annex 2 of SC10-DW05 presented detailed methods and instructions to gather enough expert knowledge to extend RES methods to estimate relative density (0-1) for four stony corals (*Goniocorella dumosa, Enallopsammia rostrata, Madrepora oculata, Solenosmilia variabilis*). Briefly, a set of instructions and worksheets were developed to gather expert input, with three input sections provided for:

1. Selection of **environmental variables** (relevant to the assessed VME indicator taxa).
2. Selection of **the shape** that best describes the perceived **relationship** between each chosen environmental variable and VME indicator taxa density. Shapes available for selection included **Trapezoid**, **Plateau** and **Linear**.
3. Selection of numerical **thresholds** (absolute and preferred; min and max) that best describe the relationship between VME indicator taxa density and a given environmental variable.

The initial models (presented in SC10-DW05) were trialled using responses from 6 experts, from the 22 that were initially approached. Some respondents seemed to misinterpret the provided instructions, which led to a series of steps taken once the work that led to SC10-DW05 was completed (post-August 2022):

1. Experts were approached with queries regarding their original responses to check whether these were caused by misinterpretation of instructions or not. The number of expert responses increased from 6 to 8.

2. Additional feedback was used to establish consensus variables, shapes and median threshold values used for the RES models.

3. The RES models were re-run (for the four stony coral taxa *Goniocorella dumosa, Enallopsammia rostrata, Madrepora oculata, Solenosmilia variabilis*) using the additional feedback gathered during steps 1 and 2.

The updated *principles-based* approach models for the four stony coral taxa (*Goniocorella dumosa, Enallopsammia rostrata, Madrepora oculata, Solenosmilia variabilis*) were then hurdled (multiplied) with the Stephenson et al. (2021a) habitat suitability models and model fits assessed using the same data and process as described for the *data-driven* approach (Pearson's correlation). For comparison, scatter plots and Pearson's correlation were assessed using the DTIS abundance data (described above) for the principles-based approach and habitat suitability model outputs previously used as estimates (or proxies for) abundance (HSI-linear and HSI ROC-linear) (SC8-DW07-rev1).

3.5 VAST modelling

The vector autoregressive spatio-temporal (VAST) modelling platform is a spatio-temporal modelling platform designed to support the provision of multiple types of assessments (i.e., stock assessments, habitat assessments) that often share common core goals to effectively inform fisheries management (Thorson, 2019). VAST can be applied using an open-source and publicly-available package (https://www.github.com/james-thorson/VAST/) within the R statistical environment (R Core Team, 2022), which was used for our case study. The VAST package (version 3.10.0) was used to build spatial models (predicting at a 1 km^2 resolution grid) for the class Demospongiae including spatial effects (from nearby observed data) and environmental covariates. Due to having the highest number of records in the DTIS dataset compiled to inform the development of density models of VME indicator taxa, and a high number of records in the presence-only data (SC10-DW05), the class Demospongiae was deemed appropriate to be used as a study taxon for the VAST modelling approach.

Biological data

Previously compiled and groomed VME indicator taxa presence-only data from Stephenson et al. (2021a) and observed abundance data (same DTIS dataset used in the density modelling of VME indicator taxa using a *data-driven* approach) were used to inform the VAST framework. Pseudo-absence data was required for model building and was generated using both target-group background (as performed in Stephenson et al. (2021a)) and random (10x as many presence-only observations) generation methods (Barbet-Massin et al., 2012; Cerasoli et al., 2017; Chefaoui & Lobo, 2008; Mateo et al., 2008; Phillips et al., 2009).

Environmental data

A sub-set of environmental variables were identified as suitable to be used in the VAST approach and subsequently collected from Georgian et al. (2019) and Stephenson et al. (2021a) (percent gravel, percent mud, slope, bathymetry, presence of seamounts, dissolved oxygen at depth and temperature). Highly correlated variables to temperature such as silicate at depth and productivity were discarded to avoid multicollinearity issues when used in a regression model. To reduce the dimensionality of the large environmental dataset a secondary analysis was performed using a Principal Components Analysis (PCA) to transform the environmental covariates into a smaller set of principal components (Goode et al., 2021).

Density modelling

To test the importance of spatial effects and environmental covariates, for each pseudo-absence generation method (target-group background, random) and for each set of environmental covariates (standard set, PCA set) models were built:

- Including spatial effects only
- Including environmental covariates only
- Including both spatial effects and environmental covariates

Akaike information criterion (AIC), percent deviance explained, and assessment of each model's uncertainty was used to select the best performing model with target-group background pseudo-absences and with randomly generated pseudo-absences. Then, K-fold cross-validation was performed on the selected models to compare the predictive performance across the pseudo-absence generation methods. Correlations (Pearson's and Spearman's) were used to assess relationships with

the observed data. Root mean square error (RMSE) and average error (AVE) metrics were estimated to compare magnitude of error between models.

3.6 Investigating the relationship between benthic bycatch biomass and density of VME indicator taxa

Benthic bycatch data provide an estimate of biomass (weight) of the caught organism/s in a defined area and/or tow. Density data refer to the number of individuals of a given taxon within an area or transect. These two metrics are not necessarily correlated, and the likelihood of correlation is greatly affected by the taxonomic resolution at which the data is grouped. For example, within the class Demospongiae (demosponges) we find species such as *Ecionemia alata* (which often grow to ~1 m in diameter) and *Aciculites pulchra* (which grow to ~20cm wide), which present obvious differences in terms of relating biomass and number of individuals. Nonetheless, we investigated the relationship between benthic bycatch data and the density/habitat suitability models of VME taxa. A previously compiled dataset of benthic bycatch records from bottom trawl fishing vessels within the SPRFMO Evaluated Area (SC8-DW11) was used to perform the investigation. Raw taxon-specific bycatch biomass records were assessed against taxon-specific models of density (presented in this paper as the models developed under the "data-driven" approach) and habitat suitability models (when used as estimates or proxies for abundance) (HSI-linear and HSI ROC-linear) from Stephenson et al. (2021) and SC10-DW05 using Pearsons correlation coefficient (Table 10).

Correlations between estimates of the biomass of VME indicator taxa on the seafloor derived from benthic bycatch and modelled estimates of density derived from DTIS video surveys are potentially complicated by the taxonomic resolution at which the data are grouped (see example above). In additional to taxon-specific differences in relationships between biomass and number of individuals, several other factors, which DTIS data is not subject to, can complicate comparisons between DTIS and bycatch data, including:

1. The **catchability of taxa by bottom trawl gear**, where the more readily caught taxa (based on morpho-characteristics i.e., upright or encrusting) and the gear characteristics (like gear type, net size, trawl length and trawl speed) may contribute disproportionately to benthic bycatch biomass associated to a tow.
2. **Location-specific catchability** where seafloor features and topography may have an influence on benthic bycatch rates by bottom trawl gear.
3. The potential influence of historical **fishing effort** on biomass estimates, with highly fished areas having lower bycatch rates as VME indicator taxa, if previously present, may have been removed by past fishing events.

Additionally, estimates of density using DTIS data (as previously described) originate from transects within mainly untrawled areas, benthic bycatch records are associated to areas where fishing has occurred. These differences between the datasets used to model density of VME indicator taxa, compared to bycatch datasets used to estimate seafloor biomass mean that correlations need to be carefully interpreted (at best) or may even be considered spurious.

3.7 VME indices

VME indices were mapped using as a basis the approach detailed by Gros et al. (2023) and adapted for SPRFMO VME indicator taxa and for modelled data by Stephenson et al. (in prep). The approach

involves three steps: 1) assessing the vulnerability of VME indicator taxa to bottom-impact fishing (see Gros et al., 2023 for details); 2) mapping richness-based (using habitat suitability models developed by Stephenson et al., 2021a and SC10-DW05) and density-based VME indices (using the density models developed herein), 3) overlapping richness- and density-based VME indices to identify areas where VMEs are most likely to occur (Stephenson et al. in prep).

Vulnerability scores were calculated for morphotaxa by Gross et al. (2023) and Stephenson et al. (in prep) based on the following criteria: rare or unique; larval dispersal; sessility; habitat forming; fragility; life history (Morato et al., 2018; Burgos et al., 2020; Gros et al., 2023). As some VME indicator taxa modelled here (Alcyonacea, Bryozoa, Crinoidea, Demospongiae, Gorgonacea Alcyoncea, and Pennatulacea) contained several morphotaxa considered separately by Gros et al. (2023) and Stephenson et al. (in prep), mean vulnerability scores of morphotaxa within VME indicator taxa groups were used.

For richness- and density-based VME indices, each modelled layer of habitat suitability or density was multiplied by corresponding vulnerability scores for respective VME indicator taxa (as per Gros et al., 2023). This process was also applied to associated uncertainty layers for presence-only and density models (SD). Vulnerability score-applied layers were then stacked (summed) into four sets of combined layers (density; density-uncertainty; richness; richness-uncertainty). As in Stephenson et al. (in prep), the uncertainty estimates generated here differ to those generated in Gros et al. (2023). Spatially explicit uncertainty estimates were calculated in a method similar to the coefficient of variation. Uncertainty estimates for the richness-based and density-based VME indices were calculated by dividing the summed richness- and density-based VME indices by respective summed vulnerability applied uncertainties (SD) for richness and density.

Areas of high richness- and density-based VME indices (90th and 95th percentiles) were then mapped. Areas of very high VME indices (95th percentile) were overlayed (richness and density VME indices). This produces a final map detailing four classes where areas of overlapping high richness- and density-based VME indices are mapped (map colours used are the same as Gros et al., 2023 for easy comparison). Natural breaks were used to map areas of low confidence for richness- and density-based indices. Three breaks were applied, and the upper break was used to show areas where comparatively low confidence is present for richness and density indices independently (adapted from Stephenson et al., in prep).

4. Results

4.1 Density models

Performance at multiple spatial scales

Taxon-specific estimates of predicted density of individuals for 15 VME indicator taxa in the study area produced good model fits (well above the subjectively defined Pearson's r >0.4 threshold) when using training data for all VME indicator taxa except for the stony coral *Solenosmilia variabilis* (0.32 with BRT) (Table 3). Conservative model fits, as assessed with iteratively (each bootstrap) withheld evaluation data, showed significantly lower values for both BRTs and RFs across all modelled taxa, with mean Pearson's r values ranging from 0.09 to 0.62 (Table 3).

Table 3 | Mean model fits based on 100 bootstraps for Boosted Regression Trees (BRTs) and Random Forest (RF) density models for the entire study area for the 15 VME indicator taxa used in the *data-driven* approach.

	Mean correlation (100 bootstraps) (Pearson's r)			
	Training data		Evaluation data	
VME indicator taxon	**RF**	**BRT**	**RF**	**BRT**
Actiniaria	0.90	0.85	0.54	0.50
Alcyonacea	0.88	0.79	0.25	0.21
Antipatharia	0.83	0.69	0.29	0.30
Brisingida	0.93	0.87	0.38	0.33
Bryozoa	0.85	0.86	0.25	0.15
Crinoidea	0.77	0.82	0.30	0.33
Demospongiae	0.87	0.89	0.32	0.24
Enallopsammia rostrata	-	-	-	-
Goniocorella dumosa	0.95	0.89	0.62	0.57
Gorgonacea Alcyonacea	0.87	0.92	0.25	0.16
Hexactinellida	0.82	0.79	0.31	0.29
Hydrozoa	0.86	0.87	0.27	0.25
Madrepora oculata	-	-	-	-
Pennatulacea	0.88	0.90	0.39	0.32
Solenosmilia variabilis	0.73	0.32	0.21	0.23
Stylasteridae	0.88	0.94	0.54	0.57
Zoantharia	0.87	0.70	0.11	0.09

Model fits were calculated again, post-model fitting based on the final ensembled density model and using all training data available (832 records). When constrained to the boundaries of the SPRFMO Evaluated Area, correlation (Pearson's r) of density models and estimates of abundance for 15 VME indicator taxa ranged from 0.26 to 0.952, with values well above 0.4 (except Bryozoa with 0.26) and with no results for the stony coral *Goniocorella dumosa*, given no DTIS transect sites detected this particular taxon outside the boundaries of the EEZs. Correlation values with the modelled taxa constrained to the boundaries of the EEZs were consistently high (> 0.7) for all taxa, with values very similar to those obtained from evaluating the models at the full study area, except for the stony coral *Solenosmilia variabilis*, where Pearson's r decreased from 0.837 to 0.354 (Table 4).

Table 4 | Correlation (Pearson's r) for the density models of 15 VME indicator taxa and their estimates of abundance (observations using DTIS data) within the boundaries of the Exclusive Economic Zones (EEZs), the SPRFMO Evaluated Area and the entire study area (a combination of the previous two). Model fits based on the final ensembled density model (BRT and RF) and the full set of training data available.

	Correlation (Pearson's r)		
VME indicator taxon	**EEZs**	**Evaluated Area**	**Study area**
No. of DTIS data points	**692**	**138**	**832**
Actiniaria	0.809	0.810	0.812
Alcyonacea	0.910	0.909	0.910
Antipatharia	0.753	0.780	0.750
Brisingida	0.961	0.923	0.958
Bryozoa	0.991	0.264	0.991
Crinoidea	0.857	0.946	0.853
Demospongiae	0.918	0.952	0.918
Goniocorella dumosa	0.897		0.897
Gorgonacea Alcyonacea	0.936	0.942	0.935
Hexactinellida	0.734	0.760	0.736
Hydrozoa	0.867	0.661	0.867
Pennatulacea	0.959	0.789	0.959
Solenosmilia variabilis	0.837	0.602	0.354
Stylasteridae	0.972	0.710	0.972
Zoantharia	0.990	0.945	0.986

Model fits for the final ensembled density models calculated using the bioregions defined in Costello et al. (2017) (Figure A1-2) yielded Pearson's r values for the "Mid-South Tropical Pacific", "New Zealand" and "Southern Ocean" bioregions. It should be noted that in the Southern Ocean bioregion, there were only six DTIS observations available for model fit calculation. Values were well above the 0.4 threshold except for Crinoidea and *Solenosmilia variabilis* in the Southern Ocean bioregion (-0.542 and 0.216 respectively) and some combinations of taxa-region correlation values were not calculated (*Goniocorella dumosa* in the Mid-South Tropical and Southern Ocean, Zoantharia and Actiniaria in the Southern Ocean) (Table A2-1).

Model fits for the final ensemble density models calculated using the FMAs within the Evaluated Area (Figure 1) yielded results for three out of the 9 FMAs (North Louisville, Central Louisville, and Northwest Challenger). Values were well above the 0.4 threshold except for Bryozoa and Crinoidea in the Northwest Challenger FMA (0.036 and -0.153 respectively). The stony coral *Goniocorella dumosa* could not be evaluated in any of the FMAs due to the lack of observational data within those areas (Table A2-2).

Spatial patterns of predicted density

Predicted density of modelled taxa represented as number of individuals per km^2 were generally concentrated in areas with lower uncertainty (where the coefficient of variation, using the same unit as modelled density, had relatively low values). For example, estimated densities of Antipatharia in some parts of the Challenger Plateau, where Pearson's correlation r value for the final ensembled model (BRT and RF) and the DTIS data in the Northwest Challenger FMA was 0.525 (Table A2-2), reached ~20,000 individuals/km^2, while modelled uncertainty levels remain relatively low (estimated to range from 0 to 400 individuals/km^2) for that particular area (Figure 3, Figure 4). Despite the relatively high correlation between the final hurdled model (0.750, Table 4) it is important to note that predicted densities were significantly lower than observed densities (Figure 5). This finding is likely attributed to the relatively few observed densities with extremely high numbers of individuals (<7 DTIS points with observations of >50,000 Antipatharia per km^2). During the bootstrapping procedure used to create the data-driven models, comparatively high-density observations would have been intermittently randomly selected for model training. Thus, the predicted densities are generally lower than the observed densities, despite relatively high correlations between predicted and observed densities for most modelled taxa.

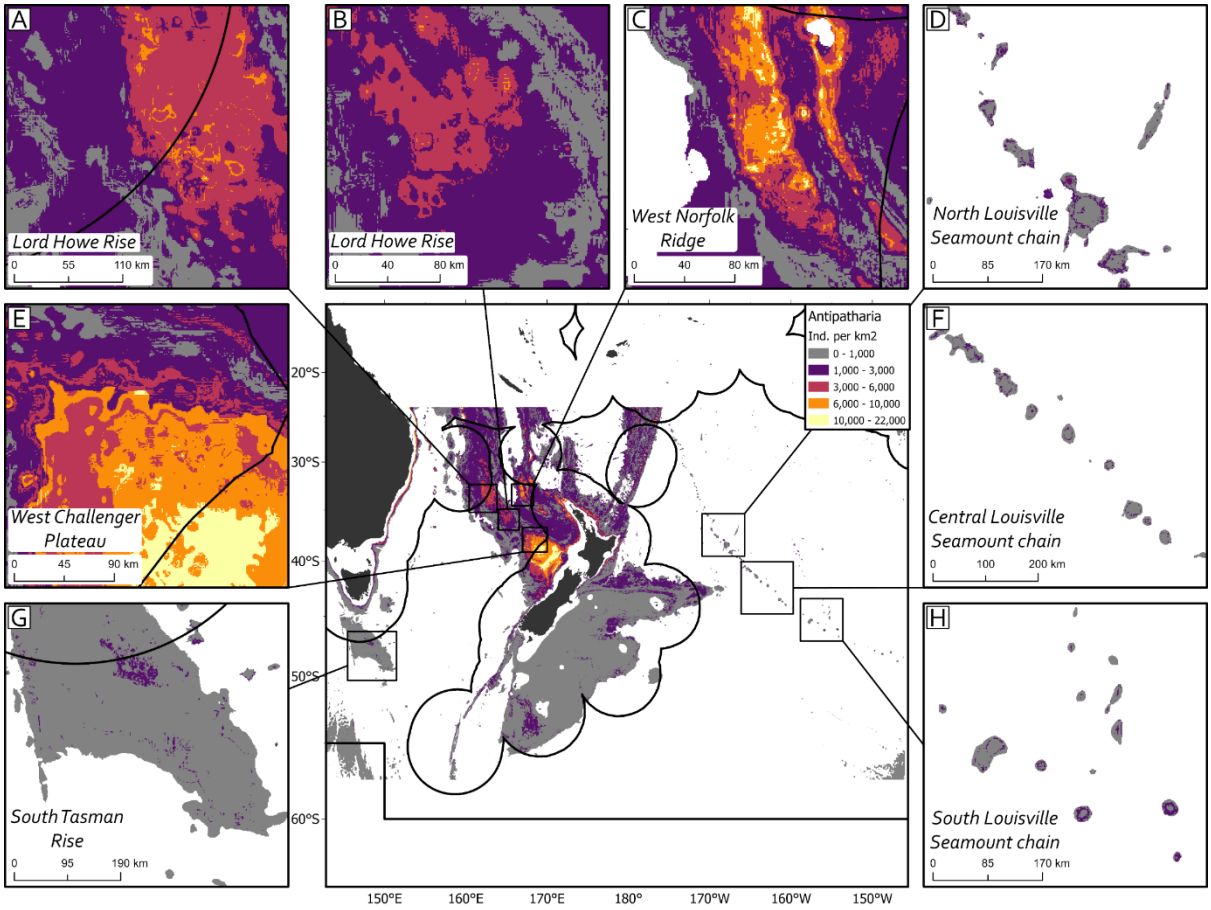

Figure 3 | Predicted density (individuals per km^2) of Antipatharia in the study area from the hurdle model approach (DTIS *data-driven* approach). Inset maps of the high seas in the study area: (a) West Lord Howe Rise; (b) East Lord Howe Rise; (c) West Norfolk Ridge; (d) North Louisville Seamount Chain; (e) West Challenger Plateau; (f) Central Louisville Seamount Chain; (g) South Tasman Rise; and (h) South Louisville Seamount Chain

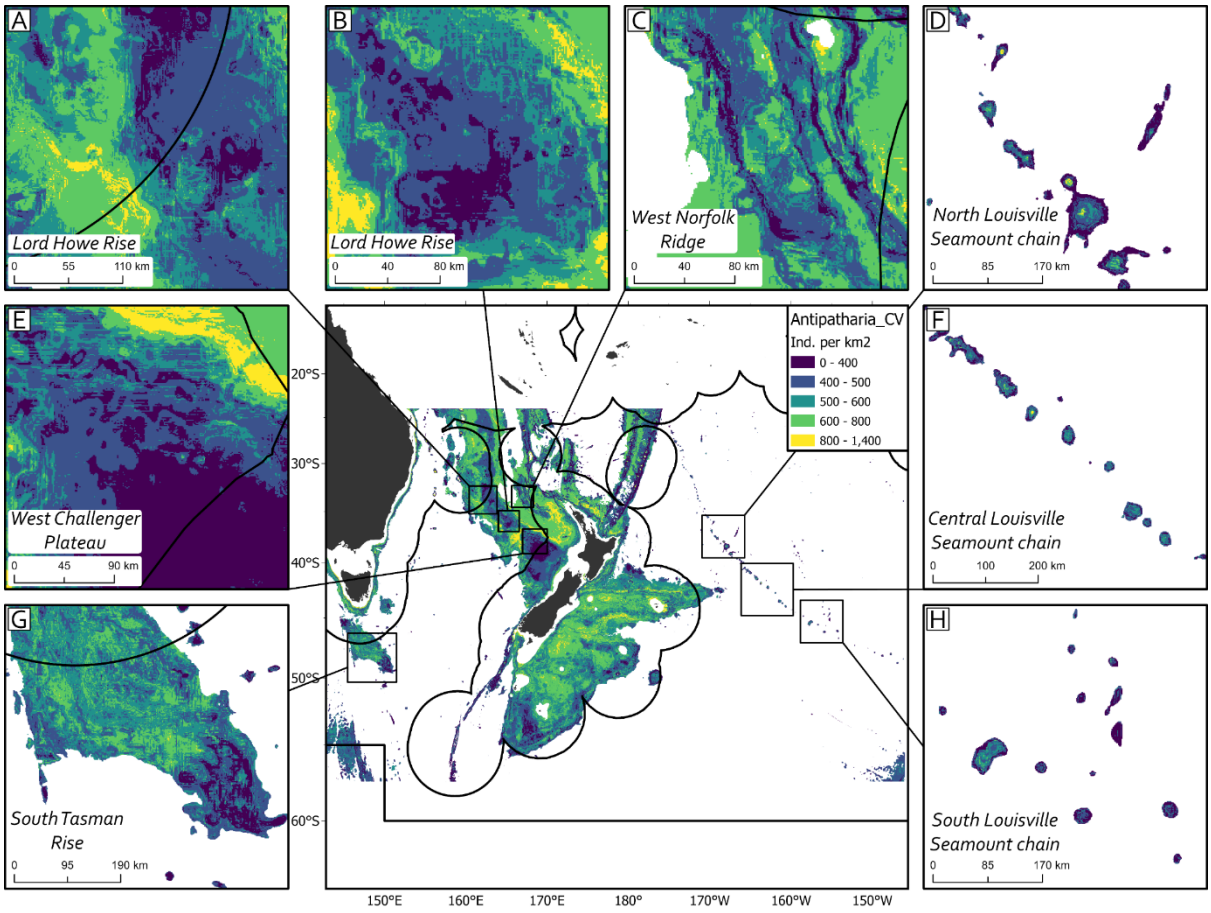

Figure 4 | Coefficient of variation (CV) (individuals per km^2) of Antipatharia in the study area from the hurdle model approach (DTIS *data-driven* approach). Inset maps of the high seas in the study area: (a) West Lord Howe Rise; (b) East Lord Howe Rise; (c) West Norfolk Ridge; (d) North Louisville Seamount Chain; (e) West Challenger Plateau; (f) Central Louisville Seamount Chain; (g) South Tasman Rise; and (h) South Louisville Seamount Chain**.**

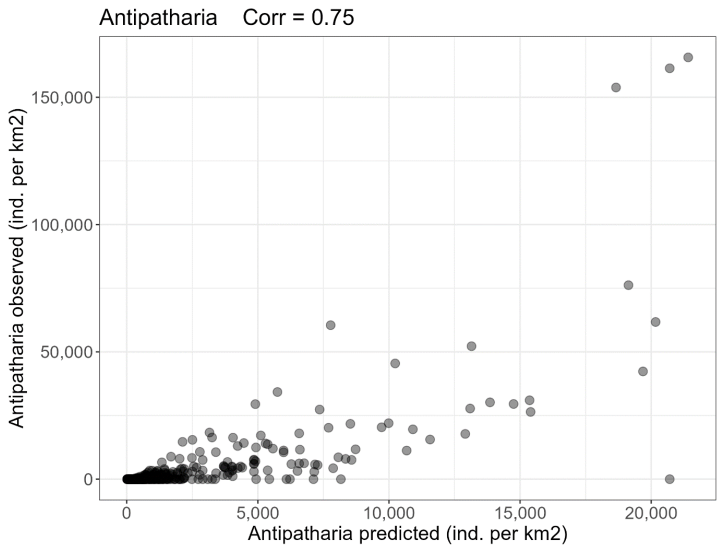

Figure 5 | Predicted estimates of density (*data-driven* approach) compared to observed estimates of density (DTIS data) for Antipatharia.

Figures for the rest of modelled VME indicator taxa can be found in Annex 3 .

Comparing density predictions

Existing habitat suitability models (Stephenson et al., 2021) for VME indicator taxa (Antipatharia, Desmospongiae, *Goniocorella dumosa*, Gorgonian Alcyonacea, Hexactinellida, Pennatulacea, Stylasteridae and *Solensomilia variabilis*) used to estimate (or proxy for) abundance using HSI-linear, ROC AUC thresholded and Power-mean versions of the model were compared to predicted estimates of density. No clear patterns were produced for Antipatharia (Figure 6), nor for other VME indicator taxa except for *Solenosmilia variabilis*, when using a randomly selected 10% of the total modelled area (Annex 2).

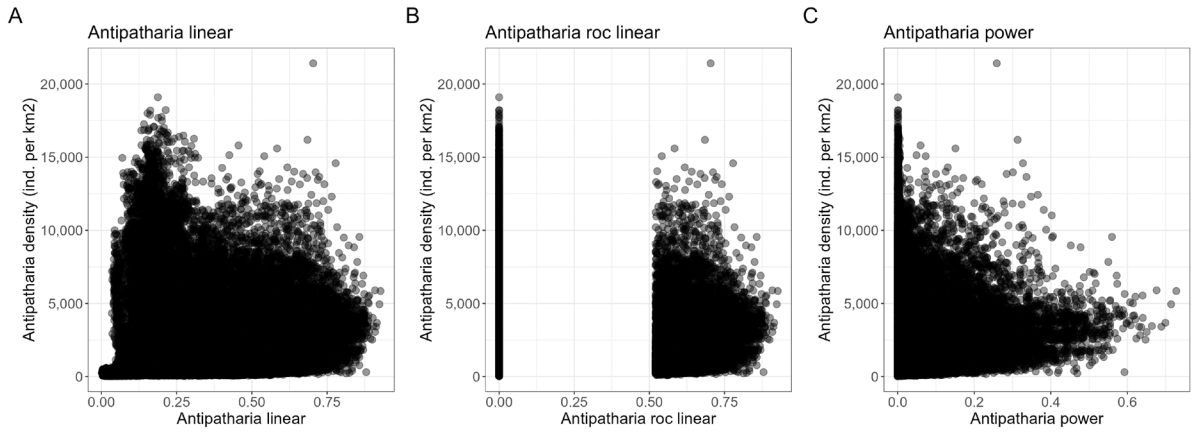

Figure 6 | Predicted estimates of density (*data-driven* approach) of Antipatharia compared to predictions from different methods previously used to estimate (or proxy for) abundance: (a) linear habitat suitability model; (b) thresholded habitat suitability model based on the ROC AUC; (c) power transformed habitat suitability model. Samples represent a randomly selected subset of 10% of the modelled area due to the high number of points.

Environmental coverage

Combined (i.e., for all modelled taxa) environmental coverage values generated were highest in the shallow to moderate depths of the study area (300–1200 m depth), both inside (e.g., on the Chatham Rise, the Kermadec Ridge, edges of the Campbell Plateau) and outside (e.g., on the South Tasman Rise, the Lord Howe Rise, the features of the Louisville Seamount Chain) New Zealand's EEZ (Figure 7).

Individual environmental coverage values were also separately generated for each modelled VME indicator taxa (Annex 4), which resulted in dissimilarities across a range of areas. Particularly for *Solenosmilia variabilis*, for which the highest environmental coverage values (~0.9 - ~1) appeared to be restricted to relatively small well-defined topographic features (e.g., on features from the Louisville Seamount Chain, the Macquarie Ridge and the Hjort Trench) (Figure A4-13). This prediction reflects the seafloor topography-related environmental variables used in the *Solenosmilia variabilis* density model (BPI-broad, seamounts and standard deviation of slope).

The proportion of combined environmental coverage values distributed within FMAs was assessed using breaks of 0.1. Low to medium environmental coverage values (from ~0 to ~0.5) generally accounted for most of the environmental coverage estimates within each FMA, with the Louisville Seamount Chain FMAs (North, Central and South) yielding the largest proportions within areas of high environmental coverage (~1) (Table 6).

Table 5 | Proportion of combined environmental coverage for all modelled VME indicator taxa within Fisheries Management Areas (FMAs)

Env. coverage interval	S. Lord Howe Rise	N. Lord Howe Rise	NW. Challenger	Westpac	West Norfolk	North Louisville	Central Louisville	South Louisville	South Tasman Rise
0 – 0.1	0.29	0.33	0.20	0.39	0.43	0.34	0.40	0.52	0.59
0.1 – 0.2	0.30	0.46	0.14	0.14	0.21	0.12	0.08	0.07	0.11
0.2 – 0.3	0.23	0.13	0.28	0.17	0.11	0.06	0.06	0.04	0.07
0.3 – 0.4	0.12	0.05	0.22	0.12	0.09	0.04	0.04	0.03	0.08
0.4 – 0.5	0.05	0.02	0.10	0.08	0.06	0.03	0.04	0.03	0.07
0.5 – 0.6	0.01	0.01	0.04	0.05	0.04	0.02	0.03	0.03	0.04
0.6 – 0.7	0.00	0.00	0.02	0.04	0.03	0.03	0.05	0.06	0.03
0.7 – 0.8	0.00	0.00	0.01	0.01	0.02	0.03	0.06	0.06	0.01
0.8 – 0.9	0.00	0.00	0.01	0.00	0.01	0.07	0.08	0.09	0.00
0.9 – 1.0	0.00	0.00	0.00	0.00	0.00	0.27	0.16	0.06	0.00

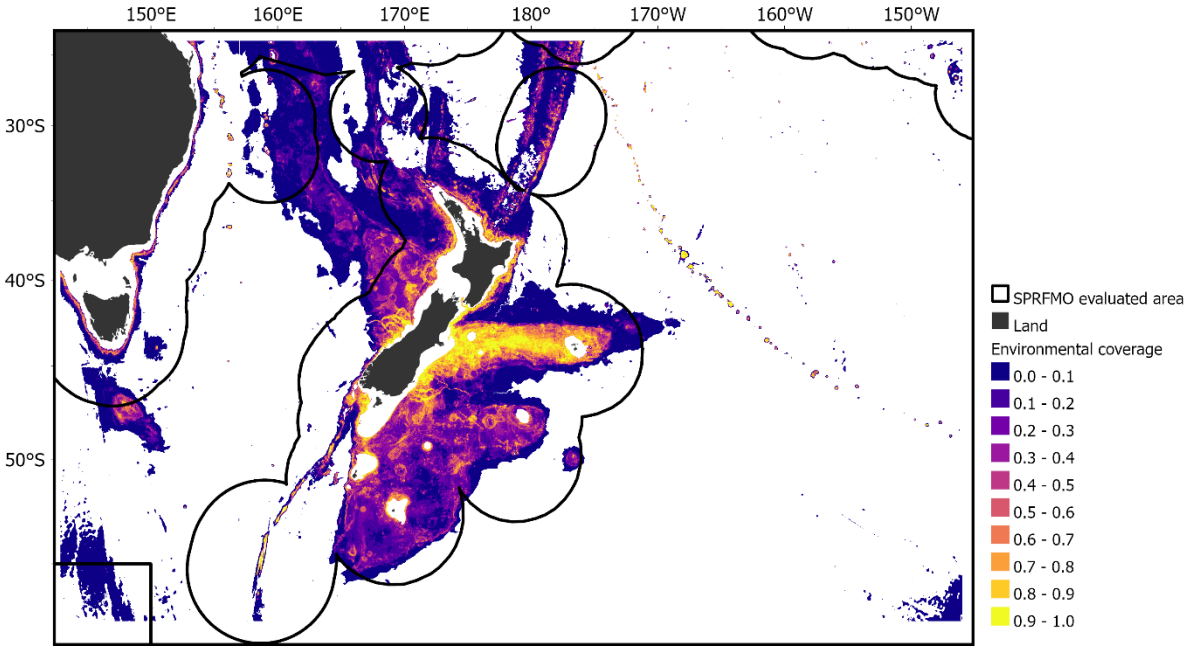

Figure 7 | Combined environmental coverage (0–1) between 200 and 3000 m depth within the study area. Low values of environmental coverage (dark blue) indicate parts of the environmental space that contained few, or no training data - meaning greater caution should be placed in the predictions of VME indicator taxa density estimates.

4.2 Relative environmental suitability (RES) models

For all four stony coral taxa (*Goniocorella dumosa, Enallopsammia rostrata, Madrepora oculata, Solenosmilia variabilis*), the environmental variables used in the *principles-based* modelling approach were similar, with aragonite saturation at depth, bathymetric position index, particulate organic carbon export and temperature being selected more than 15 times across the different VME indicator taxa, which led to the selection of these variables to inform the RES methodology, with agreement from all experts (Figure 8, Table A5-1).

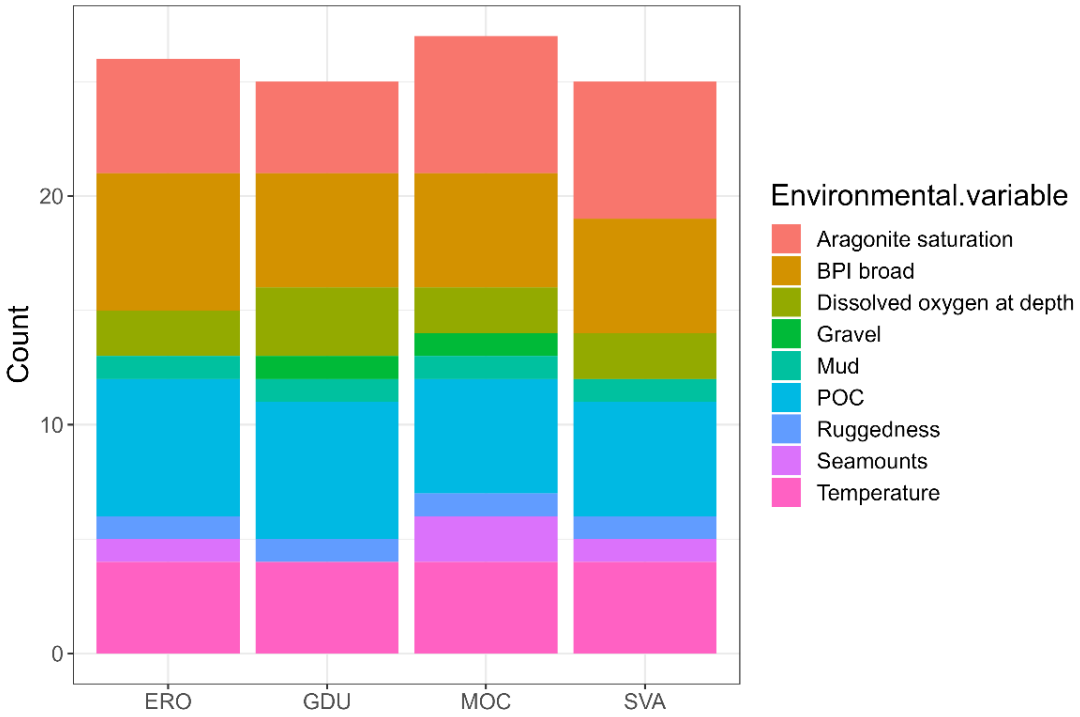

Figure 8 | Environmental variables chosen by experts following the approach originally described in SC10-DW05 for four stony coral taxa: *Goniocorella dumosa* (GDU), *Enallopsammia rostrata* (ERO), *Madrepora oculata* (MOC) and *Solenosmilia variabilis* (SVA).

Following discussion with the panel of 8 experts that provided feedback (out of the 22 initially contacted), most experts agreed on the use of the plateau shape for aragonite saturation at depth, bathymetric position index and particulate organic carbon export, while trapezoid shape was chosen by all experts for temperature. Detailed results are provided in Annex 5.

The performance of the models was assessed using DTIS imagery data (used for the *data-driven* approach). Model performance, as assessed with this completely independent evaluation data, ranged from a Pearson's correlation 0.06 to 0.35 (Table 7, Annex 6). The *principles-based* approach density models under-performed compared to the habitat suitability index models produced by Stephenson et al. (2021). For example, for *Goniocorella dumosa*, Pearson's correlation for the *principles-based* approach density model was 0.30, whereas evaluation of the habitat suitability model (HSI-linear and ROC AUC thresholded) compared to the abundance data was 0.34-0.35 respectively (Table 7). Relationships between observed *Goniocorella dumosa* density (DTIS data) compared to predictions from the *principles-based* approach density model and the habitat suitability models used to estimate (or proxy) for density (HIS-linear and ROC AUC thresholded) were similar, with the highest observed density values (from the DTIS data) being predicted as lower densities by the *principles-based* approach density model (Figure 10).

Despite showing low correlation values, the broad spatial predictions of *Goniocorella dumosa* density partly matched spatial patterns of density determined using the *data-driven* approach (Figure 9 compared with Figure A2-16) with higher relative density predicted on the Challenger Plateau and the

Chatham Rise (this species being found predominantly inside New Zealand's EEZ). Results from the rest of modelled stony coral taxa can be found in Annex 6.

Table 6 | Correlation (Pearson's r) between model predictions (RES, Habitat suitability models; Stephenson et al., 2021 [linear and ROC-linear]) for four stony coral taxa (*Goniocorella dumosa, Enallopsammia rostrata, Madrepora oculata, Solenosmilia variabilis*), and DTIS observations.

	Correlation (Pearson's r)		
Taxa	**RES**	**HSI-linear**	**HSI ROC-linear**
Enallopsammia rostrata	0.20	0.29	0.35
Goniocorella dumosa	0.30	0.35	0.34
Madrepora oculata	0.10	0.30	0.31
Solenosmilia variabilis	0.06	0.22	0.23

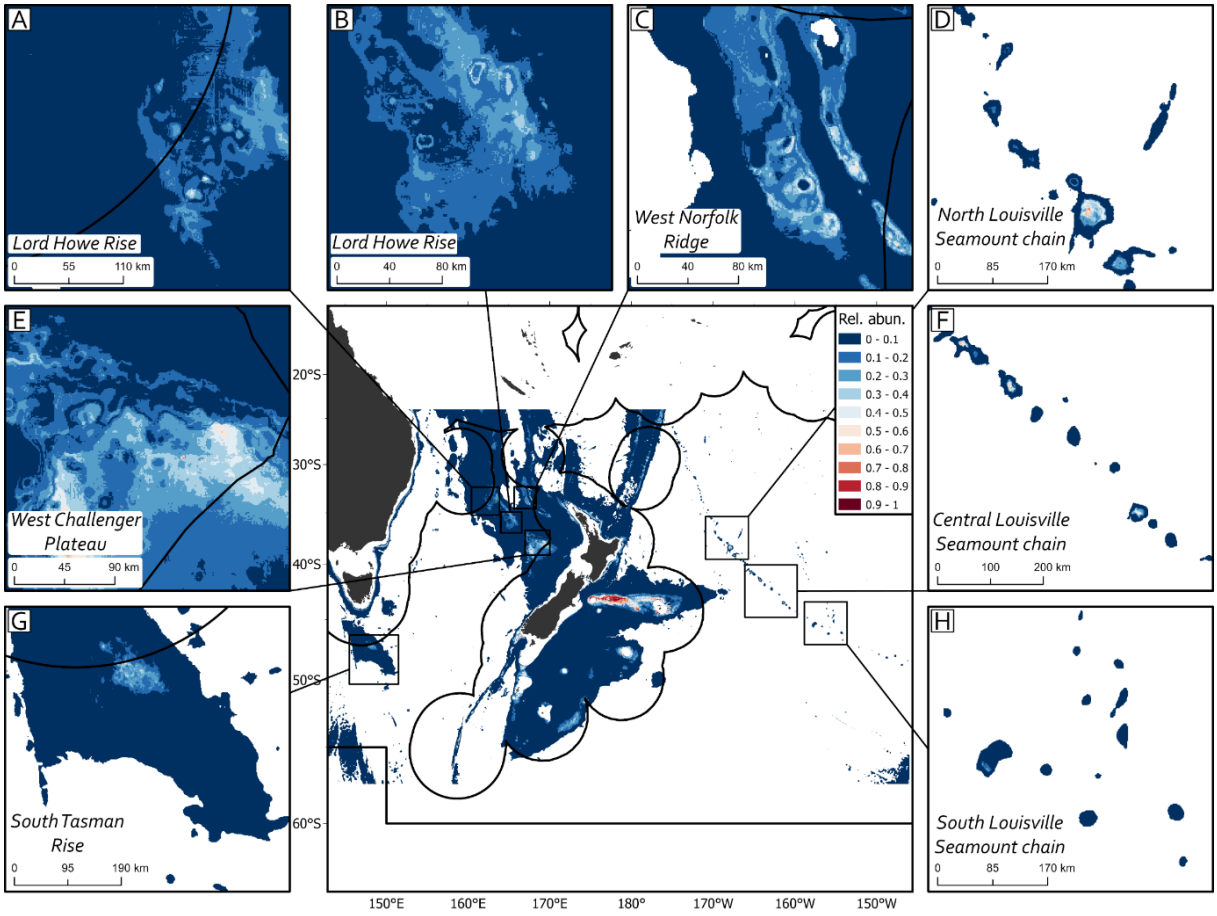

Figure 9 | Predicted relative density (0-1) in the study area from the hurdled *principles-based* approach (expert informed) for *Goniocorella dumosa*. Inset maps of the high seas in the study area: (a) West Lord Howe Rise; (b) East Lord Howe Rise; (c) West Norfolk Ridge; (d) North Louisville Seamount Chain; (e) West Challenger Plateau; (f) Central Louisville Seamount Chain; (g) South Tasman Rise; and (h) South Louisville Seamount Chain.

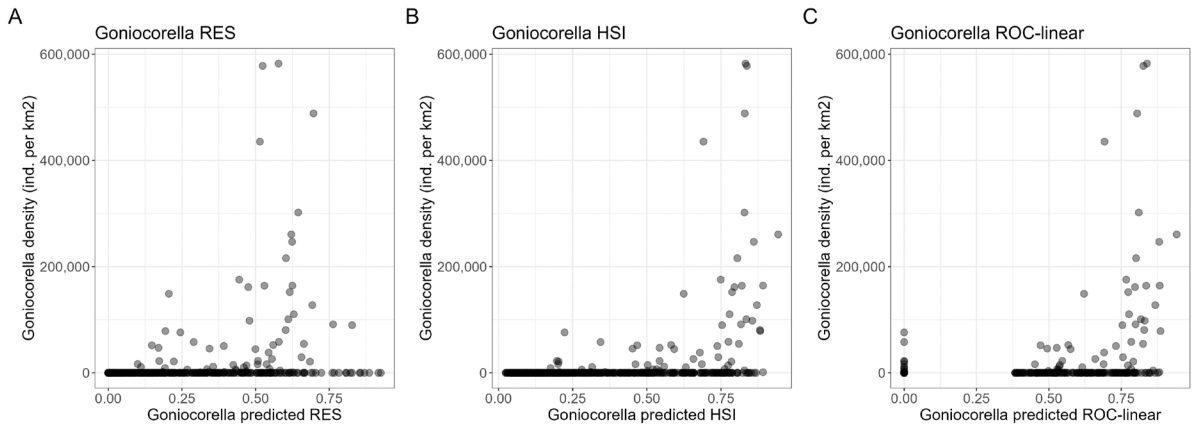

Figure 10 | Relationships between *Goniocorella dumosa* abundance (DTIS data) compared to predictions from different methods used to estimate (or proxy for) density (a) *principles-based* approach (RES); (b) habitat suitability model (HSI-linear); (c) ROC AUC thresholded habitat suitability model (ROC-linear).

4.3 VAST models

Analysis of models

Used as a measure of each model's parsimony, Aikake information criterion (AIC) was lowest for the models using spatial and environmental effects (Table 8). Models generating pseudo-absences with target-group background yielded similar AIC values when using spatial effects and either PCA or standard (untransformed) environmental covariates.

Table 7 | Aikake information criterion (AIC) and percent deviance explained for all VAST models predicting relative density of Demospongiae in the study area.

Aikake information criterion (AIC)			**Percent deviance explained**	
VAST model	**Target-group background**	**Random (10x)**	**Target-group background**	**Random (10x)**
Environmental (PCA)	14645.48	13978.01	89.0	88.8
Environmental (standard)	14624.55	13833.43	89.4	88.7
Spatial	14390.00	13911.86	94.7	95.0
Spatial and environmental (PCA)	14293.02	13463.97	94.7	95.2
Spatial and environmental (standard)	14295.65	13259.85	94.8	95.2

Percent deviance explained values were higher for models using spatial and environmental effects (Table 8). Spatial effects alone explain a greater proportion of the models' deviance then the environmental covariates, but when combined, explain the greatest amount of deviance (Table 8). Considering the AIC and deviance values and the larger uncertainty for models using PCA environmental covariates, the two models (with pseudo-absences being randomly generated and

TGB-generated) using spatial and environmental effects (standard) were used for the ensemble model mapping. Where, the ensemble predictions were made using the same approach as Stephenson et al. (2021). However, weights for the ensemble model were constructed using median Pearson's correlations (Table 9) rather than AUC.

Performance of models

Correlations of the predicted density of Demospongiae and the observed abundance (DTIS data) for both models were found to be moderate. Model bias varied significantly across cross-validation folds, suggesting a slight over-prediction for both models (Table 9). Model spread was centred around 1, indicating a positive one-to-one trend between the observed and the predicted data. Root-mean-square error (RSME) and average error (AVE) metrics (Potts and Elith, 2006) were also alike (Table 9), leading to the overall conclusion that both models performed similarly and that target-group background generation of pseudo-absences (instead of random generation) does not improve performance.

Table 8 | K-fold cross-validation results of spatial and environmental models (lowest equal AIC and highest percent deviance explained). Mean, median and range given for Pearson's correlation coefficient, Spearman's rank correlation, model bias (closer to 0, the better), model spread (closer to 1, the better), root-mean-square error (RMSE) and average error (AVE) metrics.

Model	Pearson's		Spearman's		Model bias		Model spread		RMSE		AVE	
	Mean	Median	Mean	Median	Mean	Median	Mean	Median	Mean	Median	Mean	Median
TGB	0.60	0.60 (0.20-0.93)	0.52	0.55 (0.31-0.62)	3.10	1.84 (-4.28-10.05)	1.45	1.42 (0.26-3.15)	71.17	63.14 (46.67-119.16)	-9.00	-8.98 (-17.05-1.98)
Random (10x)	0.61	0.66 (0.23-0.93)	0.54	0.56 (0.35-0.61)	4.41	3.50 (-1.78-10.76)	1.27	1.28 (0.3-2.65)	70.30	63.09 (49.76-118.27)	-7.39	-7.45 (-16.83-1.48)

Spatial patterns of predicted density

VAST ensemble predictions of relative density of Demospongiae in the study area showed 'hotspots' on the Chatham Rise, the Campbell Plateau, the Challenger Plateau and the Kermadec Ridge (Figure 11). The VAST ensemble coefficient of variation showed low uncertainty in areas overlapping or near the location of the DTIS sites, increasing as the distance to these sites also increases (Figure 12). Spatial patterns of relative density appeared to be similar to those showed by the hurdle model predicting density of Demospongiae using the *data-driven* approach (Figure A3-11) although more 'hotspots' were present in the latter.

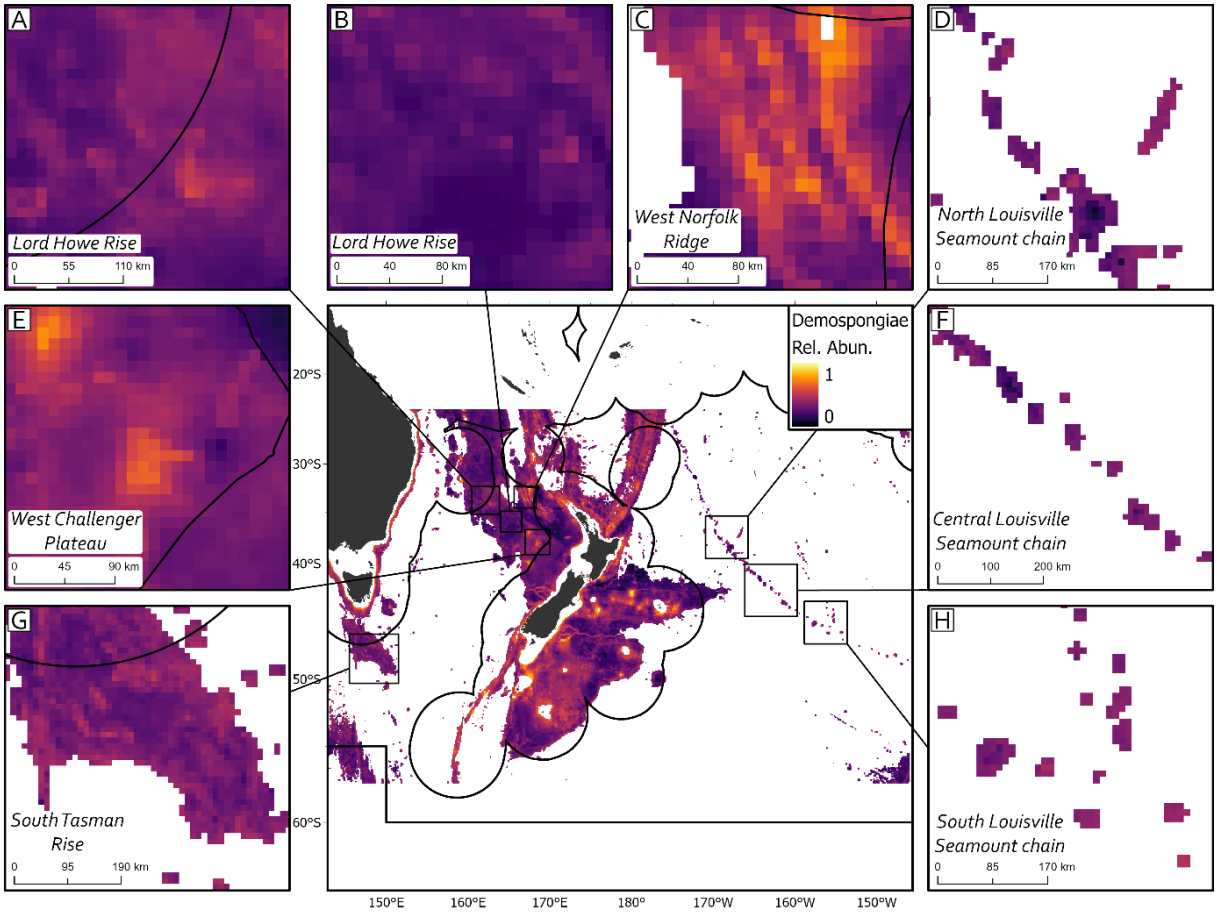

Figure 11 | VAST ensemble predicting relative density of Demospongiae. Inset maps of the high seas in the study area: (a) West Lord Howe Rise; (b) East Lord Howe Rise; (c) West Norfolk Ridge; (d) North Louisville Seamount Chain; (e) West Challenger Plateau; (f) Central Louisville Seamount Chain; (g) South Tasman Rise; and (h) South Louisville Seamount Chain.

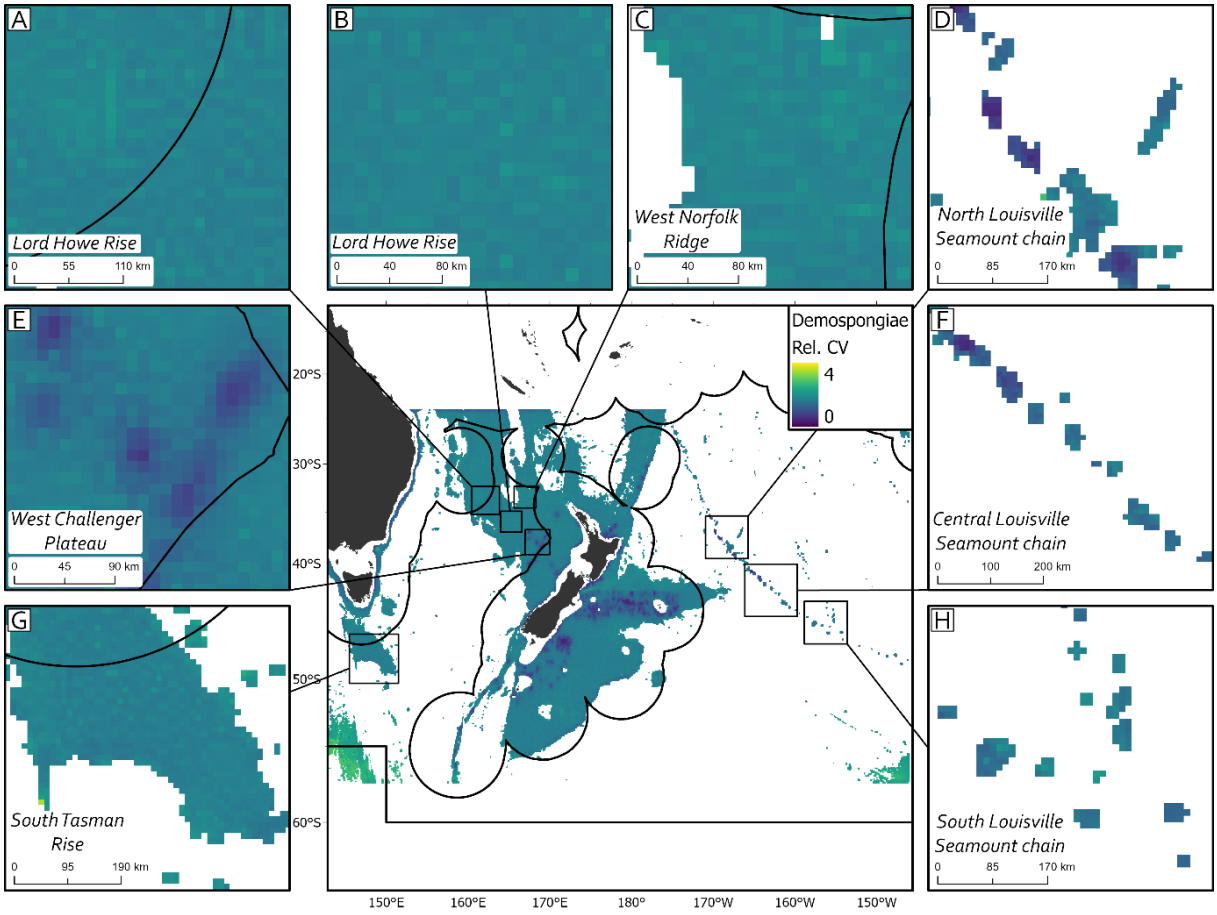

Figure 12| Coefficient of variation (CV) from the VAST ensemble predicting relative density of Demospongiae. Inset maps of the high seas in the study area: (a) West Lord Howe Rise; (b) East Lord Howe Rise; (c) West Norfolk Ridge; (d) North Louisville Seamount Chain; (e) West Challenger Plateau; (f) Central Louisville Seamount Chain; (g) South Tasman Rise; and (h) South Louisville Seamount Chain.

4.4 Investigating the relationships between benthic bycatch biomass and predicted density of VME indicator taxa

Correlations (Pearson's) between benthic bycatch biomass data from the SPRFMO Evaluated Area (data compiled for SC8-DW11) were calculated for 15 VME indicator taxa using density (hurdle) models (presented in this paper) and, estimates (or proxies for) abundance based on habitat suitability models (HSI-linear and HSI ROC-linear) from Stephenson et al (2021) and SC10-DW05 (Table 10).

Table 9 | Pearson's correlation measuring the linear relationship between benthic bycatch biomass of VME indicator taxon (using data compiled for SC8-DW11) and spatial predictions, using density models, HSI-linear and HSI ROC-linear habitat suitability models from Stephenson et al (2021) and SC10-DW05.

VME indicator taxon	Density models	HSI-linear	HSI ROC-linear
Actiniaria	0.01	0.29	0.289
Alcyonacea	0.023	0.058	0.063
Antipatharia	0.079	0.262	0.286
Brisingida	0.028	0.099	0.111
Bryozoa	-0.004	0.066	0.066
Crinoidea	0.002	0.026	0.029
Demospongiae	0.003	0.022	0.021
Goniocorella dumosa	0.03	0.034	0.035
Gorgonacea Alcyonacea	0.014	0.046	0.047
Hexactinellida	0.234	0.159	0.165
Hydrozoa	-0.014	0.047	0.041
Pennatulacea	0.17	0.087	0.086
Solenosmilia variabilis	0.178	0.165	0.185
Stylasteridae	0.386	0.134	0.141
Zoantharia	0.012	0.082	0.091

Pearson's correlation was consistently non-existent (near 0) across all VME indicator taxa density models except for Hexactinellida, Stylasteridae and *Solenosmilia variabilis*, which were marginally higher, ranging from 0.178 to 0.386 (Table 10). Correlation was also consistently low (< ~0.29) across all VME indicator taxa when calculated against the HSI-linear and HSI ROC-linear models.

4.5 VME indices

Vulnerability scores for modelled VME indicator taxa were extracted and adapted from Gros et al., 2023 and Stephenson et al., in prep. (Table 11).

Table 10 | Vulnerability scores for all modelled VME indicator taxa (either using the *data-driven* or the *principles-based* approach) were extracted and adapted from Gros et al., 2023 and Stephenson et al., in prep.

VME indicator taxon	Vulnerability score
Actiniaria	1.958
Alcyonacea	2.160
Antipatharia	2.273
Brisingida	2.098
Bryozoa	2.177
Crinoidea	2.405
Demospongiae	2.704
Goniocorella dumosa	2.776
Gorgonacea	2.624
Hexactinallida	2.776
Hydrozoa	2.550
Pennatulacea	2.389
Solenosmilia variabilis	2.776
Stylasteridae	2.614
Zoantharia	2.550

For all VME indicator taxa modelled using the *data-driven* approach, taxon-specific vulnerability scores, multiplied by both the taxon-specific estimated density and presence-only (Stephenson et al., 2021a) models were summed to create estimates of combined richness- and abundance-VME indices. The output was then mapped with the respective uncertainty layers. For exploratory purposes, a combined visualisation was produced for the top 5% of richness- and abundance-based VME indices and classified according to the four categories proposed in Gros et al., 2023 (defined as “Low abundance-high Richness”, “High Abundance-High richness”, “Low abundance-Low richness”, “High abundance-Low richness”) with two extra categories to highlight areas of low confidence (one for abundance, one for richness) (Figure 13).

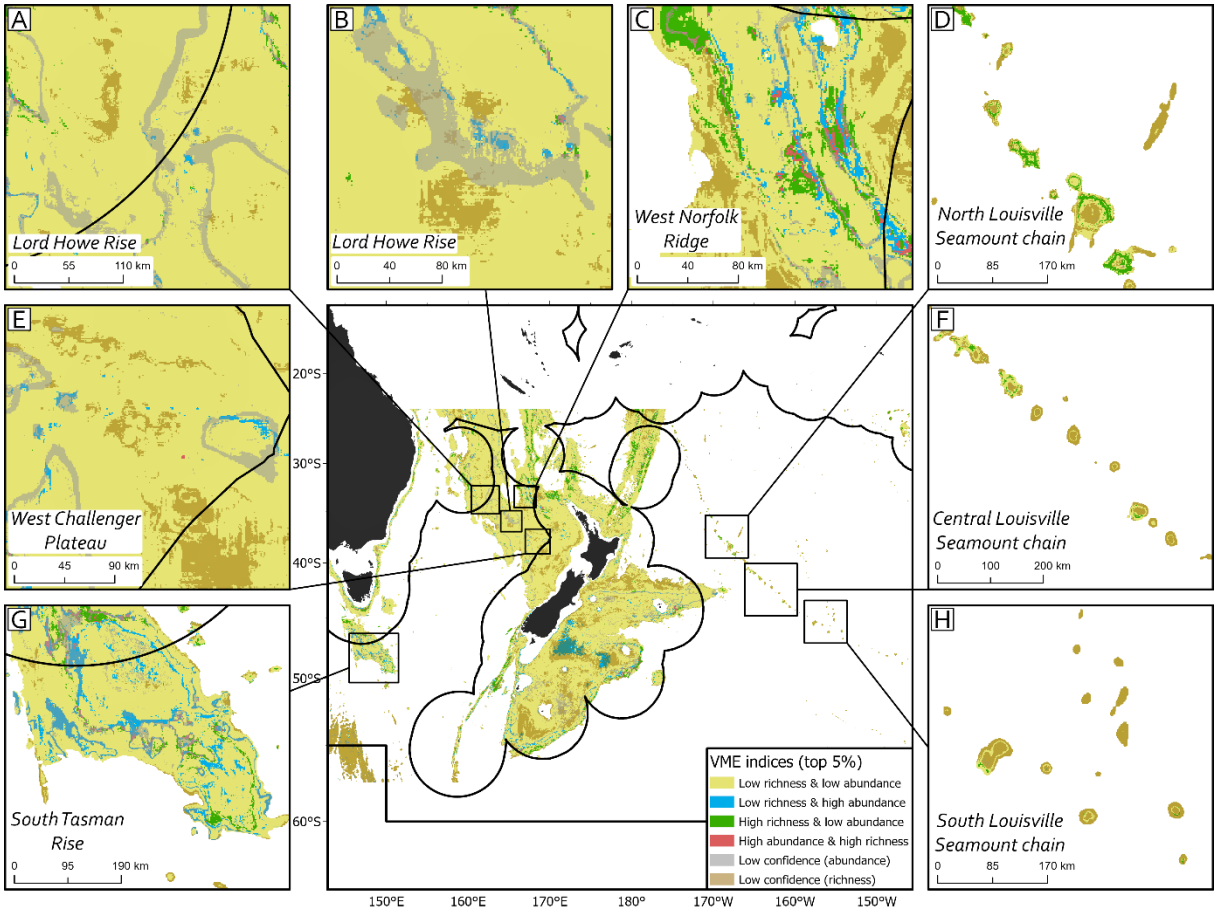

Figure 13 | Exploratory visualisation of a vulnerability weighted VME indices. The top 5% of areas for modelled VME indicator taxa richness and abundance in the study area categorised by: Low abundance-High Richness (green), High abundance-High richness (salmon), Low abundance-Low richness (beige), High abundance-Low richness (blue), Abundance Low confidence (grey) and Richness Low confidence (light brown). Inset maps of the high seas in the study area: (a) West Lord Howe Rise; (b) East Lord Howe Rise; (c) West Norfolk Ridge; (d) North Louisville Seamount Chain; (e) West Challenger Plateau; (f) Central Louisville Seamount Chain; (g) South Tasman Rise; and (h) South Louisville Seamount Chain.

5. Discussion

5.1 *Data-driven* density models

Predicted density models and their associated uncertainty estimates (coefficient of variation) were developed for 15 VME indicator taxa (Table 1). The models were developed using a *data-driven* approach previously described and trialled in SC10-DW05 and accepted by the SC.

We found that the ensemble density models performed well (Pearson's r > 0.75) at the spatial scale of the study area (the SPRFMO evaluated area and EEZ's within its boundaries) when using training data for the evaluation (which may lead to over-inflation of the performance metric), except for the stony coral *Solenosmilia variabilis* (Pearson's r = 0.35). We also found that the models generally performed well when constrained to the SPRFMO Evaluated Area (excluding the EEZ's) using training data (Peason's r > 0.65), except for Bryozoa (Pearson's r = 0.29) and *Gioniocorella dumosa* (the latter couldn't be evaluated due to the lack of training data within the Evaluated Area). Investigation of the

models at the scale of each Fishery Management Area (FMA) was only partially possible for three out of the eight FMAs, highlighting the need to acquire abundance data from these areas (and the wider Evaluated Area) for model building, training, and validation. The need for location-specific data was reinforced by the results from the investigation of the environmental coverage within FMAs, which showed little overlap of the FMAs with regions of high environmental coverage.

The final ensembled density models were evaluated using training data only, and that their predictive accuracy should be ideally assessed using completely independent data. There are other image data that may be available from other locations within the SPRFMO Evaluated Area and Australia's EEZ that could potentially allow for this independent validation test. However, these data were collected using different instruments than the DTIS imagery and a considerable amount of data grooming may be required to make them comparable to the DTIS abundance data. Existing image data collected within Australia's EEZ (Williams et al., 2020ab; Koslow et al., 2001; Althaus et al., 2009) has been recently provided to NIWA, who are currently assessing if these data are suitable and of sufficient quantity to independently evaluate the density models presented here.

As more abundance data suitable for model development and validation becomes available (from either past or future surveys), the density models that currently represent coarse taxonomic groups (e.g., Actiniaria, Demospongiae, Zoantharia) may be able to be broken down into finer taxonomic groups (e.g., as has been done for the stony corals *Goniocorella dumosa* and *Solenosmilia variabilis* from the order Scleractinia). This taxonomic refinement of the models will potentially allow ecological patterns at the species level, which may be obscured at coarser taxonomic resolutions, to emerge.

5.2 *Principles-based* (RES) density models

Principles-based (RES) density models were developed for 4 VME indicator taxa (Table 1), using an approach previously described and trialled in SC10-DW05 and accepted by the SC.

We found that the RES density models performed poorly at the full scale of the study area when using DTIS abundance data for the investigation of their performance and that, statistically, existing habitat suitability models performed better at predicting abundance.

While the *data-driven* approach provides an objective methodology for estimating the spatial distribution of density (abundance) and should remain prioritised for the development of robust density models, the *principles-based* approach remains an alternative that may continue to be explored, particularly if:

- The number of responses from experts increase (8 of the approached 22 experts participated in our approach).
- Relevant, new and/or improved environmental data becomes available.
- The methods used to gather independent expert knowledge evolve (e.g., new shapes to describe relationships between taxa and environmental variables are used).

5.3 VAST density models

A single predicted density model, and its associated uncertainty estimate, was developed for the class Demospongiae using the VAST modelling framework. This is the first instance of this methodology being used to model predicted estimates of VME indicator taxa density in the SPRFMO Evaluated Area.

The model performed moderately well when cross-validated to the DTIS data and presented broadly similar predicted patterns of the spatial distribution of density to the final *data-driven* density models.

5.4 Investigating the relationship between benthic bycatch and predictions of density

Correlations between modelled distributions of VME indicator taxa (habitat suitability models and density models) and benthic bycatch biomass data (compiled as part of SC8-DW11) were explored. No significant correlation was identified for any of the modelled taxa, with correlation results marginally increasing when assessing the relationship with habitat suitability models. The latter likely relates to the habitat suitability models being partly built using benthic bycatch presence-absence data. Before further investigations of density models and bycatch biomass data are undertaken (if any), a better understanding of the data limitations and how they affect inference from correlations between benthic bycatch and predictions of density is required. Ideally, to make valid comparisons between benthic bycatch biomass data and predictive models, it would be necessary to first build biomass models (not abundance models) and to be able to adjust the raw biomass data using robust trawl catchability estimates for VME indicator taxa.

5.5 VME indices

We used the development of the density models for the study area, and the recent adaptation of a VME-index method (Stephenson et al. In prep.), to also trial a method to quantify the vulnerability of VME indicator taxa to physical disturbance. The results characterise different levels of vulnerability to bottom trawl fishing, reflecting different levels of abundance and richness of VME indicator taxa. The resulting indices appear to be a promising approach to describing spatial vulnerability across VME indicator taxa, with the method reproducible and easily applied to other datasets and use other vulnerability criteria.

Further improvements to the application of the method could include the normalisation of abundance across taxa, which was not done in our application of the method and may have resulted in locations containing VME indicator taxa that naturally occur in high abundances being prioritised over locations containing VME indicator taxa that naturally occur at relatively lower abundances.

The identification of vulnerability hotspots could represent focal areas for preventing significant adverse impacts on VMEs. However, in our application of the approach we have used an arbitrary threshold of the top 5% to characterise hotspots of vulnerability, and further work is required to identify meaningful or evidence-based thresholds before this approach is applied to inform management decisions. Once that has been done, potential applications of VME indices include their use for risk assessment in areas where image data are available. Previously developed VME indices have been used as part of a multi-criteria approach to help inform the design of protective measures for VMEs in the North-East Atlantic (Morato et al. 2018).

6. Recommendations

It is recommended that the Scientific Committee:

- **Notes**:

- Spatial predictions of density for 15 VME indicator taxa, based on a *data-driven* approach using observed abundance data (DTIS) that has previously been endorsed by the SC, have been completed, showing promising results.
- Spatial predictions of density for 4 VME indicator taxa, based on a *principles*-based approach using on expert knowledge (RES) that has previously been endorsed by the SC, have been completed, but further work is required to fully assess the appropriateness of this approach.
- Spatial prediction of relative density for 1 VME indicator taxon based on the VAST modelling framework has been completed, with promising results.
- A method to develop VME indices that quantify the vulnerability of VME indicator taxa to physical disturbance using taxon-specific abundance and presence data has been trialled, with promising results.
- The future availability of further imagery data would help facilitate spatial predictions of density for a greater number of VME indicator taxa with increased robustness.

- **Recommends**:
  - Where feasible, that additional data is collected from areas of interest to management (e.g., FMAs) to better inform model development and validation.
  - That additional independent data, ideally providing a better coverage of the Evaluated Area, is compiled to perform a full evaluation of the density models.
  - That once density models have been fully evaluated, and if considered to be adequate to inform management decisions, they are:
    - Incorporated into the ongoing review of the effectiveness of the spatial management arrangements.
    - Fed into the VME index to quantify the vulnerability of VME indicator taxa to physical disturbance.

7. Acknowledgements

Funding for this study was provided by Fisheries New Zealand, Ministry for Primary Industries. The authors acknowledge the useful input received from members of the South Pacific Working Group. We thank all experts who provided input for the principles-based approach modelling including Chris Rooper (DFO), Chris Yesson (ZSL), Di Tracey, Malcolm Clark, and Jennifer Beaumont (all NIWA). We thank Fabrice Stephenson for advice and support that contributed to the modelling and VME indices analyses presented in this study. We thank the New Zealand Department of Conservation (DOC), Fisheries New Zealand (FNZ) and the National Institute of Water and Atmospheric Research (NIWA) for providing the DTIS imagery data. Specifically, we thank Owen Anderson, Lyndsey Holland for input and advice on the data used in the analyses.

8. References

Althaus, F., A. Williams, T. A. Schlacher, R. J. Kloser, M. A. Green, B. A. Barker, N. J. Bax, P. Brodie, and Monica A. Schlacher-Hoenlinger. 2009. Impacts of bottom trawling on deep-coral ecosystems of seamounts are long-lasting. *Marine Ecology Progress Series* 397 (2009): 279-294.

Anderson, O.F., Guinotte, J., Rowden, A.A., Clark, M.R., Mormede, S., Davies, A.J. (2016). Field validation of habitat suitability models for Vulnerable Marine Ecosystems in the South Pacific Ocean:

implications for the use of broad-scale models in fisheries management. *Ocean and Coastal Management* 120: 110-126.

Anderson, O.F., Guinotte, J.M., Rowden, A.A., Tracey, D.M., Mackay, K.A., Clark, M.R. (2016). Habitat suitability models for predicting the occurrence of vulnerable marine ecosystems in seas around New Zealand. *Deep-Sea Research I*, 115: 265-292.

Anderson, O.; Schnabel, K.; Bowden, D.; Davey, N.; Hart, A. (in press). Identification of protected coral hotspots using species distribution modelling. DRAFT Report Prepared for Project POP2021-02, Conservation Services Programme, Department of Conservation

Barbet-Massin, M., Jiguet, F., Albert, C. H., & Thuiller, W. (2012). Selecting pseudo-absences for species distribution models: How, where and how many? Methods in Ecology and Evolution, 3(2), 327-338.

Burgos, J. M., Buhl-Mortensen, L., Buhl-Mortensen, P., Ólafsdóttir, S. H., Steingrund, P., Ragnarsson, S. Á., & Skagseth, Ø. (2020). Predicting the distribution of indicator taxa of vulnerable marine ecosystems in the Arctic and sub-arctic waters of the Nordic Seas. Frontiers in Marine Science, 7, 131.

Cerasoli, F., Iannella, M., D'Alessandro, P., & Biondi, M. (2017). Comparing pseudo-absences generation techniques in Boosted Regression Trees models for conservation purposes: A case study on amphibians in a protected area. PLoS One, 12(11), e0187589.

Chefaoui, R. M., & Lobo, J. M. (2008). Assessing the effects of pseudo-absences on predictive distribution model performance. Ecological Modelling, 210(4), 478-486.

Clark, M. R., Wood, B., Mackay, K., Anderson, O. F., Hart, A., Rickard, G., Rowden, A. A. (2022). Underwater Topographic Features in the New Zealand region: development of an updated 'SEAMOUNT' database and information on the extent and intensity of deep-sea trawl fisheries on them. New Zealand Aquatic Environment and Biodiversity Report No. 291. 28 p.

Elith, J. and Leathwick, J.R., 2009. Species distribution models: ecological explanation and prediction across space and time. *Annual review of ecology, evolution, and systematics*, 40, pp.677-697.

Ellis, N., Smith, S. J., & Pitcher, C. R. (2012). Gradient forests: calculating importance gradients on physical predictors. Ecology, 93(1), 156-168.

Georgian, S. E., O. F. Anderson, and A. A. Rowden. 2019. Ensemble habitat suitability modeling of vulnerable marine ecosystem indicator taxa to inform deep-sea fisheries management in the South Pacific Ocean. *Fisheries Research* 211:256-274.

Goode, S.L., Rowden, A.A., Bowden, D.A., Clark, M.R., Stephenson, F. (2021). Fine-scale mapping of mega-epibenthic communities and their patch characteristics on two New Zealand seamounts. Frontiers in Marine Science, 8:765407.

Gros, C., Jansen, J., Untiedt, C., Pearman, T. R., Downey, R., Barnes, D. K., ... & Hill, N. A. (2023). Identifying vulnerable marine ecosystems: an image-based vulnerability index for the Southern Ocean seafloor. *ICES Journal of Marine Science*, *80*(4), 972-986.

Guisan, A., and N. E. Zimmermann. 2000. Predictive habitat distribution models in ecology. Ecological Modelling 135:147-186.

Kaschner, K., R. Watson, A. W. Trites, and D. Pauly. 2006. Mapping world-wide distributions of marine mammal species using a relative environmental suitability (RES) model. Marine Ecology Progress Series 316:285-310.

Koslow et al. (2001). Seamount benthic macrofauna off southern Tasmania: community structure and impacts of trawling. Marine Ecology Progress Series, 213, pp.111-125.

Mateo, R. G., Croat, T. B., Felicísimo, Á. M., & Munoz, J. (2010). Profile or group discriminative techniques? Generating reliable species distribution models using pseudo-absences and target-group absences from natural history collections. Diversity and distributions, 16(1), 84-94.

Morato, T., Pham, C. K., Pinto, C., Golding, N., Ardron, J. A., Duran Munoz, P., & Neat, F. (2018). A multi criteria assessment method for identifying Vulnerable Marine Ecosystems in the North-East Atlantic. *Frontiers in Marine Science*, *5*, 460.

Phillips, S. J., Dudík, M., Elith, J., Graham, C. H., Lehmann, A., Leathwick, J., & Ferrier, S. (2009). Sample selection bias and presence-only distribution models: implications for background and pseudo-absence data. Ecological Applications, 19(1), 181-197.

Potts, J. M., & Elith, J. (2006). Comparing species abundance models. *Ecological Modelling*, 199(2), 153-163.

Rowden A. A., Anderson O. F., Georgian S. E., Bowden D. A., Clark M. R., Pallentin A., Miller A. 2017. High-resolution habitat suitability models for the conservation and management of vulnerable marine ecosystems on the Louisville Seamount Chain, South Pacific Ocean. Frontiers in Marine Science, 4: 335.

Stephenson, F., A. A. Rowden, O. F. Anderson, C. R. Pitcher, M. H. Pinkerton, G. Petersen, and D. A. Bowden. 2021. Presence-only habitat suitability models for vulnerable marine ecosystem indicator taxa in the South Pacific have reached their predictive limit. *ICES Journal of Marine Science*

Stephenson, F., Bowden, D. A., Finucci, B., Anderson, O. F., & Rowden, A. A. (2021b). Developing updated predictive models for benthic taxa and communities across Chatham Rise and Campbell Plateau using photographic survey data. *New Zealand Aquatic Environment and Biodiversity Report No. 276*. p. 86.

Stephenson, F., Bowden, D., A., Rowden, A., A., Anderson, O., Bennion, M. Finucci, B., Pinkerton, M., Goode, S., Chin, C., Davey, N., Hart, A., Stewart, R., Clark, M. (In prep.). Using joint species distribution modelling to predict distributions of seafloor taxa and identify vulnerable marine ecosystems in New Zealand waters.

Stephenson, F., Goetz, K., Sharp, B. R., Mouton, T. L., Beets, F. L., Roberts, J., ... & Lundquist, C. J. (2020). Modelling the spatial distribution of cetaceans in New Zealand waters. *Diversity and Distributions*, *26*(4), 495-516.

Thorson, J.T., 2019. Guidance for decisions using the Vector Autoregressive Spatio-Temporal (VAST) package in stock, ecosystem, habitat and climate assessments. *Fisheries Research* 210, 143–161.

Watson, H., J. G. Hiddink, M. J. Hobbs, T. M. Brereton, and M. J. Tetley. 2013. 'The utility of relative environmental suitability (RES) modelling for predicting distributions of seabirds in the North Atlantic', *Marine Ecology Progress Series*, 485: 259-73

Williams, A., Althaus, F., Maguire, K., Green, M., Untiedt, C., Alderslade, P., Clark, M.R., Bax, N. and Schlacher, T.A., 2020. The fate of deep-sea coral reefs on seamounts in a fishery-seascape: what are the impacts, what remains, and what is protected? *Frontiers in Marine Science*, p.798.

Williams, A., Althaus, F., Green, M., Maguire, K., Untiedt, C., Mortimer, N., Jackett, C.J., Clark, M., Bax, N., Pitcher, R. and Schlacher, T., 2020. True size matters for conservation: a robust method to determine the size of deep-sea coral reefs shows they are typically small on seamounts in the Southwest Pacific Ocean. *Frontiers in Marine Science*, *7*, p.187.

Yesson, C., Clark, M. R., Taylor, M. L., Rogers, A. D. (2011) The global distribution of seamounts based on 30 arc seconds bathymetry data. Deep Sea Research Part I: Oceanographic Research Papers, 58 (4). pp. 442-453.

Annex 1 - Deep Towed Imaging System (DTIS) Data

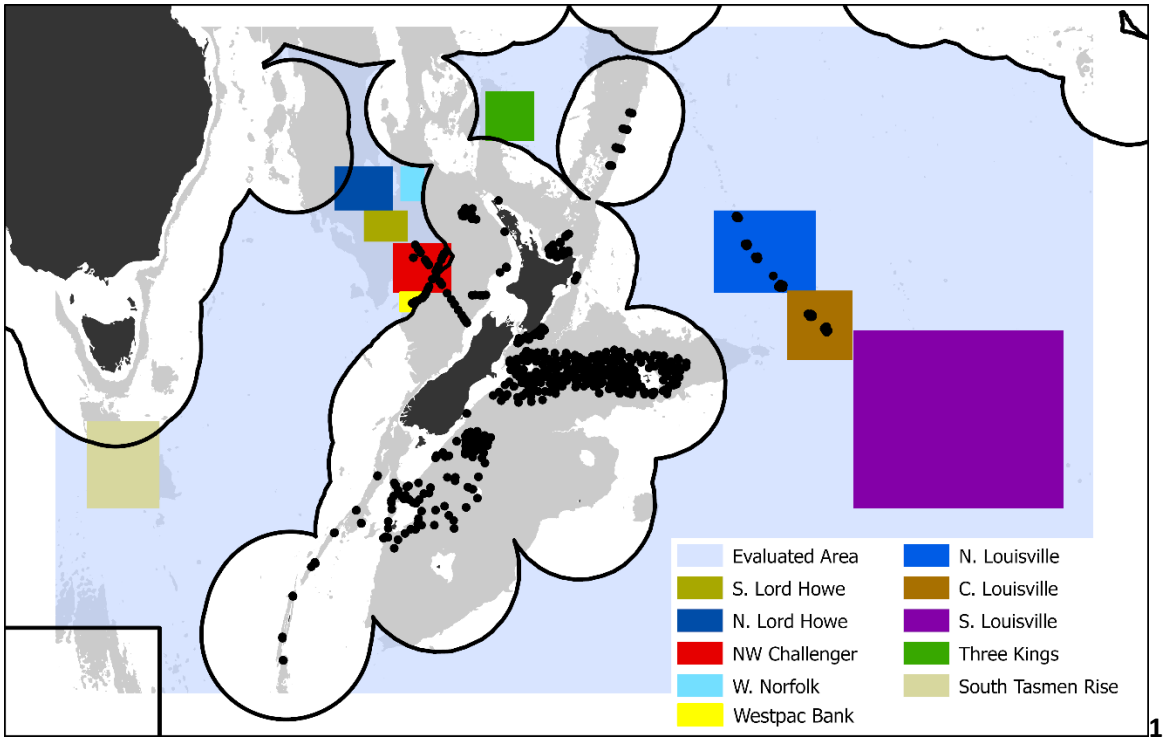

Figure A1-2 | Location of all DTIS sites (black points) in relation to all the Fishery Management Areas (FMAs) present in the Evaluated Area (in light blue).

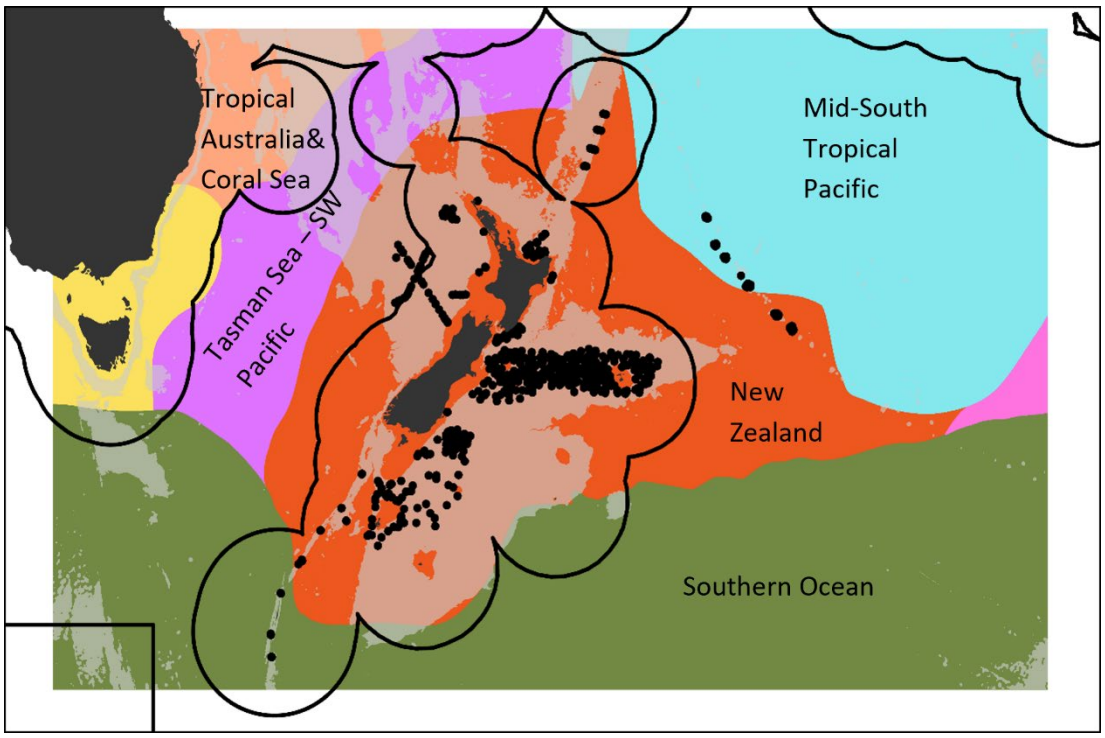

Figure A1-3 | Location of all DTIS sites in relation to the bioregions defined in Costello et al. (2017).

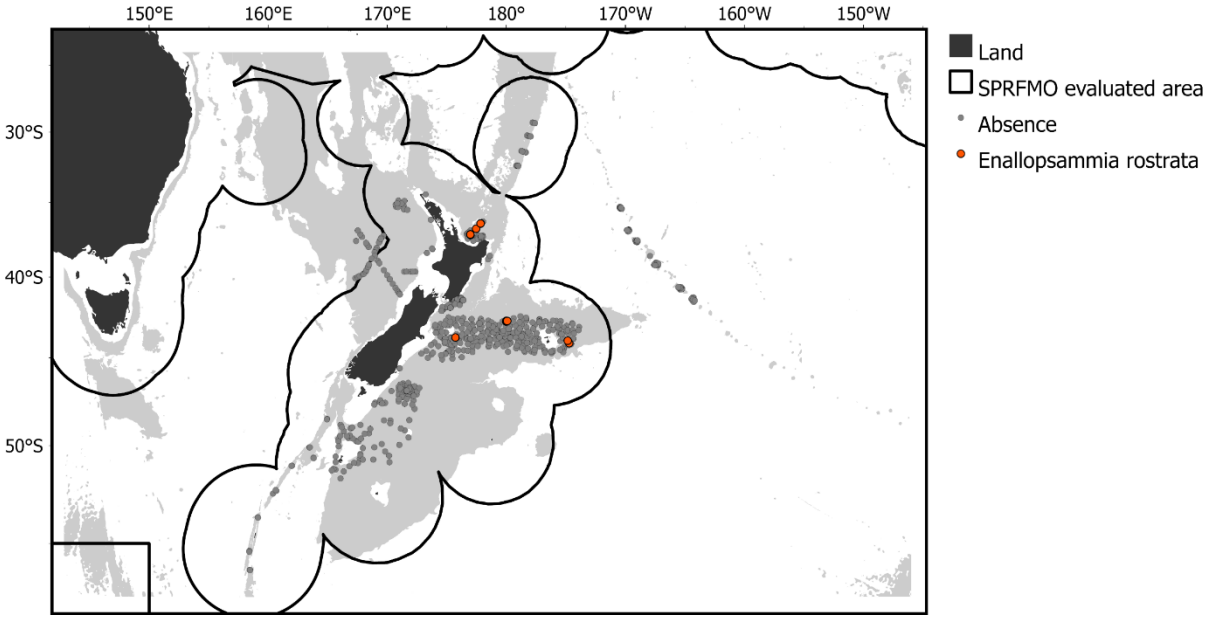

Figure A1-4 | DTIS sites that provided estimates of abundance for *Enallopsammia rostrata* (CSS). DTIS sites where Enallopsammia rostrata as absent are shown as grey dots. Black lines indicate the boundaries between the SPRFMO Evaluated Area and the multiple Exclusive Economic Zones.

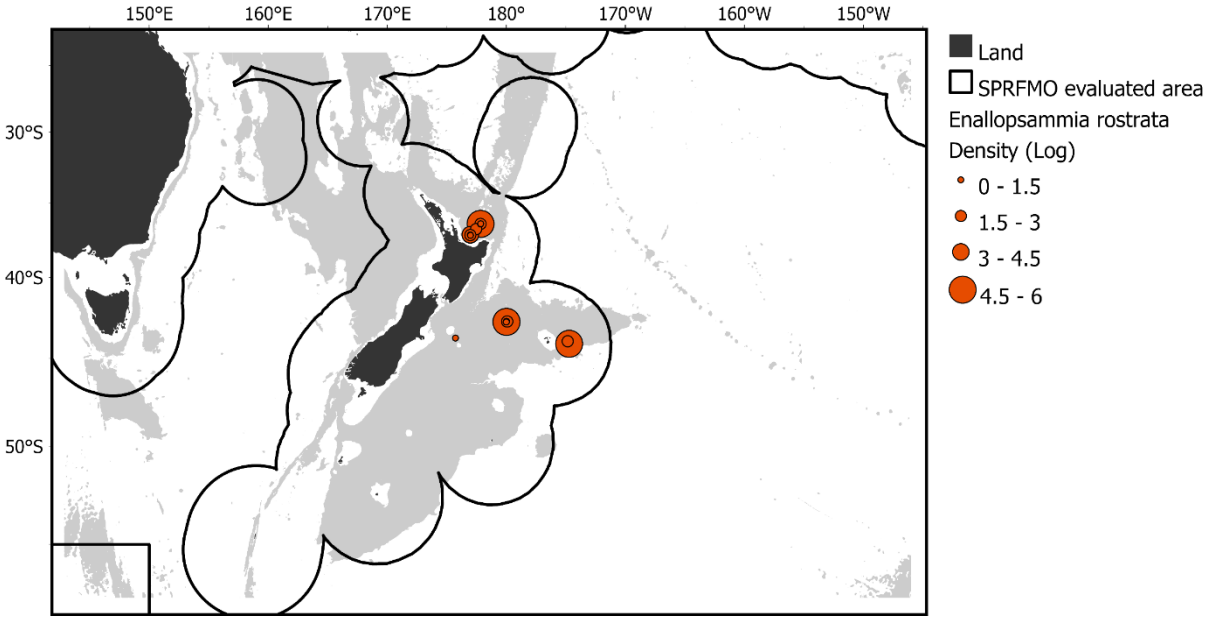

Figure A1-5 | DTIS sites that provided estimates of VME indicator taxa abundance data for *Enallopsammia rostrata* (CSS). Size represents density (log). Black lines indicate the boundaries between the SPRFMO Evaluated Area and the multiple Exclusive Economic Zones.

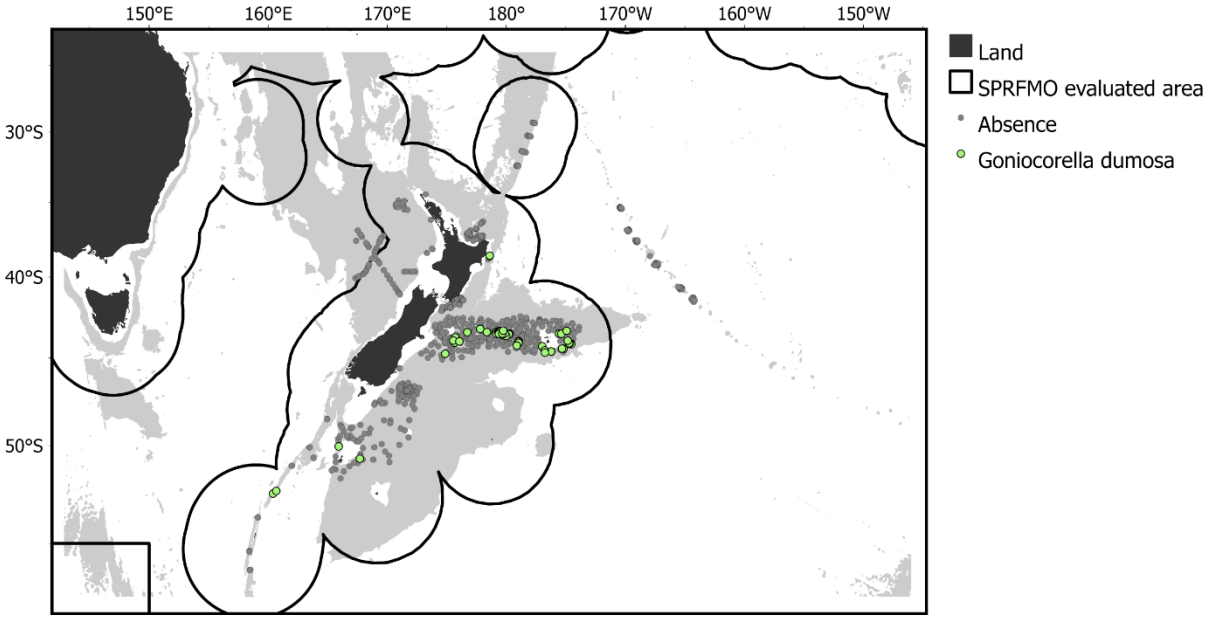

Figure A1-6 | DTIS sites that provided estimates of abundance for *Goniocorella dumosa* (CSS). DTIS sites where Goniocorella dumosa was absent are shown as grey dots. Black lines indicate the boundaries between the SPRFMO Evaluated Area and the multiple Exclusive Economic Zones.

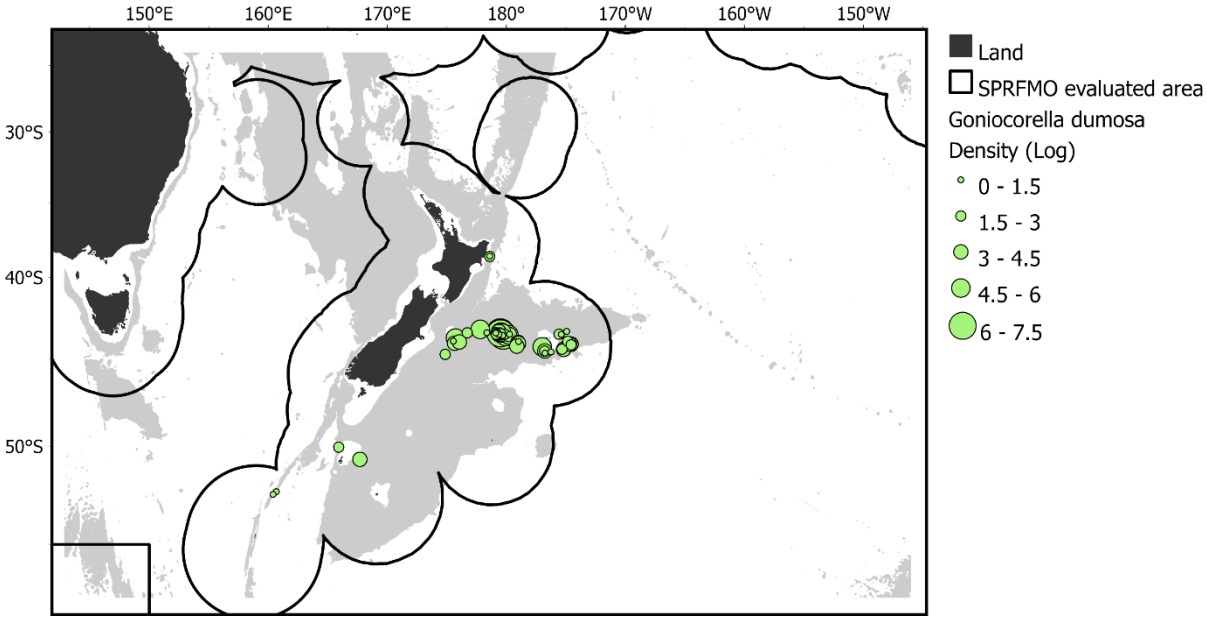

Figure A1-7 | DTIS sites that provided estimates of VME indicator taxa abundance data for *Goniocorella dumosa* (CSS). Size represents density (log). Black lines indicate the boundaries between the SPRFMO Evaluated Area and the multiple Exclusive Economic Zones.

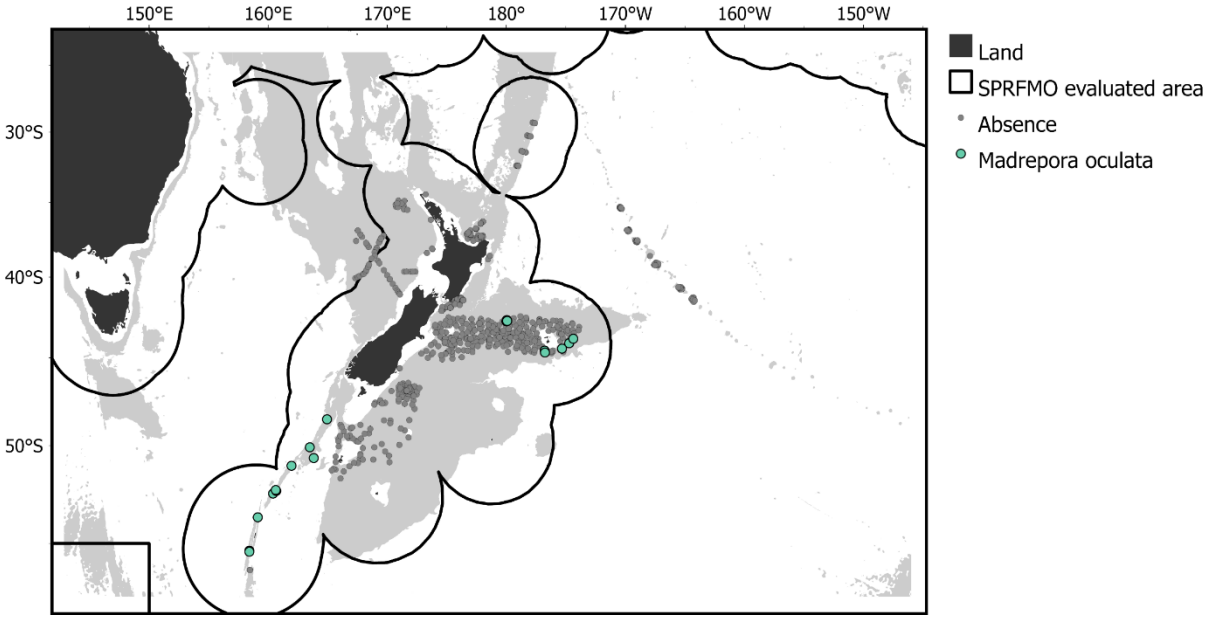

Figure A1-8 | DTIS sites that provided estimates of abundance for *Madrepora Oculata* (CSS). DTIS sites where Madrepora oculata was absent are shown as grey dots. Black lines indicate the boundaries between the SPRFMO Evaluated Area and the multiple Exclusive Economic Zones.

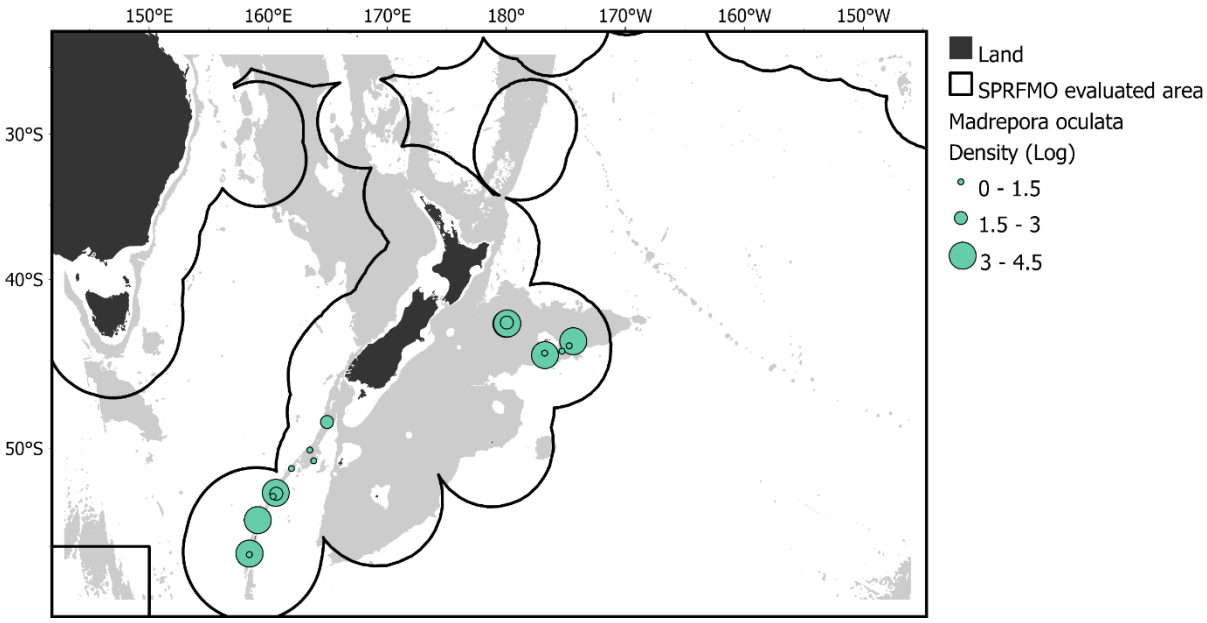

Figure A1-9 | DTIS sites that provided estimates of VME indicator taxa abundance data for *Madrepora oculata* (CSS). Size represents density (log). Black lines indicate the boundaries between the SPRFMO Evaluated Area and the multiple Exclusive Economic Zones.

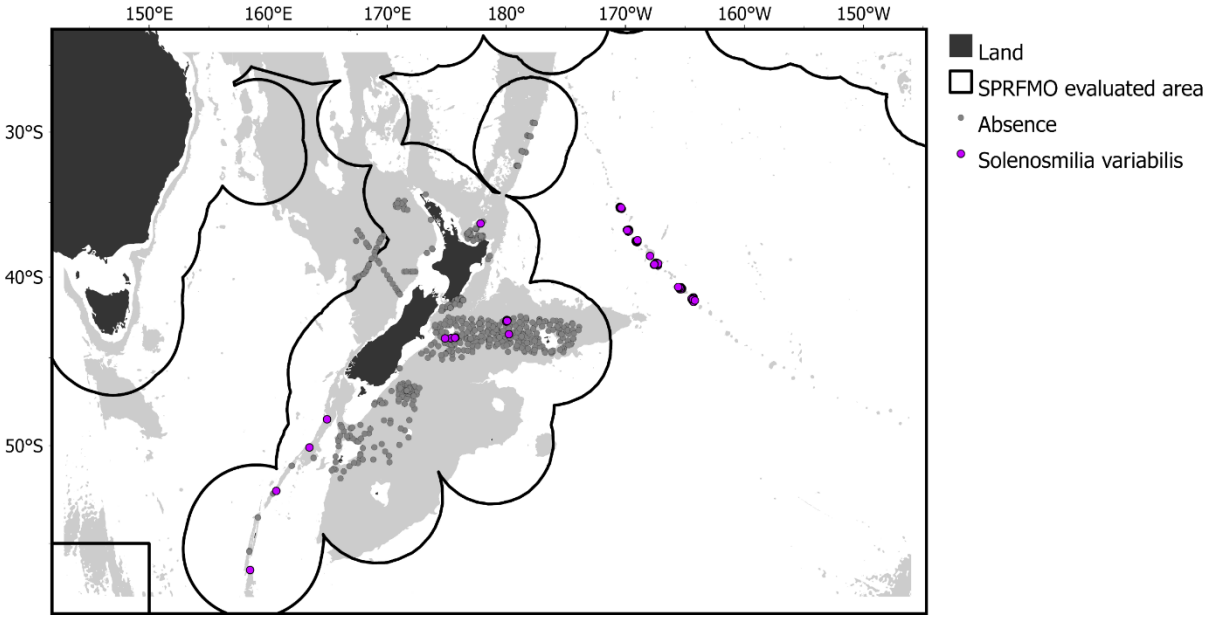

Figure A1-10 | DTIS sites that provided estimates of abundance for *Solenosmilia variabilis*. DTIS sites where Solenosmilia variabilis (CSS) was absent are shown as grey dots. Black lines indicate the boundaries between the SPRFMO Evaluated Area and the multiple Exclusive Economic Zones.

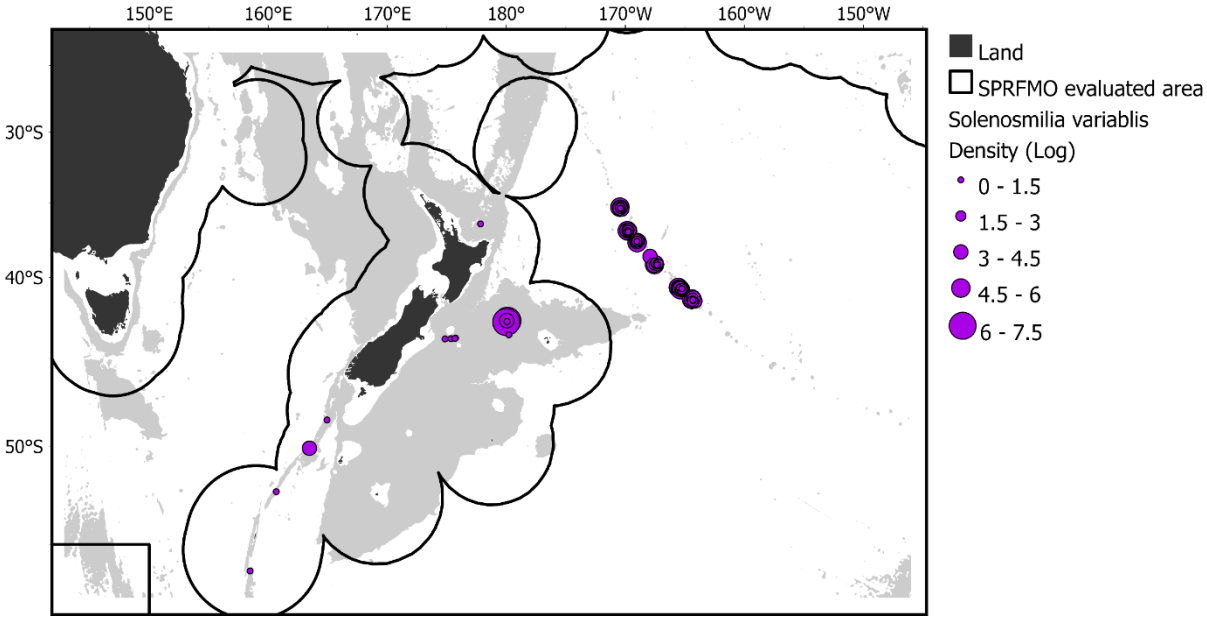

Figure A1-11 | DTIS sites that provided estimates of VME indicator taxa abundance data for *Solenosmilia variabilis* (CSS). Size represents density (log). Black lines indicate the boundaries between the SPRFMO Evaluated Area and the multiple Exclusive Economic Zones.

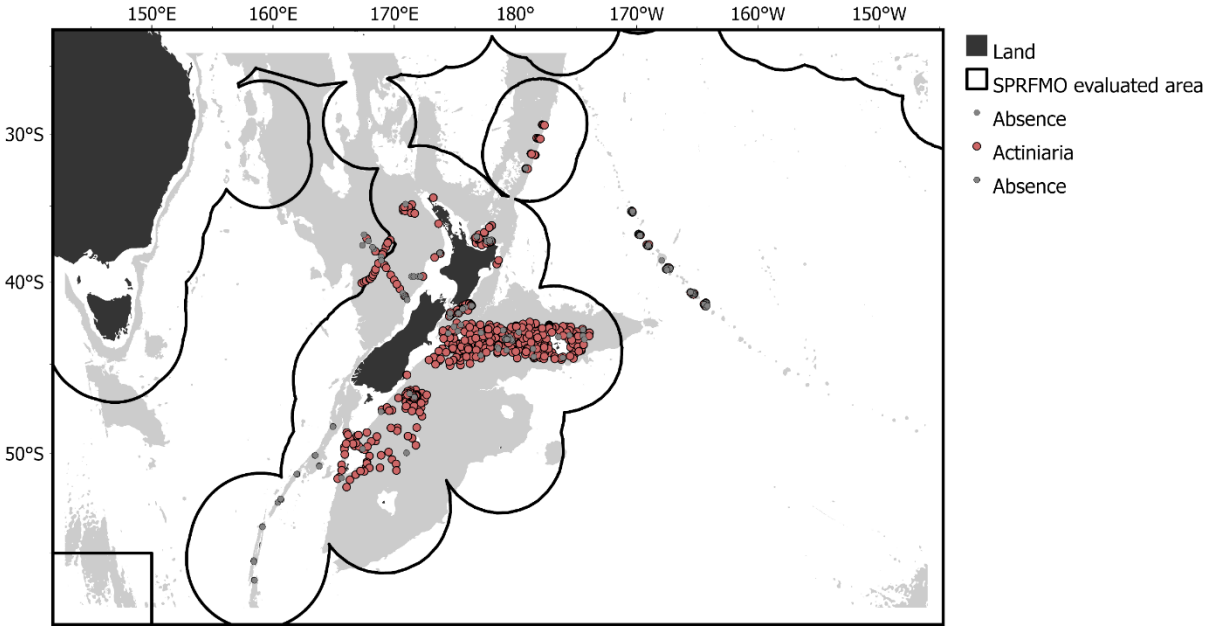

Figure A1-12 | DTIS sites that provided estimates of abundance for Actinaria (ATX). DTIS sites where Actinaria were absent are shown as grey dots. Black lines indicate the boundaries between the SPRFMO Evaluated Area and the multiple Exclusive Economic Zones.

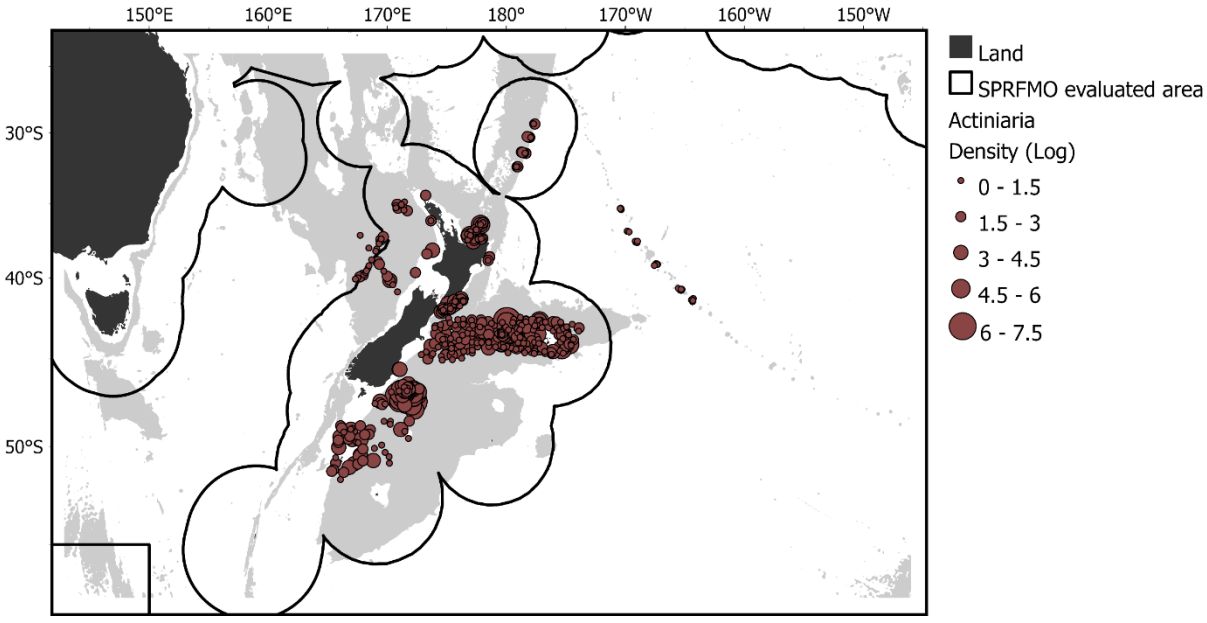

Figure A1-13 | DTIS sites that provided estimates of VME indicator taxa abundance data for Actinaria (ATX). Size represents density (log). Black lines indicate the boundaries between the SPRFMO Evaluated Area and the multiple Exclusive Economic Zones.

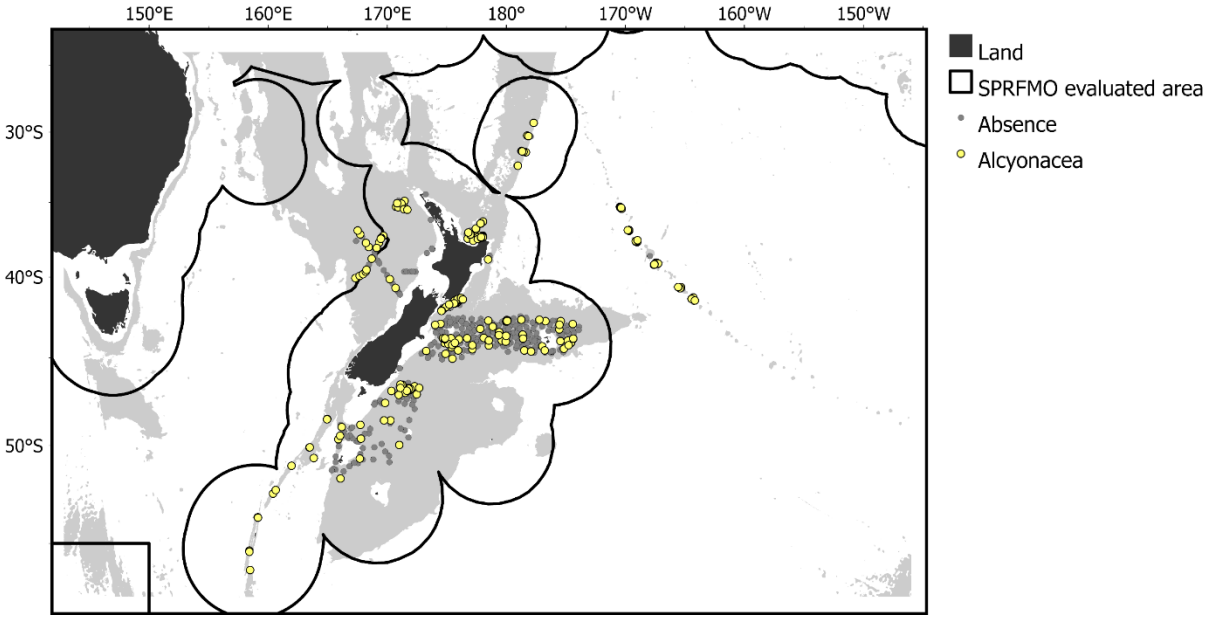

Figure A1-14 | DTIS sites that provided estimates of abundance for Alcyonacea (AJZ). DTIS sites where Alcyonacea were absent are shown as grey dots. Black lines indicate the boundaries between the SPRFMO Evaluated Area and the multiple Exclusive Economic Zones.

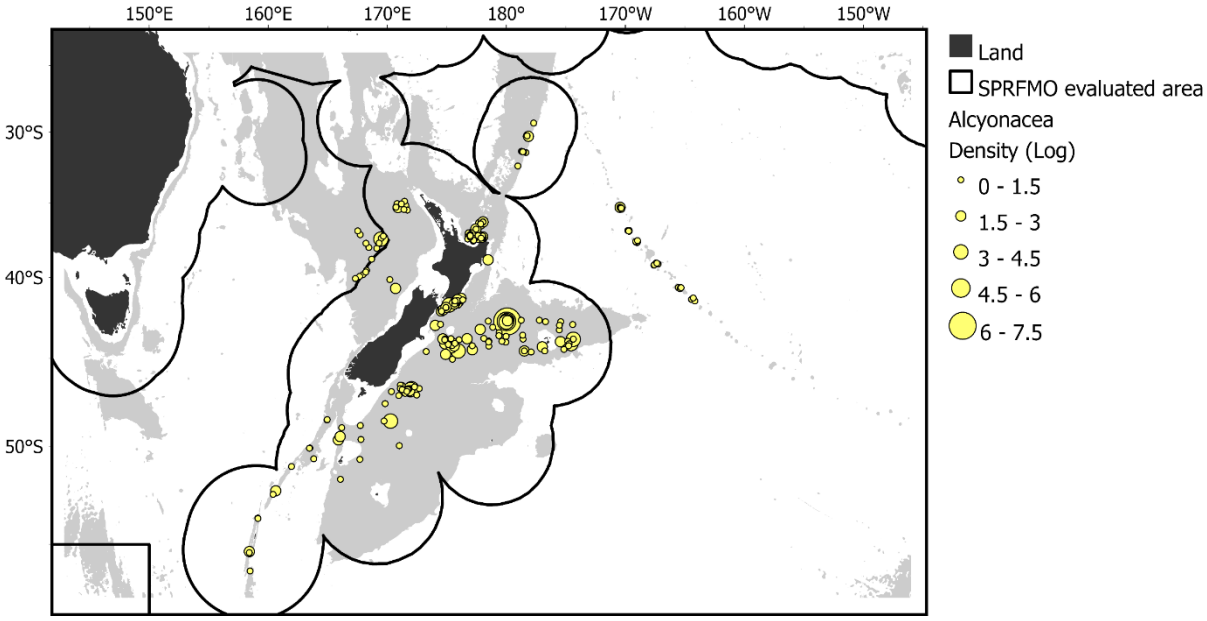

Figure A115 | DTIS sites that provided estimates of VME indicator taxa abundance data for Alcyonacea (AJZ). Size represents density (log). Black lines indicate the boundaries between the SPRFMO Evaluated Area and the multiple Exclusive Economic Zones.

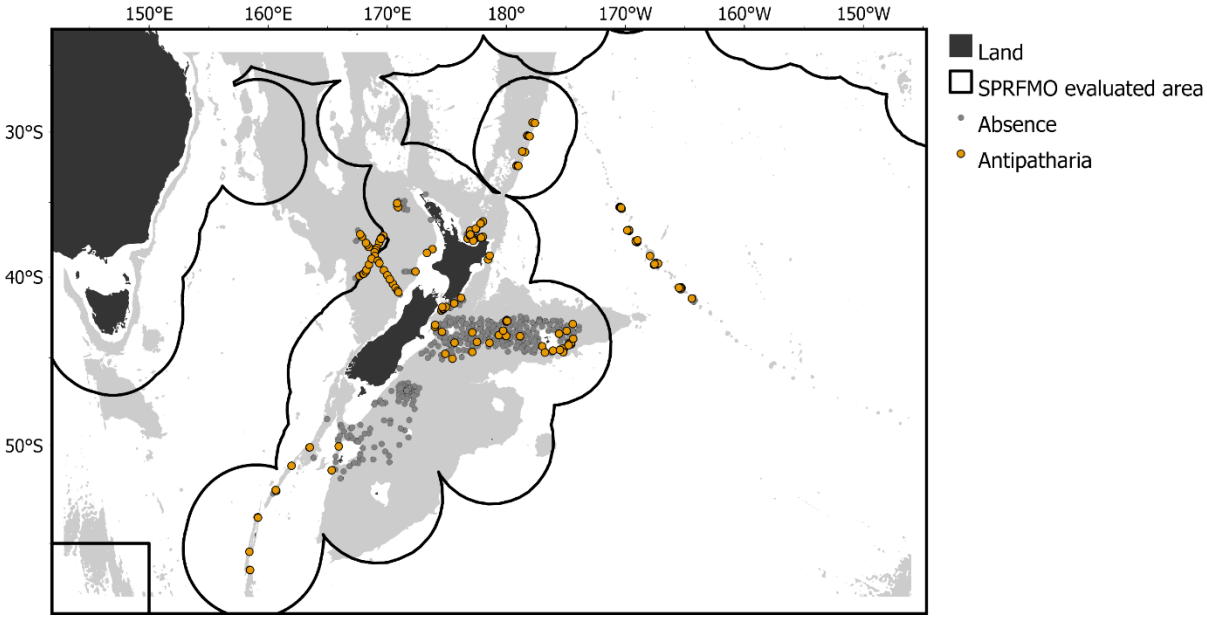

Figure A1-16 | DTIS sites that provided estimates of abundance for Antipatharia (AQZ). DTIS sites where Antipatharia were absent are shown as grey dots. Black lines indicate the boundaries between the SPRFMO Evaluated Area and the multiple Exclusive Economic Zones.

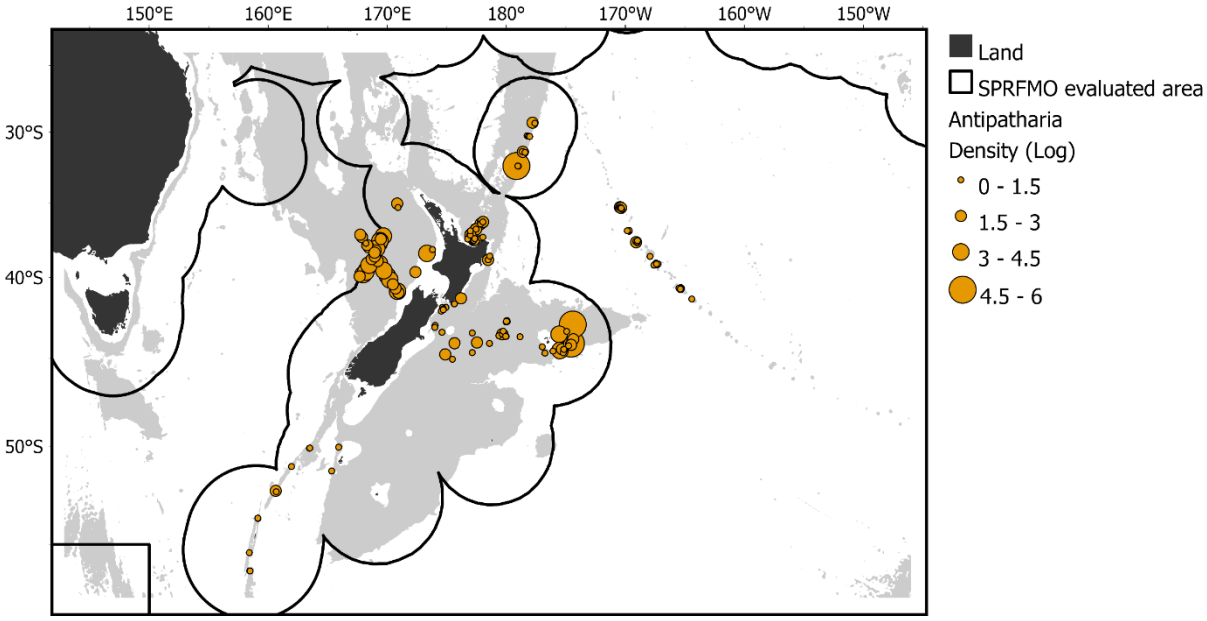

Figure A1-17 | DTIS sites that provided estimates of VME indicator taxa abundance data for Antipatharia (AQZ). Size represents density (log). Black lines indicate the boundaries between the SPRFMO Evaluated Area and the multiple Exclusive Economic Zones.

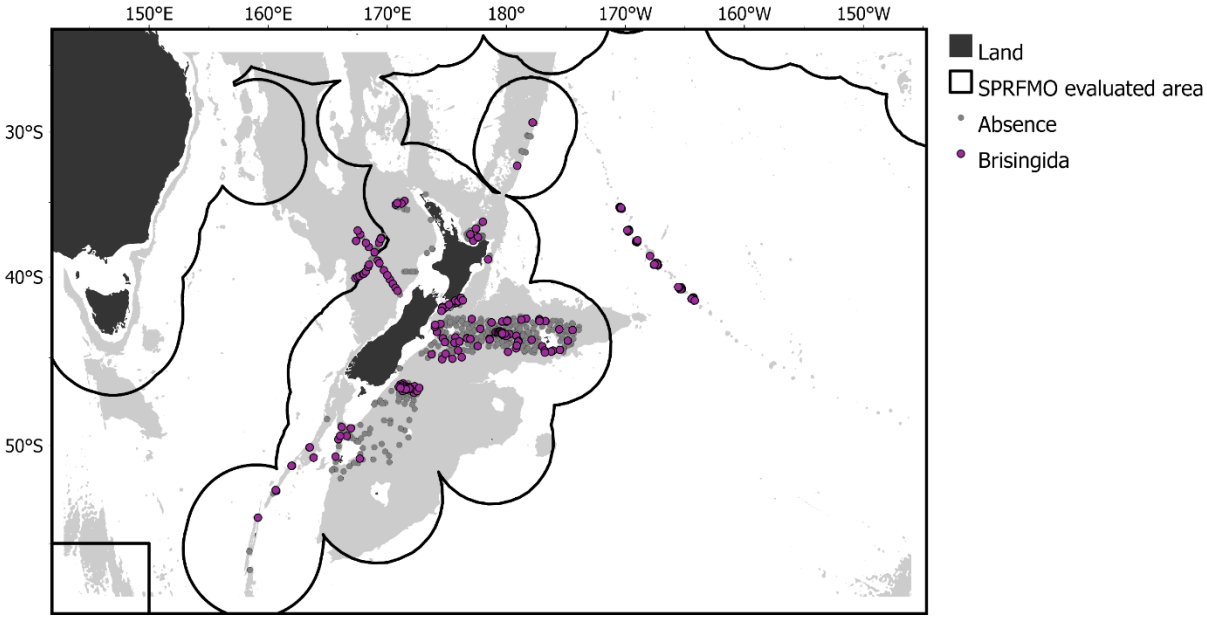

Figure A1-18 | DTIS sites that provided estimates of abundance for Brisingida (BHZ). DTIS sites where Brisingida were absent are shown as grey dots. Black lines indicate the boundaries between the SPRFMO Evaluated Area and the multiple Exclusive Economic Zones.

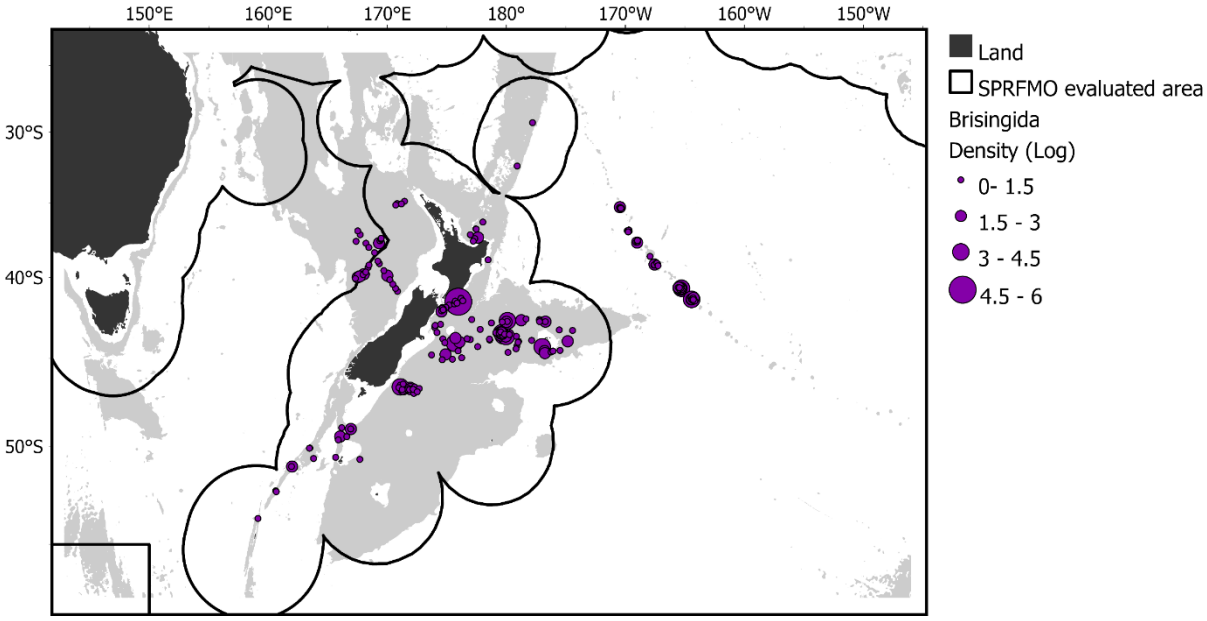

Figure A1-19 | DTIS sites that provided estimates of VME indicator taxa abundance data for Brisingida (BHZ). Size represents density (log). Black lines indicate the boundaries between the SPRFMO Evaluated Area and the multiple Exclusive Economic Zones.

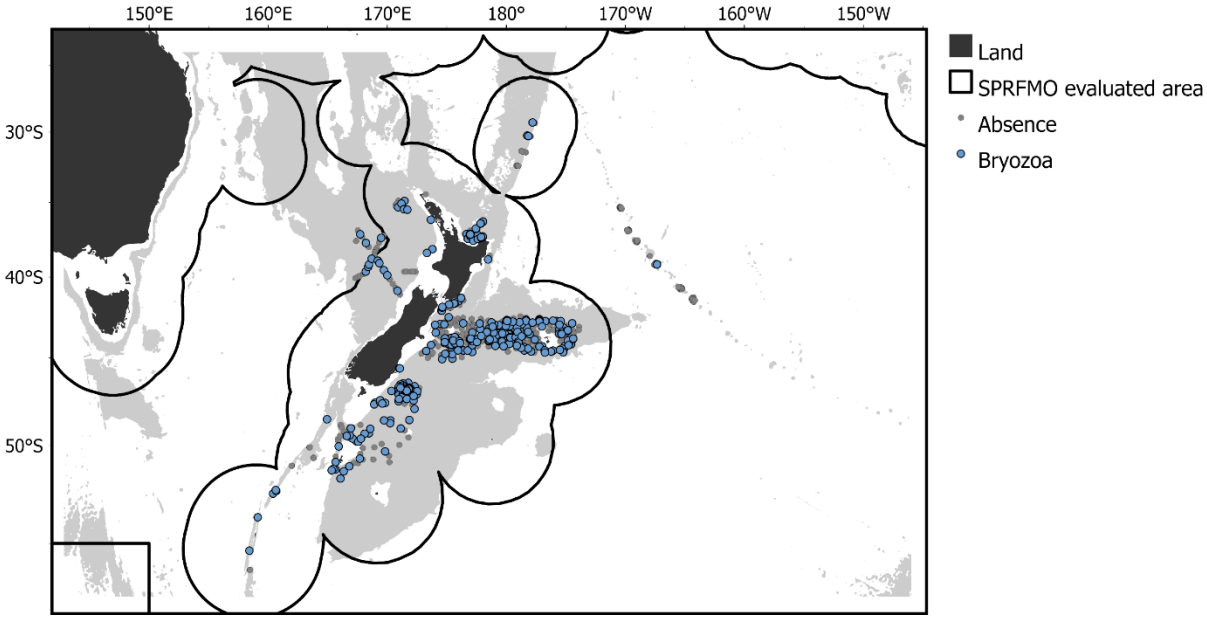

Figure A1-20 | DTIS sites that provided estimates of abundance for Bryozoa (BZN). DTIS sites where Bryozoa were absent are shown as grey dots. Black lines indicate the boundaries between the SPRFMO Evaluated Area and the multiple Exclusive Economic Zones.

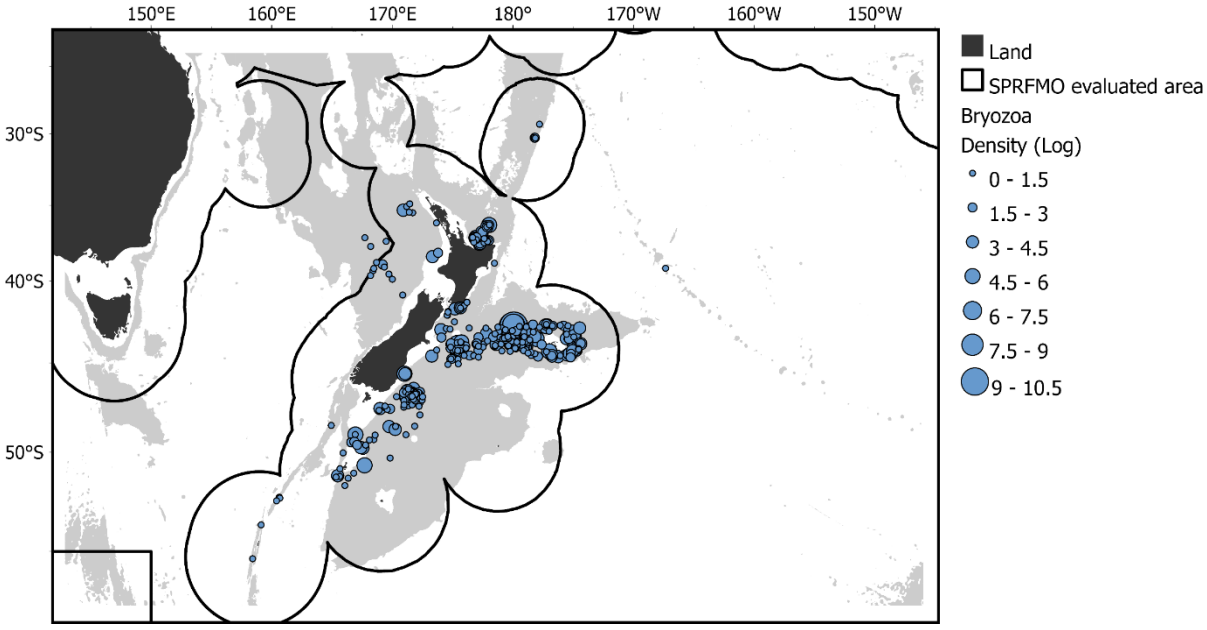

Figure A1-21 | DTIS sites that provided estimates of VME indicator taxa abundance data for Bryozoa (BZN). Size represents density (log). Black lines indicate the boundaries between the SPRFMO Evaluated Area and the multiple Exclusive Economic Zones.

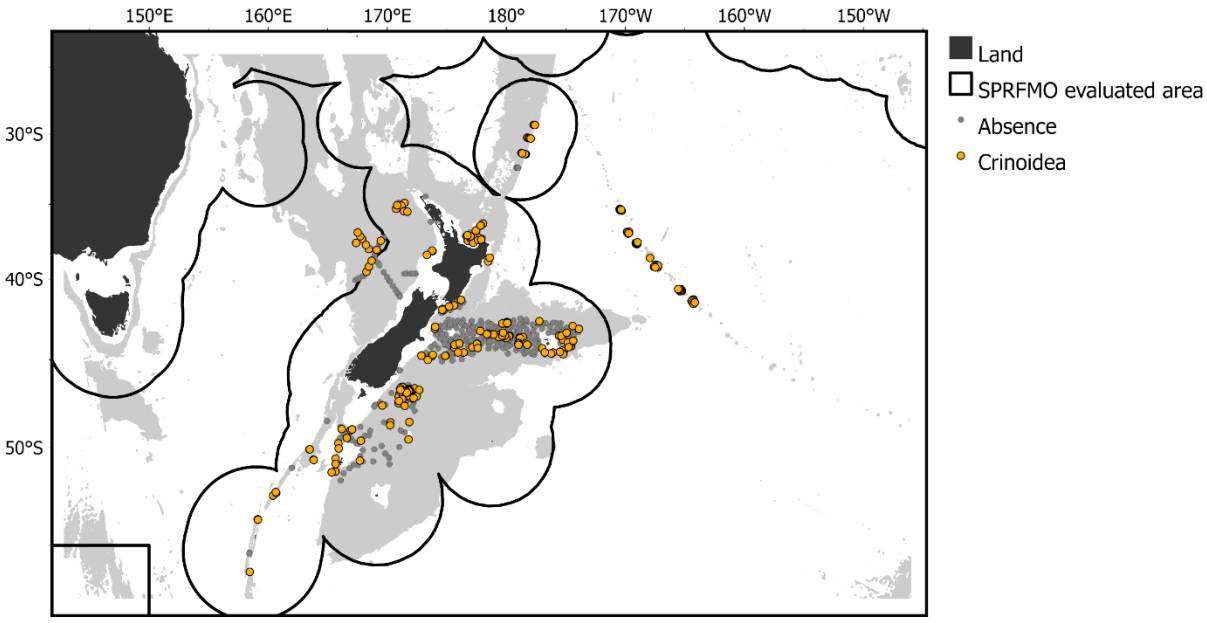

Figure A1-22 | DTIS sites that provided estimates of abundance for Crinoidea (CWD). DTIS sites where Crinoidea were absent are shown as grey dots. Black lines indicate the boundaries between the SPRFMO Evaluated Area and the multiple Exclusive Economic Zones.

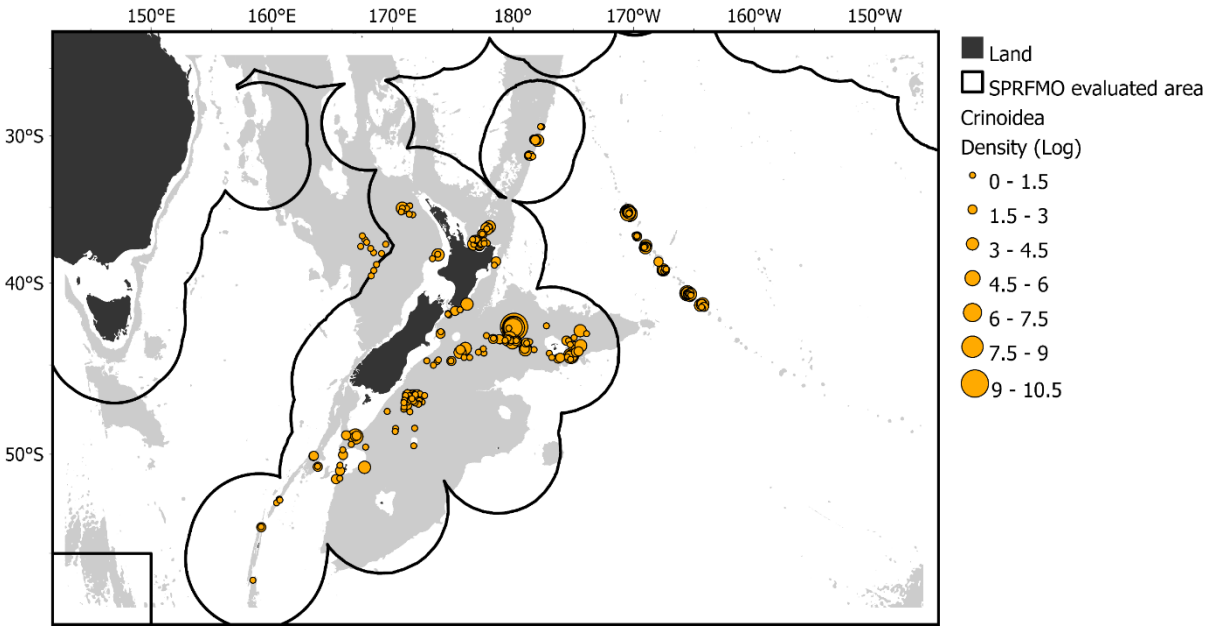

Figure A1-23 | DTIS sites that provided estimates of VME indicator taxa abundance data for Crinoidea (CWD). Size represents density (log). Black lines indicate the boundaries between the SPRFMO Evaluated Area and the multiple Exclusive Economic Zones.

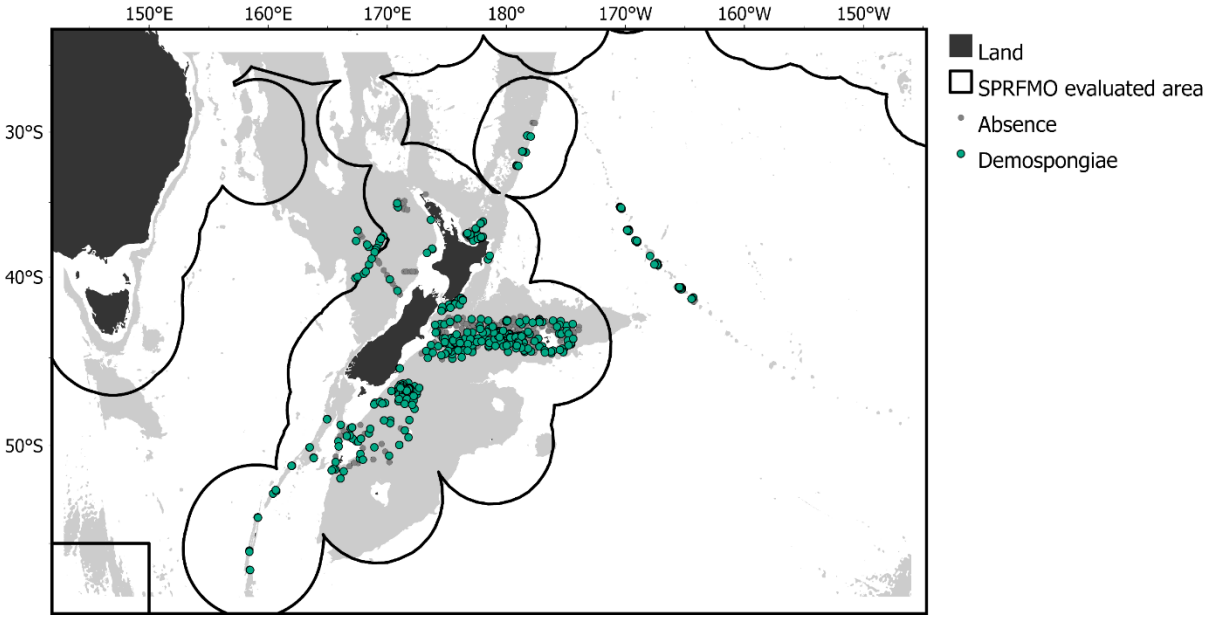

Figure A1-24 | DTIS sites that provided estimates of abundance for Demospongiae (PFR). DTIS sites where Demospongiae were absent are shown as grey dots. Black lines indicate the boundaries between the SPRFMO Evaluated Area and the multiple Exclusive Economic Zones.

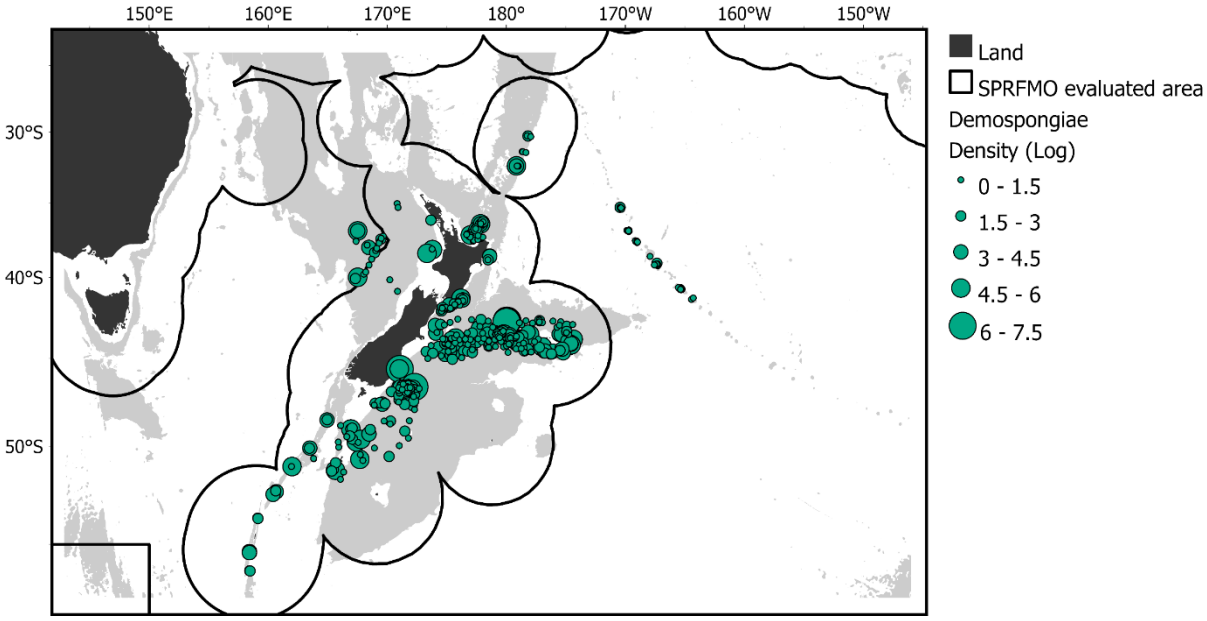

Figure A1-25 | DTIS sites that provided estimates of VME indicator taxa abundance data for Demospongiae (PFR). Size represents density (log). Black lines indicate the boundaries between the SPRFMO Evaluated Area and the multiple Exclusive Economic Zones.

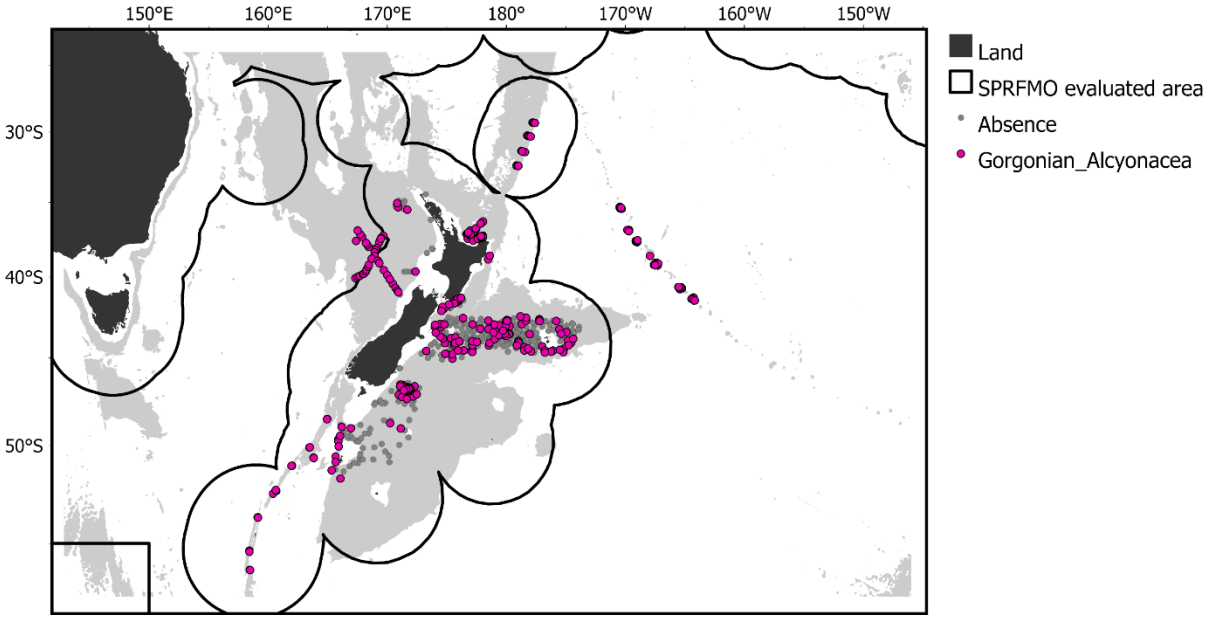

Figure A1-26 | DTIS sites that provided estimates of abundance for Gorgonian Alcyonacea (GGW). DTIS sites where Gorgonian Alcyonacea were absent are shown as grey dots. Black lines indicate the boundaries between the SPRFMO Evaluated Area and the multiple Exclusive Economic Zones

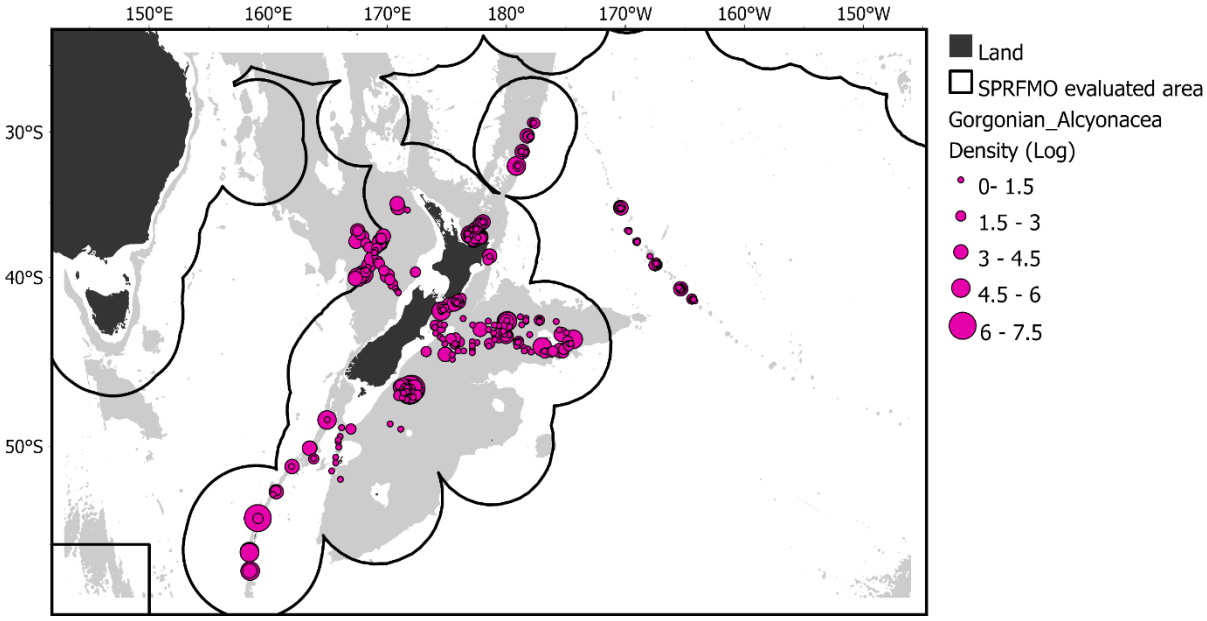

Figure A1-27 | DTIS sites that provided estimates of VME indicator taxa abundance data for Gorgonian Alcyonacea (GGW). Size represents density (log). Black lines indicate the boundaries between the SPRFMO Evaluated Area and the multiple Exclusive Economic Zones.

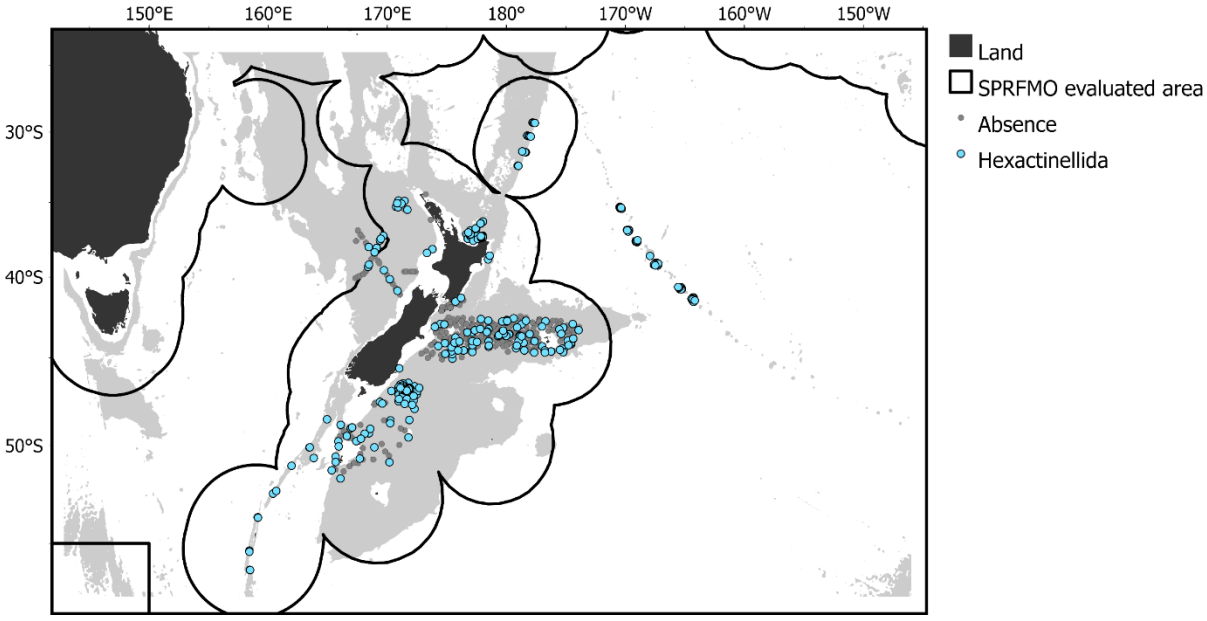

Figure A1-28 | DTIS sites that provided estimates of abundance for Hexactinellida (PFR). DTIS sites where Hexactinellida were absent are shown as grey dots. Black lines indicate the boundaries between the SPRFMO Evaluated Area and the multiple Exclusive Economic Zones

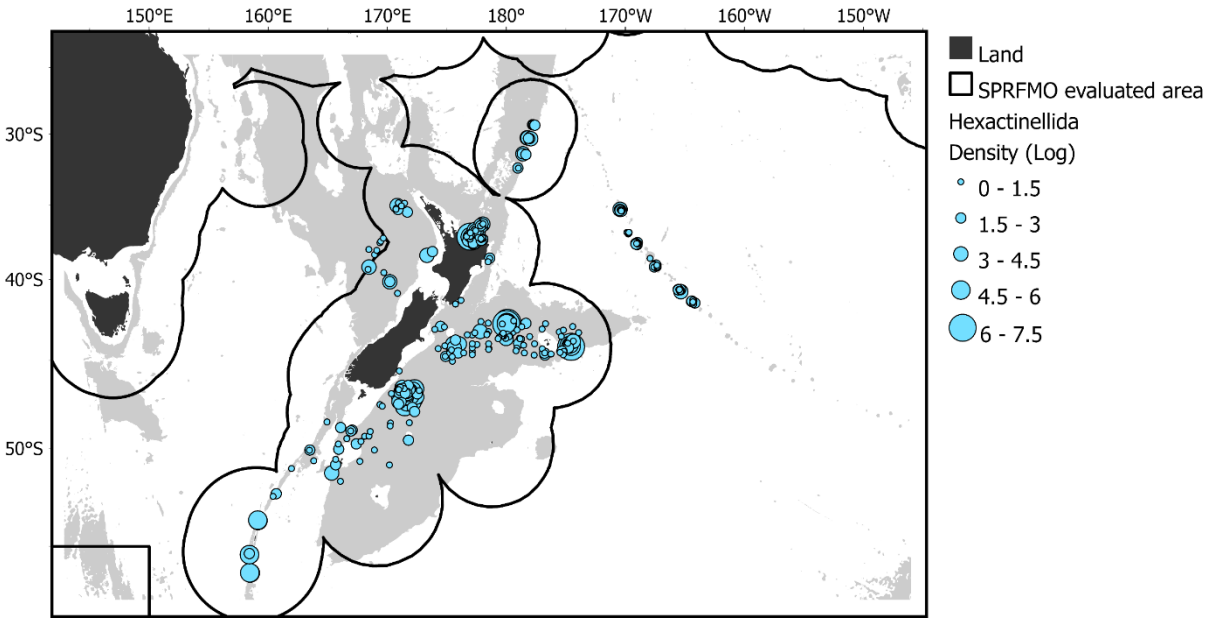

Figure A1-29 | DTIS sites that provided estimates of VME indicator taxa abundance data for Hexactinellida (PFR). Size represents density (log). Black lines indicate the boundaries between the SPRFMO Evaluated Area and the multiple Exclusive Economic Zones.

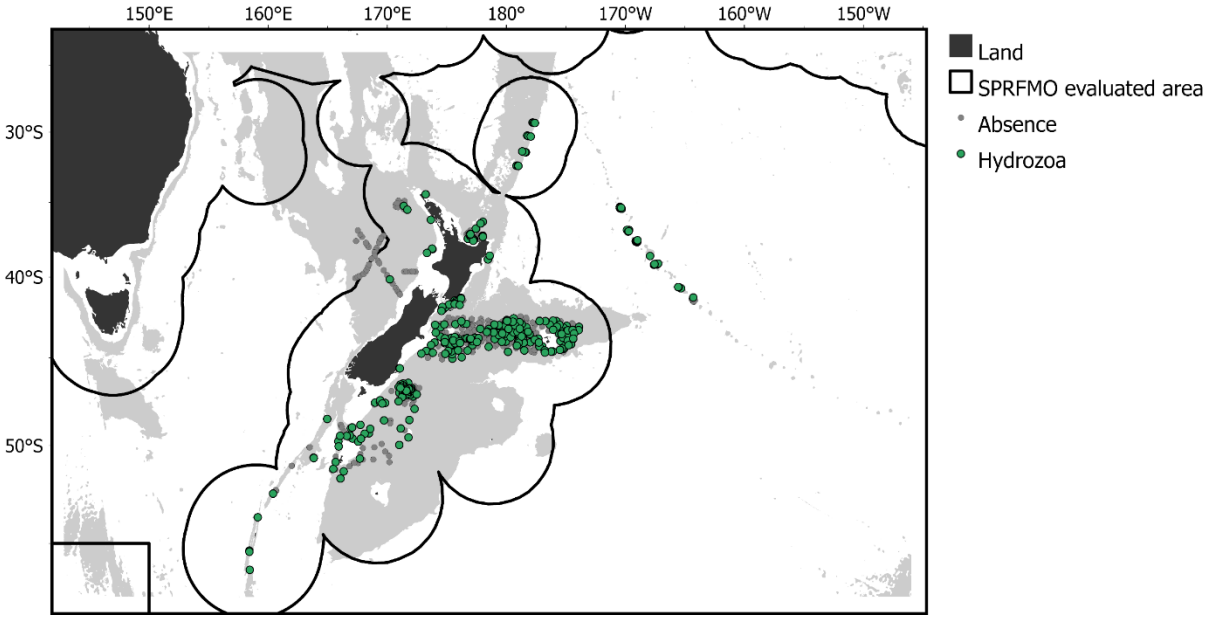

Figure A1-30 | DTIS sites that provided estimates of abundance for Hydrozoa (HQZ). DTIS sites where Hydrozoa were absent are shown as grey dots. Black lines indicate the boundaries between the SPRFMO Evaluated Area and the multiple Exclusive Economic Zones

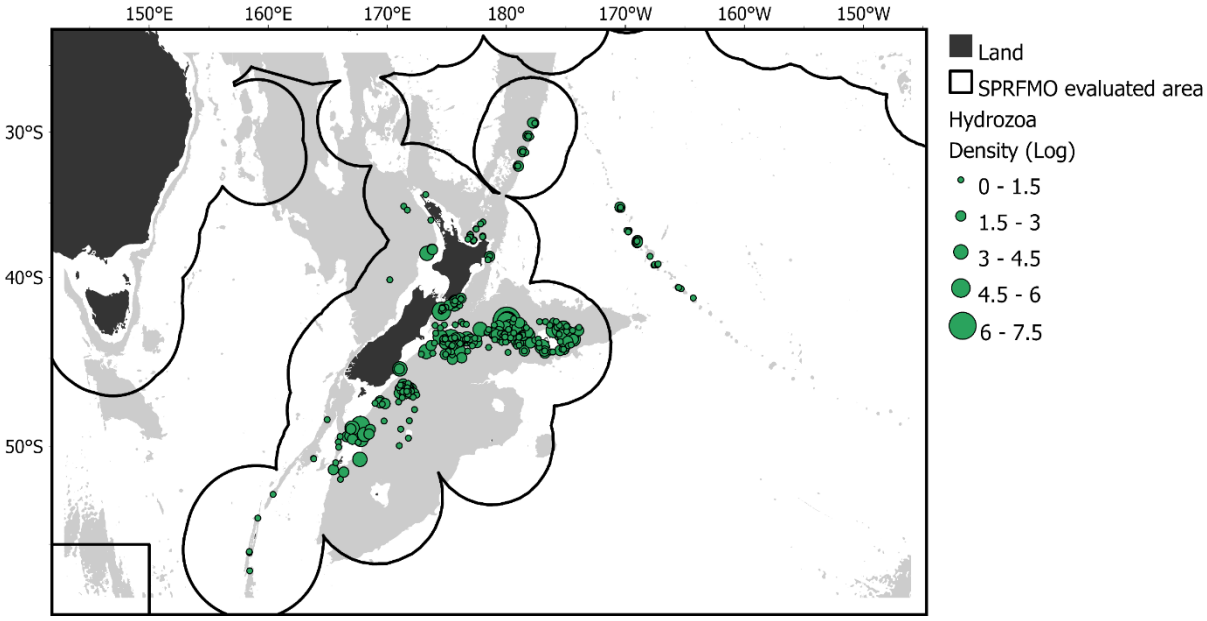

Figure A1-31 | DTIS sites that provided estimates of VME indicator taxa abundance data for Hydrozoa (HQZ). Size represents density (log). Black lines indicate the boundaries between the SPRFMO Evaluated Area and the multiple Exclusive Economic Zones.

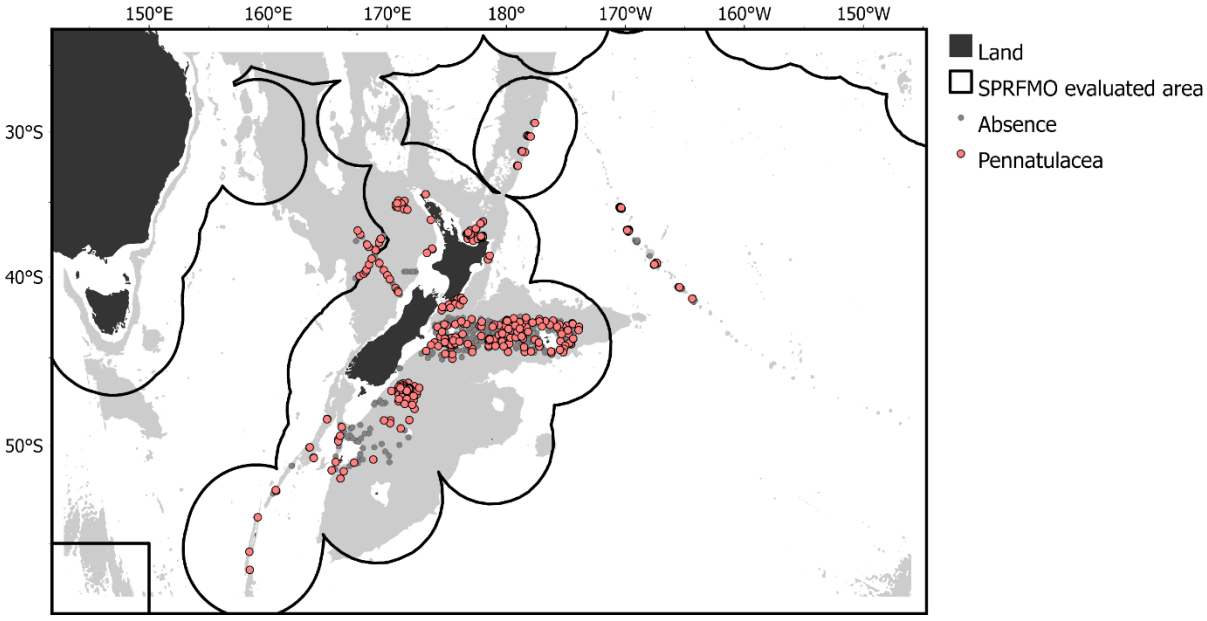

Figure A1-32 | DTIS sites that provided estimates of abundance for Pennatulacea (NTW). DTIS sites where Pennatulacea were absent are shown as grey dots. Black lines indicate the boundaries between the SPRFMO Evaluated Area and the multiple Exclusive Economic Zones

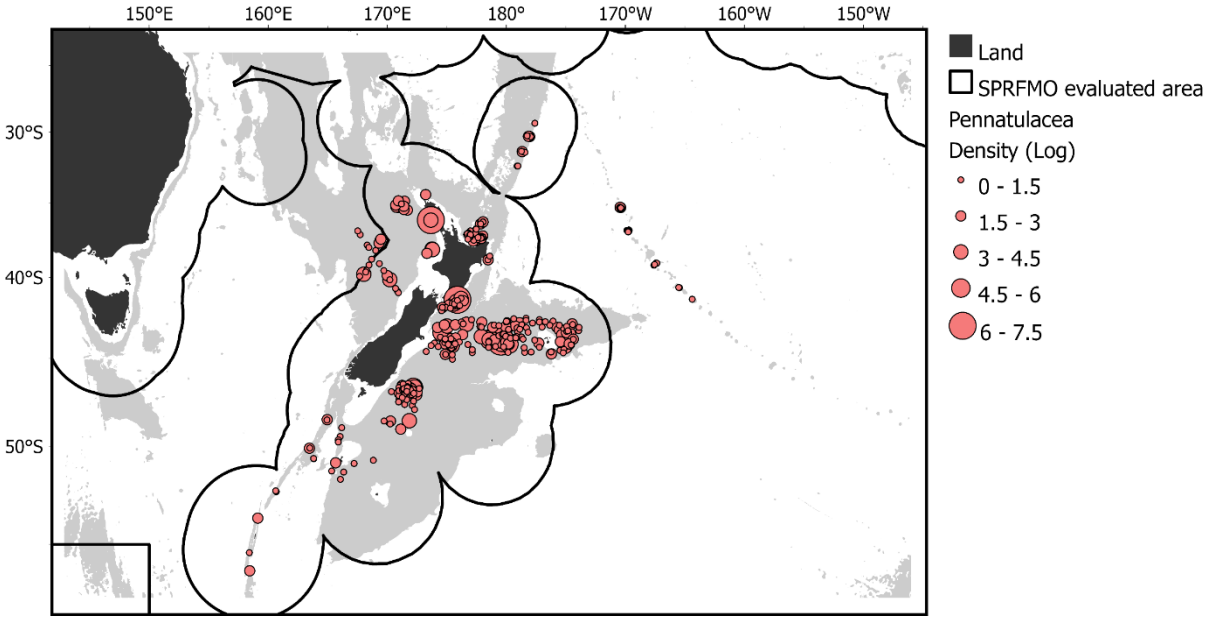

Figure A1-33 | DTIS sites that provided estimates of VME indicator taxa abundance data for Pennatulacea (NTW). Size represents density (log). Black lines indicate the boundaries between the SPRFMO Evaluated Area and the multiple Exclusive Economic Zones.

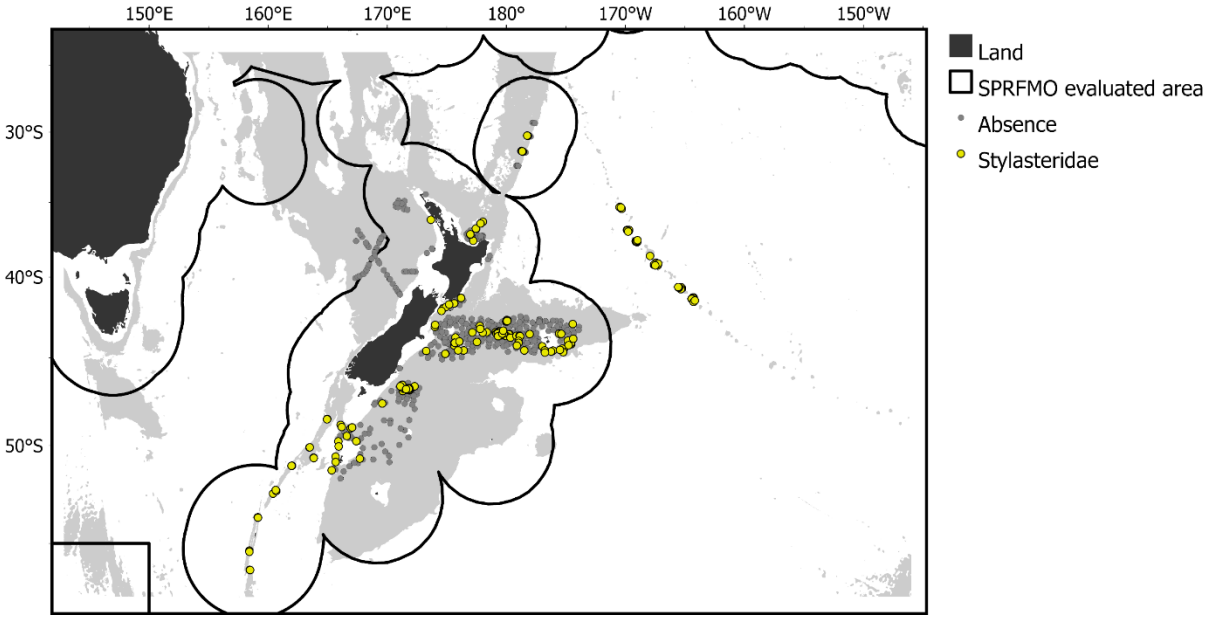

Figure A1-34 | DTIS sites that provided estimates of abundance for Stylasteridae (AXT). DTIS sites where Stylasteridae were absent are shown as grey dots. Black lines indicate the boundaries between the SPRFMO Evaluated Area and the multiple Exclusive Economic Zones

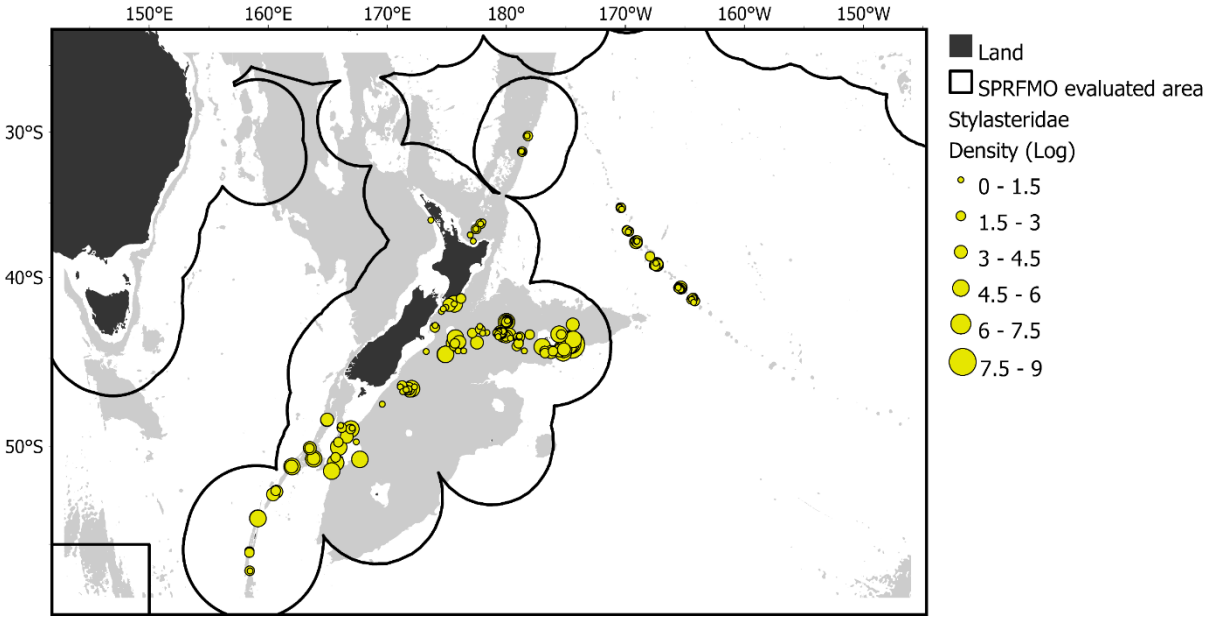

Figure A1-35 | DTIS sites that provided estimates of VME indicator taxa abundance data for Stylasteridae (AXT). Size represents density (log). Black lines indicate the boundaries between the SPRFMO Evaluated Area and the multiple Exclusive Economic Zones.

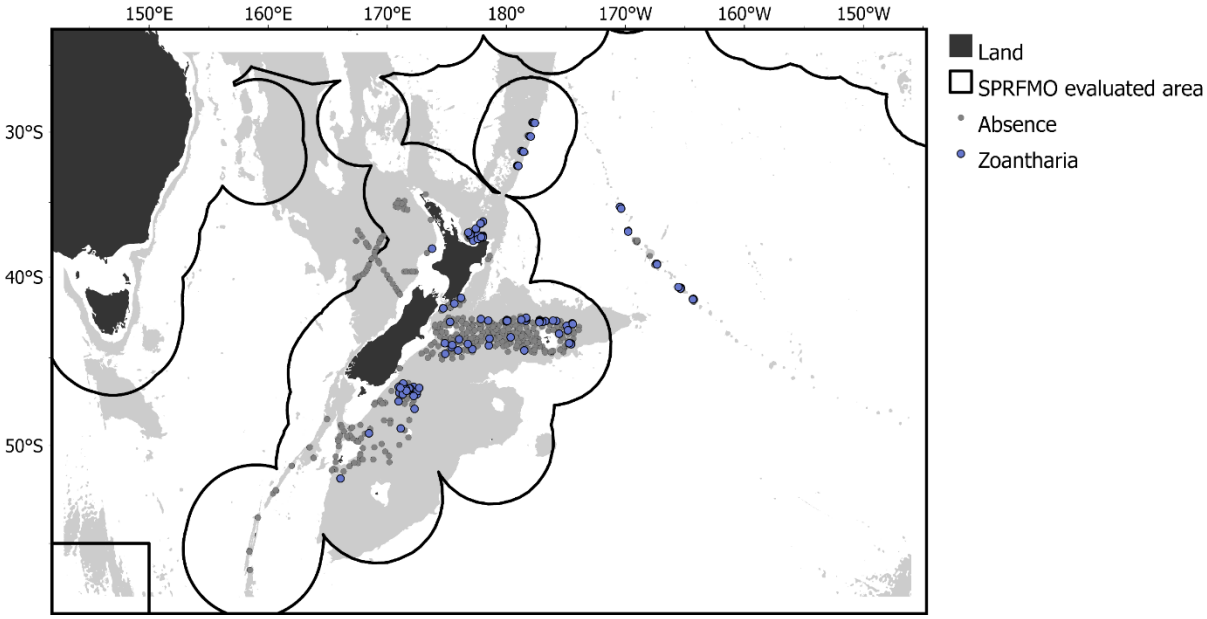

Figure A1-36 | DTIS sites that provided estimates of abundance for Zoantharia (ZOT). DTIS sites where Zoantharia were absent are shown as grey dots. Black lines indicate the boundaries between the SPRFMO Evaluated Area and the multiple Exclusive Economic Zones

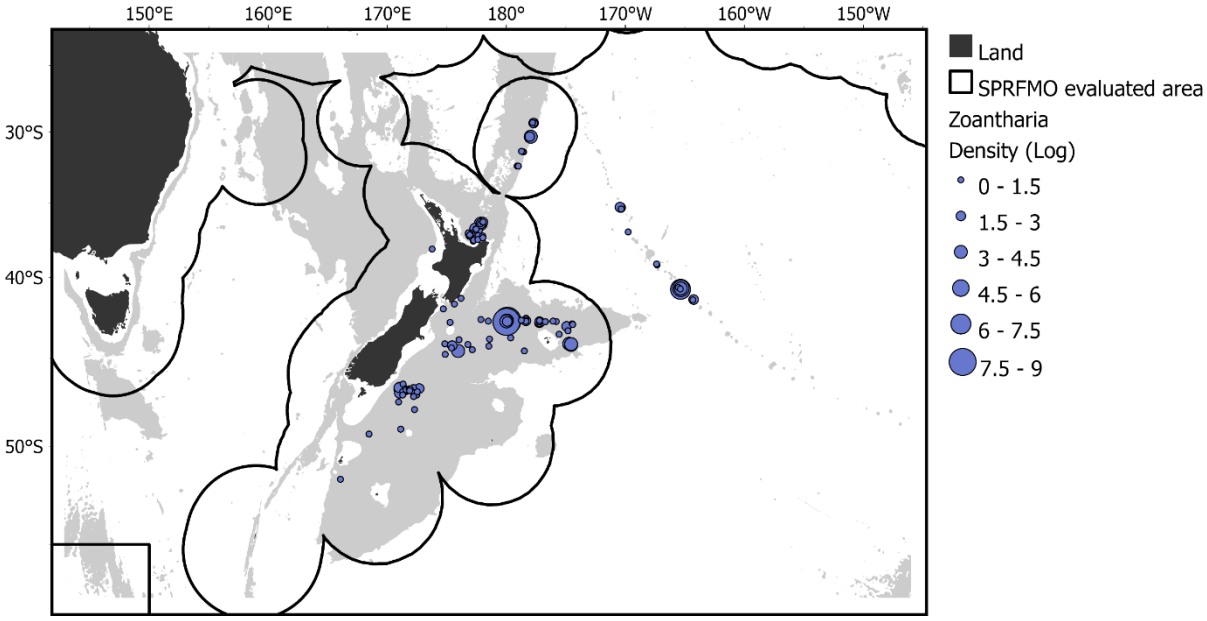

Figure A1-37 | DTIS sites that provided estimates of VME indicator taxa abundance data for Zoantharia (ZOT). Size represents density (log). Black lines indicate the boundaries between the SPRFMO Evaluated Area and the multiple Exclusive Economic Zones.

Annex 2 – Investigation of data-driven models

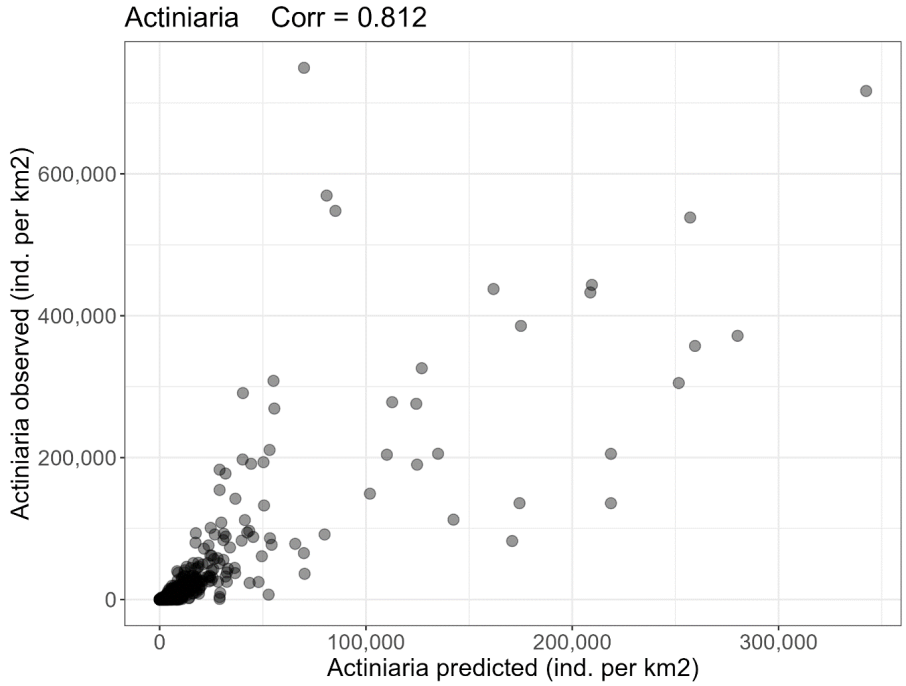

Figure A2-1 | Predicted estimates of density (*data-driven* approach) compared to observed estimates of density (DTIS data) for Actinaria.

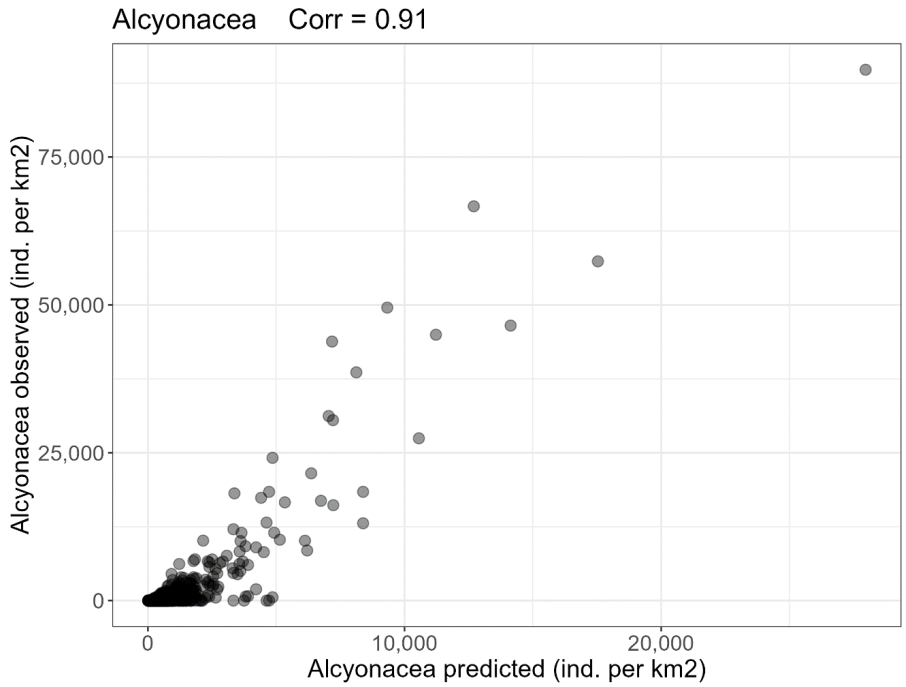

Figure A2-2 | Predicted estimates of density (*data-driven* approach) compared to observed estimates of density (DTIS data) for Alcyonacea.

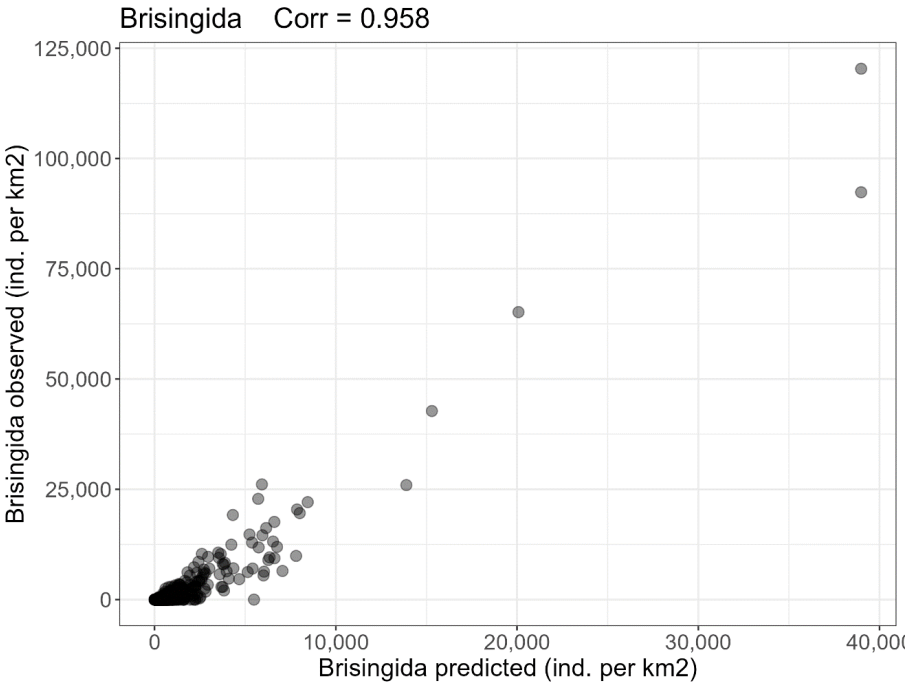

Figure A2-3 | Predicted estimates of density (*data-driven* approach) compared to observed estimates of density (DTIS data) for Brisingida.

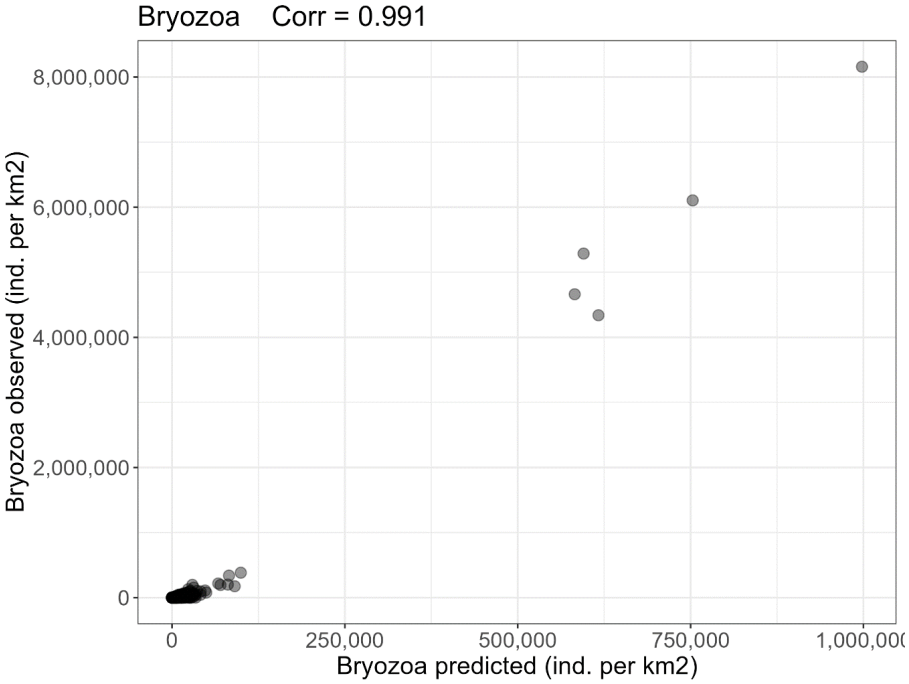

Figure A2-4 | Predicted estimates of density (*data-driven* approach) compared to observed estimates of density (DTIS data) for Bryozoa.

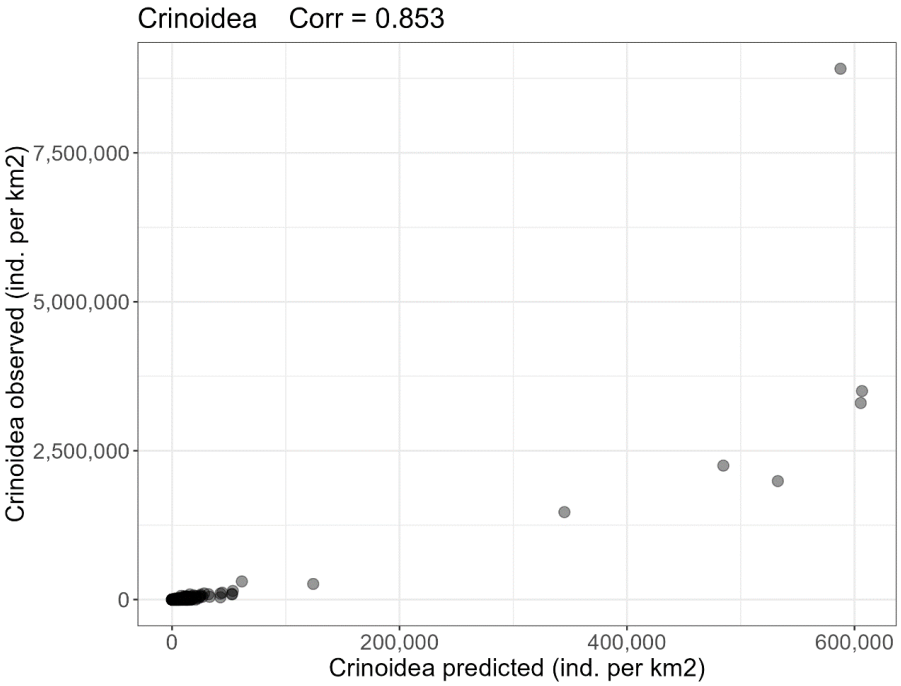

Figure A2-5 | Predicted estimates of density (*data-driven* approach) compared to observed estimates of density (DTIS data) for Crinoidea.

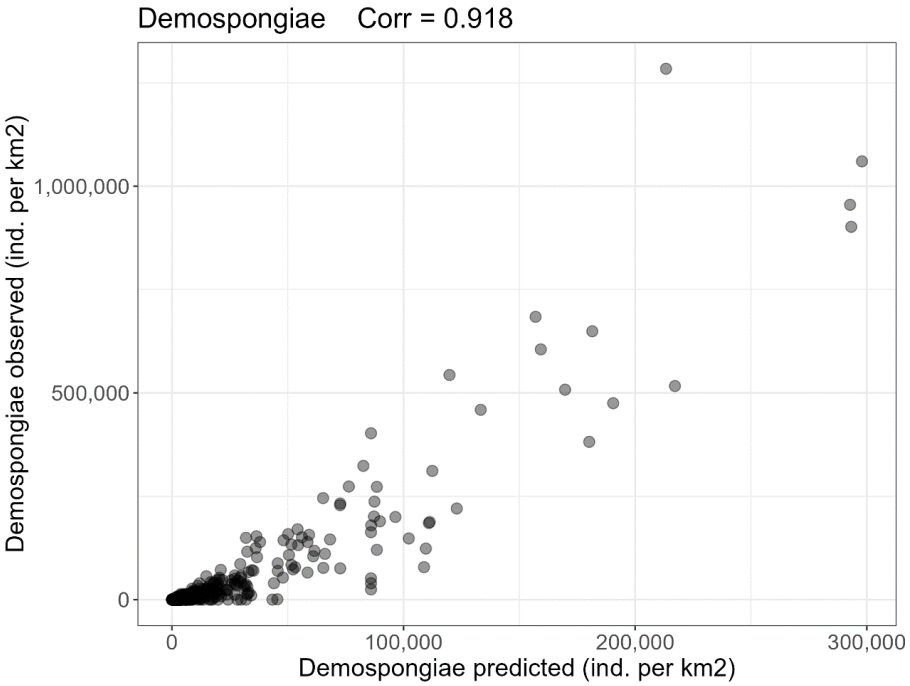

Figure A2-6 | Predicted estimates of density (*data-driven* approach) compared to observed estimates of density (DTIS data) for Desmospongiae.

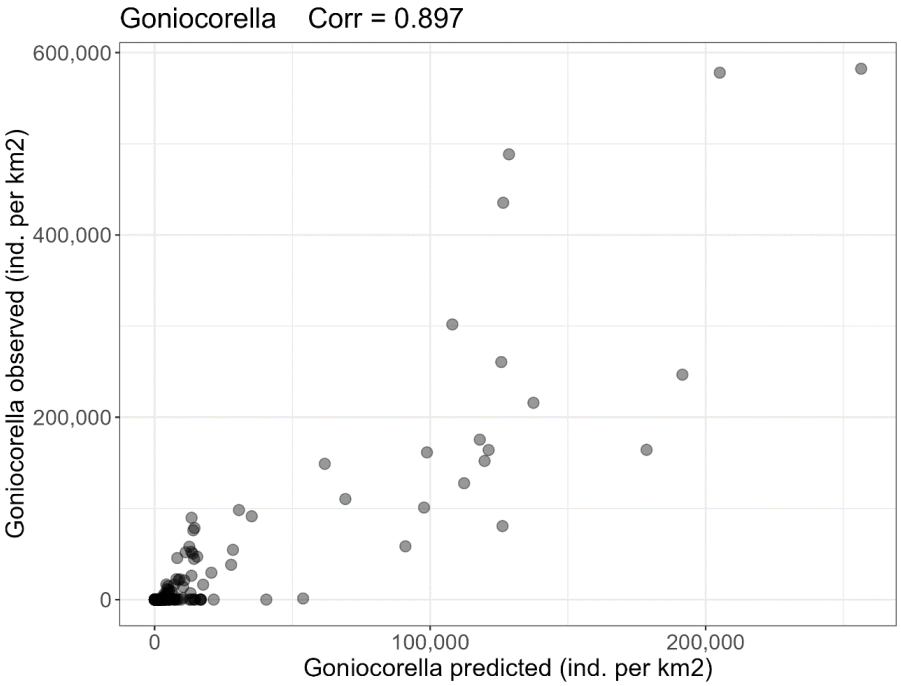

Figure A2-7 | Predicted estimates of density (*data-driven* approach) compared to observed estimates of density (DTIS data) for *Goniocorella dumosa*.

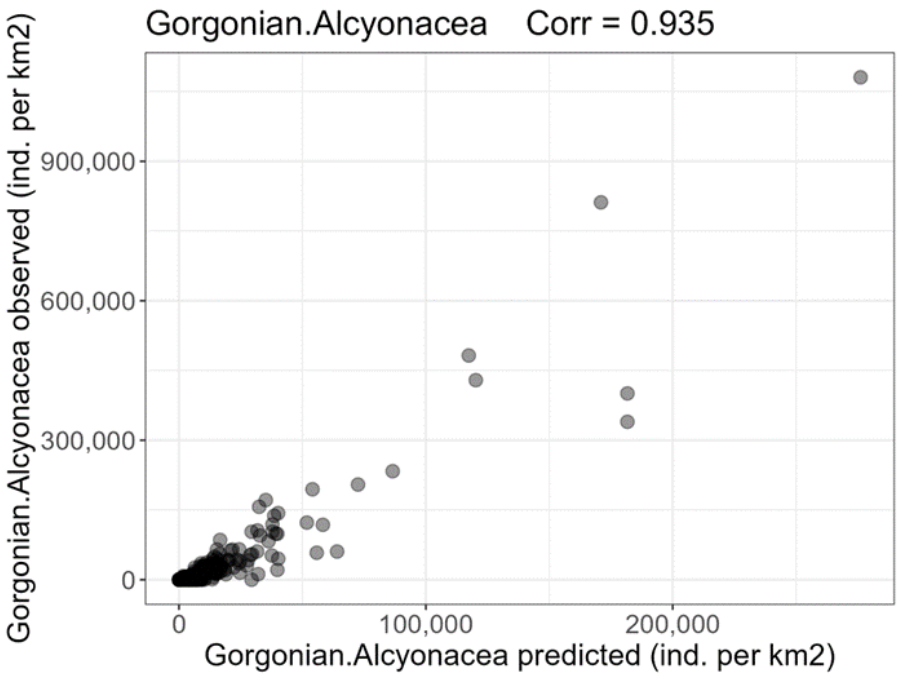

Figure A2-8 | Predicted estimates of density (*data-driven* approach) compared to observed estimates of density (DTIS data) for Gorgonian Alcyonacea.

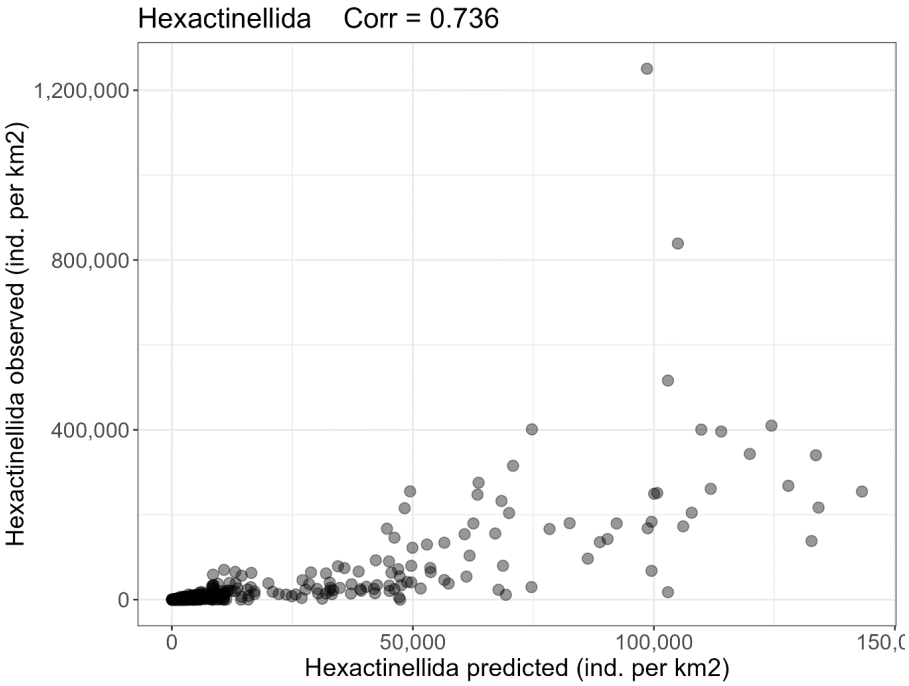

Figure A2-9 | Predicted estimates of density (*data-driven* approach) compared to observed estimates of density (DTIS data) for Hexactinellida.

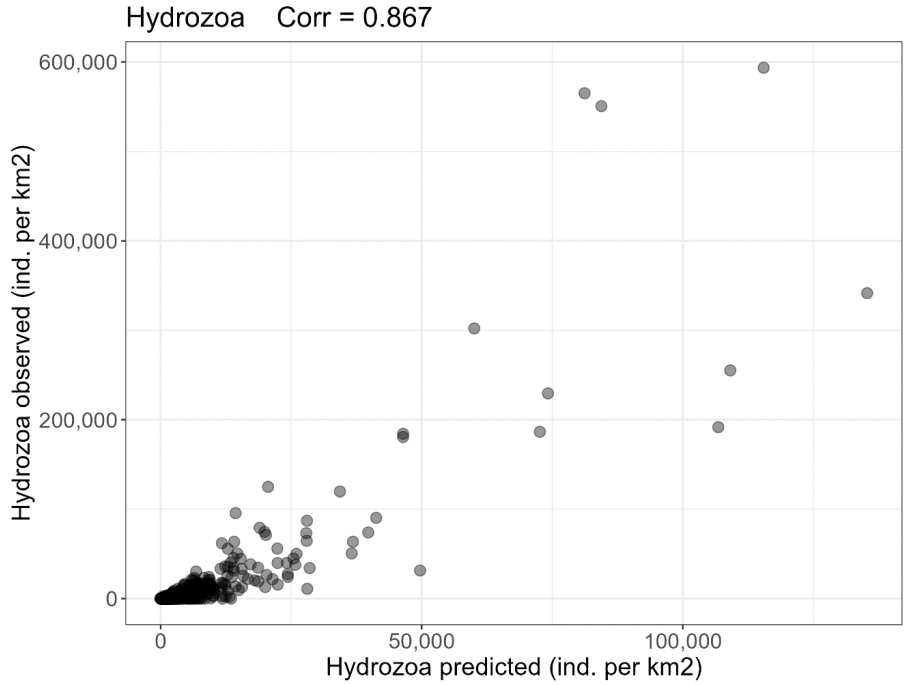

Figure A2-10 | Predicted estimates of density (*data-driven* approach) compared to observed estimates of density (DTIS data) for Hydrozoa.

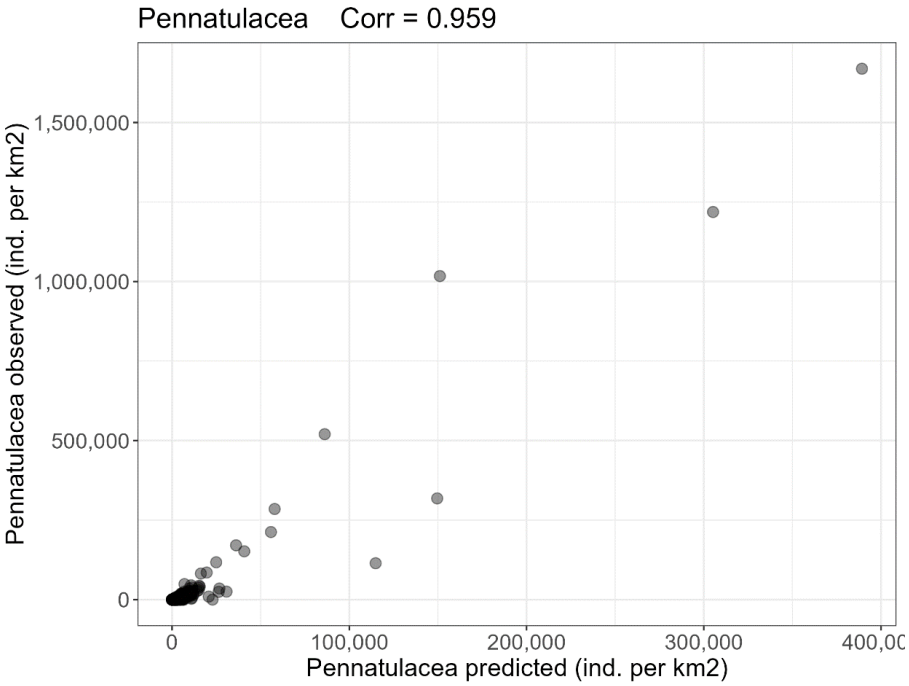

Figure A2-11 | Predicted estimates of density (*data-driven* approach) compared to observed estimates of density (DTIS data) for Pennatulacea.

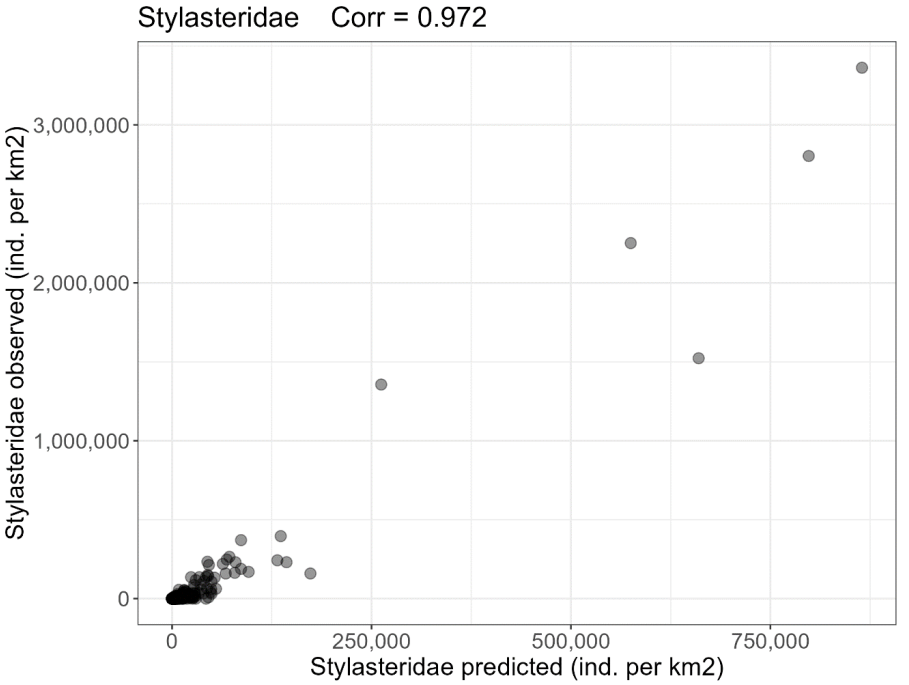

Figure A2-12 | Predicted estimates of density (*data-driven* approach) compared to observed estimates of density (DTIS data) for Stylasteridae.

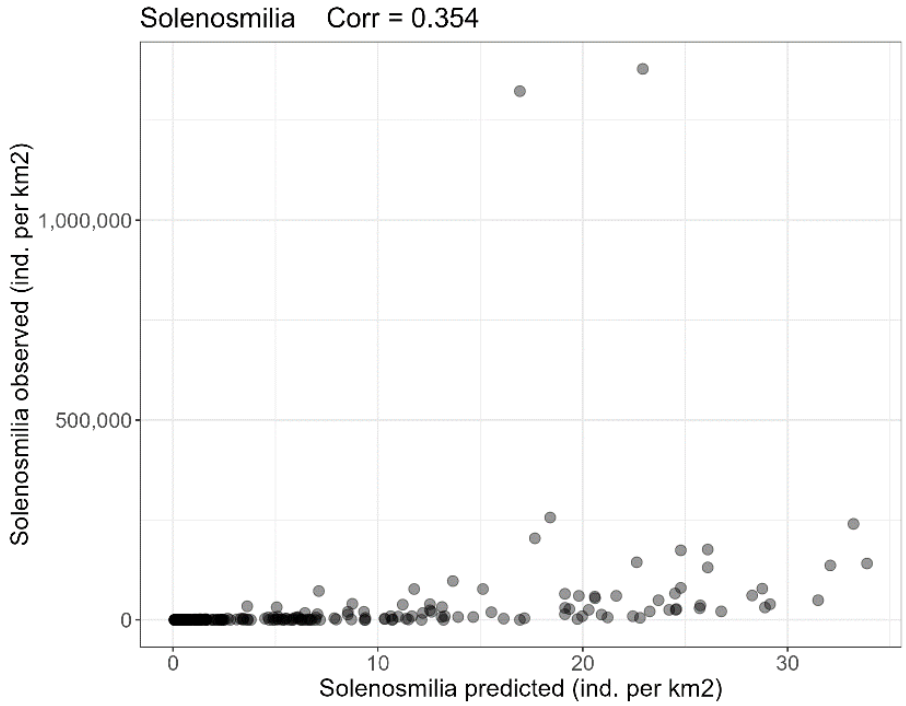

Figure A2-13 | Predicted estimates of density (*data-driven* approach) compared to observed estimates of density (DTIS data) for *Solenosmilia variabilis*.

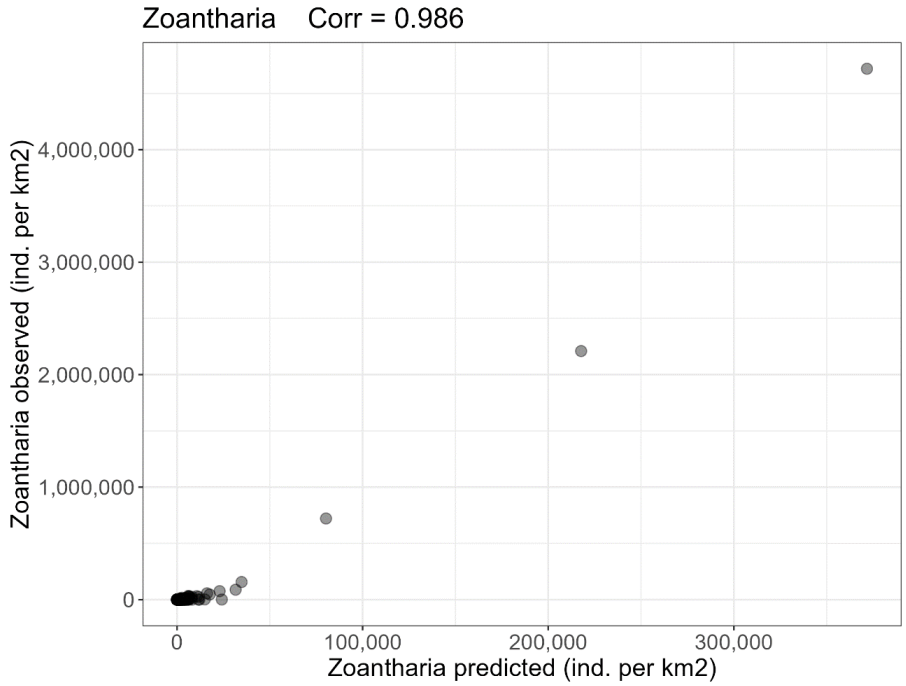

Figure A2-14 | Predicted estimates of density (*data-driven* approach) compared to observed estimates of density (DTIS data) for Zoantharia.

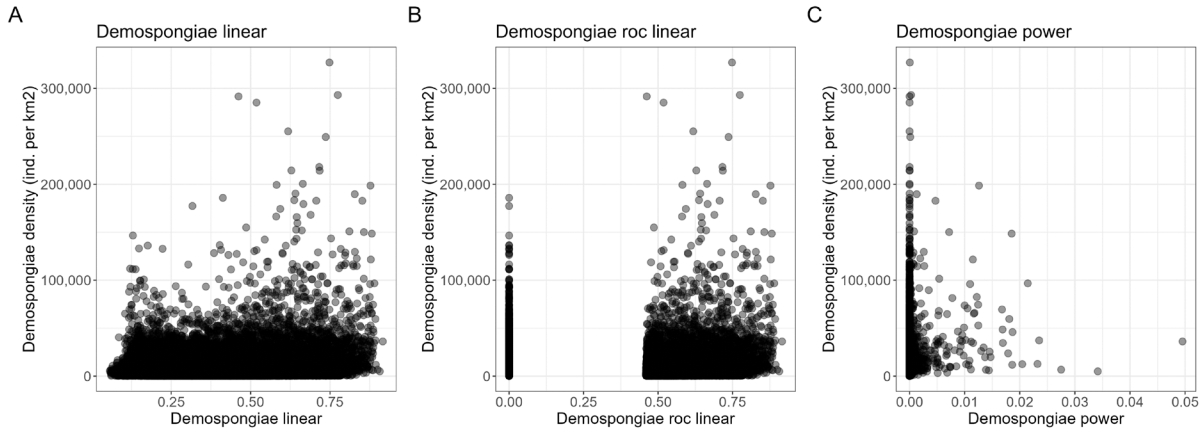

Figure A2-15 | Predicted estimates of density (*data-driven* approach) of Demospongiae compared to predictions from different methods previously used to estimate (or proxy for) abundance (a) habitat suitability modelling; (b) thresholded habitat suitability model based on the ROC AUC; (c) Power transformed habitat suitability model. Samples represent a randomly selected subset of 10% of the modelled area due to the high number of points.

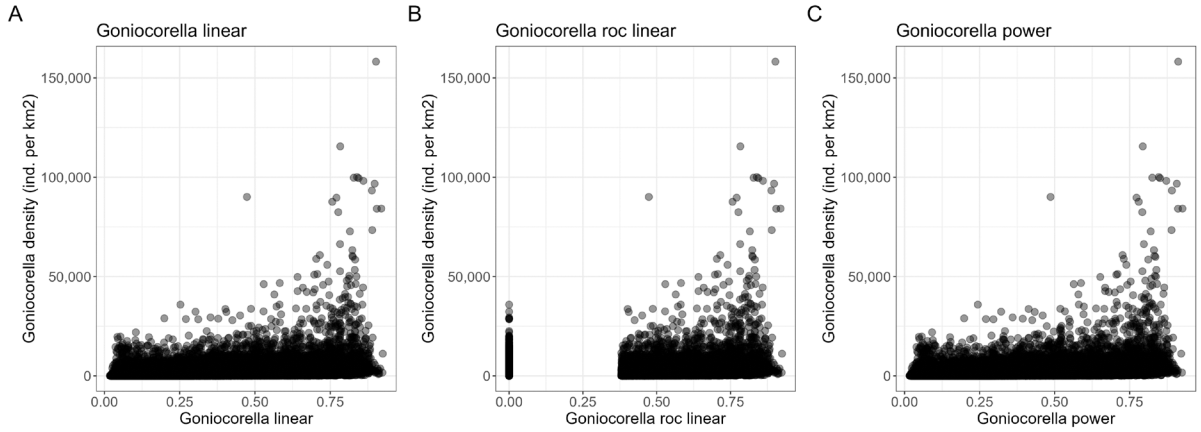

Figure A2-16 | Predicted estimates of density (*data-driven* approach) of *Goniocorella dumosa* compared to predictions from different methods previously used to estimate (or proxy for) abundance (a) habitat suitability modelling; (b) thresholded habitat suitability model based on the ROC AUC; (c) Power transformed habitat suitability model. Samples represent a randomly selected subset of 10% of the modelled area due to the high number of points.

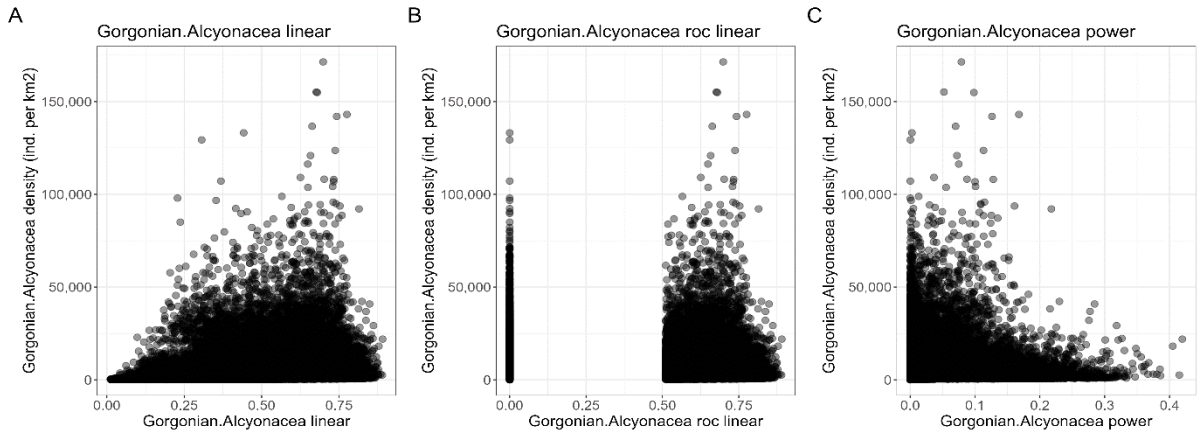

Figure A2-17 | Predicted estimates of density (*data-driven* approach) of Gorgonian Alcyonacea compared to predictions from different methods previously used to estimate (or proxy for) abundance (a) habitat suitability modelling; (b) thresholded habitat suitability model based on the ROC AUC; (c) Power transformed habitat suitability model. Samples represent a randomly selected subset of 10% of the modelled area due to the high number of points.

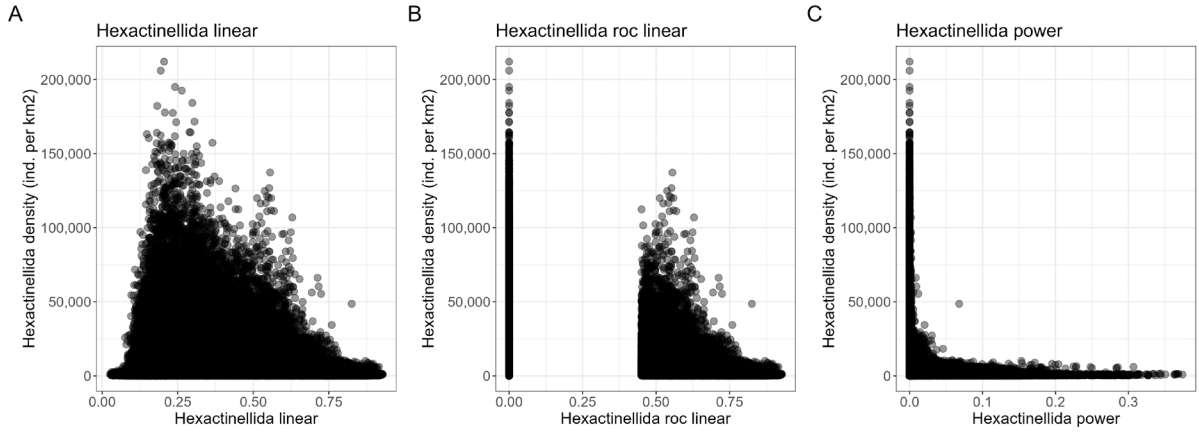

Figure A2-18 | Predicted estimates of density (*data-driven* approach) of Hexactinellida compared to predictions from different methods previously used to estimate (or proxy for) abundance (a) habitat suitability modelling; (b) thresholded habitat suitability model based on the ROC AUC; (c) Power transformed habitat suitability model. Samples represent a randomly selected subset of 10% of the modelled area due to the high number of points.

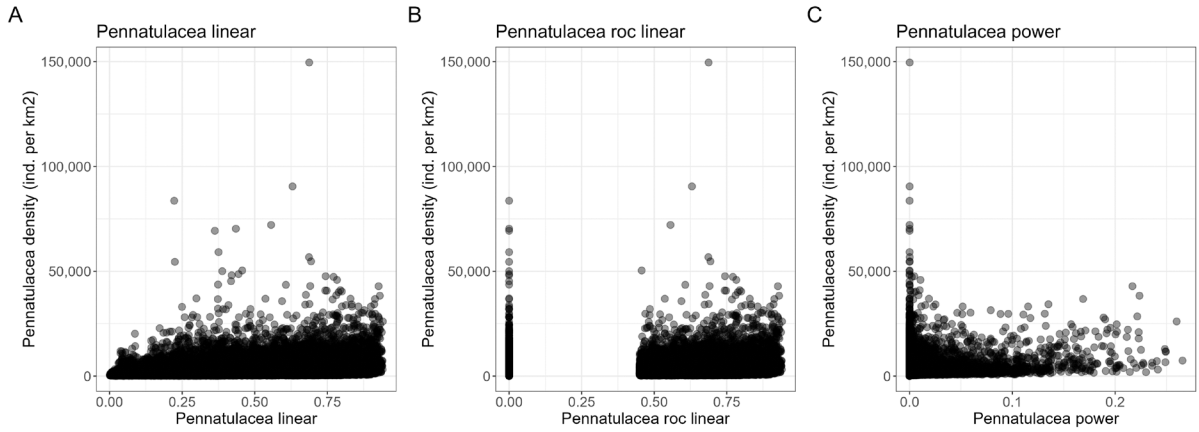

Figure A2-19 | Predicted estimates of density (*data-driven* approach) of Pennatulacea compared to predictions from different methods previously used to estimate (or proxy for) abundance (a) habitat suitability modelling; (b) thresholded habitat suitability model based on the ROC AUC; (c) Power transformed habitat suitability model. Samples represent a randomly selected subset of 10% of the modelled area due to the high number of points.

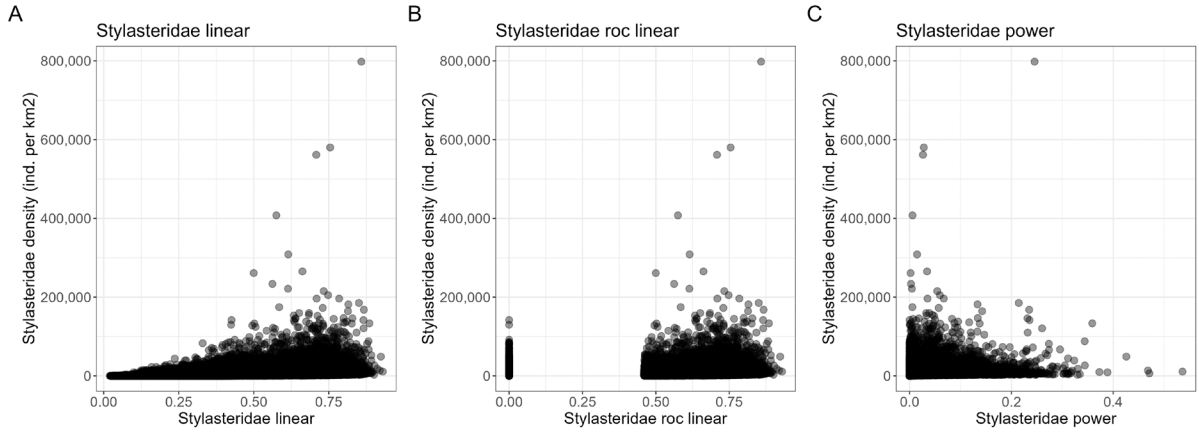

Figure A2-20 | Predicted estimates of density (*data-driven* approach) of Stylasteridae compared to predictions from different methods previously used to estimate (or proxy for) abundance (a) habitat suitability modelling; (b) thresholded habitat suitability model based on the ROC AUC; (c) Power transformed habitat suitability model. Samples represent a randomly selected subset of 10% of the modelled area due to the high number of points.

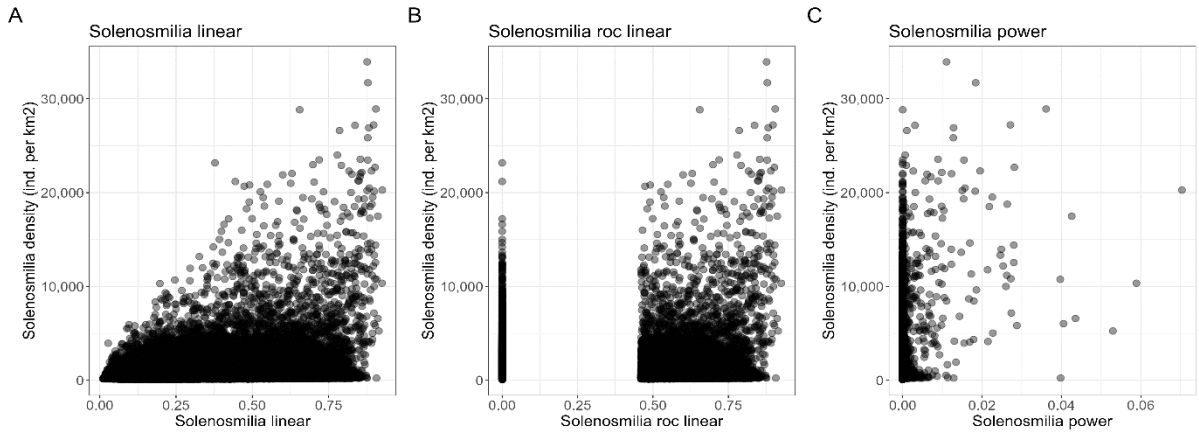

Figure A2-21| Predicted estimates of density (*data-driven* approach) of *Solenosmilia variabilis* compared to predictions from different methods previously used to estimate (or proxy for) abundance (a) habitat suitability modelling; (b) thresholded habitat suitability model based on the ROC AUC; (c) Power transformed habitat suitability model. Samples represent a randomly selected subset of 10% of the modelled area due to the high number of points.

Table A11 | Correlation (Pearson's r) for the density models of 15 VME indicator taxa and their estimates of abundance (using DTIS data) within the boundaries of the bioregions (from Costello et al., 2017) overlapping the area of the study. Cell values with '-' indicate that there was not enough data to evaluate performance and 'NA' values indicate that correlation could not be calculated, with all data being 0.

	Correlation (Pearson's r)				
VME indicator taxon	**Tropical Australia & Coral Sea**	**Tasman Sea – SW Pacific**	**Mid-South Tropical Pacific**	**New Zealand**	**Southern Ocean**
No. of DTIS data points	**0**	**0**	**73**	**753**	**6**
Actiniaria	-	-	0.712	0.81	NA
Alcyonacea	-	-	0.724	0.91	0.933
Antipatharia	-	-	0.828	0.75	0.559
Brisingida	-	-	0.825	0.958	0.582
Bryozoa	-	-	0.453	0.991	0.639
Crinoidea	-	-	0.96	0.857	-0.542
Demospongiae	-	-	0.731	0.918	0.808
Goniocorella dumosa	-	-	NA	0.897	NA
Gorgonacea Alcyonacea	-	-	0.86	0.93	0.987
Hexactinellida	-	-	0.734	0.728	0.947
Hydrozoa	-	-	0.899	0.867	0.691
Pennatulacea	-	-	0.81	0.959	0.984
Solenosmilia variabilis	-	-	0.617	0.372	0.216
Stylasteridae	-	-	0.786	0.972	0.93
Zoantharia	-	-	0.758	0.986	NA

Table A2-12 | Correlation (Pearson's r) for the final ensembled (BRT and RF) density models of 15 VME indicator taxa and their estimates of abundance (observations using DTIS data) within the boundaries of the Fishery Management Areas (FMAs) within the Evaluated Area. Cell values with '-' indicate that there was not enough data to evaluate performance.

	Correlation (Pearson's r)								
VME indicator taxon	**S. Lord Howe**	**N. Lord Howe**	**NW. Challenger**	**W. Norfolk**	**N. Louisville**	**C. Louisville**	**S. Louisville**	**Westpac Bank**	**South Tasman**
No. of DTIS data points	**0**	**0**	**17**	**0**	**73**	**45**	**0**	**3**	**0**
Actiniaria	-	-	0.847	-	0.712	0.84	-	-0.99	-
Alcyonacea	-	-	0.94	-	0.724	0.78	-	0.49	-
Antipatharia	-	-	0.525	-	0.828	0.495	-	0.99	-
Brisingida	-	-	0.949	-	0.825	0.941	-	0.95	-
Bryozoa	-	-	0.036	-	0.453	-	-	-	-
Crinoidea	-	-	-0.153	-	0.96	0.871	-	-	-
Demospongiae	-	-	0.951	-	0.731	0.743	-	1.0	-
Goniocorella dumosa	-	-	-	-	-	-	-	-	-
Gorgonacea Alcyonacea	-	-	0.851	-	0.86	0.742	-	0.91	-
Hexactinellida	-	-	0.101	-	0.734	0.852	-	-	-
Hydrozoa	-	-	-	-	0.899	0.784	-	-	-
Pennatulacea	-	-	0.731	-	0.81	0.804	-	0.84	-
Solenosmilia variabilis	-	-	-	-	0.617	0.518	-	-	-
Stylasteridae	-	-	-	-	0.786	0.611	-	-	-
Zoantharia	-	-	-	-	0.758	0.949	-	-	-

Annex 3 - Data-driven models

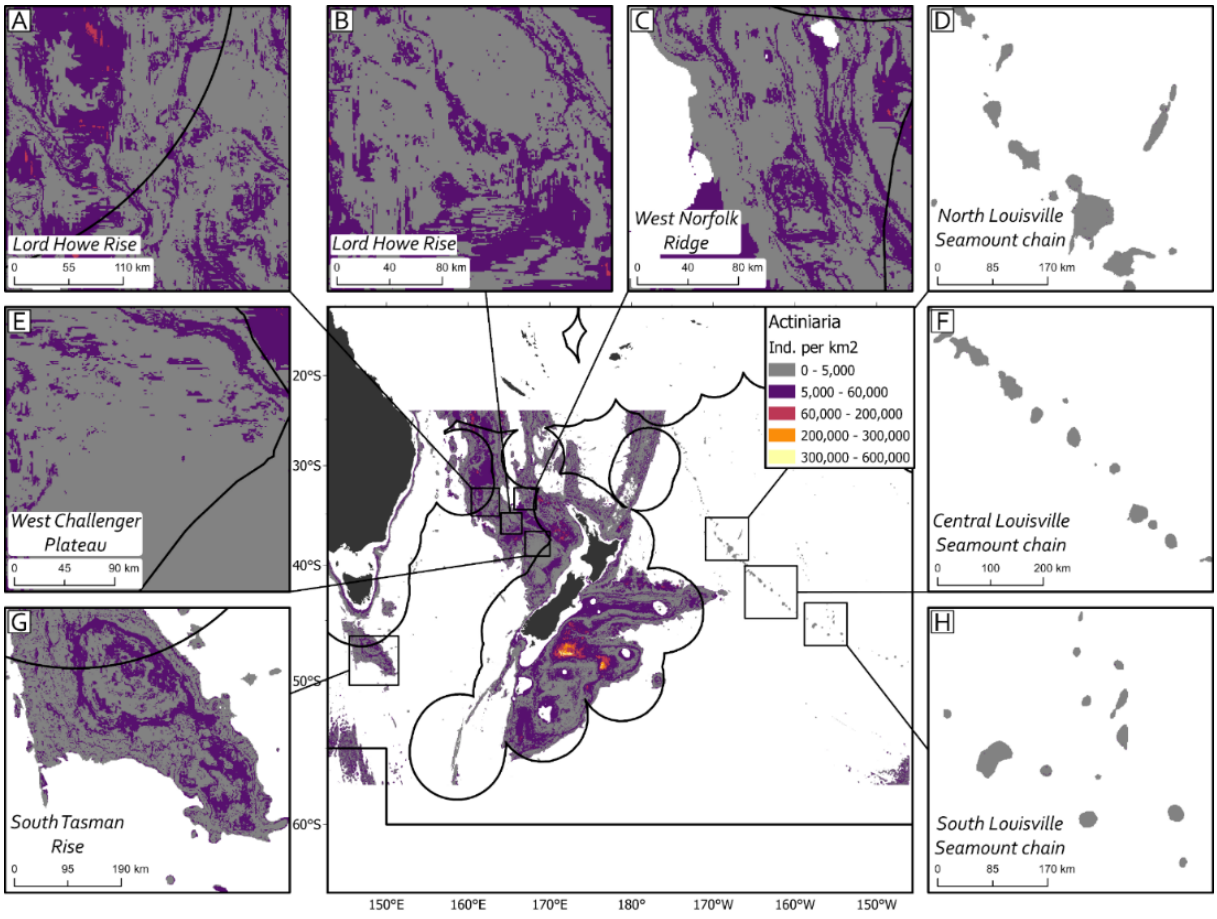

Figure A3-1 | Predicted density (individuals per km^2) of Actinaria in the study area from the hurdle model approach (DTIS *data-driven* approach). Inset maps of the high seas in the study area: (a) West Lord Howe Rise; (b) East Lord Howe Rise; (c) West Norfolk Ridge; (d) North Louisville Seamount Chain; (e) West Challenger Plateau; (f) Central Louisville Seamount Chain; (g) South Tasman Rise; and (h) South Louisville Seamount Chain**.**

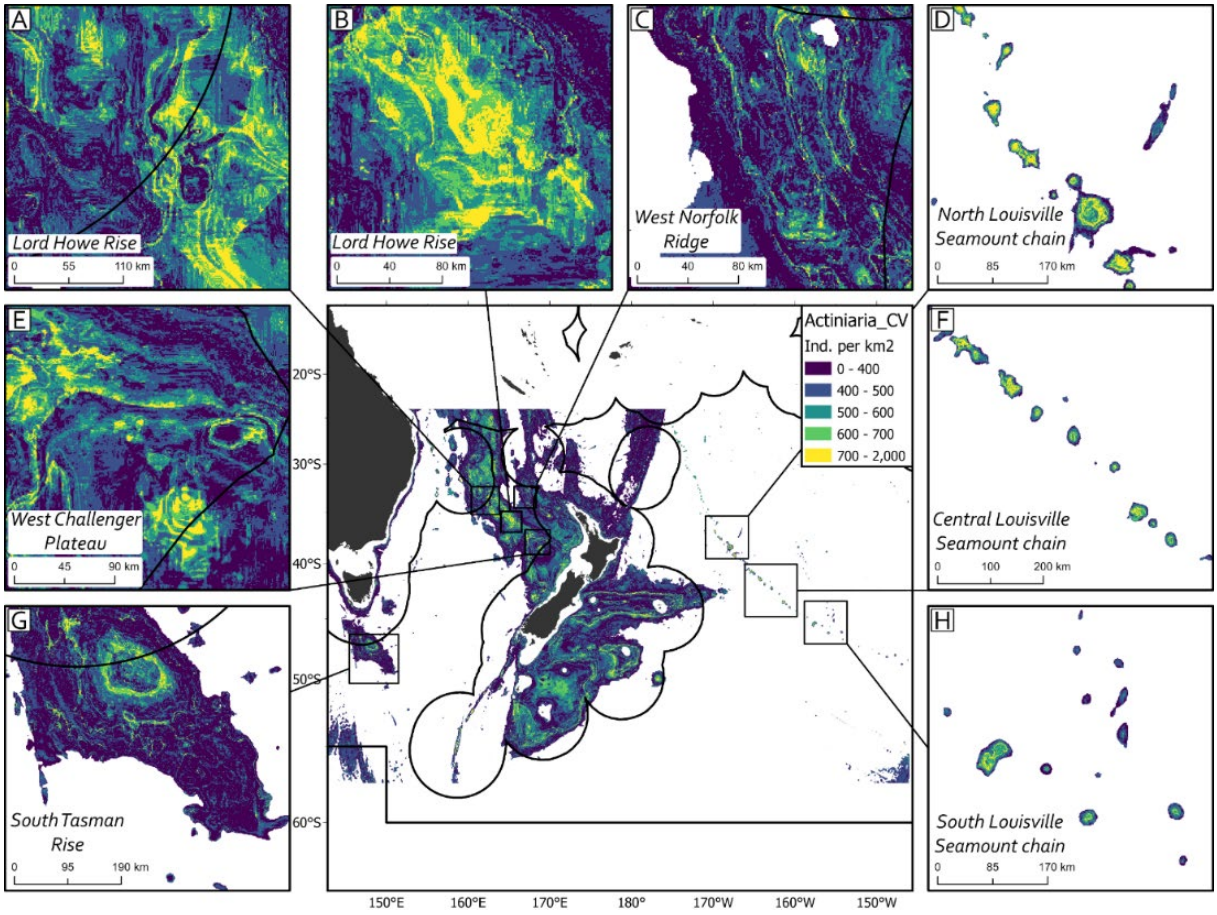

Figure A3-2 | Coefficient of variation (CV) (individuals per km^2) of Actinaria in the study area from the hurdle model approach (DTIS *data-driven* approach). Inset maps of the high seas in the study area: (a) West Lord Howe Rise; (b) East Lord Howe Rise; (c) West Norfolk Ridge; (d) North Louisville Seamount Chain; (e) West Challenger Plateau; (f) Central Louisville Seamount Chain; (g) South Tasman Rise; and (h) South Louisville Seamount Chain**.**

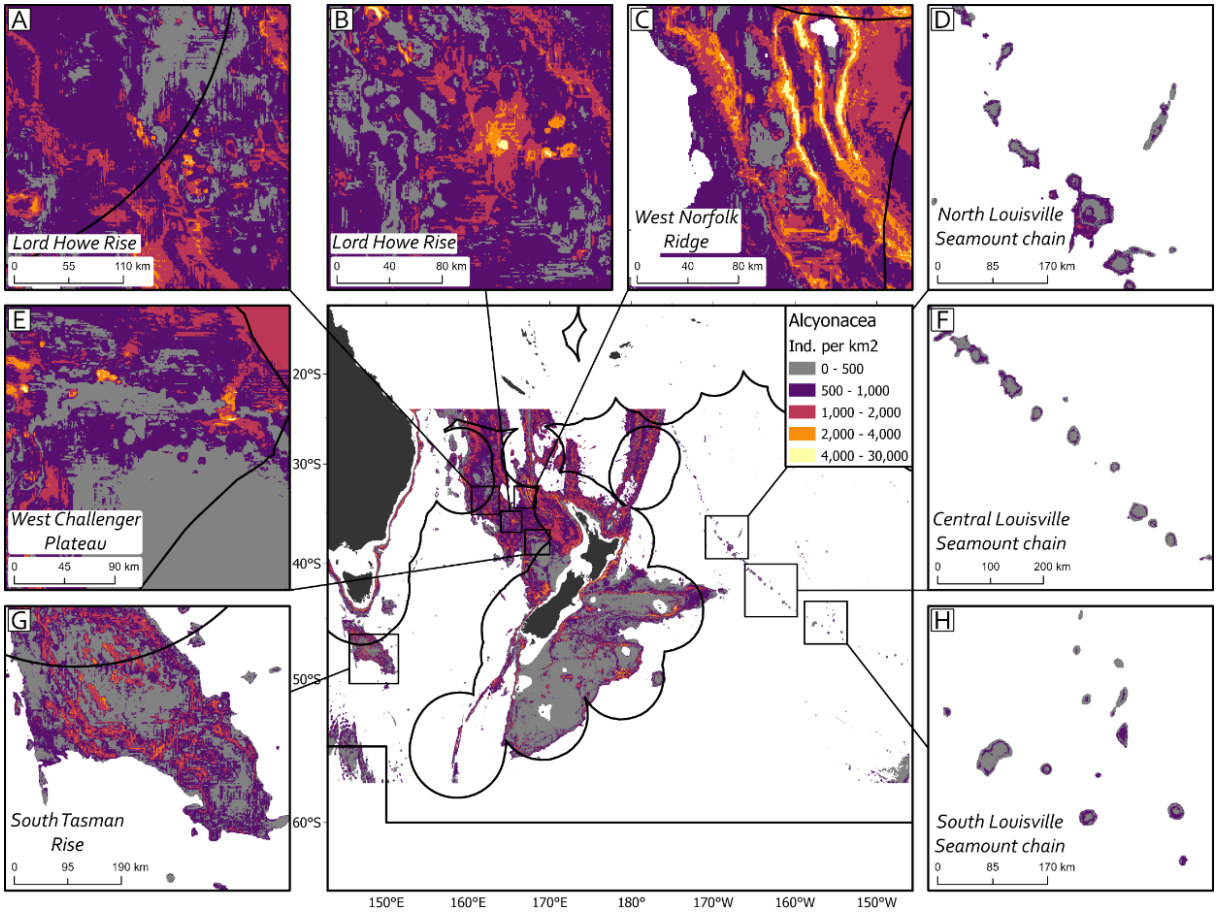

Figure A3-3 | Predicted density (individuals per km^2) of Alcyonacea in the study area from the hurdle model approach (DTIS *data-driven* approach). Inset maps of the high seas in the study area: (a) West Lord Howe Rise; (b) East Lord Howe Rise; (c) West Norfolk Ridge; (d) North Louisville Seamount Chain; (e) West Challenger Plateau; (f) Central Louisville Seamount Chain; (g) South Tasman Rise; and (h) South Louisville Seamount Chain**.**

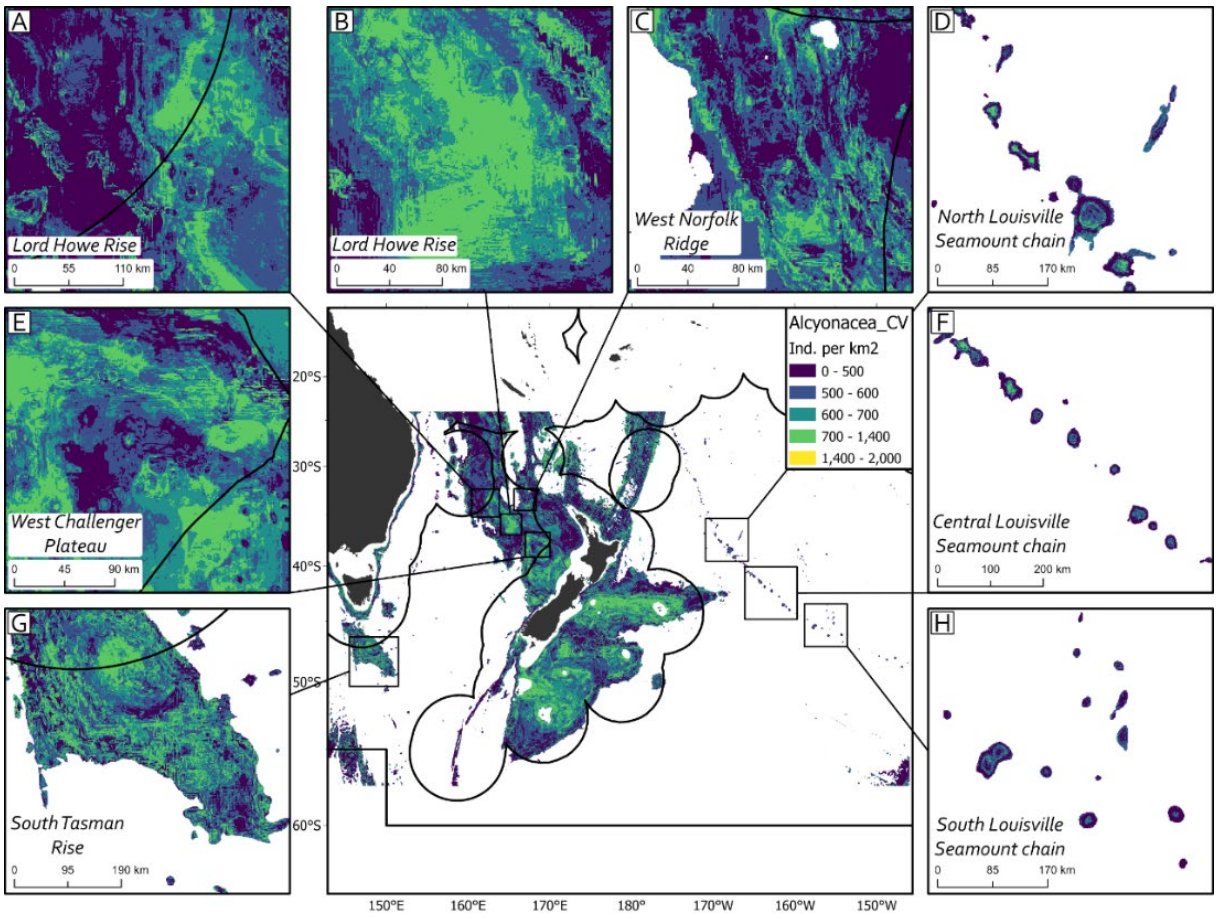

Figure A3-4 | Coefficient of variation (CV) (individuals per km^2) of Alcyonacea in the study area from the hurdle model approach (DTIS *data-driven* approach). Inset maps of the high seas in the study area: (a) West Lord Howe Rise; (b) East Lord Howe Rise; (c) West Norfolk Ridge; (d) North Louisville Seamount Chain; (e) West Challenger Plateau; (f) Central Louisville Seamount Chain; (g) South Tasman Rise; and (h) South Louisville Seamount Chain**.**

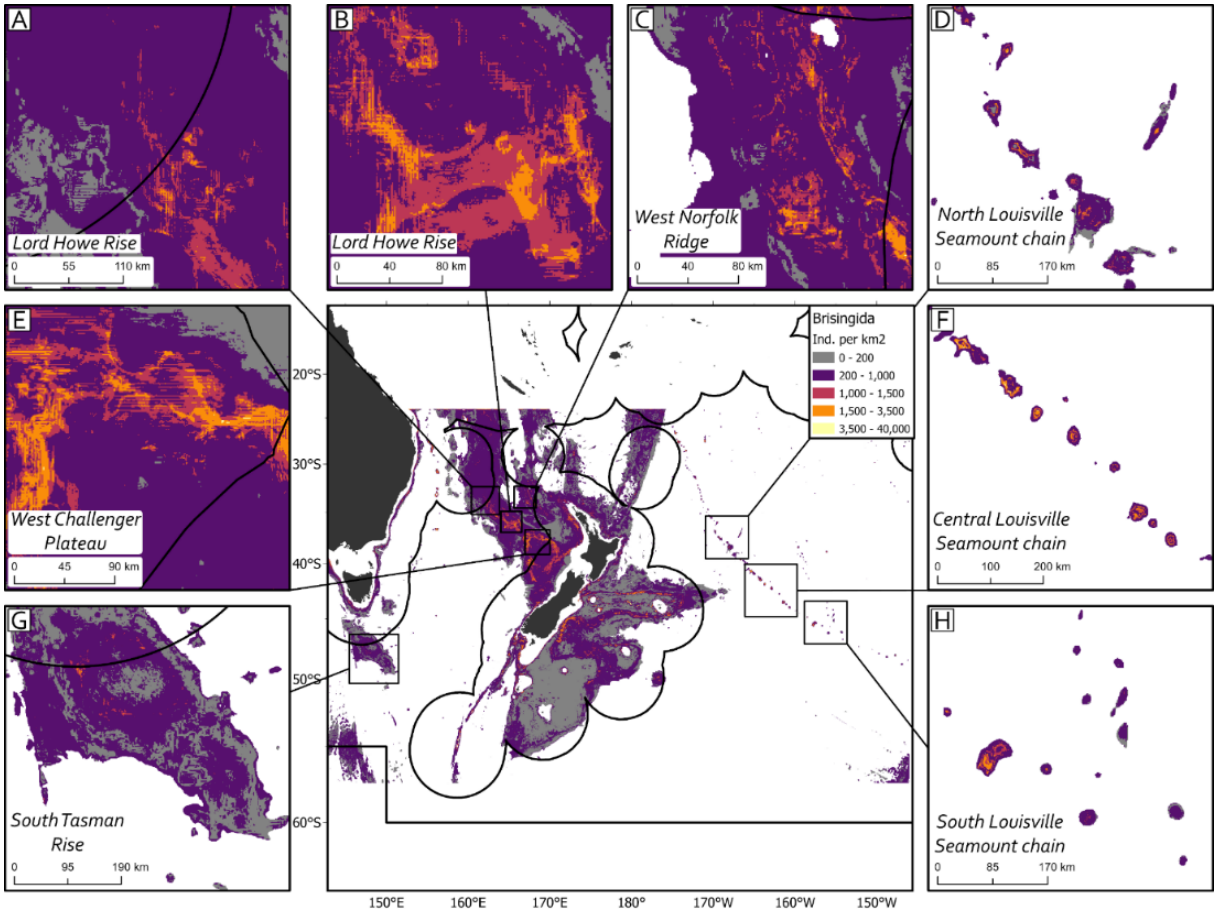

Figure A3-5 | Predicted density (individuals per km^2) of Brisingida in the study area from the hurdle model approach (DTIS *data-driven* approach). Inset maps of the high seas in the study area: (a) West Lord Howe Rise; (b) East Lord Howe Rise; (c) West Norfolk Ridge; (d) North Louisville Seamount Chain; (e) West Challenger Plateau; (f) Central Louisville Seamount Chain; (g) South Tasman Rise; and (h) South Louisville Seamount Chain**.**

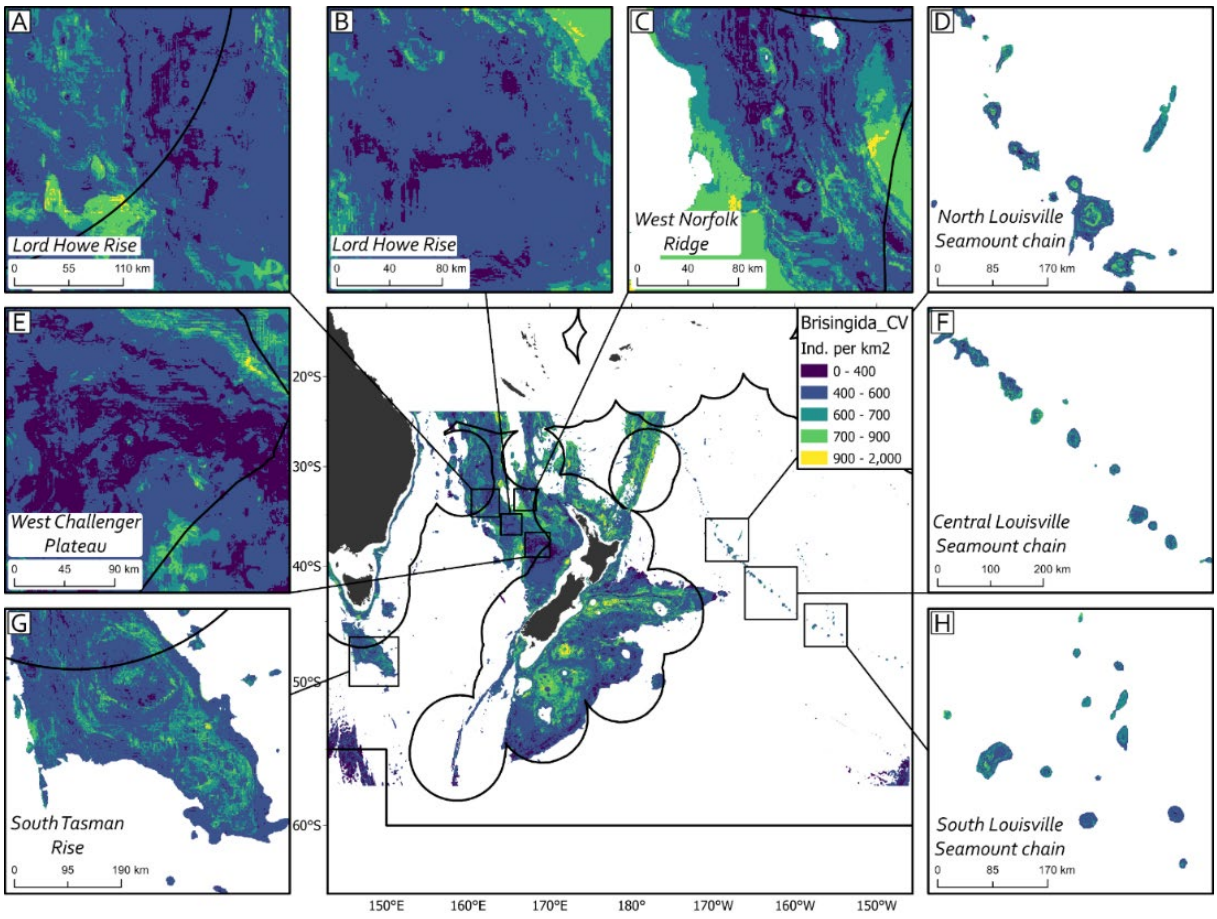

Figure A3-6 | Coefficient of variation (CV) (individuals per km^2) of Brisingida in the study area from the hurdle model approach (DTIS *data-driven* approach). Inset maps of the high seas in the study area: (a) West Lord Howe Rise; (b) East Lord Howe Rise; (c) West Norfolk Ridge; (d) North Louisville Seamount Chain; (e) West Challenger Plateau; (f) Central Louisville Seamount Chain; (g) South Tasman Rise; and (h) South Louisville Seamount Chain**.**

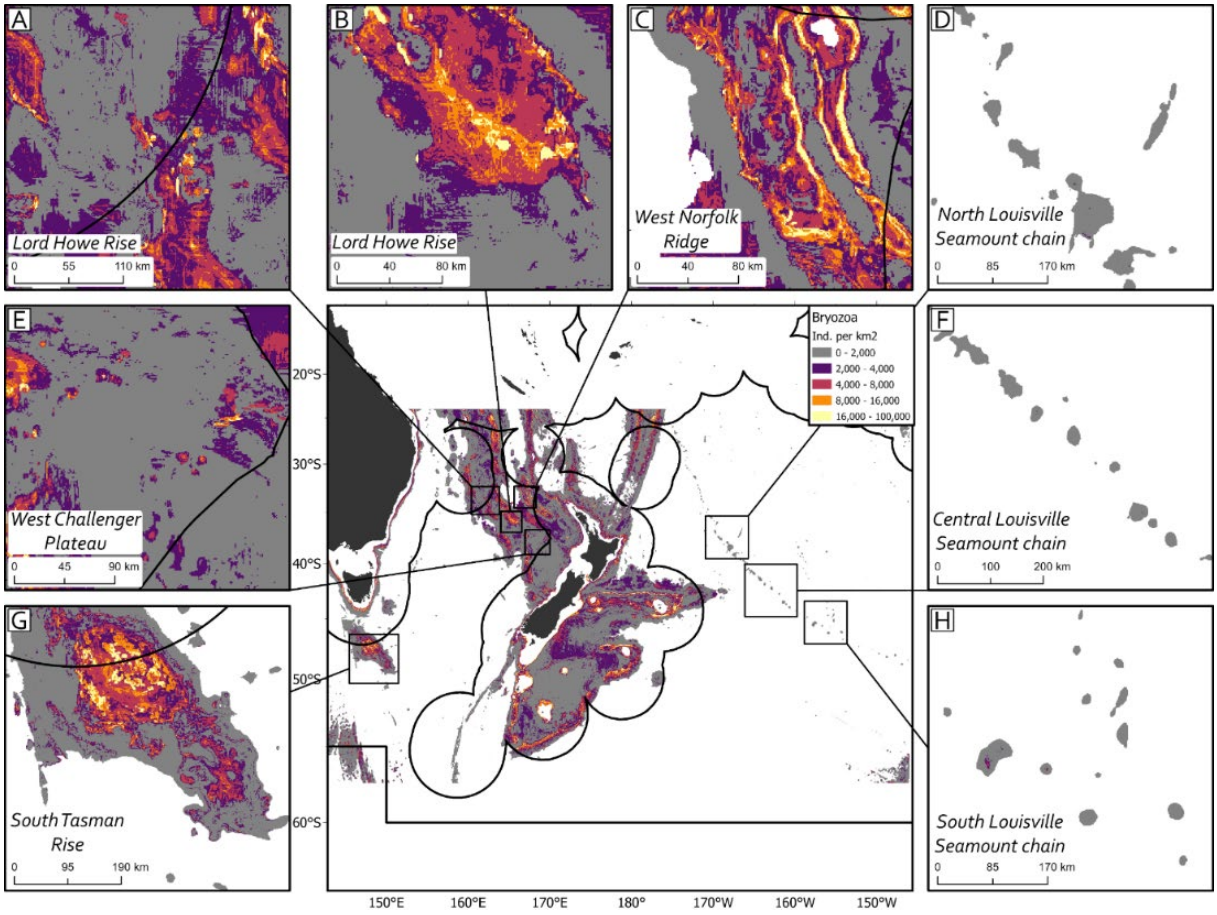

Figure A3-7 | Predicted density (individuals per km^2) of Bryozoa in the study area from the hurdle model approach (DTIS *data-driven* approach). Inset maps of the high seas in the study area: (a) West Lord Howe Rise; (b) East Lord Howe Rise; (c) West Norfolk Ridge; (d) North Louisville Seamount Chain; (e) West Challenger Plateau; (f) Central Louisville Seamount Chain; (g) South Tasman Rise; and (h) South Louisville Seamount Chain**.**

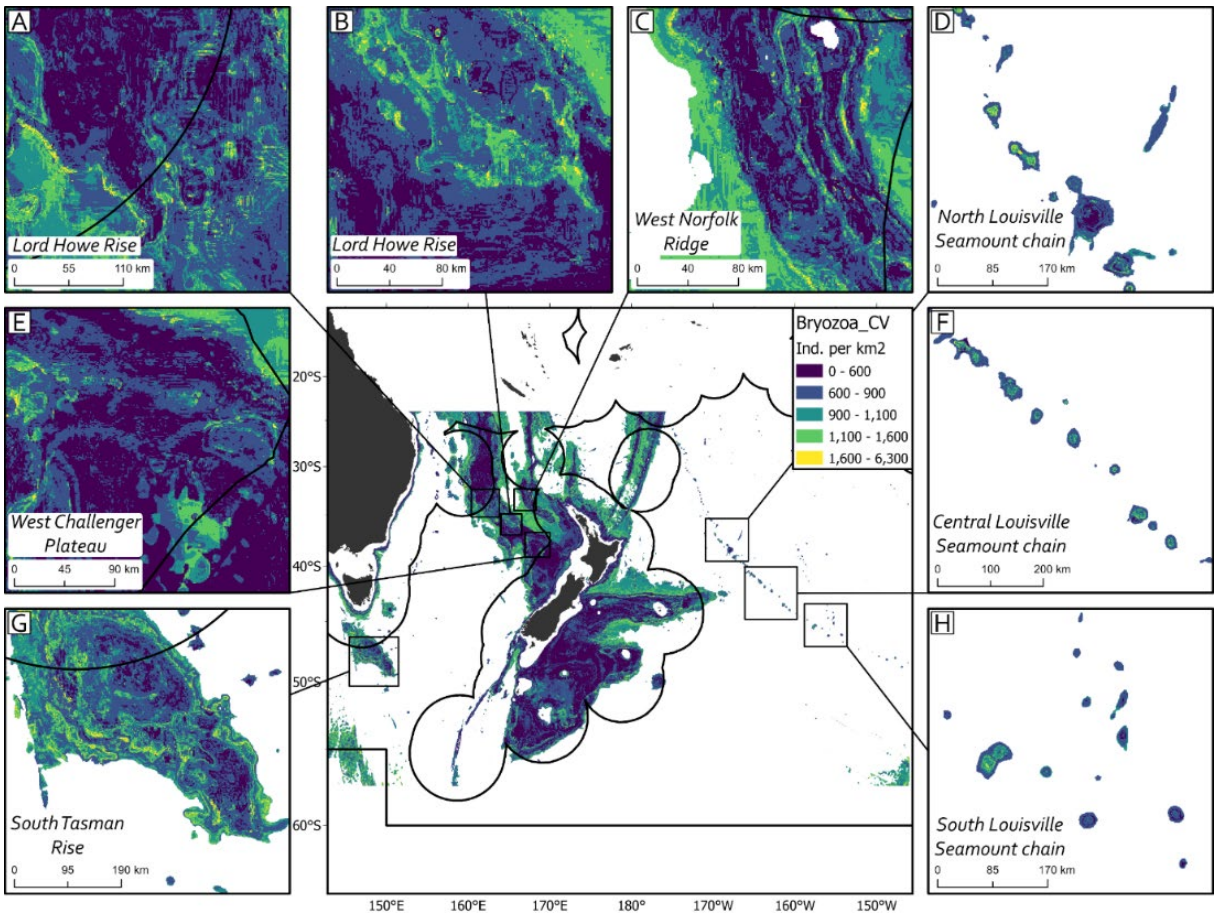

Figure A3-8 | Coefficient of variation (CV) (individuals per km^2) of Bryozoa in the study area from the hurdle model approach (DTIS *data-driven* approach). Inset maps of the high seas in the study area: (a) West Lord Howe Rise; (b) East Lord Howe Rise; (c) West Norfolk Ridge; (d) North Louisville Seamount Chain; (e) West Challenger Plateau; (f) Central Louisville Seamount Chain; (g) South Tasman Rise; and (h) South Louisville Seamount Chain**.**

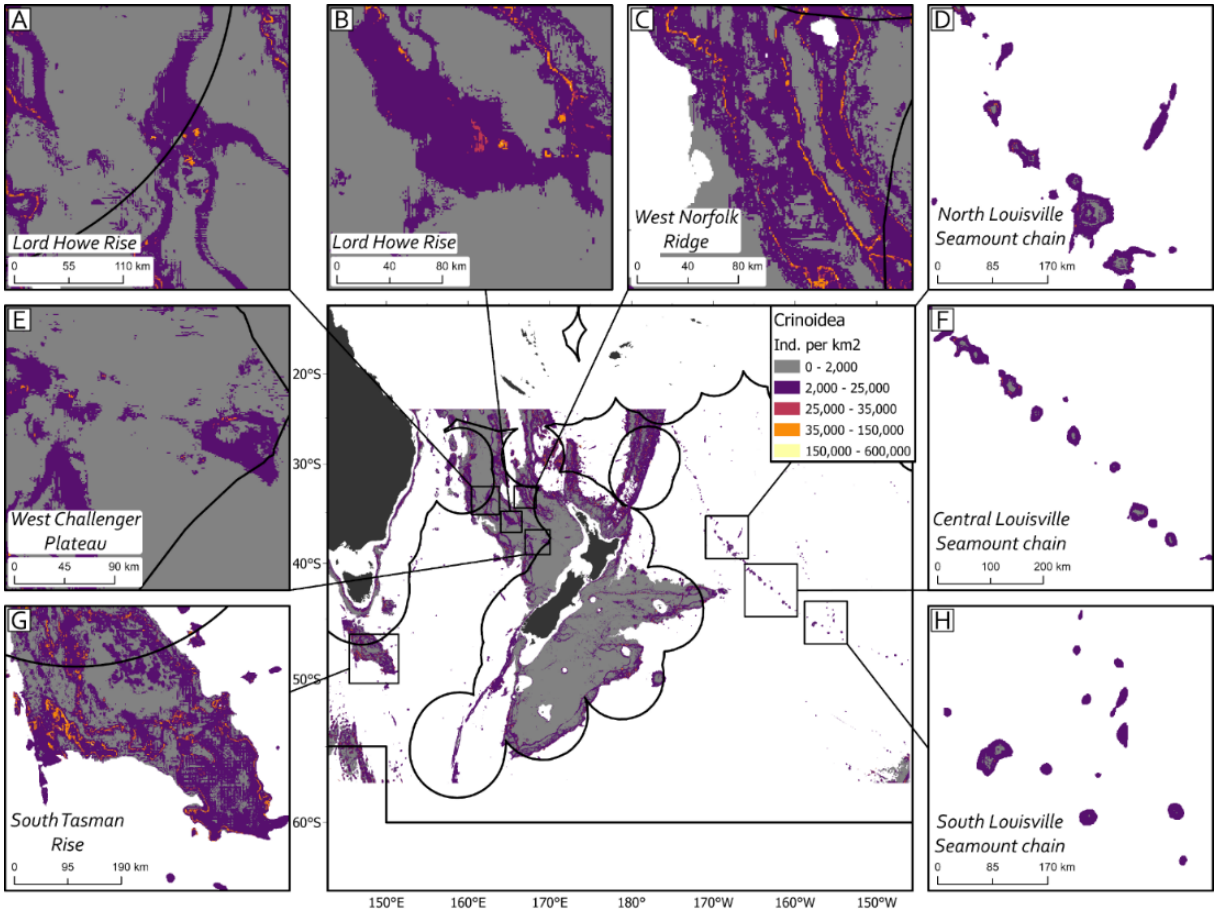

Figure A3-9 | Predicted density (individuals per km^2) of Crinoidea in the study area from the hurdle model approach (DTIS *data-driven* approach). Inset maps of the high seas in the study area: (a) West Lord Howe Rise; (b) East Lord Howe Rise; (c) West Norfolk Ridge; (d) North Louisville Seamount Chain; (e) West Challenger Plateau; (f) Central Louisville Seamount Chain; (g) South Tasman Rise; and (h) South Louisville Seamount Chain.

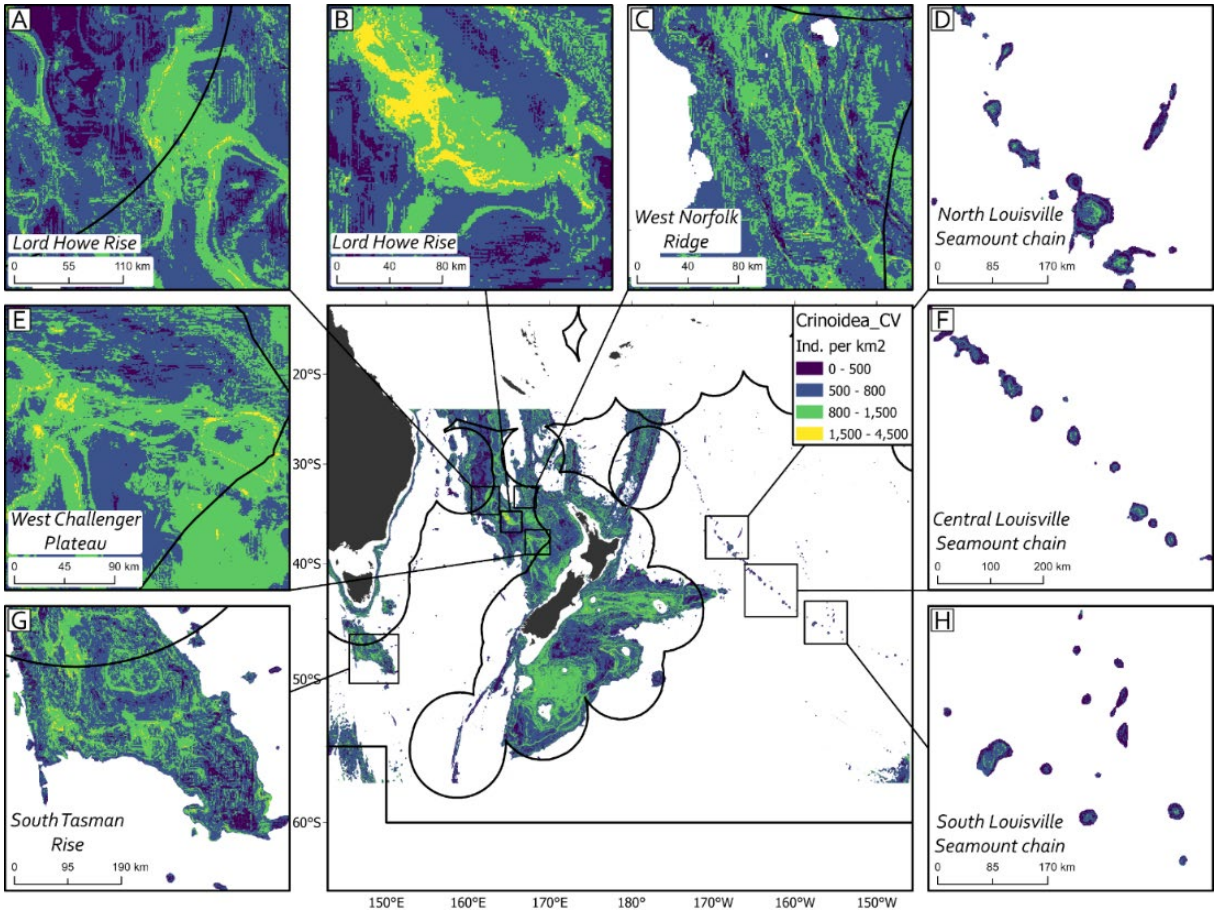

Figure A3-10 | Coefficient of variation (CV) (individuals per km^2) of Crinoidea in the study area from the hurdle model approach (DTIS *data-driven* approach). Inset maps of the high seas in the study area: (a) West Lord Howe Rise; (b) East Lord Howe Rise; (c) West Norfolk Ridge; (d) North Louisville Seamount Chain; (e) West Challenger Plateau; (f) Central Louisville Seamount Chain; (g) South Tasman Rise; and (h) South Louisville Seamount Chain**.**

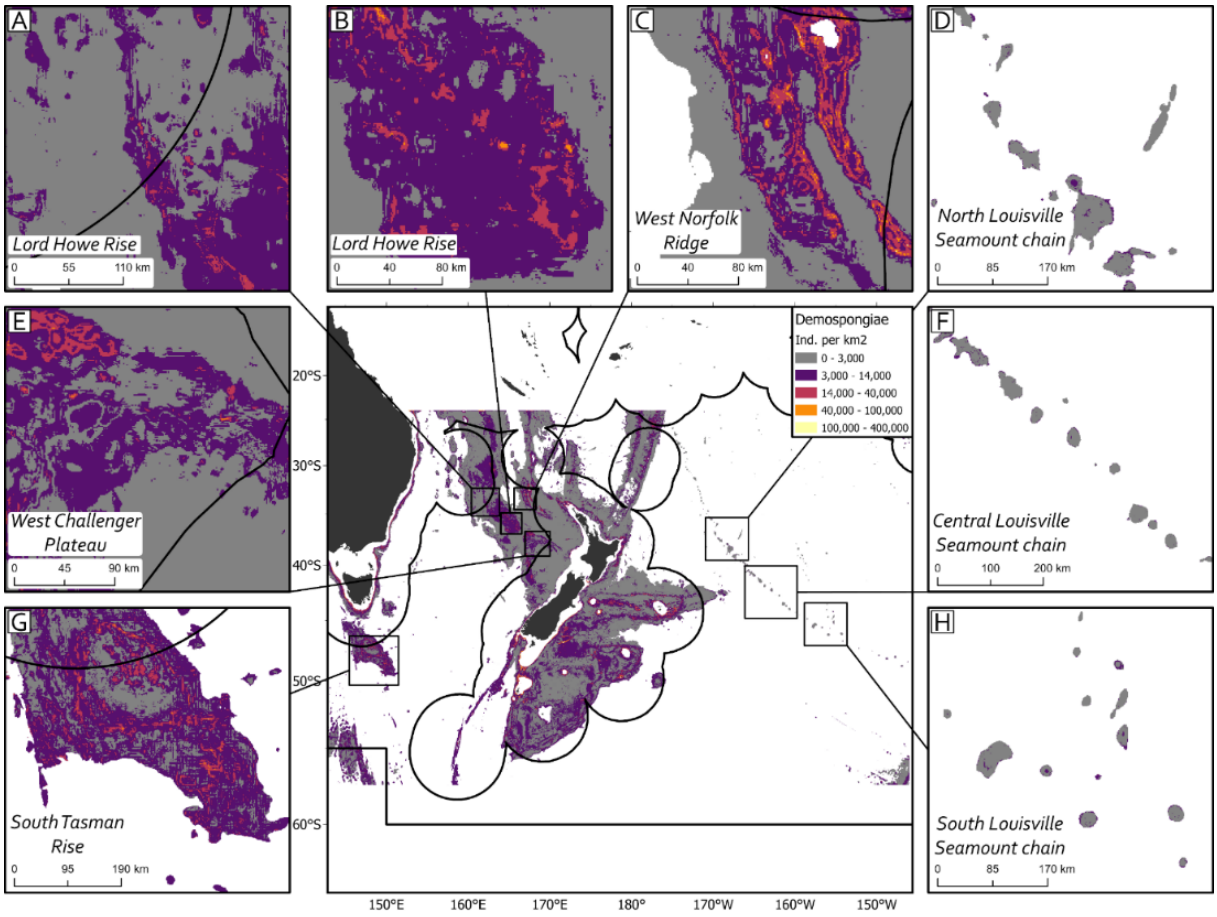

Figure A3-11 | Predicted density (individuals per km^2) of Demospongiae in the study area from the hurdle model approach (DTIS *data-driven* approach). Inset maps of the high seas in the study area: (a) West Lord Howe Rise; (b) East Lord Howe Rise; (c) West Norfolk Ridge; (d) North Louisville Seamount Chain; (e) West Challenger Plateau; (f) Central Louisville Seamount Chain; (g) South Tasman Rise; and (h) South Louisville Seamount Chain.

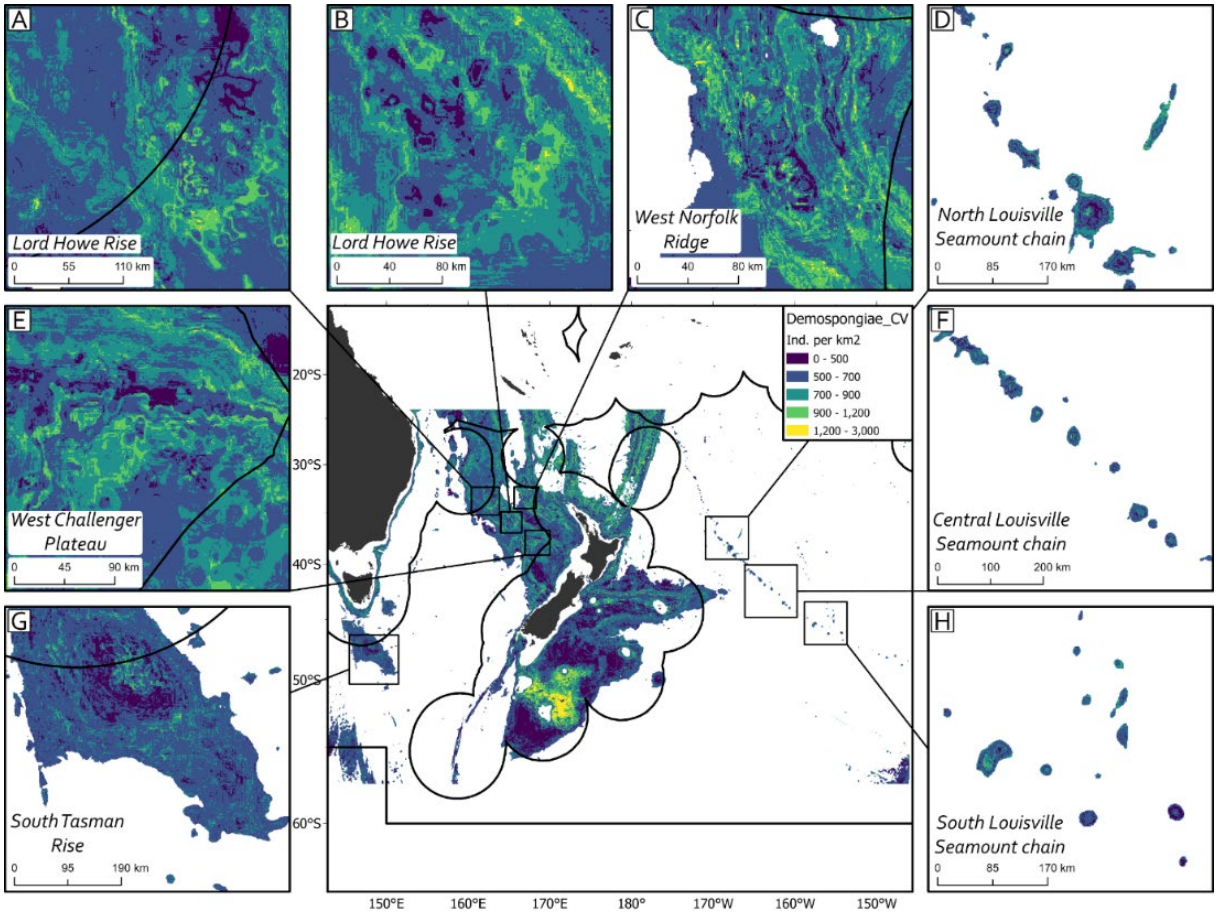

Figure A3-12 | Coefficient of variation (CV) (individuals per km^2) of Desmospongiae in the study area from the hurdle model approach (DTIS *data-driven* approach). Inset maps of the high seas in the study area: (a) West Lord Howe Rise; (b) East Lord Howe Rise; (c) West Norfolk Ridge; (d) North Louisville Seamount Chain; (e) West Challenger Plateau; (f) Central Louisville Seamount Chain; (g) South Tasman Rise; and (h) South Louisville Seamount Chain**.**

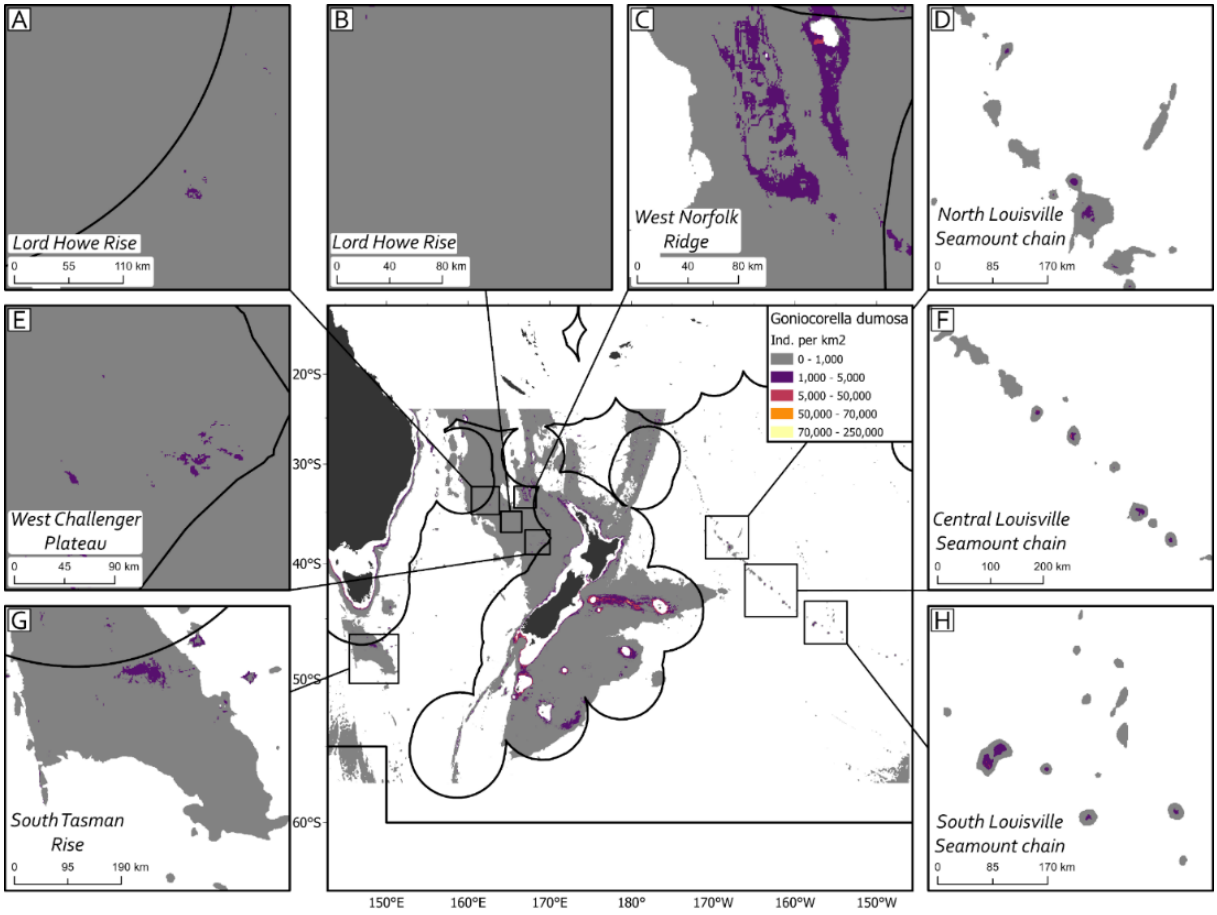

Figure A3-13 | Predicted density (individuals per km^2) of *Goniocorella dumosa* in the study area from the hurdle model approach (DTIS *data-driven* approach). Inset maps of the high seas in the study area: (a) West Lord Howe Rise; (b) East Lord Howe Rise; (c) West Norfolk Ridge; (d) North Louisville Seamount Chain; (e) West Challenger Plateau; (f) Central Louisville Seamount Chain; (g) South Tasman Rise; and (h) South Louisville Seamount Chain**.**

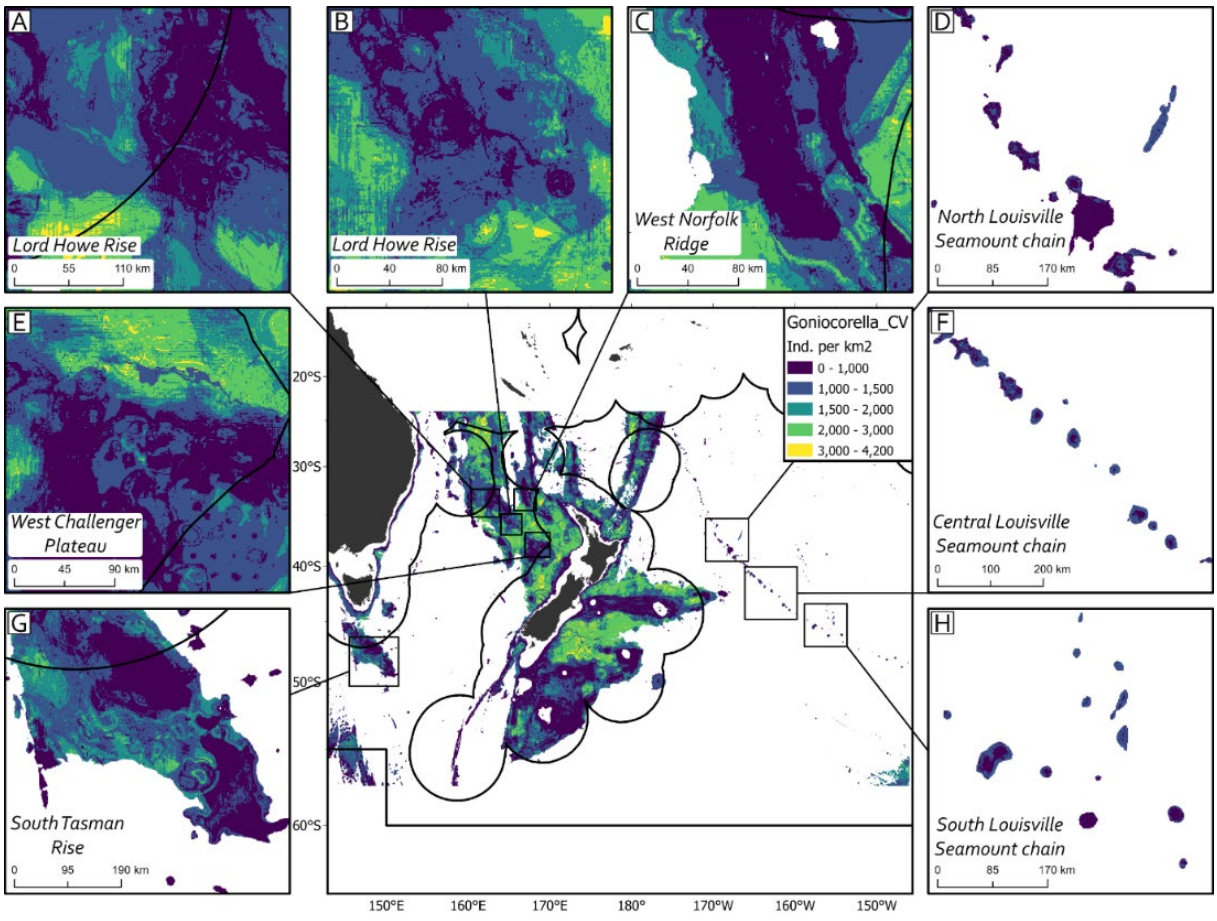

Figure A3-14 | Coefficient of variation (CV) (individuals per km^2) of *Goniocorella dumosa* in the study area from the hurdle model approach (DTIS *data-driven* approach). Inset maps of the high seas in the study area: (a) West Lord Howe Rise; (b) East Lord Howe Rise; (c) West Norfolk Ridge; (d) North Louisville Seamount Chain; (e) West Challenger Plateau; (f) Central Louisville Seamount Chain; (g) South Tasman Rise; and (h) South Louisville Seamount Chain**.**

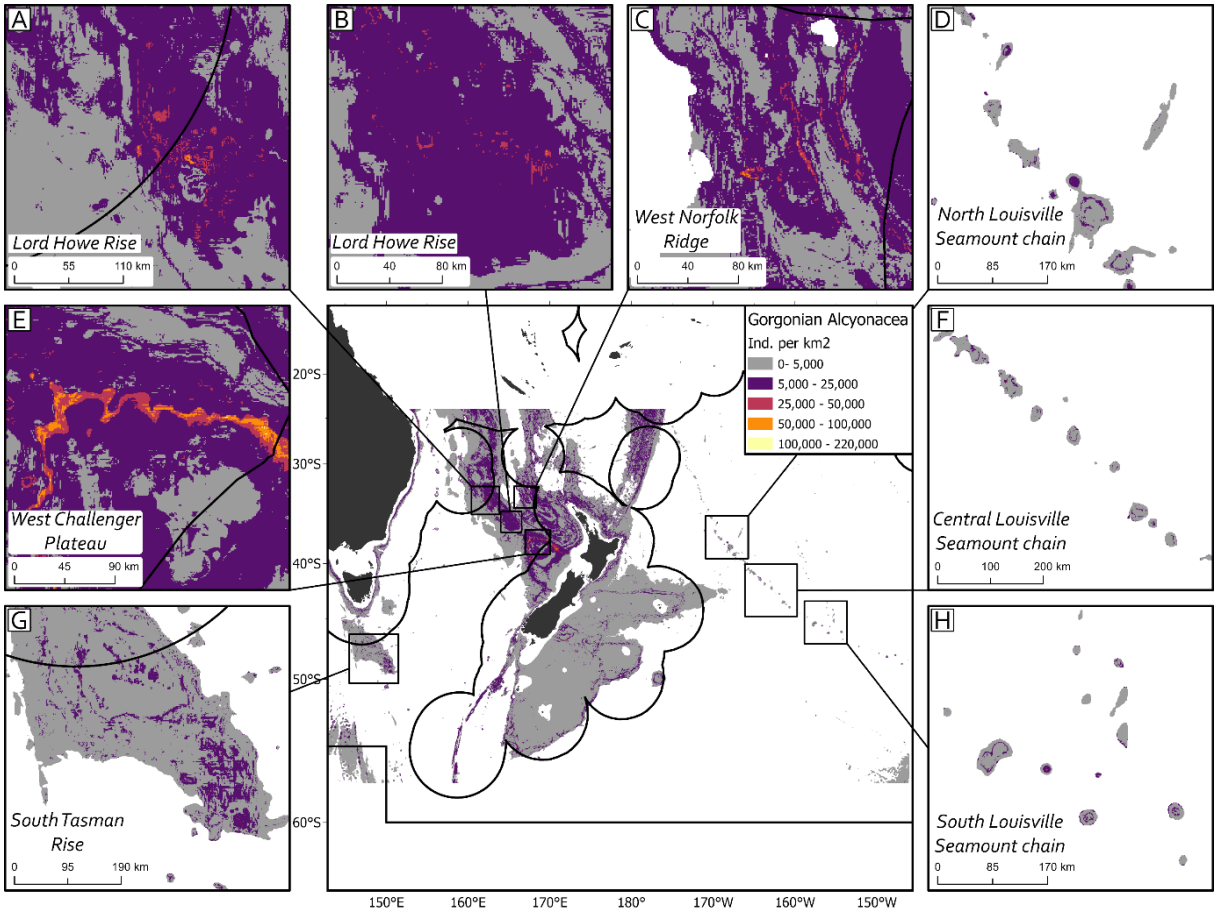

Figure A3-15 | Predicted density (individuals per km^2) of Gorgonian Alcyonacea in the study area from the hurdle model approach (DTIS *data-driven* approach). Inset maps of the high seas in the study area: (a) West Lord Howe Rise; (b) East Lord Howe Rise; (c) West Norfolk Ridge; (d) North Louisville Seamount Chain; (e) West Challenger Plateau; (f) Central Louisville Seamount Chain; (g) South Tasman Rise; and (h) South Louisville Seamount Chain**.**

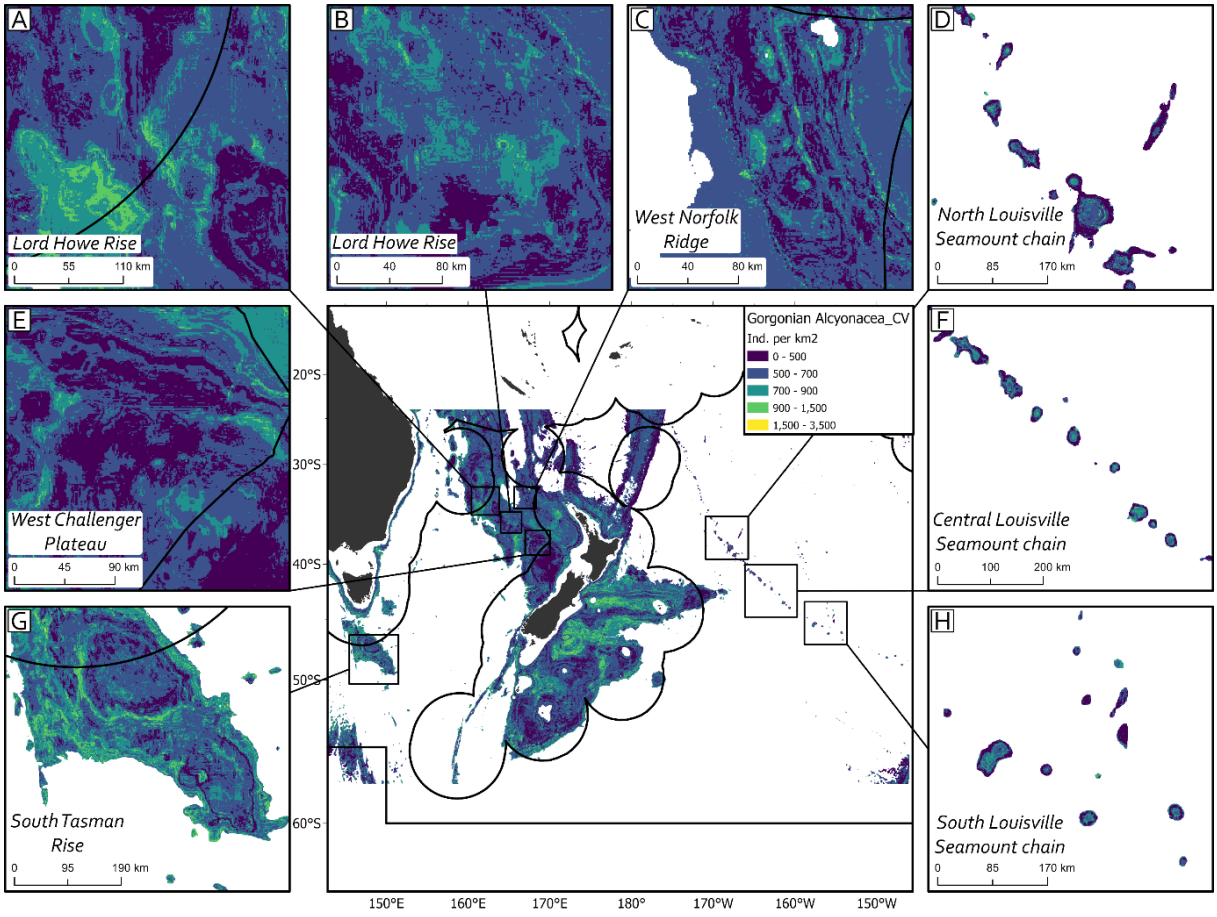

Figure A3-16 | Coefficient of variation (CV) (individuals per km^2) of Gorgonian Alcyonacea in the study area from the hurdle model approach (DTIS *data-driven* approach). Inset maps of the high seas in the study area: (a) West Lord Howe Rise; (b) East Lord Howe Rise; (c) West Norfolk Ridge; (d) North Louisville Seamount Chain; (e) West Challenger Plateau; (f) Central Louisville Seamount Chain; (g) South Tasman Rise; and (h) South Louisville Seamount Chain**.**

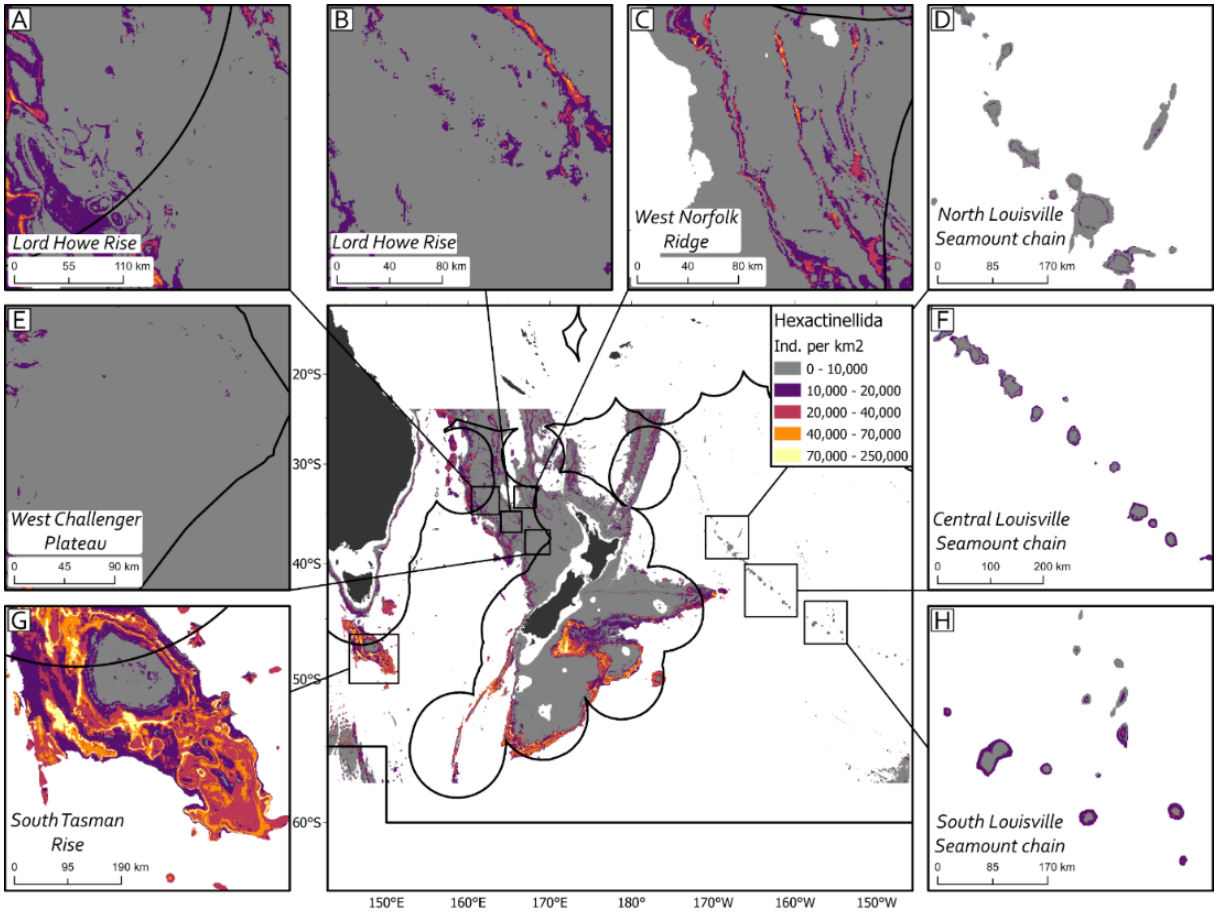

Figure A3-17 | Predicted density (individuals per km^2) of Hexactinellida in the study area from the hurdle model approach (DTIS *data-driven* approach). Inset maps of the high seas in the study area: (a) West Lord Howe Rise; (b) East Lord Howe Rise; (c) West Norfolk Ridge; (d) North Louisville Seamount Chain; (e) West Challenger Plateau; (f) Central Louisville Seamount Chain; (g) South Tasman Rise; and (h) South Louisville Seamount Chain**.**

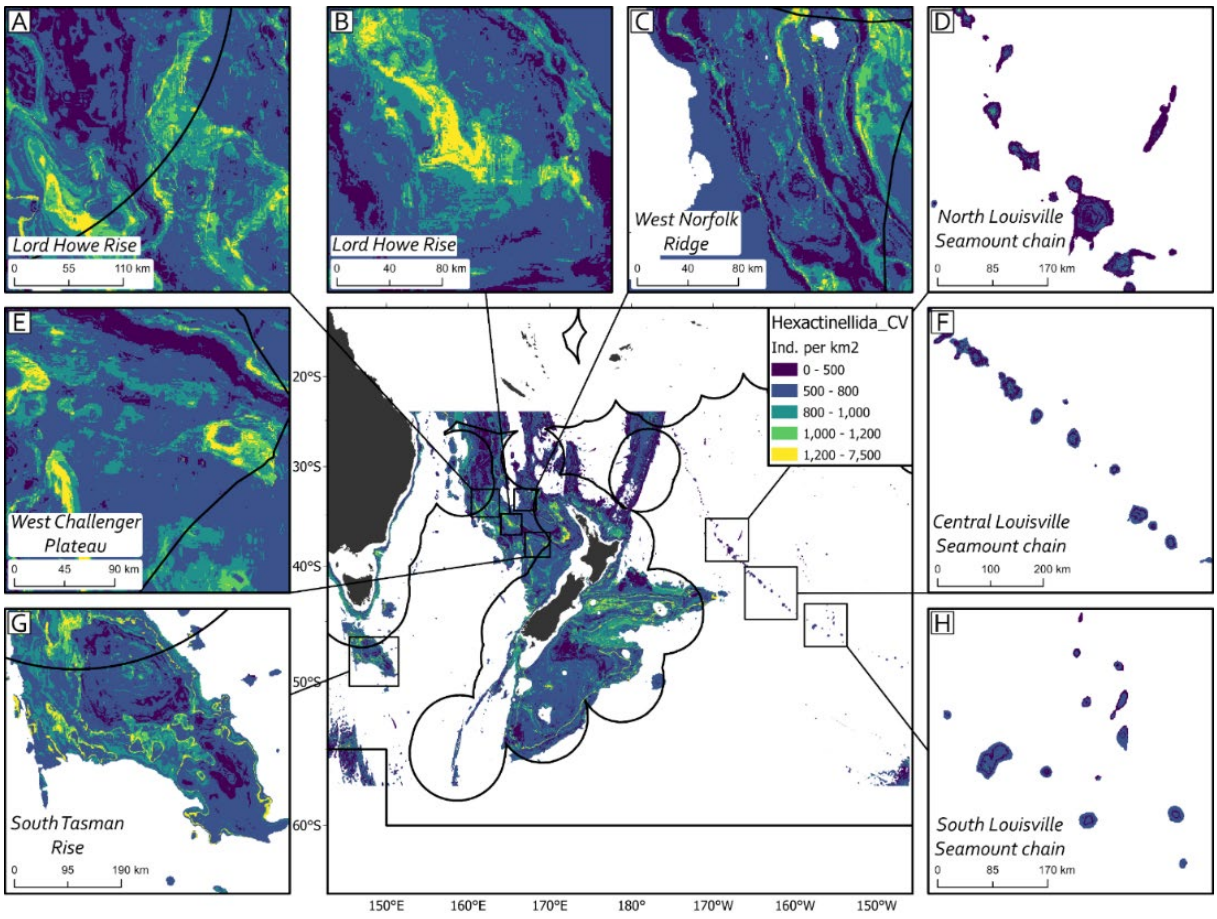

Figure A3-18 | Coefficient of variation (CV) (individuals per km^2) of Hexactinellida in the study area from the hurdle model approach (DTIS *data-driven* approach). Inset maps of the high seas in the study area: (a) West Lord Howe Rise; (b) East Lord Howe Rise; (c) West Norfolk Ridge; (d) North Louisville Seamount Chain; (e) West Challenger Plateau; (f) Central Louisville Seamount Chain; (g) South Tasman Rise; and (h) South Louisville Seamount Chain.

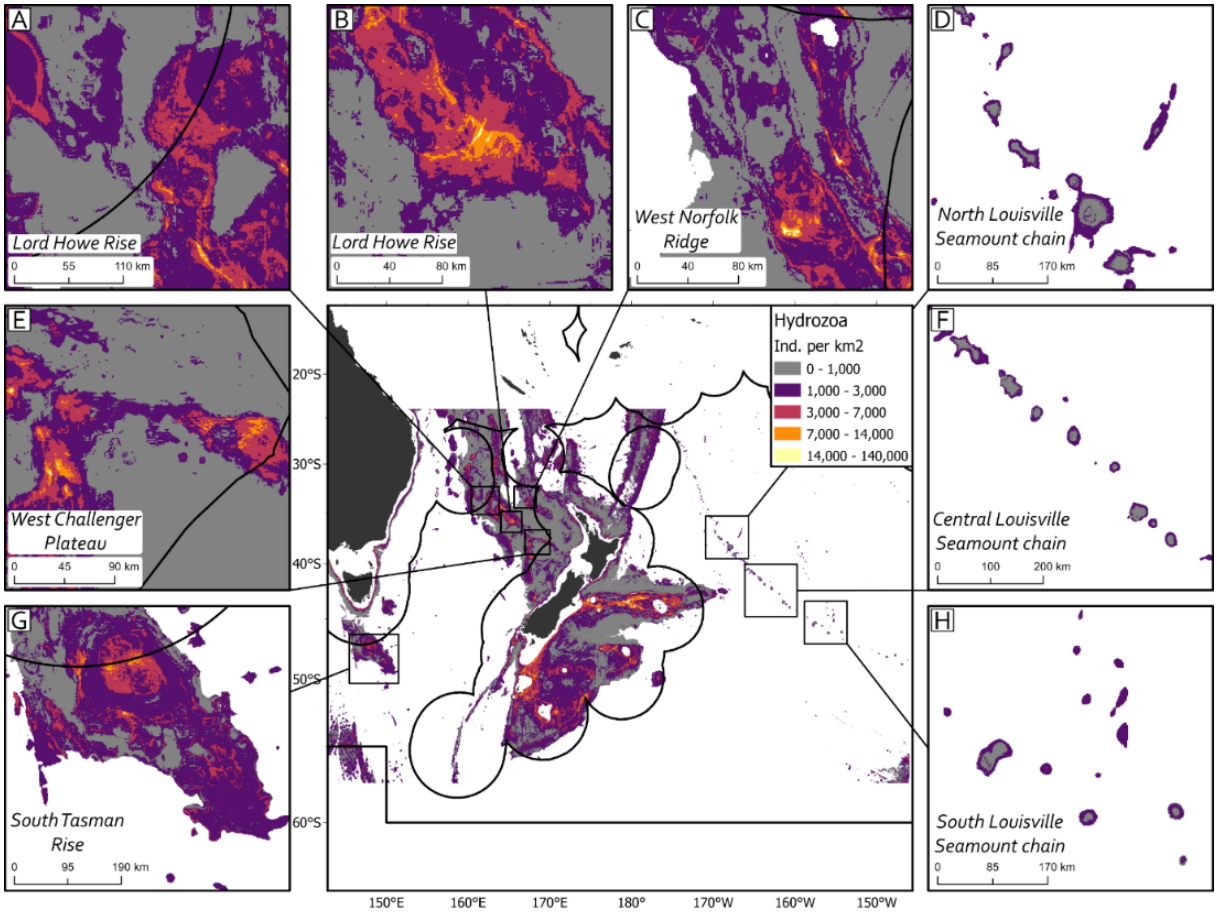

Figure A3-19 | Predicted density (individuals per km^2) of Hydrozoa in the study area from the hurdle model approach (DTIS *data-driven* approach). Inset maps of the high seas in the study area: (a) West Lord Howe Rise; (b) East Lord Howe Rise; (c) West Norfolk Ridge; (d) North Louisville Seamount Chain; (e) West Challenger Plateau; (f) Central Louisville Seamount Chain; (g) South Tasman Rise; and (h) South Louisville Seamount Chain**.**

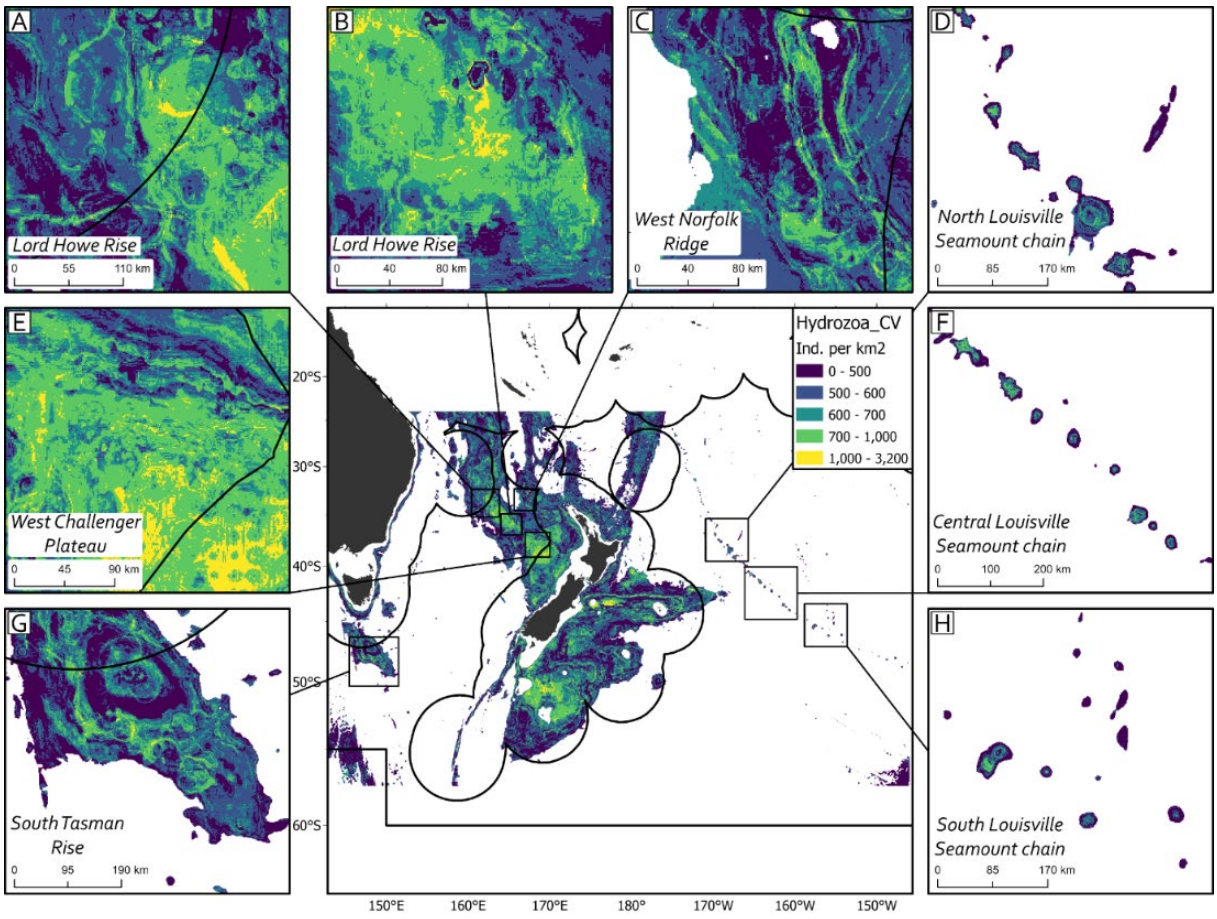

Figure A3-20 | Coefficient of variation (CV) (individuals per km^2) of Hydrozoa in the study area from the hurdle model approach (DTIS *data-driven* approach). Inset maps of the high seas in the study area: (a) West Lord Howe Rise; (b) East Lord Howe Rise; (c) West Norfolk Ridge; (d) North Louisville Seamount Chain; (e) West Challenger Plateau; (f) Central Louisville Seamount Chain; (g) South Tasman Rise; and (h) South Louisville Seamount Chain**.**

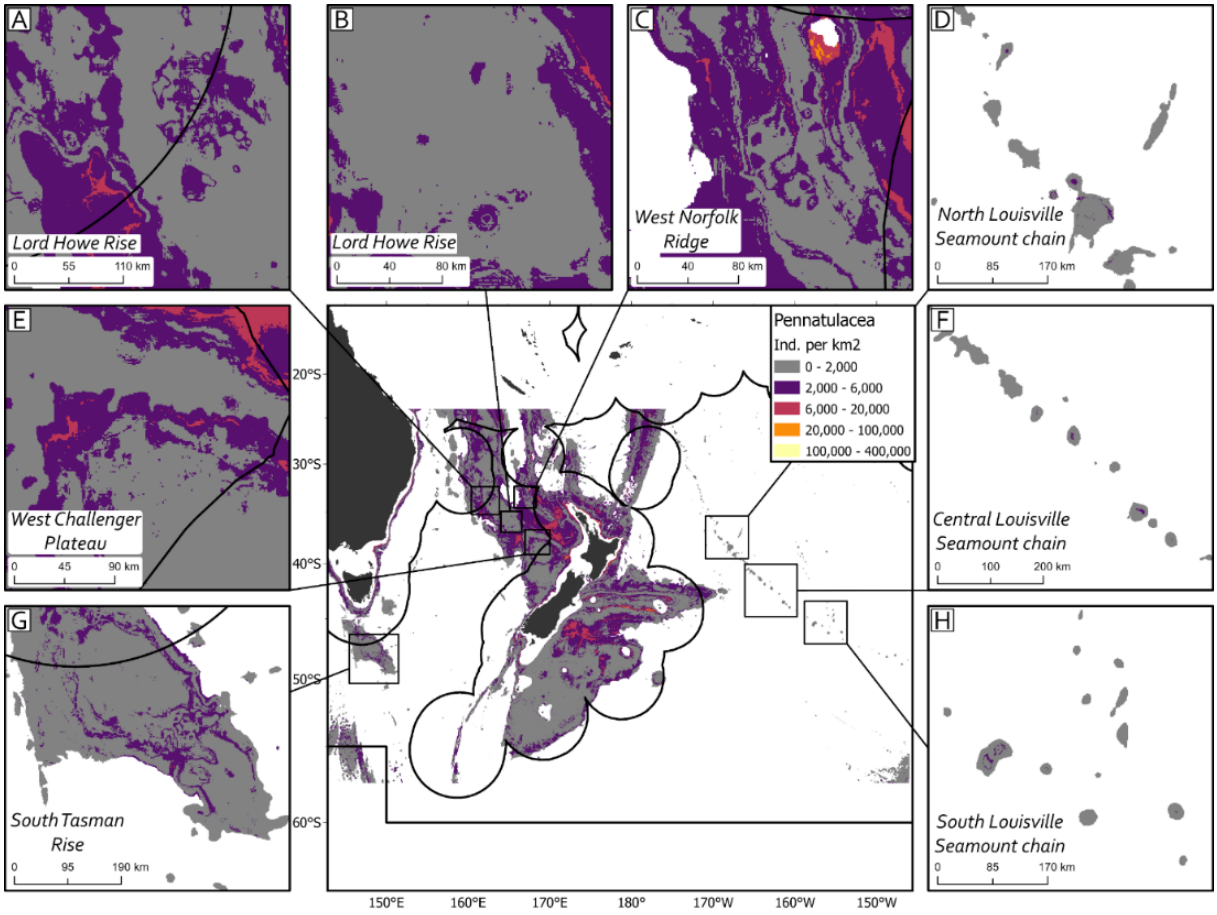

Figure A3-21 | Predicted density (individuals per km^2) of Pennatulacea in the study area from the hurdle model approach (DTIS *data-driven* approach). Inset maps of the high seas in the study area: (a) West Lord Howe Rise; (b) East Lord Howe Rise; (c) West Norfolk Ridge; (d) North Louisville Seamount Chain; (e) West Challenger Plateau; (f) Central Louisville Seamount Chain; (g) South Tasman Rise; and (h) South Louisville Seamount Chain**.**

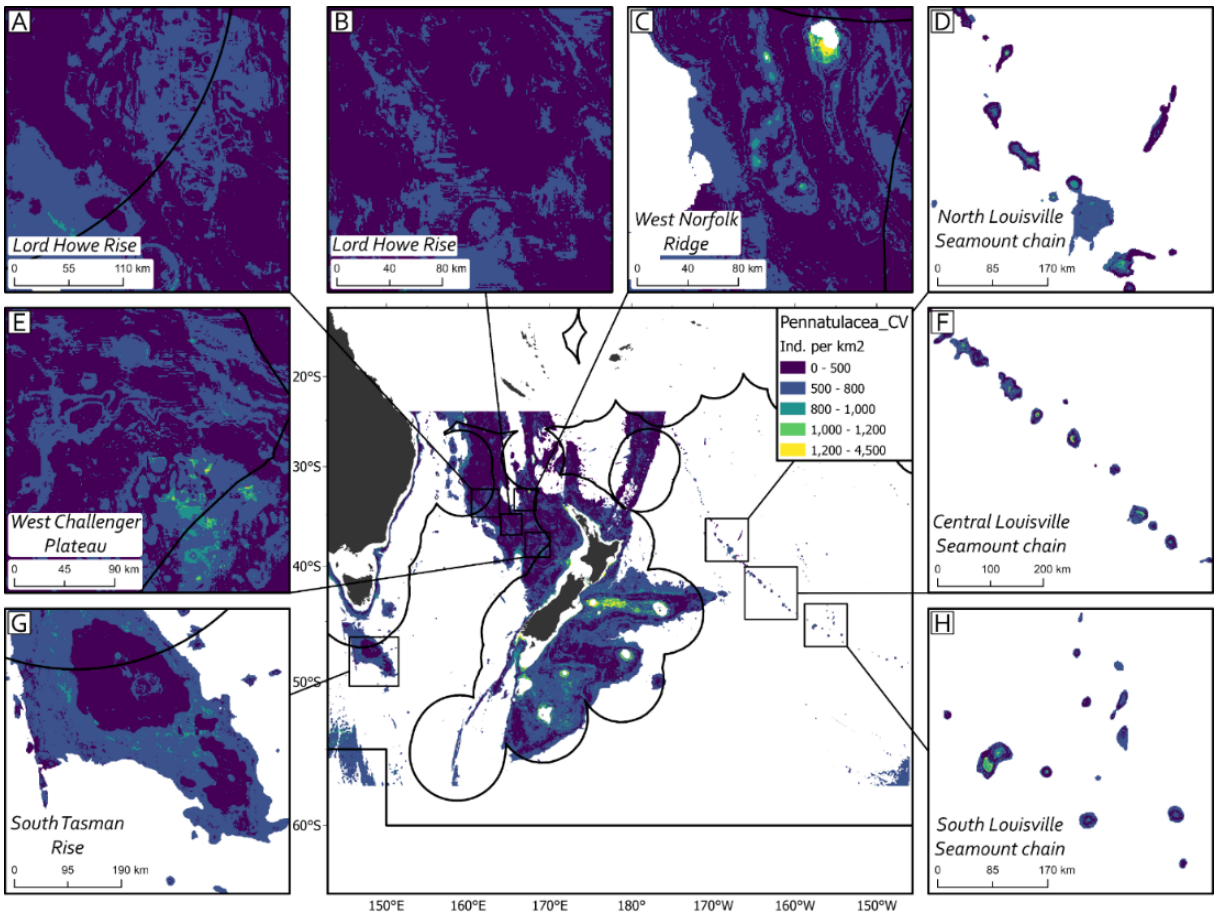

Figure A3-22 | Coefficient of variation (CV) (individuals per km^2) of Pennatulacea in the study area from the hurdle model approach (DTIS *data-driven* approach). Inset maps of the high seas in the study area: (a) West Lord Howe Rise; (b) East Lord Howe Rise; (c) West Norfolk Ridge; (d) North Louisville Seamount Chain; (e) West Challenger Plateau; (f) Central Louisville Seamount Chain; (g) South Tasman Rise; and (h) South Louisville Seamount Chain**.**

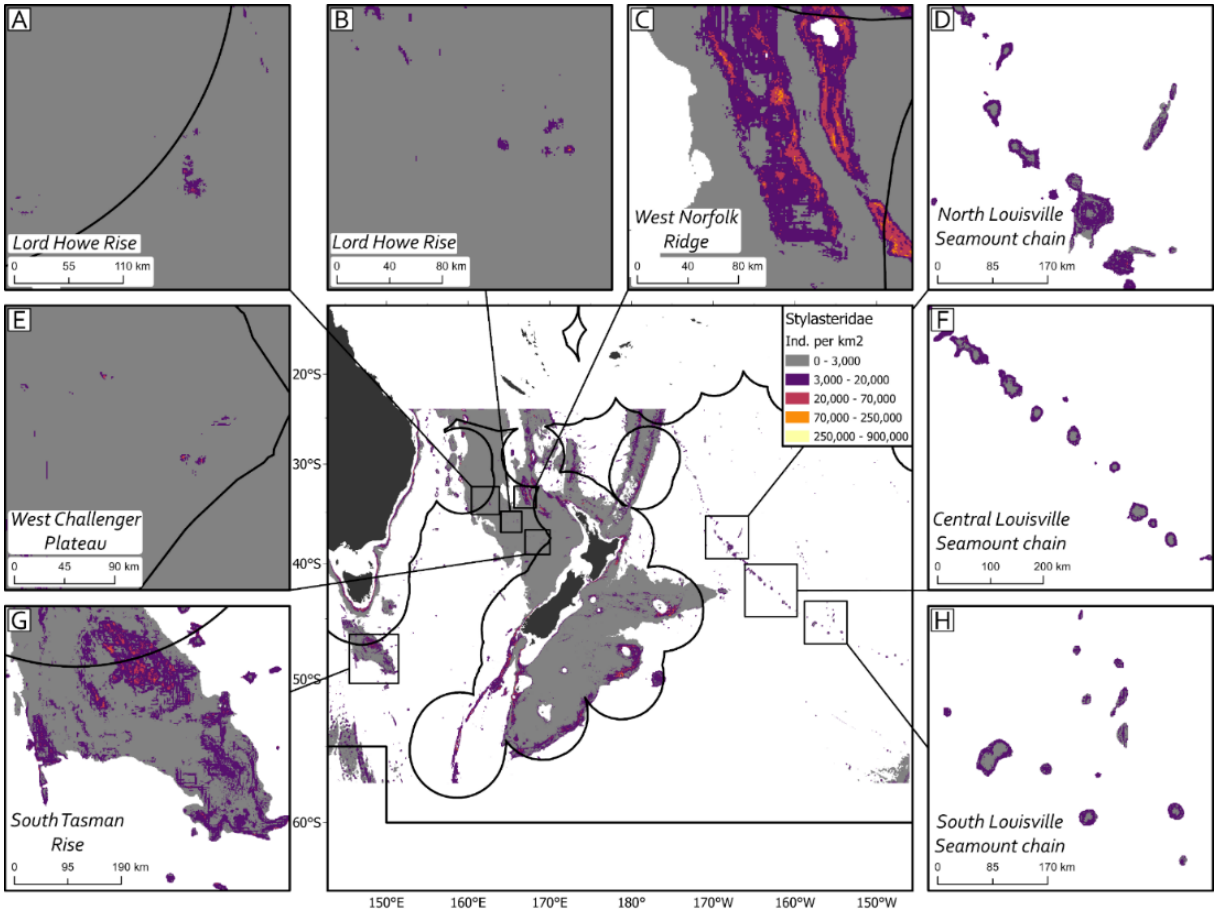

Figure A3-23 | Predicted density (individuals per km^2) of Stylasteridae in the study area from the hurdle model approach (DTIS *data-driven* approach). Inset maps of the high seas in the study area: (a) West Lord Howe Rise; (b) East Lord Howe Rise; (c) West Norfolk Ridge; (d) North Louisville Seamount Chain; (e) West Challenger Plateau; (f) Central Louisville Seamount Chain; (g) South Tasman Rise; and (h) South Louisville Seamount Chain.

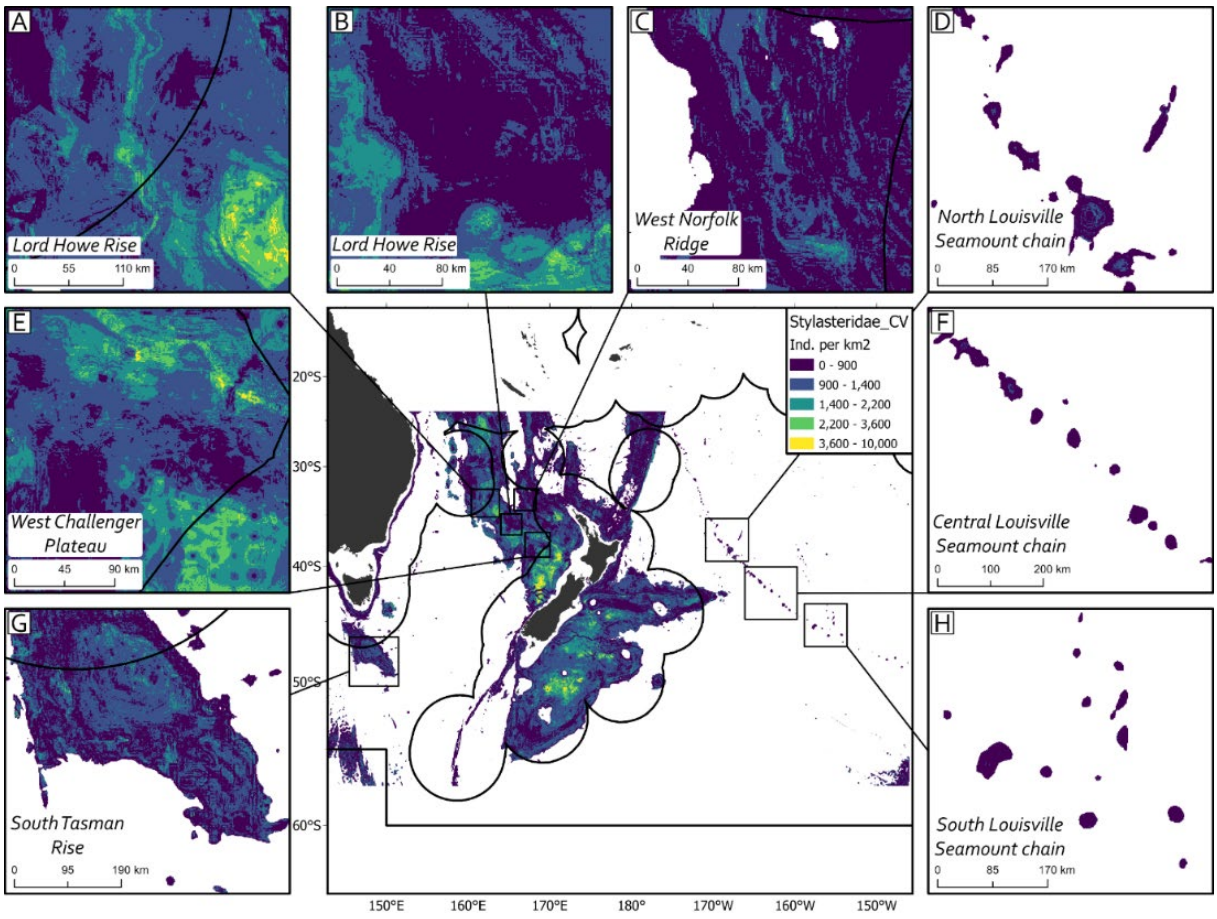

Figure A3-24 | Coefficient of variation (CV) (individuals per km^2) of Stylasteridae in the study area from the hurdle model approach (DTIS *data-driven* approach). Inset maps of the high seas in the study area: (a) West Lord Howe Rise; (b) East Lord Howe Rise; (c) West Norfolk Ridge; (d) North Louisville Seamount Chain; (e) West Challenger Plateau; (f) Central Louisville Seamount Chain; (g) South Tasman Rise; and (h) South Louisville Seamount Chain**.**

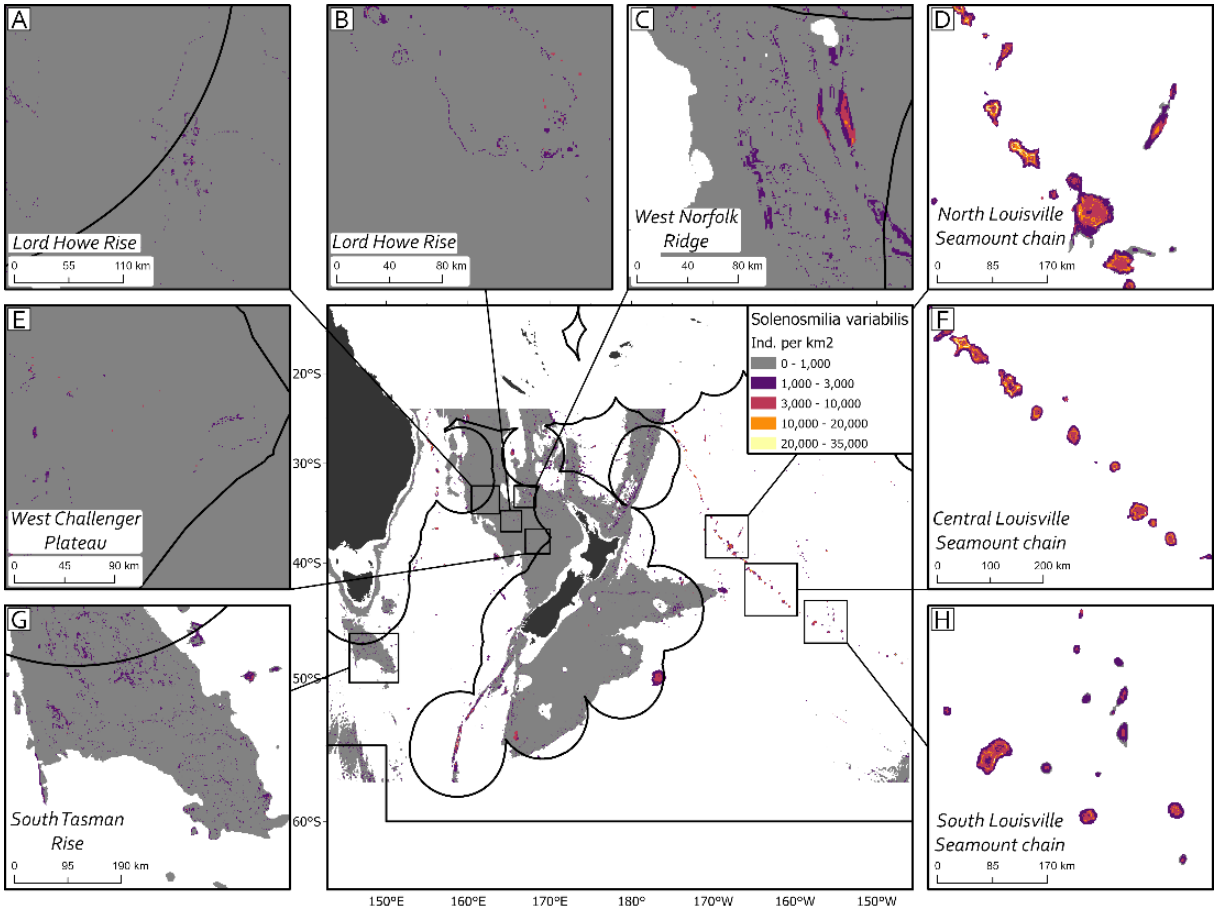

Figure A325 | Predicted density (individuals per km^2) of *Solenosmilia variabilis* in the study area from the hurdle model approach (DTIS *data-driven* approach). Inset maps of the high seas in the study area: (a) West Lord Howe Rise; (b) East Lord Howe Rise; (c) West Norfolk Ridge; (d) North Louisville Seamount Chain; (e) West Challenger Plateau; (f) Central Louisville Seamount Chain; (g) South Tasman Rise; and (h) South Louisville Seamount Chain.

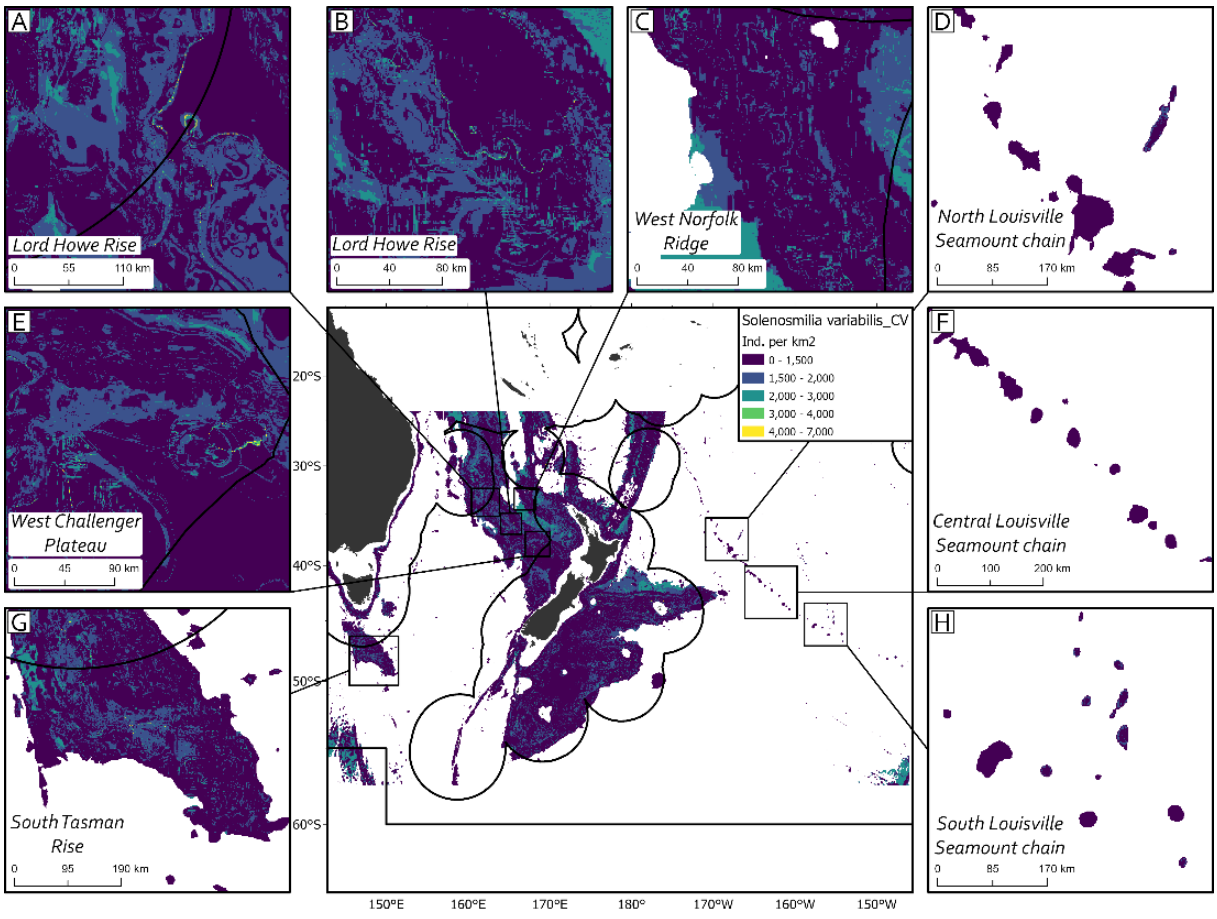

Figure A3-26 | Coefficient of variation (CV) (individuals per km^2) of *Solenosmilia variabilis* in the study area from the hurdle model approach (DTIS *data-driven* approach). Inset maps of the high seas in the study area: (a) West Lord Howe Rise; (b) East Lord Howe Rise; (c) West Norfolk Ridge; (d) North Louisville Seamount Chain; (e) West Challenger Plateau; (f) Central Louisville Seamount Chain; (g) South Tasman Rise; and (h) South Louisville Seamount Chain**.**

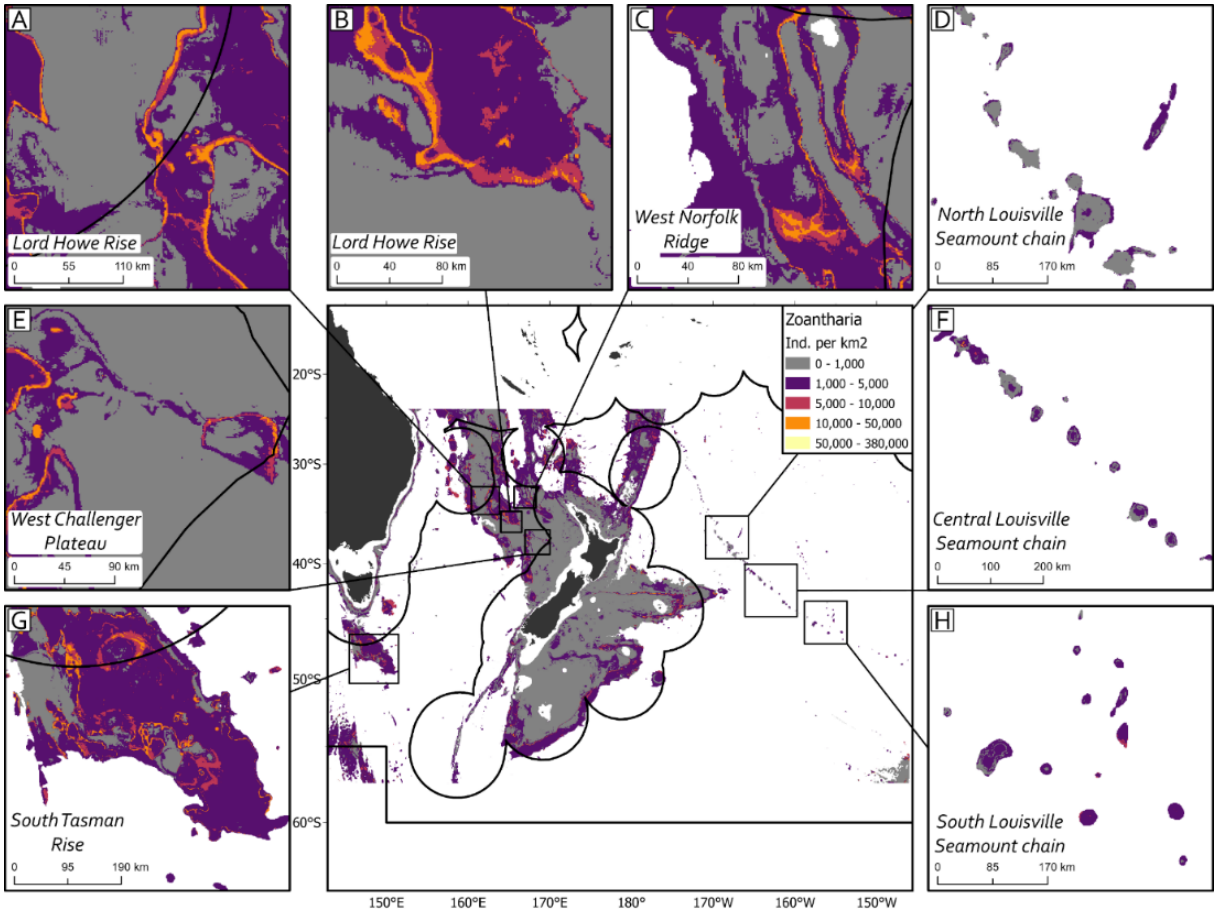

Figure A3-27 | Predicted density (individuals per km^2) of Zoantharia in the study area from the hurdle model approach (DTIS *data-driven* approach). Inset maps of the high seas in the study area: (a) West Lord Howe Rise; (b) East Lord Howe Rise; (c) West Norfolk Ridge; (d) North Louisville Seamount Chain; (e) West Challenger Plateau; (f) Central Louisville Seamount Chain; (g) South Tasman Rise; and (h) South Louisville Seamount Chain.

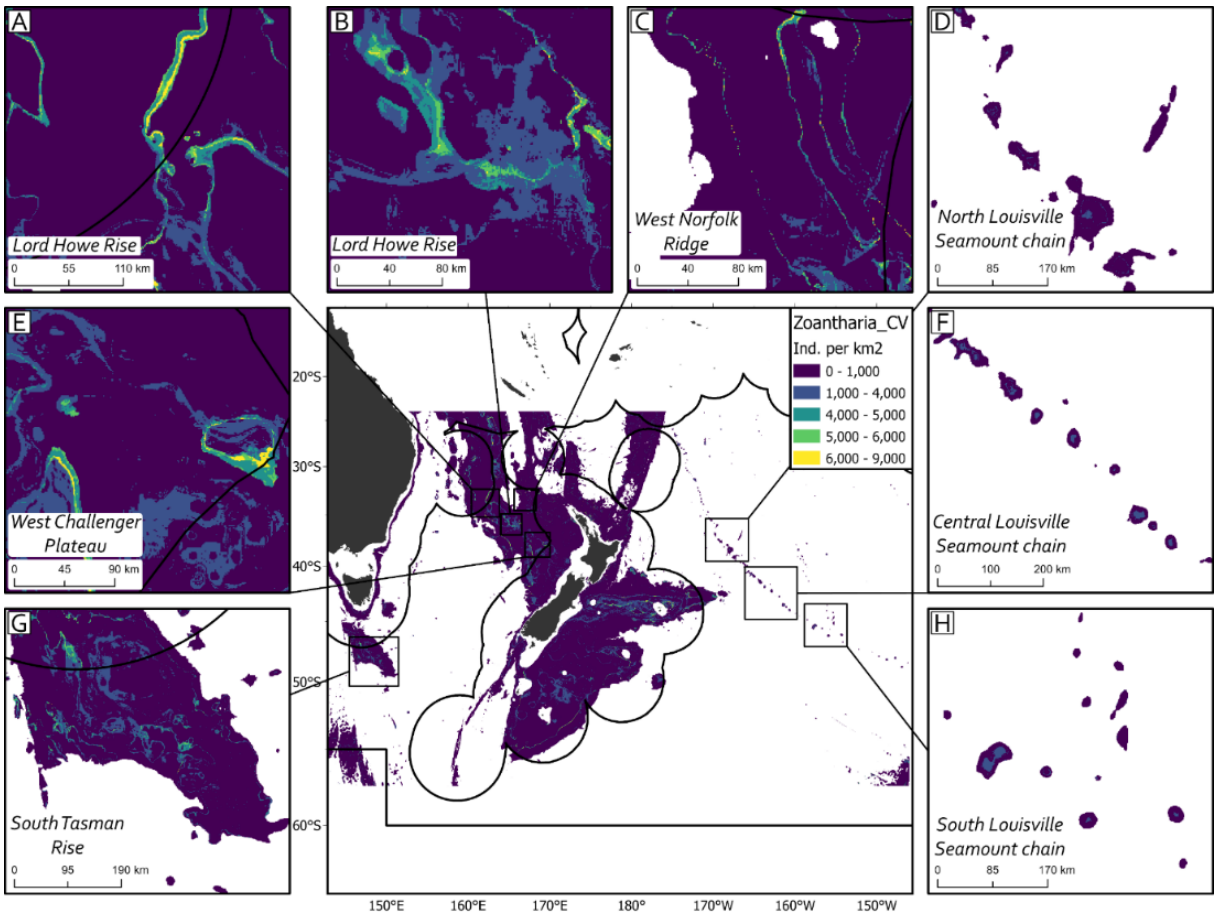

Figure A3-28 | Coefficient of variation (CV) (individuals per km^2) of Zoantharia in the study area from the hurdle model approach (DTIS *data-driven* approach). Inset maps of the high seas in the study area: (a) West Lord Howe Rise; (b) East Lord Howe Rise; (c) West Norfolk Ridge; (d) North Louisville Seamount Chain; (e) West Challenger Plateau; (f) Central Louisville Seamount Chain; (g) South Tasman Rise; and (h) South Louisville Seamount Chain.

Annex 4 - Environmental coverage for data-driven models

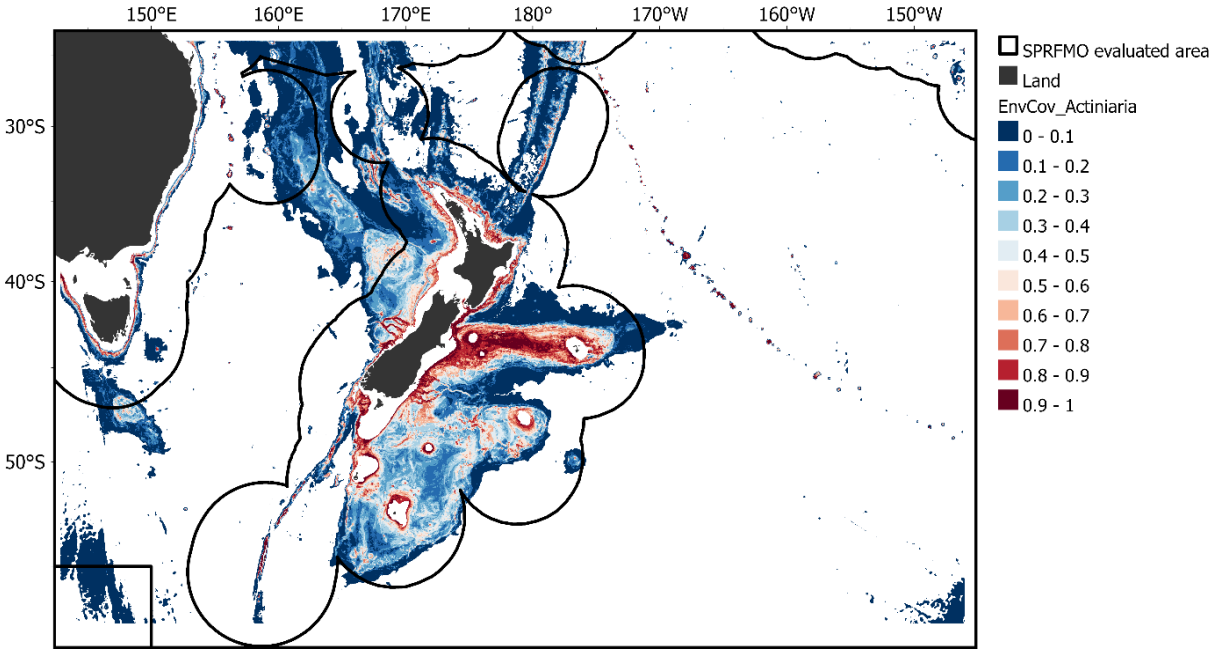

Figure A4-1 | Environmental coverage for Actinaria, ranging from low (0) to high (1) between 200 and 3000 m depth within the study area. Developed for Actinaria based on the taxon-specific environmental variables shown in Table 2.

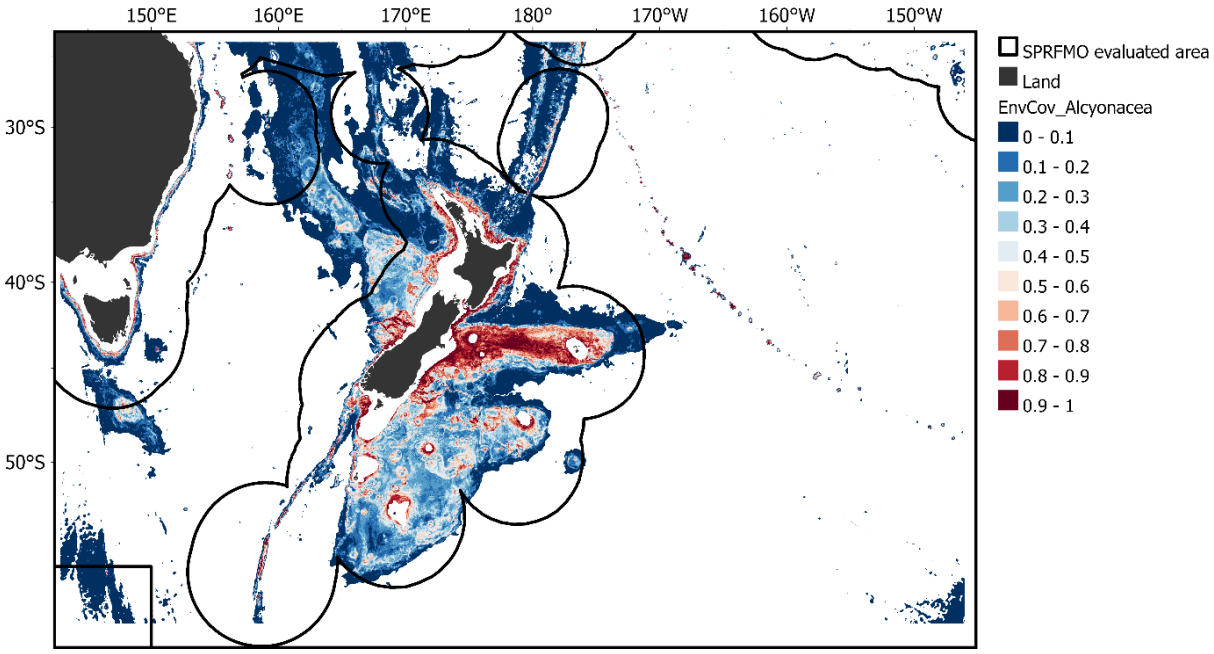

Figure A4-2 | Environmental coverage for Alcyonacea, ranging from low (0) to high (1) between 200 and 3000 m depth within the study area. Developed for Alcyonacea based on the taxon-specific environmental variables shown in Table 2.

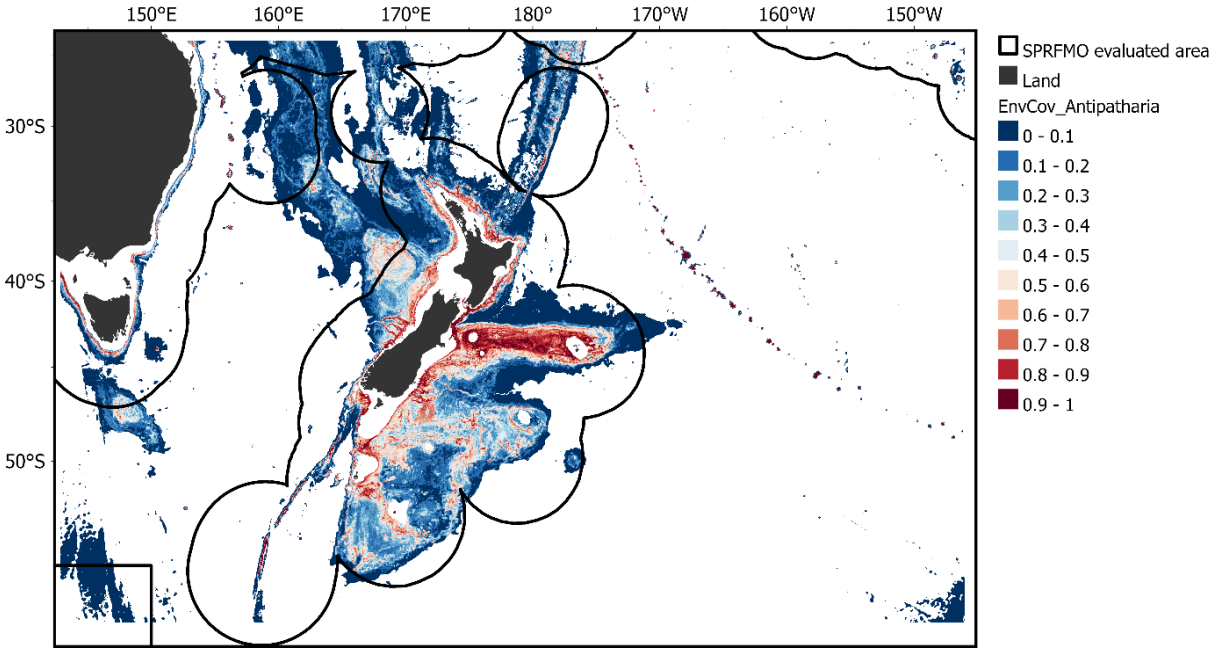

Figure A4-3 | Environmental coverage for Antipatharia, ranging from low (0) to high (1) between 200 and 3000 m depth within the study area. Developed for Antipatharia based on the taxon-specific environmental variables shown in Table 2.

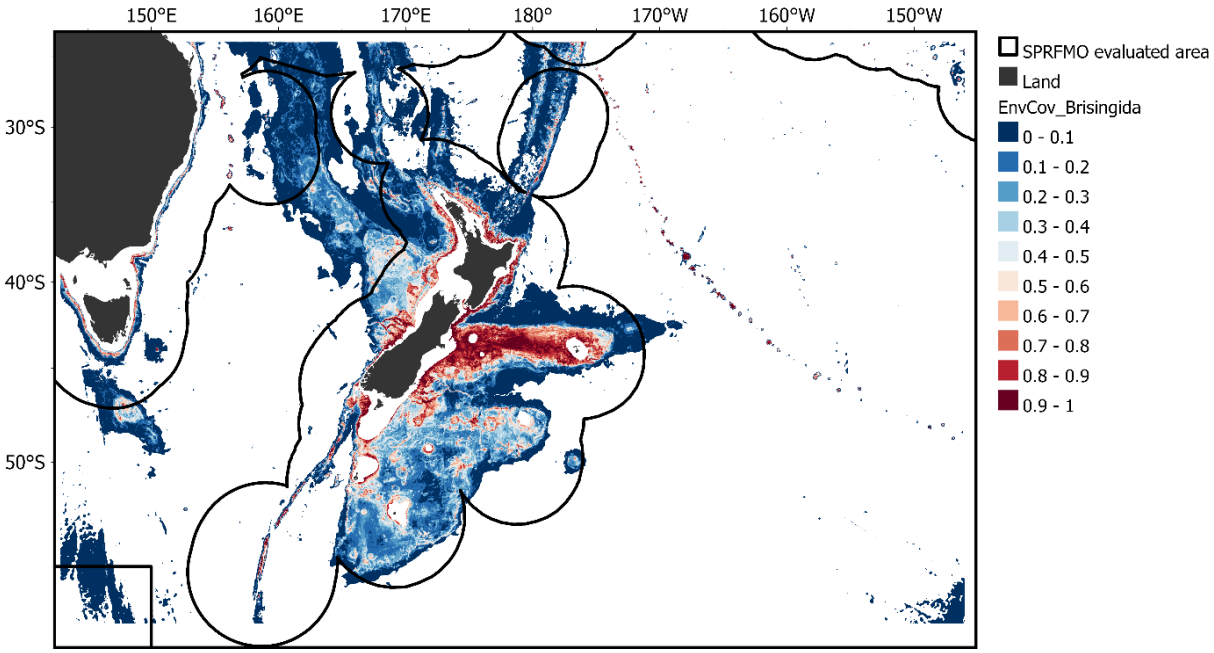

Figure A44 | Environmental coverage for Brisingida, ranging from low (0) to high (1) between 200 and 3000 m depth within the study area. Developed for Brisingida based on the taxon-specific environmental variables shown in Table 2.

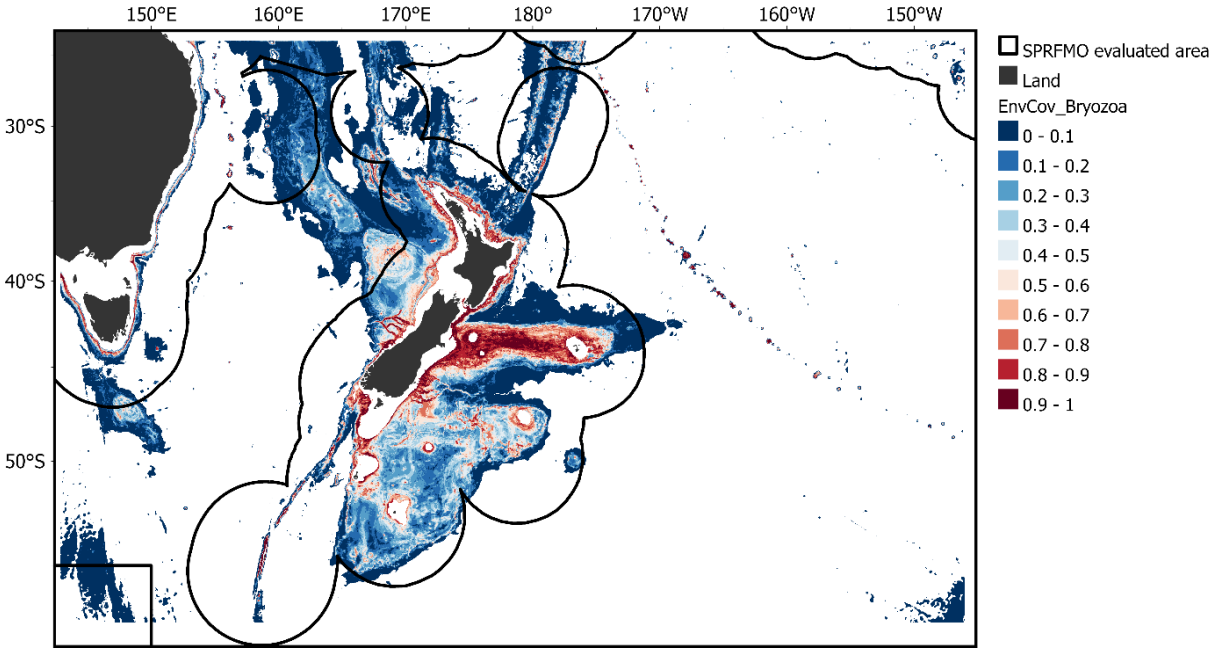

Figure A4-5 | Environmental coverage for Bryozoa, ranging from low (0) to high (1) between 200 and 3000 m depth within the study area. Developed for Bryozoa based on the taxon-specific environmental variables shown in Table 2.

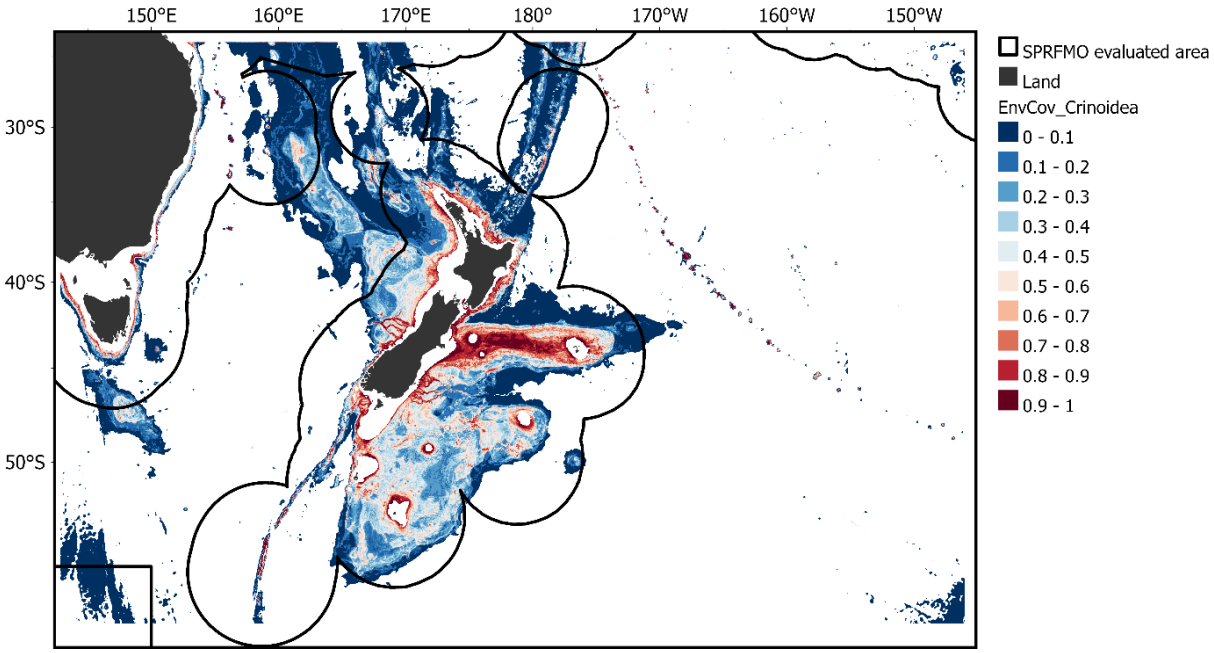

Figure A4-6 | Environmental coverage for Crinoidea, ranging from low (0) to high (1) between 200 and 3000 m depth within the study area. Developed for Crinoidea based on the taxon-specific environmental variables shown in Table 2.

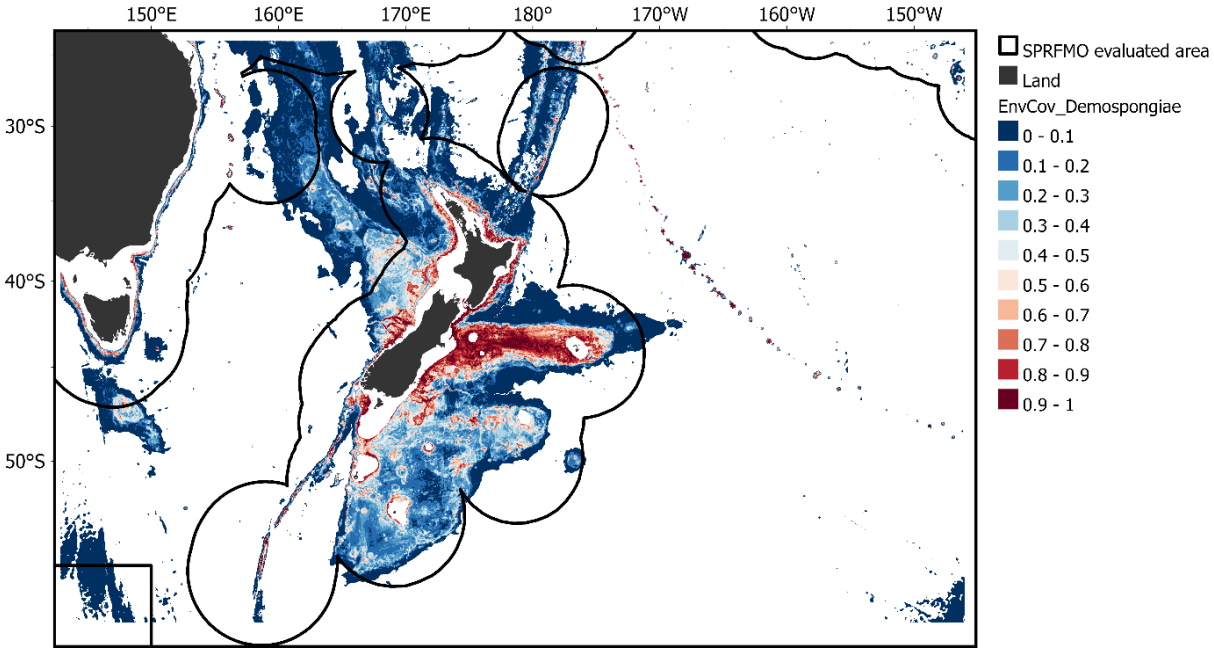

Figure A4-7 | Environmental coverage for Demospongiae, ranging from low (0) to high (1) between 200 and 3000 m depth within the study area. Developed for Demospongiae based on the taxon-specific environmental variables shown in Table 2.

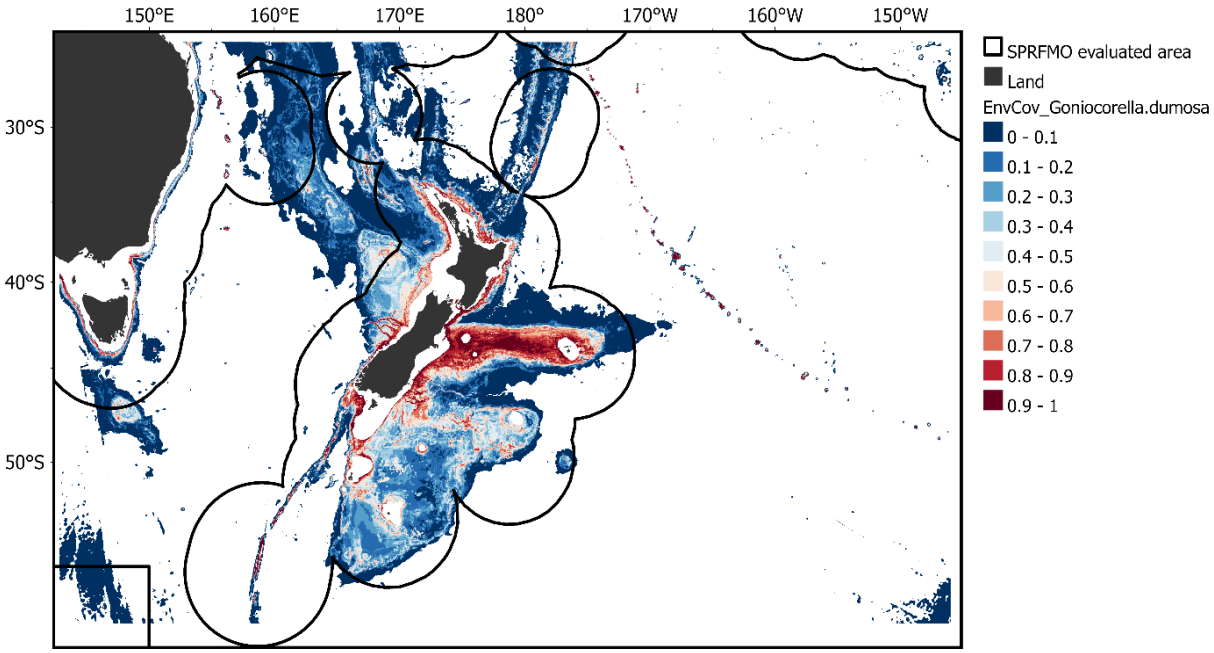

Figure A4-8 | Environmental coverage for *Goniocorella dumosa*, ranging from low (0) to high (1) between 200 and 3000 m depth within the study area. Developed for *Goniocorella dumosa* based on the taxon-specific environmental variables shown in Table 2.

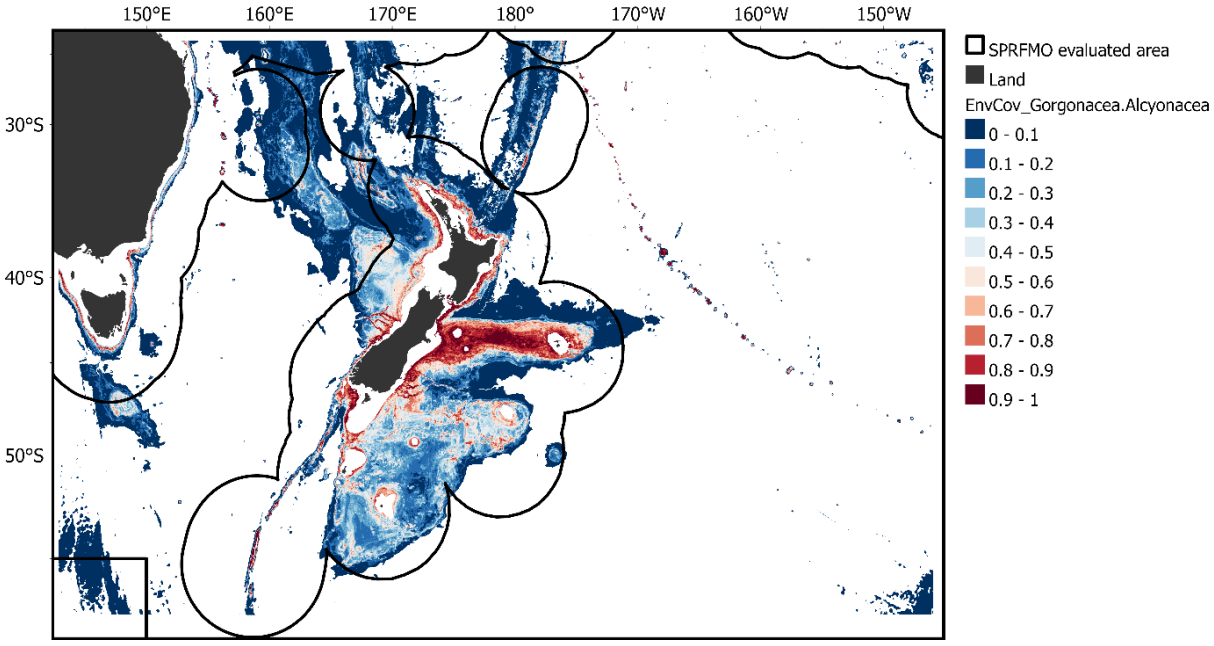

Figure A4-9 | Environmental coverage for Gorgonian Alcyonacea, ranging from low (0) to high (1) between 200 and 3000 m depth within the study area. Developed for Gorgonian Alcyonacea based on the taxon-specific environmental variables shown in Table 2.

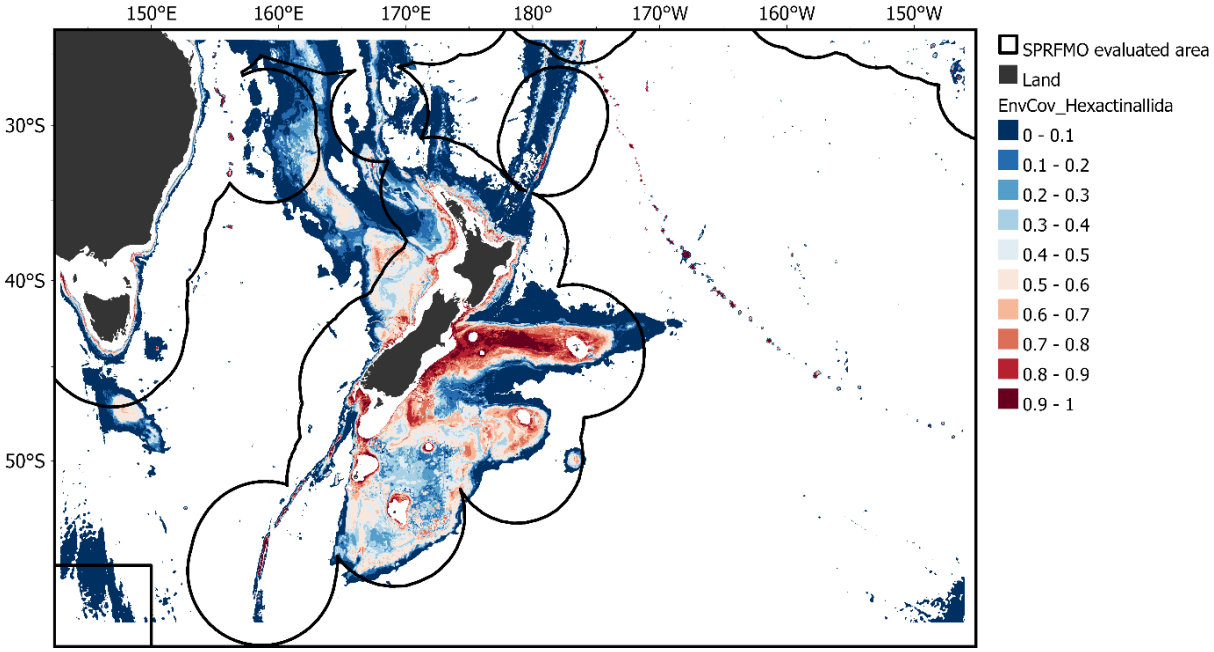

Figure A4-10 | Environmental coverage for Hexactinellida, ranging from low (0) to high (1) between 200 and 3000 m depth within the study area. Developed for Hexactinellida based on the taxon-specific environmental variables shown in Table 2.

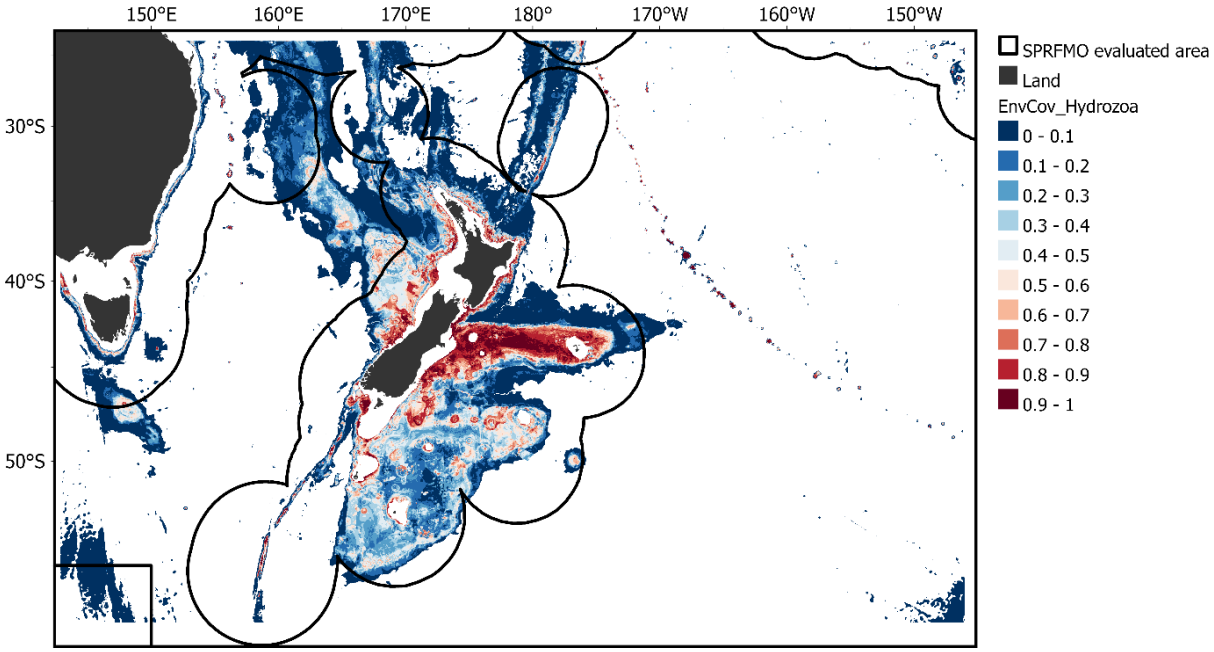

Figure A411 | Environmental coverage for Hydrozoa, ranging from low (0) to high (1) between 200 and 3000 m depth within the study area. Developed for Hydrozoa based on the taxon-specific environmental variables shown in Table 2.

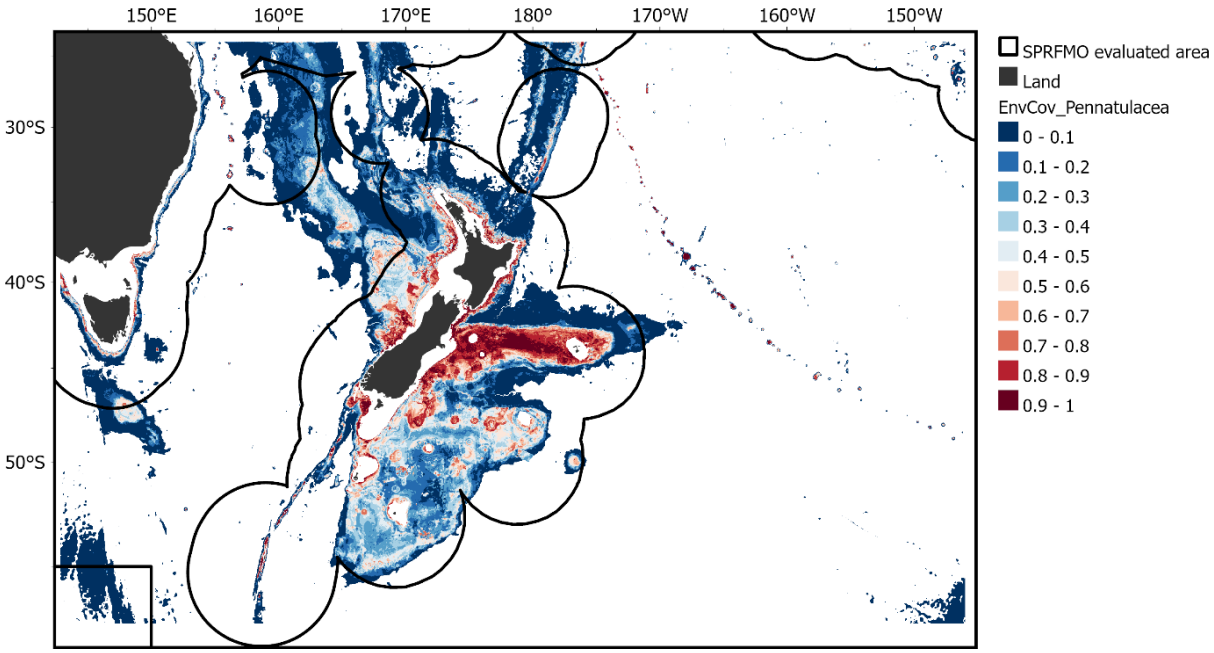

Figure A4-12 | Environmental coverage for Pennatulacea, ranging from low (0) to high (1) between 200 and 3000 m depth within the study area. Developed for Pennatulacea based on the taxon-specific environmental variables shown in Table 2.

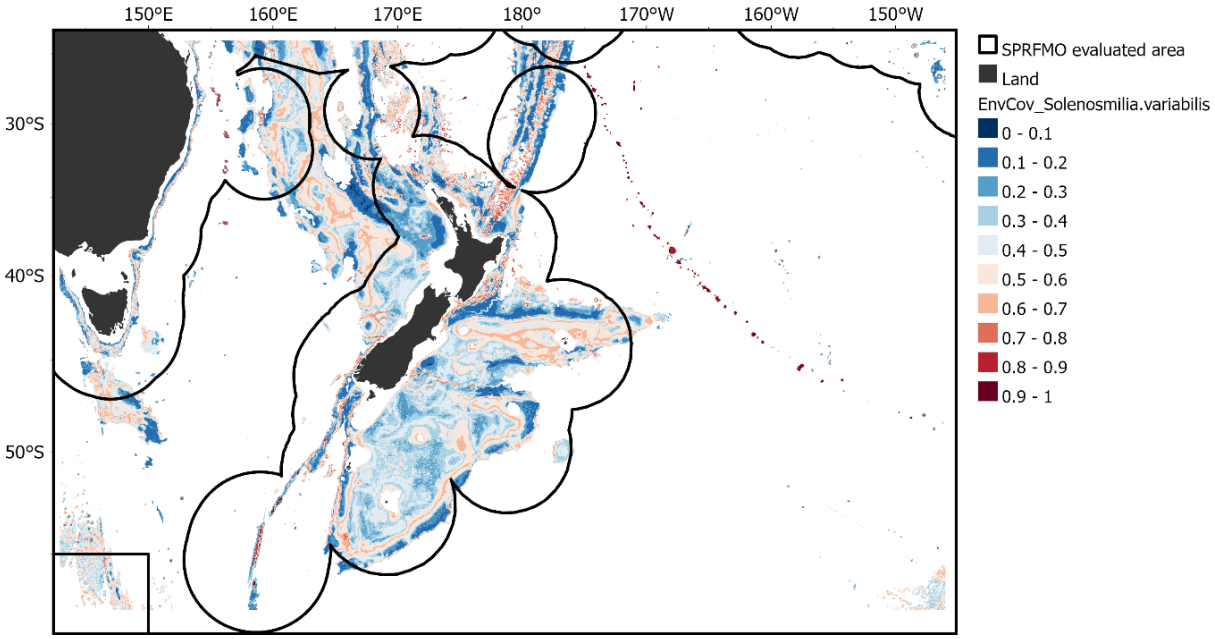

Figure A4-13 | Environmental coverage for *Solenosmilia variabilis*, ranging from low (0) to high (1) between 200 and 3000 m depth within the study area. Developed for *Solenosmilia variabilis* based on the taxon-specific environmental variables shown in Table 2.

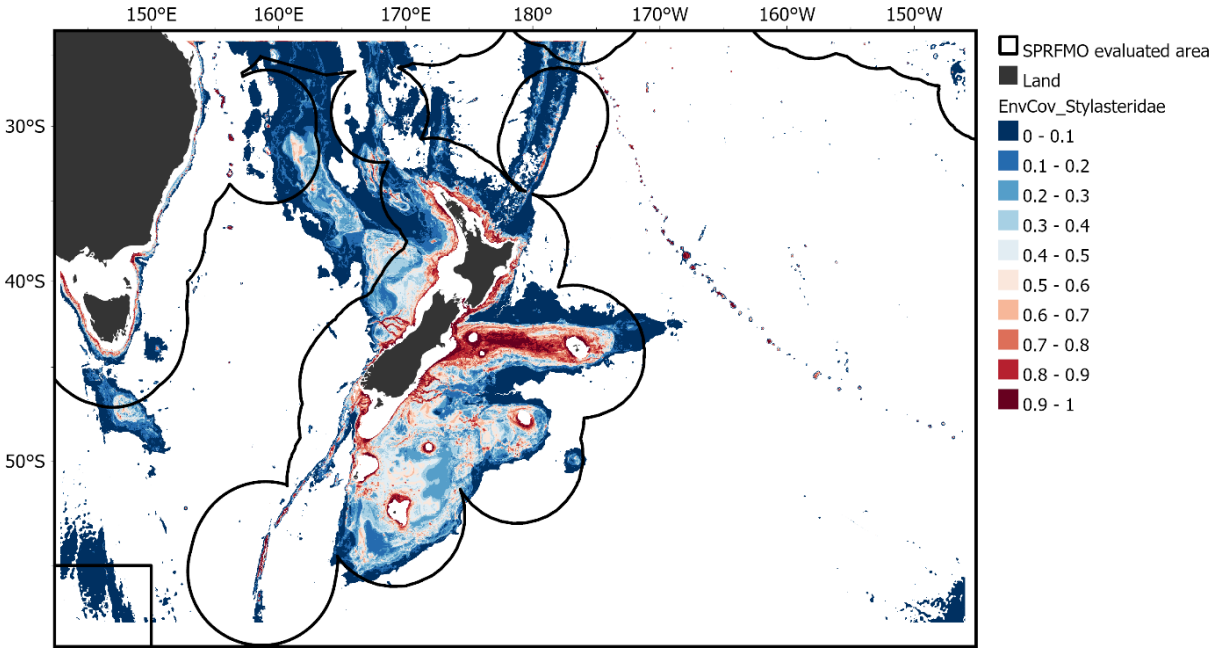

Figure A4-14 | Environmental coverage for Stylasteridae, ranging from low (0) to high (1) between 200 and 3000 m depth within the study area. Developed for Stylasteridae based on the taxon-specific environmental variables shown in Table 2.

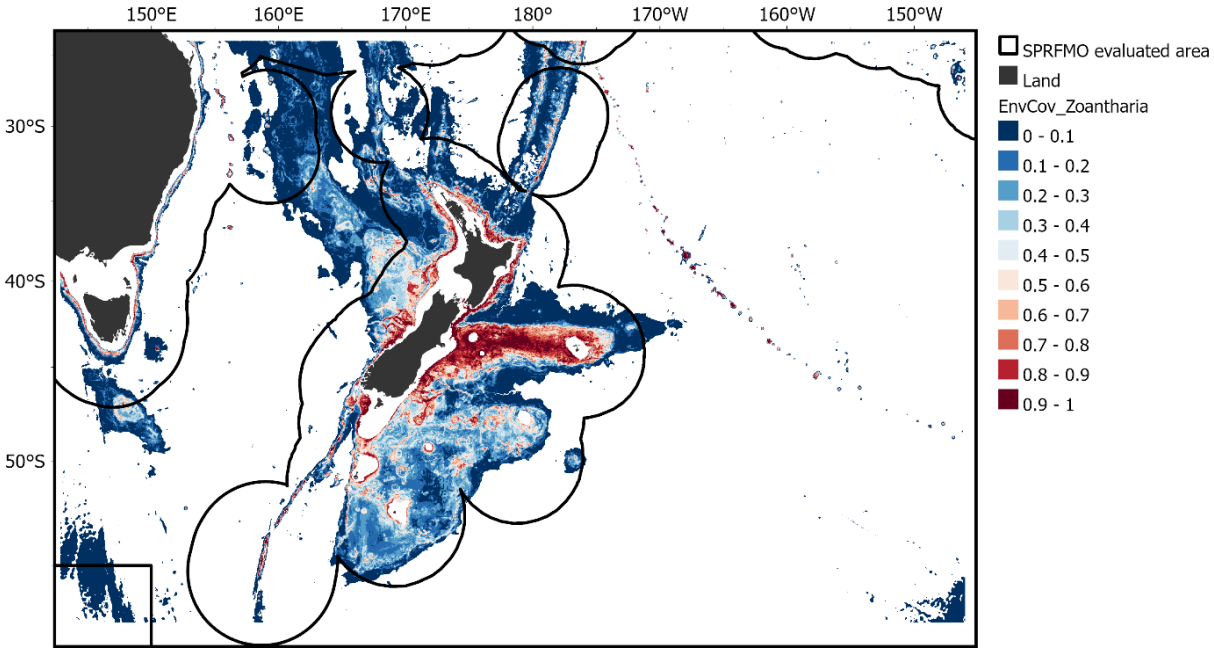

Figure A4-15 | Environmental coverage for Zoantharia, ranging from low (0) to high (1) between 200 and 3000 m depth within the study area. Developed for Zonatharia based on the taxon-specific environmental variables shown in Table 2.

Annex 5 – Relative environmental suitability (RES) models - Experts results

Table A5-113 | Number of experts that selected the top-4 most selected environmental variables

	No. of experts that selected each environmental variable			
Taxa	**Aragonite saturation at depth**	**Bathymetric position index**	**Particulate organic carbon export**	**Temperature at depth**
Enallopsammia rostrata	5	6	6	4
Goniocorella dumosa	6	5	5	4
Madrepora oculata	6	5	5	4
Solenosmilia variabilis	4	5	6	4

Table A5-2 | Anonymised expert input for the *principles-based* approach (RES models) applied to 4 stony coral taxa (GDU: Goniocorella dumosa; SVA: Solenosmilia variabilis; MOC: Madrepora oculata; ERO: Enallopsammia rostrata). Experts are anonymised and numbered (1-8). POC: particulate organic carbon export. The input in the table below has been amended following requests to each expert for clarification or additional information.

VME indicator taxa	Expert	Environmental variable	Shape	Absolute min	Preferred min	Preferred max	Absolute max
GDU	1	BPI-broad	Plateau	0	200	1000	
	1	POC	Linear	0	5		
	2	Aragonite saturation	Plateau	0	2.5		
	2	Dissolved oxygen at depth	Linear decay				
	2	Mud	Linear decay				
	2	Temperature	Trapezoid	0	2	7	7
	3	BPI-broad	Plateau	0	500		
	3	Dissolved oxygen at depth	Plateau	3	4		
	3	POC	Plateau	2	4		
	3	Temperature	Trapezoid	3	5	10	14
	4	BPI-broad	Linear	250	350	500	1000
	4	POC	Trapezoid	15	20	35	40
	4	Temperature	Trapezoid	4	5	10	15
	5	Aragonite saturation	Trapezoid	0.07	0.47	3.2	3.2
	5	POC	Linear	0.44	0.44		
	5	Ruggedness	Linear	0	1		
	5	Temperature	Trapezoid	3	8	10	12
	6	BPI-broad	Trapezoid	0	500	2000	3000
	6	Gravel	Plateau	5	20		
	6	POC	Plateau	5	20		
	7	Aragonite saturation	Plateau	0.8	1.5		
	7	BPI-broad	Plateau	-500	500		
	7	Dissolved oxygen at depth	Plateau	3.5	4.5		
	7	POC	Linear	2	5		

VME indicator taxa	Expert	Environmental variable	Shape	Absolute min	Preferred min	Preferred max	Absolute max
SVA	1	BPI-broad	Plateau	0	1000	4000	
	1	POC	Linear	0	5		
	2	Aragonite saturation	Plateau	0	2.5		
	2	Dissolved oxygen at depth	Linear decay				
	2	Mud	Linear decay				
	2	Temperature	Trapezoid	0	2	7	7
	3	Aragonite saturation	Plateau	1	1		
	3	BPI-broad	Trapezoid	0	500	3500	3500
	3	POC	Plateau	2	4		
	3	Temperature	Trapezoid	5	5	10	10
	4	Aragonite saturation	Trapezoid	0.7	1	1.6	2
	4	BPI-broad	Linear	300	500	>500	
	4	POC	Plateau	12	15	20	30
	4	Temperature	Trapezoid	4	5	10	15
	5	Aragonite saturation	Trapezoid	0.07	0.47	3.2	3.2
	5	POC	Linear	0	0.44		
	5	Seamounts	Linear	0	1	0.27	0.27
	5	Temperature	Trapezoid	3	8	6	8
	6	Aragonite saturation	Plateau	0.47	1		
	6	BPI-broad	Trapezoid	1000	2500	4000	4500
	6	Seamount	Linear	0	1		
	7	Aragonite saturation	Plateau	0.7	0.9		
	7	BPI-broad	Plateau	-500	400		
	7	Dissolved oxygen at depth	Plateau	3.5	4.5		
	7	POC	Linear	2	5		
MOC	1	BPI-broad	Plateau	0	1000	4000	
	1	POC	Linear	0	5		
	2	Aragonite saturation	Plateau	0	2.5		
	2	Dissolved oxygen at depth	Linear decay				
	2	Mud	Linear decay				
	2	Temperature	Trapezoid	0	2	7	7
	3	Gravel	Plateau	5	10		
	3	Aragonite saturation	Plateau	1	1		
	3	POC	Plateau	2	4		
	3	Temperature	Trapezoid	5	5	10	14
	4	BPI-broad	Linear	300	500	>500	
	4	POC	Plateau	12	15	20	30
	4	Temperature	Trapezoid	4	5	10	15
	5	Aragonite saturation	Trapezoid	0.07	0.47	3.2	3.2
	5	POC	Linear	0	0.44		
	5	Seamounts	Linear	0	1	0.27	0.27
	5	Temperature	Trapezoid	3	8	6	8
	8	BPI-broad	Plateau	0	2000	4500	
	8	Seamounts	Linear	0	1		
	6	Aragonite saturation	Plateau	0.47	1		

VME indicator taxa	Expert	Environmental variable	Shape	Absolute min	Preferred min	Preferred max	Absolute max
	6	BPI-broad	Trapezoid	1000	2500	4000	4500
	6	Seamounts	Linear	0	1		
	7	Aragonite saturation	Plateau	0.8	1		
	7	BPI-broad	Plateau	-500	300		
	7	Dissolved oxygen at depth	Plateau	3.5	4.5		
	7	POC	Linear	2	5		
ERO	1	BPI-broad	Plateau	0	500	2000	
	1	POC	Linear	0	5		
	2	Aragonite saturation	Plateau	0	2.5		
	2	Dissolved oxygen at depth	Linear decay				
	2	Mud	Linear decay				
	2	Temperature	Trapezoid	0	2	7	7
	3	Aragonite saturation	Plateau	1	1		
	3	BPI-broad	Trapezoid	0	500	3500	3500
	3	POC	Plateau	2	4		
	3	Temperature	Trapezoid	5	5	10	10
	4	BPI-broad	Linear	350	500	>500	
	4	POC	Plateau	12	15	20	30
	4	Temperature	Trapezoid	4	5	10	15
	5	Aragonite saturation	Trapezoid	0.07	0.47	3.2	3.2
	5	POC	Linear	0	0.44		
	5	Seamounts	Linear	0	1	0.27	0.27
	5	Temperature	Trapezoid	3	5	6	8
	8	BPI-broad	Plateau	0	2000	4500	
	8	Seamounts	Linear	0	1		
	6	BPI-broad	Trapezoid	500	1000	4000	4500
	6	POC	Plateau	5	10		
	7	Aragonite saturation	Plateau	0.8	0.9		
	7	BPI-broad	Plateau	-1000	900		
	7	Dissolved oxygen at depth	Plateau	3.5	4.5		
	7	POC	Linear	2	5		

Table A5-3 | List of experts contacted for the *principles-based* approach. Experts' name and affiliated institution shown, as well as, whether expert has provided input, or has declined to provide input. Note: some experts may not have provided input or declined to provide input due to the timeline given for feedback.

Name	Institution	Input received	Used in RES model
Di Tracey	NIWA	Y	Y
Owen Anderson	NIWA	Y	Y
Dave Bowden	NIWA	Y	Y
Ashley Rowden	NIWA	Y	Y
Malcolm Clark	NIWA	Y	Y
Jenny Beaumont	NIWA	Y	Y
Kareen Schnabel	NIWA	Declined	
Sonia Rowley	UH		
Santiago Herrera	LU		
Vonda Wareham	FOC		
Vreni Haussermann	SSU	Declined	
Chris Yesson	ZSL	Y	Y
Franzis Althaus	CSIRO		
Thomas Schlacher	USC		
Pal Mortensen	IMR		
Les Watling	UH		
Rhian Waller	UM		
Anna Metaxas	DU		
Kerry Howell	PU		
Chris Rooper	DFO	Y	Y
Andrew Davies	URI		
Lyndsey Holland	DOC	Declined	

Annex 6 - Relative environmental suitability (RES) models

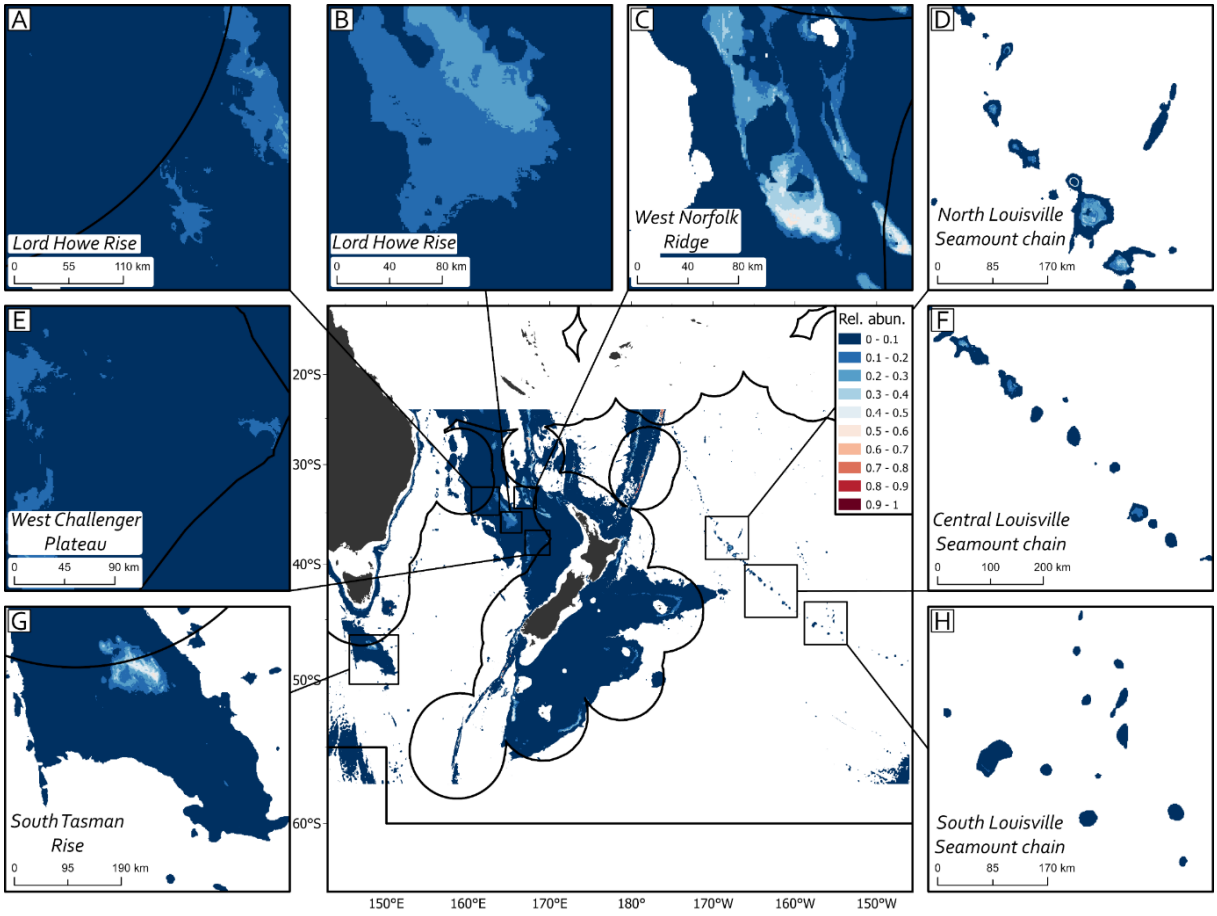

Figure A6-1 | Predicted relative density (0-1) in the study area from the hurdled *principles-based* approach (expert informed) for *Enallopsammia rostrata*. Inset maps of the high seas in the study area: (a) West Lord Howe Rise; (b) East Lord Howe Rise; (c) West Norfolk Ridge; (d) North Louisville Seamount Chain; (e) West Challenger Plateau; (f) Central Louisville Seamount Chain; (g) South Tasman Rise; and (h) South Louisville Seamount Chain**.**

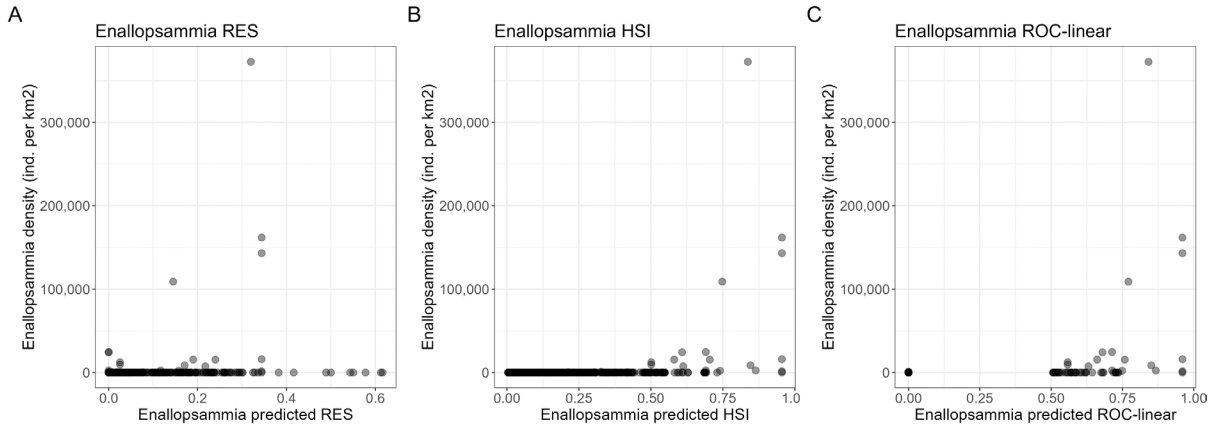

Figure A6-2 | Relationships between *Enallopsammia rostrata* abundance (DTIS data) compared to predictions from different methods used to estimate (or proxy for) abundance (a) *principles-based* approach (RES); (b) habitat suitability model (HSI-linear); (c) ROC AUC thresholded habitat suitability model (ROC-linear).

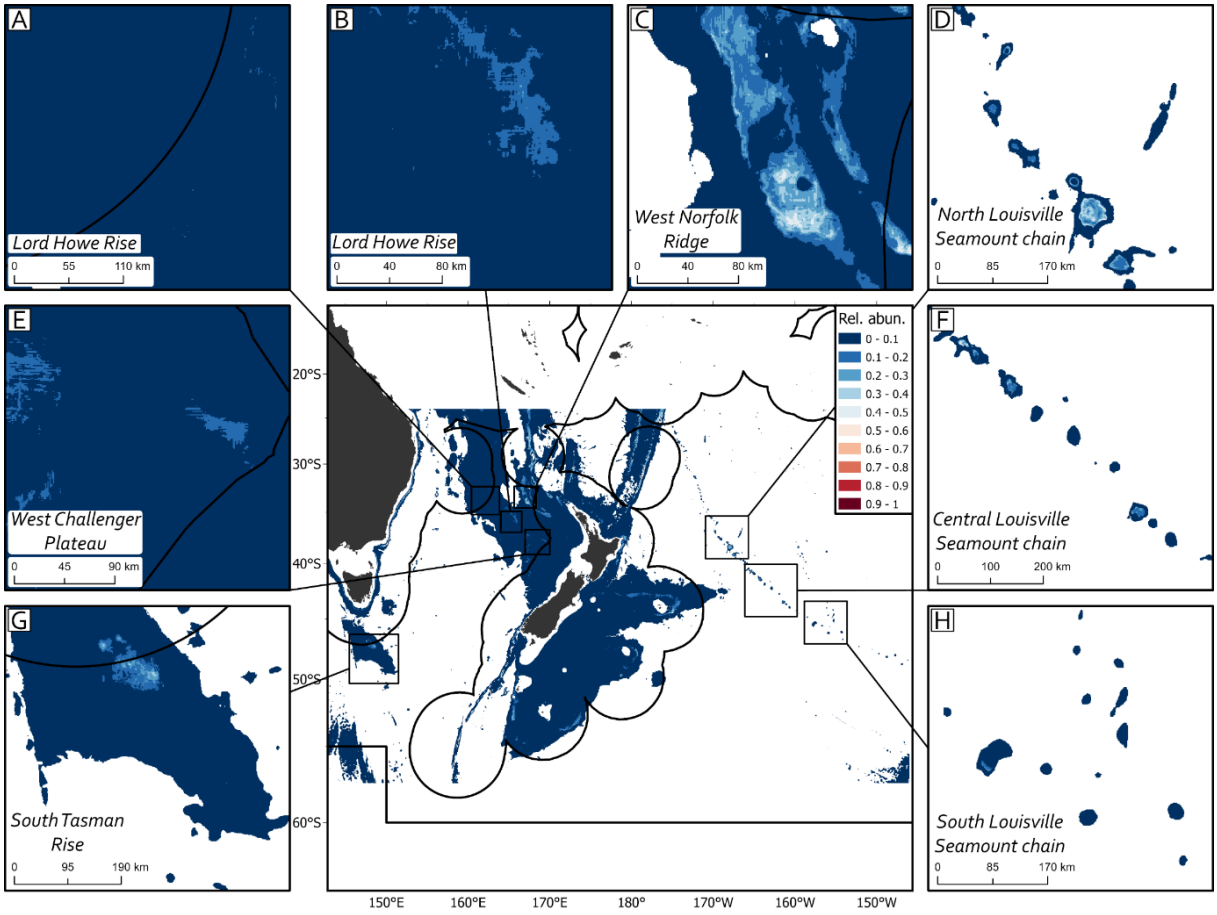

Figure A6-3 | Predicted relative density (0-1) in the study area from the hurdled *principles-based* approach (expert informed) for *Madrepora oculata*. Inset maps of the high seas in the study area: (a) West Lord Howe Rise; (b) East Lord Howe Rise; (c) West Norfolk Ridge; (d) North Louisville Seamount Chain; (e) West Challenger Plateau; (f) Central Louisville Seamount Chain; (g) South Tasman Rise; and (h) South Louisville Seamount Chain.

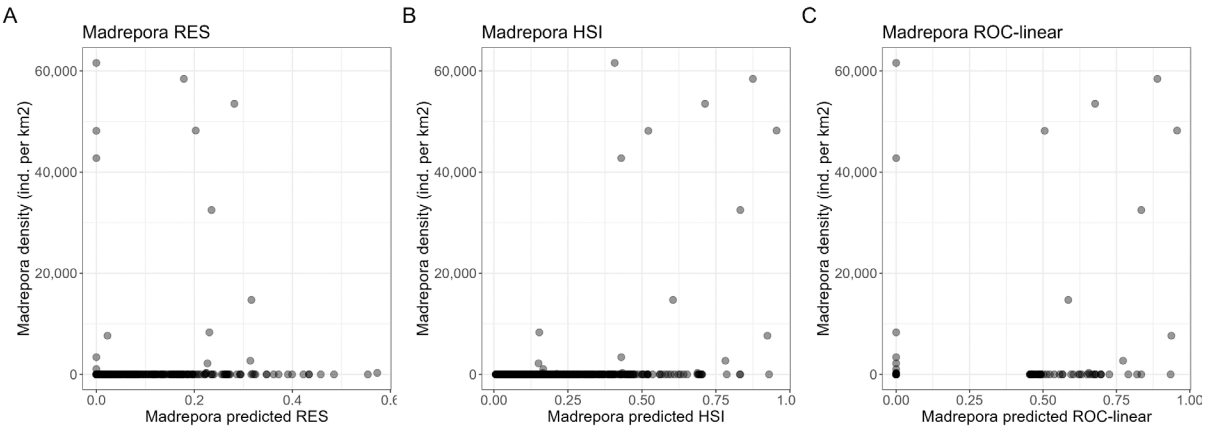

Figure A6-4 | Relationships between *Madrepora oculata* abundance (DTIS data) compared to predictions from different methods used to estimate (or proxy for) abundance (a) *principles-based* approach (RES); (b) habitat suitability model (HSI-linear); (c) ROC AUC thresholded habitat suitability model (ROC-linear).

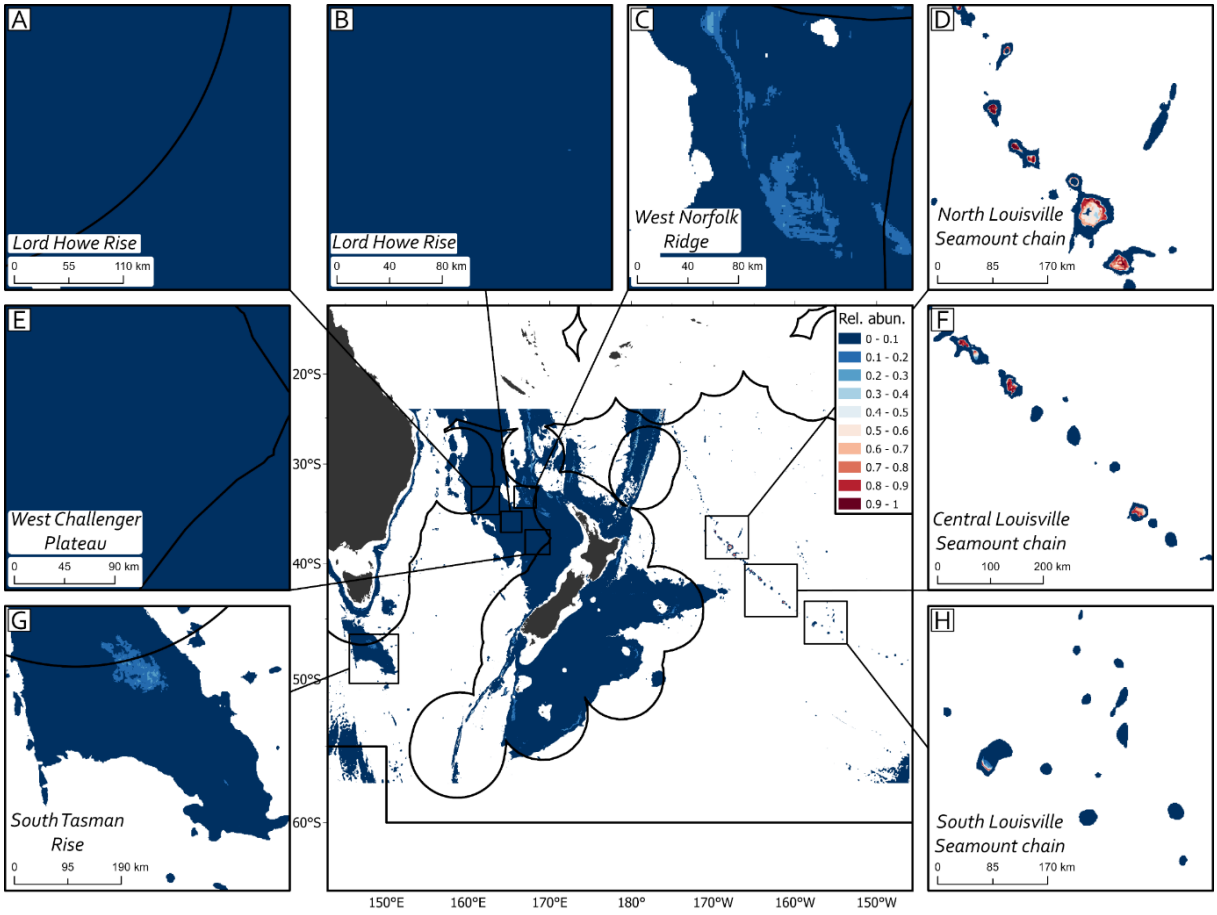

Figure A6-5 | Predicted relative density (0-1) in the study area from the hurdled *principles-based* approach (expert informed) for *Solenosmilia variabilis*. Inset maps of the high seas in the study area: (a) West Lord Howe Rise; (b) East Lord Howe Rise; (c) West Norfolk Ridge; (d) North Louisville Seamount Chain; (e) West Challenger Plateau; (f) Central Louisville Seamount Chain; (g) South Tasman Rise; and (h) South Louisville Seamount Chain.

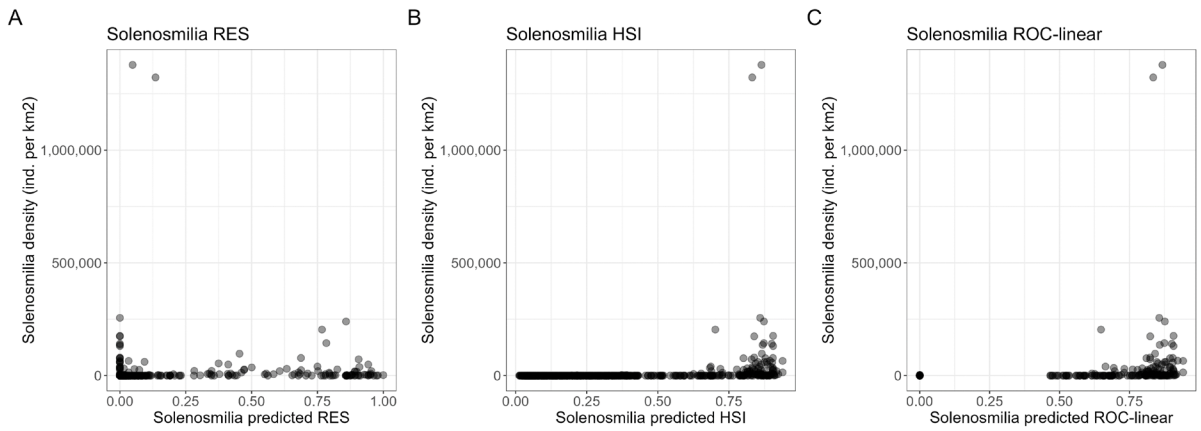

Figure A6-6 | Relationships between *Solenosmilia variabilis* abundance (DTIS data) compared to predictions from different methods used to estimate (or proxy for) abundance (a) *principles-based* approach (RES); (b) habitat suitability model (HSI-linear); (c) ROC AUC thresholded habitat suitability model (ROC-linear).

Annex 7 - VAST models

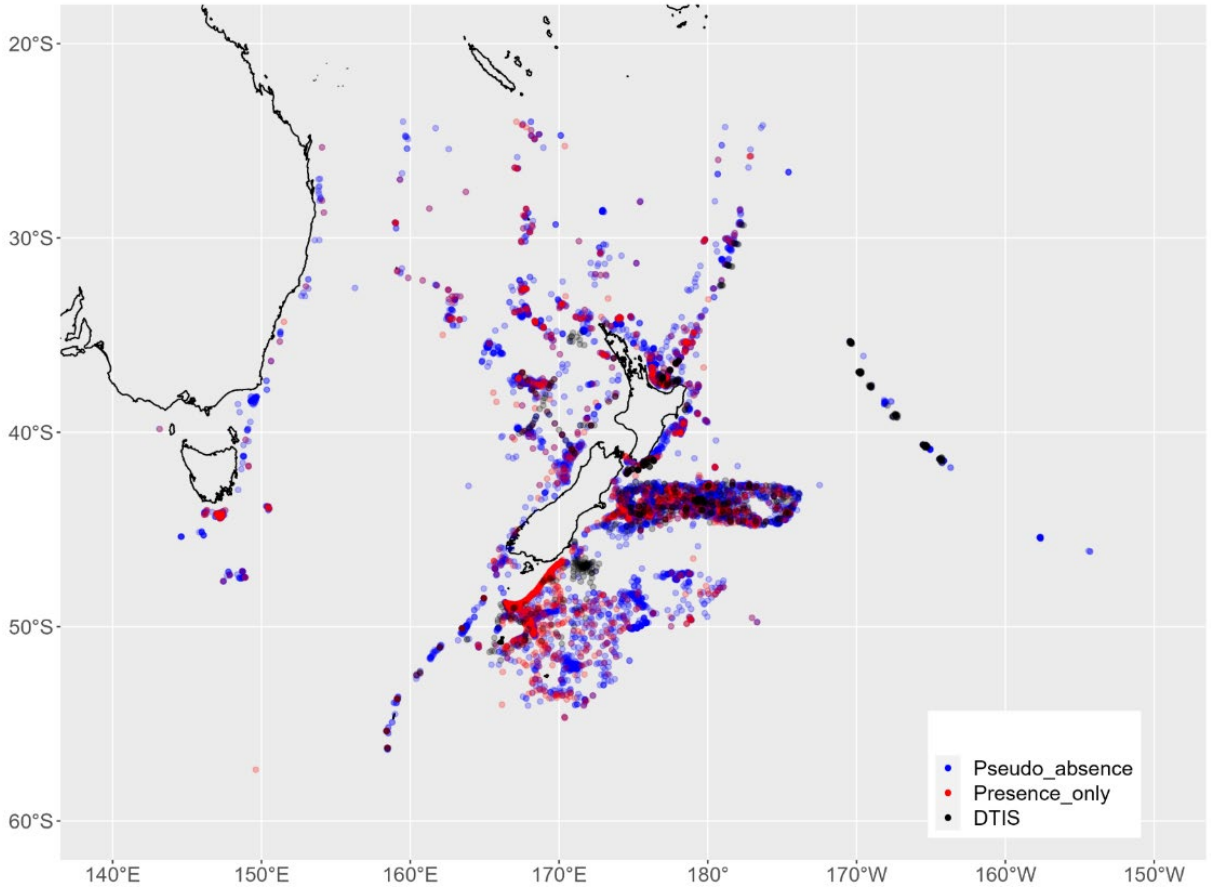

Figure A7-1 | Location of pseudo-absence records (n=8193) for Demospongiae using target group background (TGB) generation within the study area.

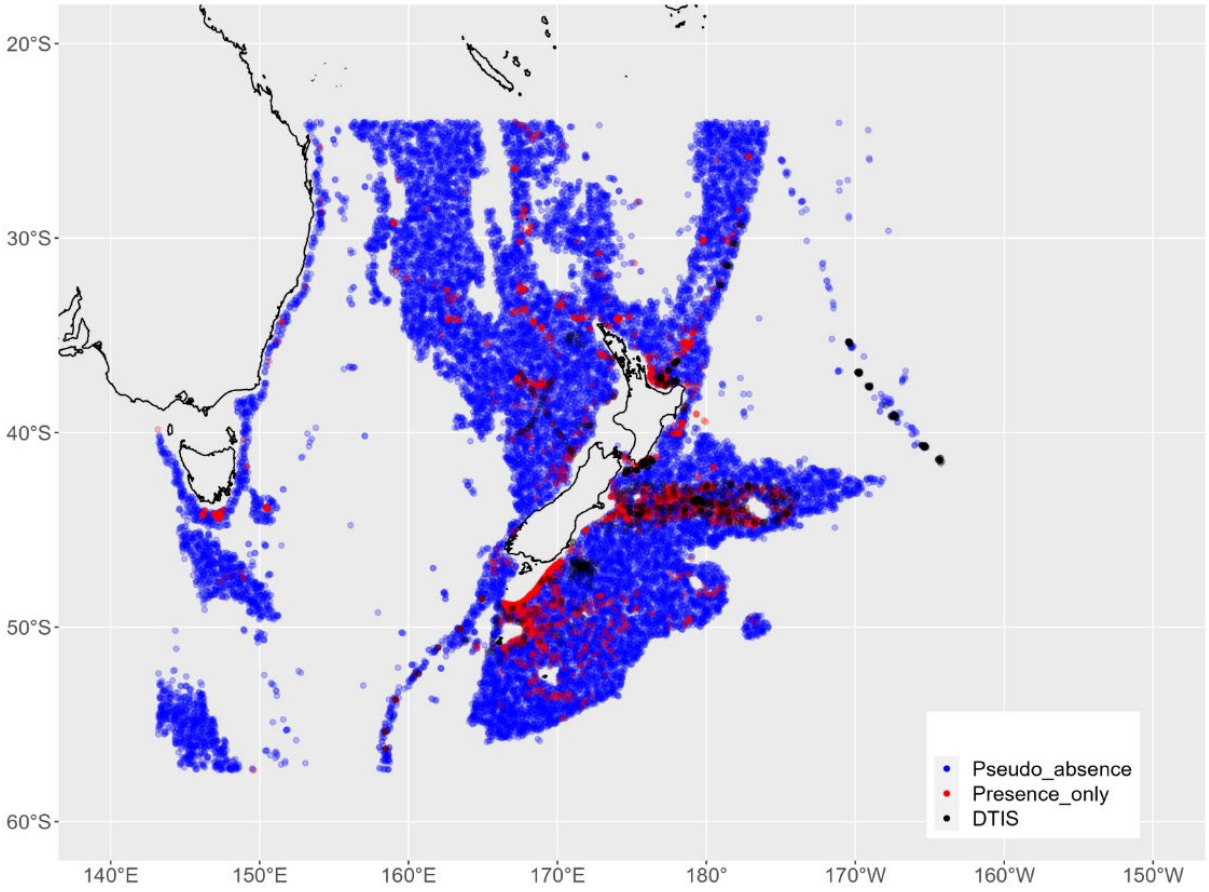

Figure A7-2 | Location of pseudo-absence records (n=22110) for Demospongiae using random generation (10x) within the study area.

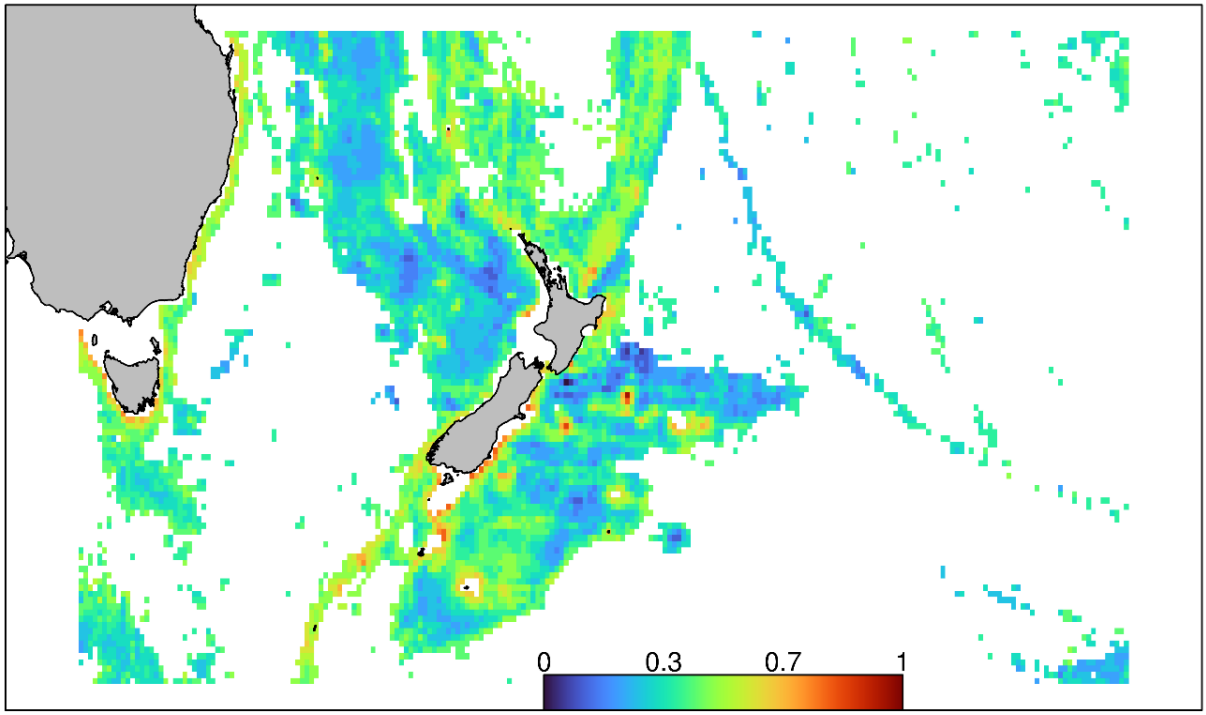

Figure A7-3 | VAST spatial model (spatial and environmental effects) predicting relative density of Demospongiae with target-group background (TGB) generated pseudo-absences within the study area.

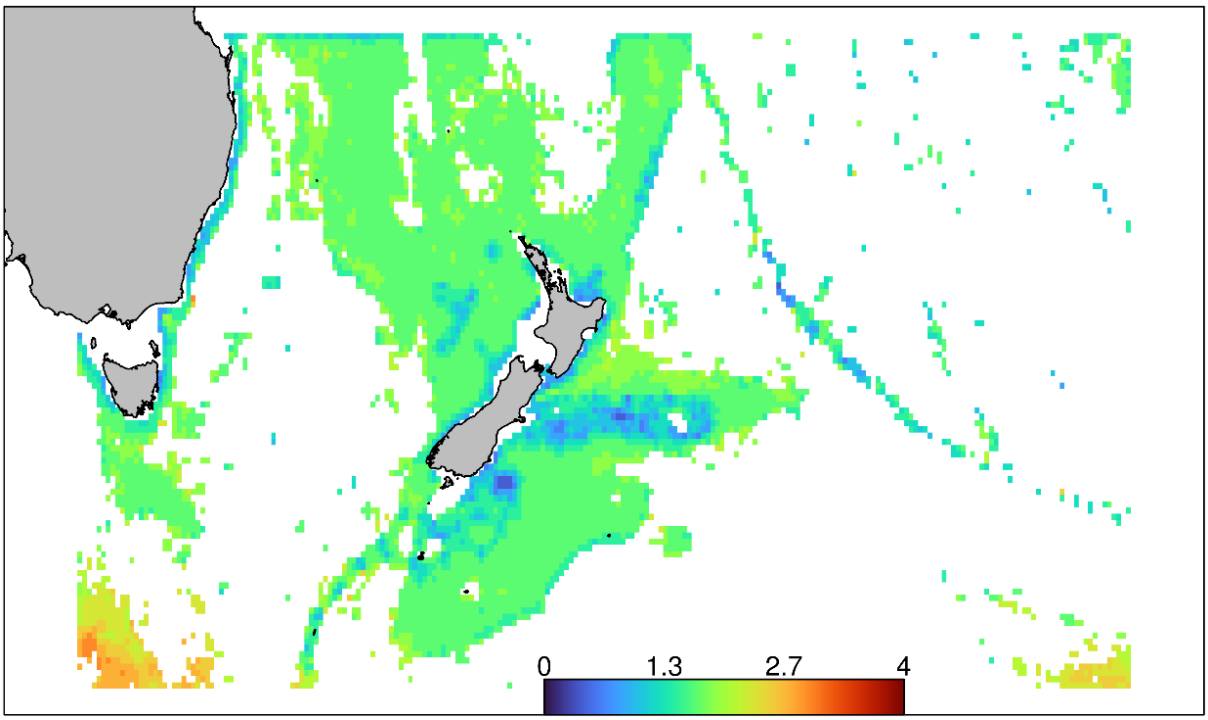

Figure A7-4 | Coefficient of variation from the VAST spatial model (spatial and environmental effects) predicting relative density of Demospongiae with target-group background (TGB) generated pseudo-absences within the study area.

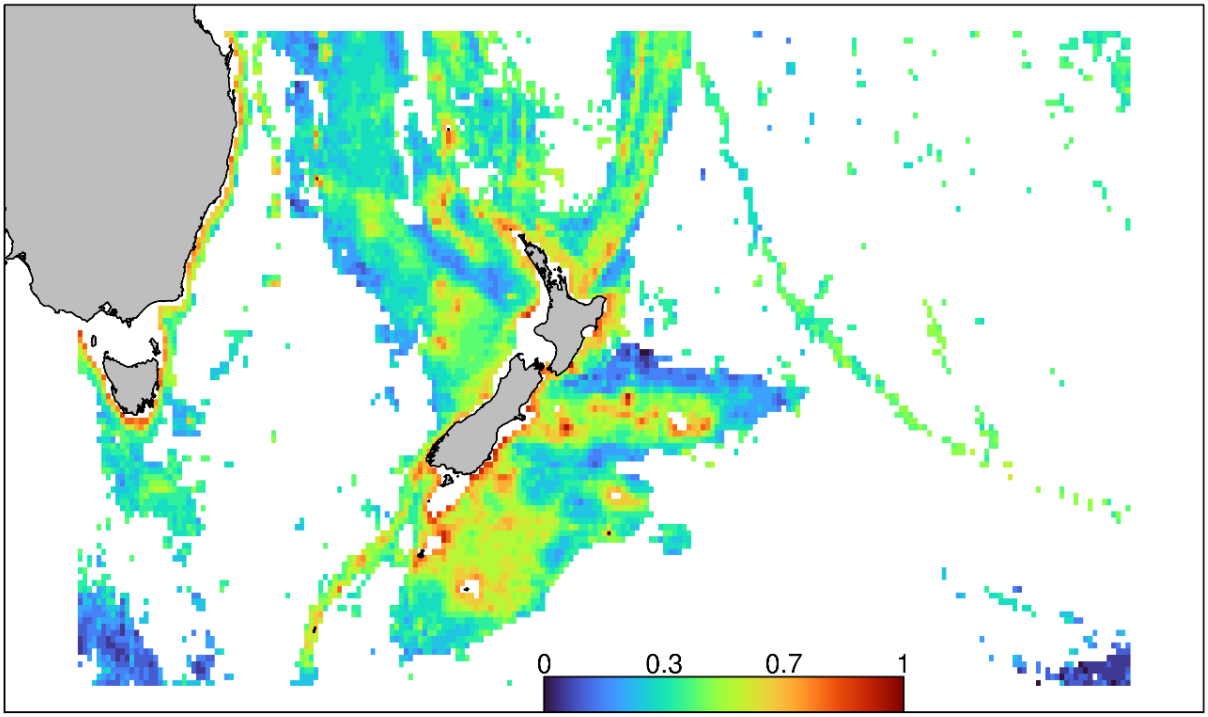

Figure A7-5 | VAST spatial model (spatial and environmental effects) predicting relative density of Demospongiae with randomly generated (10x) pseudo-absences within the study area.

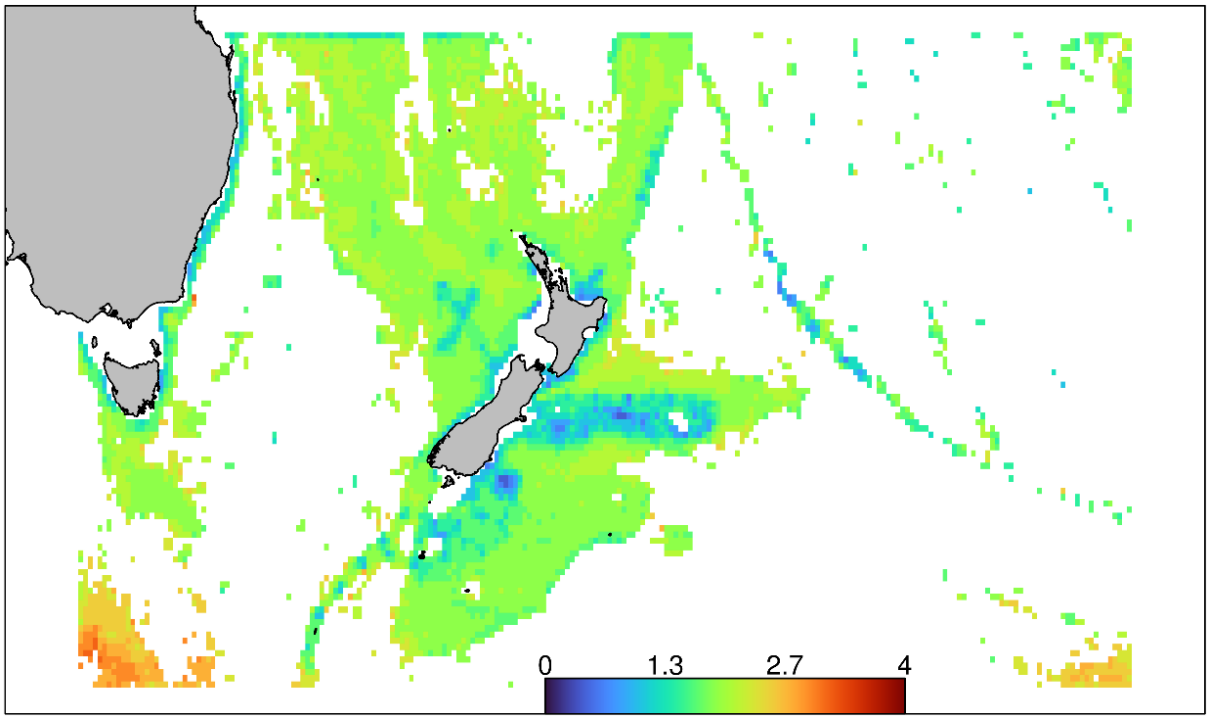

Figure A7-6 | Coefficient of variation from the VAST spatial model (spatial and environmental effects) predicting relative density of Demospongiae with randomly generated (10x) pseudo-absences within the study area.